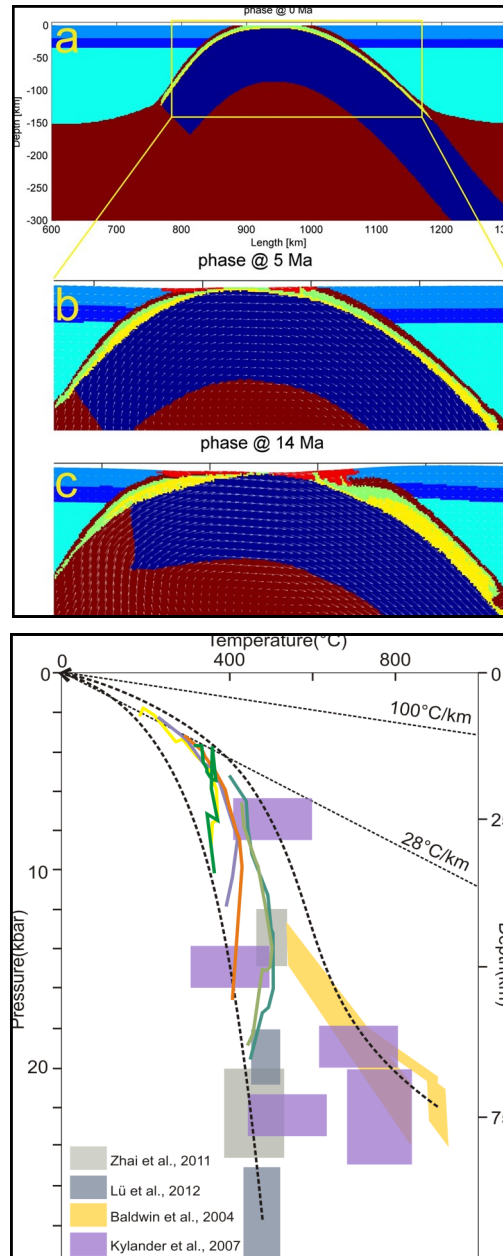
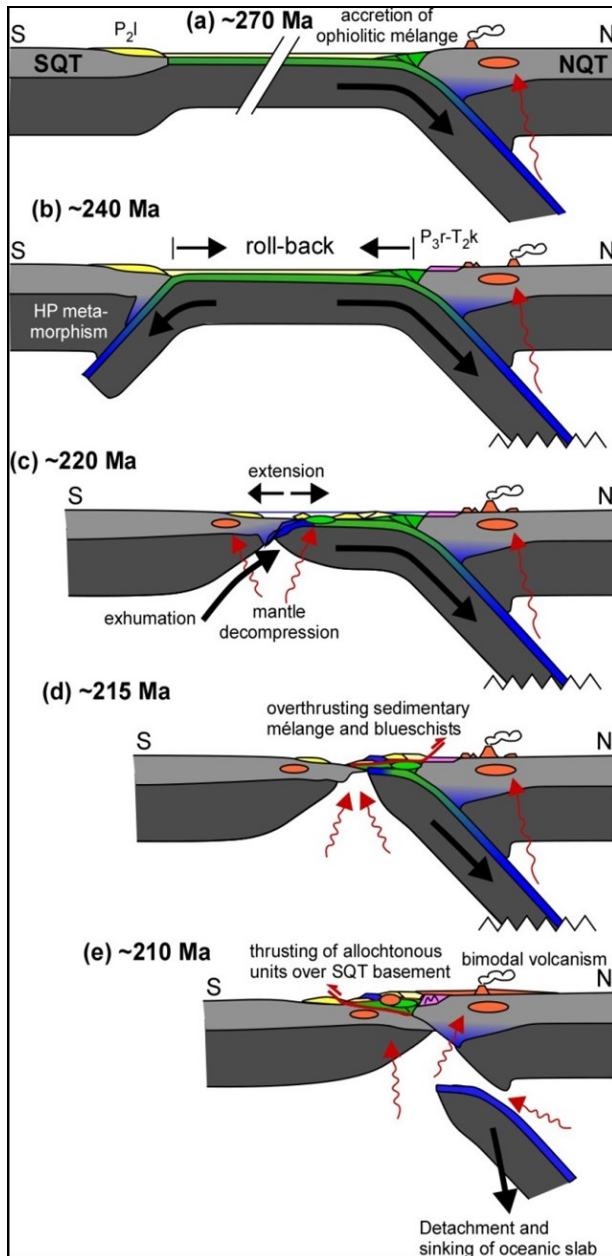


Tectonic evolution of the Qiangtang terrane, Central Tibetan Plateau



Tectonic evolution of the Qiangtang terrane, central Tibetan Plateau

Dissertation

der Mathematisch-Naturwissenschaftlichen Fakultät
der Eberhard Karls Universität Tübingen
zur Erlangung des Grades eines
Doktors der Naturwissenschaften
(Dr. rer. nat.)

vorgelegt von
Zhongbao Zhao
aus Shanxi, China

Tübingen, 2015

Erklärung

Ich erkläre hiermit, dass ich die zur Promotion eingereichte Arbeit selbständig verfasst, nur die angegebenen Quellen und Hilfsmittel benutzt und wörtlich oder inhaltlich übernommene Stellen als solche gekennzeichnet habe. Ich erkläre, dass die Richtlinien zur Sicherung guter wissenschaftlicher Praxis der Universität Tübingen (Beschluss des Senats vom 25.5.2000) beachtet wurden. Ich versichere an Eides statt, dass diese Angaben wahr sind und dass ich nichts verschwiegen habe. Mir ist bekannt, dass die falsche Abgabe einer Versicherung an Eides statt mit Freiheitsstrafe bis zu drei Jahren oder mit Geldstrafe bestraft wird.

Tübingen, June 2015

Datum der mündlichen Prüfung: 28th. August 2015

Dekan: **Prof. Dr. Wolfgang Rosenstiel**

1. Berichterstatter: **Prof. Dr. Paul D Bons**

2. Berichterstatter: **Prof. Dr. Genhou Wang**

Thesis organization and list of publications

This PhD-thesis is organized in a cumulative manner. It is separated into 6 chapters. Here, the general organization of the thesis and a list of included publications are given. Chapter 1 presents an introduction covering the context and the main ideas of the thesis. In Chapter 2-4 three different research papers which were published in the framework of the present study are represented. Chapter 5 represents results from (U-Th)/He thermochronology that are going to be a paper written for concerning on Cretaceous uplifting and shortening of Qiangtang terrane. Chapter 6 use numerical modeling methods prove our new exhumation mechanism which is also going to publish soon. Chapter 7 recapitulates the conclusions and open research questions are given.

Publications

- Zhao, Z.**, Bons, P., Wang, G., Soesoo, A., and Liu, Y.: Tectonic evolution and high-pressure rock exhumation in the Qiangtang Terrane, Central Tibet, *Solid Earth*, 6, 457-473, 2015.
- Zhao, Z.**, Bons, P. D., Wang, G., Liu, Y., and Zheng, Y.: Origin and pre-Cenozoic evolution of the south Qiangtang basement, Central Tibet, *Tectonophysics*, 623, 52-66, <http://dx.doi.org/10.1016/j.tecto.2014.03.016>, 2014.
- Yang, Y., **Zhao, Z. B.**, Yuan, T. Y., Liu, Y., and Li, C. Y.: Ordovician parallel unconformity in Qiangtang terrane, northern Tibet: Implications to Early Paleozoic evolution of northern Tibetan region. *Acta Petrologica Sinica*, 30, 2381-2392, 2014.
- Z. Zhao.**, P. D. Bons., K. Stübner., T. A. Ehlers and G. Wang.: Early Cretaceous exhumation of the Qiangtang Culmination and collision of the Qiangtang and Lhasa terranes, central Tibet. (In preparation)
- Paul D. Bons., Evgene Burov., Enrique Gomez-Rivas., Alavar Soesoo., Douwe D.J. van Hinsbergen., Kun Wang., **Zhongbao Zhao** (alphabetical order): Subduction reversal: an efficient mechanism for the exhumation of Ultra-high-pressure rocks. (In preparation)

Abstract

The highest plateau in the world has attracted geologist's attention for centuries. Significant crustal shortening, which led to the eventual construction of the Cenozoic Tibetan Plateau, began in the Himalaya in the south and the Qilian Shan in the north (over than 1000km) at approximately the Middle Cenozoic. The Paleozoic and Mesozoic tectonic histories in the Himalayan-Tibetan orogeny exerted a strong control on the Cenozoic strain history and strain distribution. Moreover, the Tibetan plateau formed by several terrane slices each of which is about several hundred kilometer wide. Assuming that the lithosphere thickness is also on the 100 km scale, the small width-thickness ratio must have induced a strong influence of mantle dynamics on crustal deformation because of the strong crustal deformation that is located mainly at the continent edges.

The Qiangtang terrane in Central Tibet, with its high-pressure rocks, is a key area to unravel the evolution of the Paleo-Tethys. The presence of widespread Mesozoic subduction mélangé and high-pressure rocks in the Qiangtang terranes can have importance consequences for the formation of the Cenozoic Tibetan plateau. Long-lasting and detailed mapping work offer us the possibly to unravel the geological evolution of the Qiangtang terrane and further test existing geodynamic models in order to better understand the evolution of small terranes.

1:50,000 mapping results from the Rongma area in the central Qiangtang terrane show that the Qiangtang metamorphic belt can be separated into a Paleozoic autochthonous basement and an overlying allochthonous thrust stack of subduction mélangé that contains high-pressure rocks and Permian sediments. Detrital zircon ages (youngest peak at 591 Ma) and an ~ 470 Ma granite intrusion age constrain the age of the Qiangtang Basement to be between the Late Precambrian to Middle Ordovician. This is in agreement with the observed unconformity between basement and overlying Mid-Late Ordovician strata. Based on detrital age spectra and an Early Ordovician unconformity we prefer that the Qiangtang terrane has Gondwana affinity during the Early Paleozoic.

The occurrence of Late Triassic eclogite and glaucophane-bearing schists in the Central Qiangtang terrane indicates the existence of a suture zone between the North and South Qiangtang terranes before the Late Triassic. Detailed 3D mapping analyses indicate that the high-pressure rocks were exhumed from underneath the south Qiangtang terrane in an extensional setting caused by the pull of the northward subducting slab of the Shuanghu-Tethys. High-pressure rocks, sedimentary mélangé and margin sediments were thrust on top of the ophiolitic mélangé that was scraped off the subducting plate. Both

units were subsequently thrust on top of the south Qiangtang terrane continental basement. These conclusions are also supported by sediments and magma ages.

Onset of Late Triassic sedimentation marked the end of the amalgamation of both Qiangtang terranes and the beginning of spreading between Qiangtang and north Lhasa to the south, leading to the deposition of thick flysch deposits in the Jurassic. Strongly folded Jurassic flysch is unconformably overlain by weakly deformed mid-Cretaceous conglomerate and volcanics. This relationship demonstrates closure of Banggong Hu-Nujiang Ocean during Early Cretaceous. Collision between the Lhasa and Qiangtang terranes led to fast exhumation in the Qiangtang terrane during ~140-90 Ma, with exhumation rates about 0.15-0.3 mm/y. The Qiangtang terrane was above sea level up to the mid-Cretaceous and experienced significant denudation prior to mid-Cretaceous times. This model implies substantial crustal thickening and perhaps plateau formation in central Tibet prior to the Indo-Asian collision.

A new model for the exhumation of (ultra-) high-pressure ((U)HP) rocks was developed, based on the observation of exhumed and obducted (U)HP rocks in the study area. It is suggested that exhumation was caused here by pulling up of the subducted slab in a double divergent subduction setting. The long northward subducting slab is envisaged to have extracted the short southward subducting slab. This model was further investigated with numerical modelling. It is suggested that the proposed mechanism may explain the very fast and recent exhumation of eclogites of the d'Entrecasteaux Island off the coast of Papua New Guinea, as well as the fast opening of the Woodlark Basin.

Zusammenfassung

Das höchste Plateau der Welt hat seit Jahrhunderten die Aufmerksamkeit von Geologen auf sich gezogen. Eine wesentliche Verkürzung der Erdkruste von mehr als 1000 km begann im Süden des Himalaya und dem Norden des Qilian Shan etwa im mittleren Känozoikum. Die tektonische Geschichte des Himalaya-Tibet-Orogens im Paläozoikum und Mesozoikum nahm einen starken Einfluss auf Geschichte und Verteilung der Deformation zu dieser Zeit. Außerdem entstand das Tibetplateau aus mehreren Terranstücken, welche jeweils über eine Breite von mehreren hundert Kilometer verfügen. Unter der Annahme, dass die Stärke des lithosphärischen Mantels ebenfalls etwa bei 100 km liegt, müssen kleinere Dicke-Breite Verhältnisse auf einen starken Einfluss der Manteldynamik auf die Krustendeformation hinweisen, da die starke Krustendeformation hauptsächlich auf den Kontinentalrand bezogen ist.

Mit seinen Hochdruckgesteinen ist das Qiangtang Terran in Zentraltibet eine Schlüsselregion, um die Evolution der Paleo-Thetys zu enträtseln. Das Vorliegen einer ausgedehnten Subduktionsmélange zusammen mit Hochdruckgesteinen im Qiangtang Gebiet kann wichtige Konsequenzen für die Entstehung des känozoischen Tibetplateaus haben. Lange und detaillierte Kartierungen bieten die Möglichkeit, die geologische Geschichte des Qiangtang Gebietes zu erklären und ferner existierende geodynamische Modelle zu testen, um die Entstehung kleiner Terrane zu verstehen.

Die Ergebnisse der Kartierungen im Maßstab 1:50,000 aus der Rongma Region im zentralen Qiangtang Terran zeigen die mögliche Einteilung des metamorphen Qiangtanggürtels in ein paläozoisches autochtones Grundgebirge und einen darüberliegenden allochthonen Stapel von Überschiebungen der Subduktionsmélange, die Hochdruckgesteine und permische Sedimente beinhalten. Detritische Zirkonalter (jüngstes Maximum bei etwa 591 Ma) und eine ca. 470 Ma alte Granitintrusion schränken das Alter des Qiangtang Grundgebirges auf das späte Präkambrium bis mittlere Ordovizium ein. Dies stimmt mit der Beobachtung einer Diskordanz zwischen dem Grundgebirge und darüberliegenden mittelordovizischen Einheiten überein. Basierend auf detritischen Altersspektren und der frühordovizischen Diskordanz bevorzugen wir die Interpretation, dass das Qiangtang Terran im frühen Paläozoikum Gondwana zugehörig war.

Das Vorkommen von spättriassischen Eklogiten und Glaukophanschiefern im zentralen Qiangtang Terran zeigt die Existenz einer Suturzone zwischen dem Nord- und Süd-Qiangtang Terran vor der späten Trias an. Detaillierte dreidimensionale Kartenanalysen weisen darauf hin, dass die Hochdruckgesteine unterhalb des Süd-Qiangtang Terrans in einem Extensionsmilieu exhumiert wurden, das von dem Zug der nordwärts gerichteten Subduktion der Platte der Shuanghu-Tethys verursacht wurde. Hochdruckgesteine,

sedimentäre Mélanges und Sedimente des Kontinentalrands wurden auf die ophiolitische Mélange geschoben, die von der subduzierenden Platte abgeschnitten wird. Anschließend wurden beide Einheiten über das kontinentale Grundgebirge des Süd-Qiangtangs geschoben. Diese Schlussfolgerungen werden auch durch Sedimente und Magmaalter unterstützt.

Das Einsetzen der Sedimentation in der späten Trias markiert das Ende des Zusammenschlusses beider Qiangtang Terrane und den Beginn der Spreizung zwischen Qiangtang und Nord-Lhasa, was im Jura zur Ablagerung von mächtigem Flysch im Süden des Qiangtang führte. Der stark verfaltete jurassische Flysch wird diskordant von schwach deformierten Konglomeraten und Vulkaniten aus der mittleren Kreide überlagert. Die Schließung des Banggong Hu-Nujiang Ozeans während der mittleren Kreide wird durch diesen Zusammenhang verdeutlicht. Die Kollision zwischen den Lhasa und Qiangtang Terranen führte zur schnellen Hebung des Süd-Qiangtang Terrans zwischen 140-190 Ma mit Hebungsraten zwischen 0,12-0,15 Millimetern pro Jahr. In der mittleren Kreide befand sich das Qiangtang Terran über dem Meeresspiegel und erfuhr bedeutende Denudation vor der mittleren Kreide. Dieses Modell impliziert eine erhebliche Verdickung der Kruste und vielleicht die Entstehung eines Plateaus in Zentraltibet vor der Indien-Asien Kollision.

Ein neues Modell für die Hebung von (Ultra-) Hochdruckgesteinen wurde auf Grundlage von Beobachtungen von herausgehobenen und obduzierten (Ultra-) Hochdruckgesteinen im Arbeitsgebiet entwickelt. Es wird vorgeschlagen, dass die Hebung hier durch den Zug der subduzierten Platte in einem Umfeld von divergierender Doppel-Subduktion verursacht wurde. Dabei wird erwogen, dass die lange, nordwärts subduzierende Platte die kurze südwärts subduzierende Platte extrahiert hat. Dieses Modell wurde weiterführend mit Hilfe numerischer Modelle untersucht. Es wird gezeigt, dass der vorgestellte Mechanismus die sehr schnelle Hebung von Eklogiten der d'Entrecasteaux Inseln vor der Küste Papua Neuguineas und ebenso die schnelle Öffnung des Woodlark Beckens erklären könnte.

Acknowledgement

I am deeply indebted to my doctoral supervisor **Paul D. Bons** for his fundamental role in my Ph.D work. Firstly, many thanks to Paul who accepted me as Ph.D students four years ago. Paul provided me with every bit of guidance, assistance, and expertise that I needed during my Ph.D study. He is the man who gives me full encouragement when I felt funk to venture into research on my research and branch out into new research areas. At the same time he was continuing to contribute valuable feedback, advice and all these really benefited me so much.

I also would like to thank my second supervisor **Genhou Wang** at China University of Geosciences, Beijing, for the substantial influence on my research and abundant financial supports without it I could not continue my study anymore. I gratefully acknowledge my colleges from Tibetan mapping group for their accompanying and helps in such a danger environment on Tibetan Plateau.

I would particularly like to acknowledge **Prof. Yan Liu**, **Prof. Guoli Yuan** and **Alavar Soesoo**, who have long been an inspiring figure for me. Working together with them, I am leaning not only academic knowledge but also how to become a better being. I am very thankful to **Evgene Burov**, who guide me with numerical modeling works at Paris last year, after that I fall in love with modeling works.

The structural group at Uni-Tuebingen is not a large group, but all members are so nice. **Enrique Gomez-Rivas**, **Till Sachau**, **K. Stübner**, **Maria-Gema Llorens**, **Anett Weisheit**, **Cathi Bauman**, **Florian Steinbach**, **Tamara de Riese** and so on. They played a crucial role in my academic career and made me surviving in Tübingen.

I owe a great debt of gratitude to my ex-girlfriend **Wen Zhang**, together with whom I experienced my valuable and eventful ten years. Without her, I would not harvest much more than I expected. I am particularly thankful to my friends in Tübingen for all the great times that we have shared. They enrich of my knowledge and life during staying in German.

I am deeply thankful to my family for their love, support, and sacrifices. Without them, this thesis would never have been written. This last word of acknowledgment I have saved for my dear **parents**, who have educated me all these years and have made them the best years of my life until now.

感谢爸妈这么多年的无私奉献和良好教育,没有良好的环境我不会有放眼世界的机会。

Zhongbao Zhao
Tübingen
July 2015

Contents

Abstract	IV
Zusammenfassung	VI
Acknowledgement	VIII
<i>Chapter 1: Introduction</i>	11
1.1 Motivation of this thesis.....	11
1.2 Geological setting around Qiangtang terrane.....	13
1.3 Geological evolution within the Qiangtang Terrane	19
1.4 Summary main points around and within Qiangtang terrane.....	21
1.5 Review of existing exhumation models	24
1.6 Organization of the thesis	25
References.....	26
<i>Chapter 2: Origin and pre-Cenozoic evolution of the south Qiangtang basement, Central Tibet</i>	38
1. Introduction.....	39
2. Geology of the Rongma area	41
3. Geochronology work in central Qiangtang terrane.....	52
4. Discussion	56
5. Conclusions.....	62
References.....	63
<i>Chapter 3: Ordovician parallel unconformity in Qiangtang terrane, northern Tibet: Implications to Early Paleozoic evolution of northern Tibet regions</i>	68
1. Introduction.....	69
2. Geological background	70
3. Unconformity between Rongma Group and Tashishan Group.....	71
4. Analysis methods	74
5. Analysis results	75
6. Discussion	77
7. Conclusion	80
<i>Chapter 4: Tectonic evolution and high-pressure rock exhumation in the Qiangtang terrane, central Tibet</i>	82
1. Introduction.....	83
2. Regional setting	84

3. The basic stratigraphic and lithological frame in the Qiangtang terrane	88
4. Structures and tectonics of the mélangé in mapping area	96
5. Discussion	100
6. Conclusions	106
References	108
<i>Chapter 5: Early Cretaceous exhumation of the Qiangtang Culmination and collision of the Qiangtang and Lhasa terranes, central Tibet</i>	<i>114</i>
1. Introduction	114
2. Geological setting	116
3. Mesozoic tectonics of the Rongma area	118
4. U-Th/He dating	121
5. Discussions	123
6. Conclusions	126
References	127
<i>Chapter 6: Subduction reversal: an efficient mechanism for the exhumation of ultra-high-pressure rocks</i>	<i>132</i>
References	140
<i>Chapter 7: Main conclusions and further questions</i>	<i>143</i>
7.1 The mélangé in central Qiangtang clarified into several different units.	143
7.2 Structural relationships of different units	144
7.3 Simplified tectonically evolution model of Qiangtang terrane.	145
7.4 New efficient exhumation model of high-pressure rocks.	146
7.5 Open questions and further research aims.	146
Appendix	147
<i>Appendix A: Original paper (in Chinese) for Chapter 3</i>	<i>147</i>
<i>Appendix B: Table of thermochronologic data (chapter 5)</i>	<i>148</i>
<i>Appendix C: Numerical setup (chapter 6)</i>	<i>149</i>
CV	150

Chapter 1: Introduction

1.1 Motivation of this thesis

The Tibetan plateau, which is the most spectacular present-day example of the consequences of subduction-collision orogeny, is marked by a width of ~2500 km between the Western (Nanga Parbat) and Eastern Syntaxis (Namche Barwa). It occupies the E–W trending high Himalaya, which includes the world’s highest mountains, the Karakorum in the south and the Tibetan Plateau in the north. This system was largely created by the collision of India and Asia in the early Eocene (e.g. Najman et al. 2010) and is part of the greater Himalayan-Alpine system, extending from the Mediterranean Sea in the west to the Sumatra arc of Indonesia to the east (Yin and Harrison 2000). The plateau was developed by the closure of the Tethys oceans between Laurasia in the north and Gondwana in the south since the Paleozoic (e.g. Şengör, 1990; Sengor and Natalin, 1996).

The Tibetan plateau consists of six main terranes, including Kunlun-Qaidam, Songpan–Ganzi, north- and south-Qiangtang, Lhasa and Himalaya terranes. From north to south, separated by the Kunlun-Anyenagen, Jinsha-Tethys, Longmu Co-Shuanghu, Banggong-Nujiang and Yarlung Zangbo suture zones (Fig. 1) (Şengör, 1990; Yin and Harrison, 2000). To the northwest the plateau is bounded by Altyn Tagh fault from the Tarim basin and it connects with Pamir Plateau to southwest (e.g. Angiolini et al., 2013). To the north of the Tibetan Plateau, the Qilianshan–Kunlun orogenic system was formed by the northward subduction of the Kunlun-Anyenagen Tethys Ocean lithosphere and the southward subduction of the Paleo-Asian Ocean lithosphere during the Early Paleozoic (e.g., Pan et al., 2012). The Tibetan Plateau thrusts onto the Sichuan basin on its eastern margin and extends to southeast along Sanjiang area joining to Southeast Asian (Metcalf, 2013). The India continent indented the Tibetan Plateau northward during Cenozoic times at the Yarlung-Zangbo suture zone and created the largest plateau in the world (Xu et al., 2014c). Within this orogeny, ophiolites and ophiolitic mélangé zones preserved in the Jinsha-Tethys, Longmu Co-Shuanghu and Bangong-Nujiang suture zones document the histories of complex island-arc formation, back-arc spreading, back-arc basin closure, arc–arc collision, and arc–continent collision during the Late Paleozoic to Mesozoic. After indentation between India and Eurasia plates, all these small terranes and tethyan suture zones were joined together (e.g., Pan et al., 2012).

During the last three decades, extensive geological knowledge of the Proto-, Paleo- and Meso-Tethys oceans was accumulated in central Tibetan plateau. Nonetheless, details of the geological evolution are still hotly debated, which encourages us to work more on this enigmatic and magnificent geological structure: the Tibetan Plateau. During 2008 to 2014, the geological survey team from China University of

Chapter 1

Geoscience mapped a 60 x 180 km² area in the centre of the Qiangtang terrane, covering the Paleotethys (Longmu Co-Shuanghu suture zone) subduction mélange with high-pressure rocks (e.g., Zhai et al., 2011a; Zhai et al., 2011b). This detailed field mapping works provided new and better understanding of the evolution of the Qiangtang Terrane.

This thesis is based on parts of mapping results and data synthesis both from our observation and the literature. Based on this, it was possible to confirm the presence of a south Qiangtang basement, to separate the subduction mélange into three main units, and to propose a new exhumation model for the high-pressure rocks. Moreover, the Mesozoic evolution is discussed, combining new thermochronological data and structural relationships in the field.

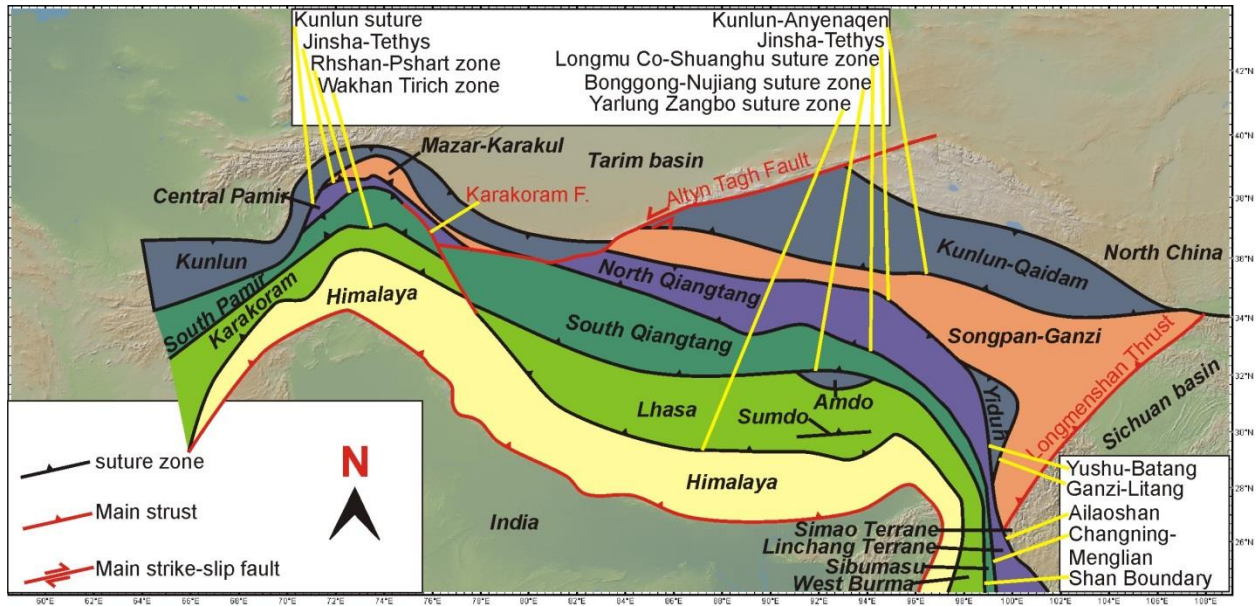


Fig. 1 Present tectonic setting of Tibet, SE Pamir and Sanjiang area, together sandwiched between the Eurasian plate to the north and the Indian plate to the south. Modified from Angiolini et al. (2013), Zhu et al., (2012), Pan et al. (2012).

In next section (1.2), I will briefly introduce the geological background of the surroundings of the Qiangtang terrane. The Qiangtang terrane itself and the Longmu Co-Shuanghu suture zone (LSS) will be focused on in section 1.3. A summary of the main argument for the tectonic evolution of these areas is presented in section 1.4. Because blueschists and eclogites are found in the central Qiangtang terrane (e.g., Liu et al., 2011), a new model for their exhumation during closure of LSS in Late Triassic is proposed. Hence, the current exhumation models are reviewed in section 1.5. A more detailed thesis structure is presented in 1.6.

1.2 Geological setting around Qiangtang terrane

In this section, the Songpan-Ganzi Flysch belt and Lhasa terrane, located north and south from Qiangtang terrane separately, will be introduced firstly. The Jinsha Tethys formerly separated the Songpan-Ganzi and Qiangtang terranes, while the Banggong-Nujiang suture zone (Meso-Tethys) is located between the Lhasa and Qiangtang terranes (Fig. 1). Both sutures are also presented. The evolution of the Yarlung Zangbo suture zone is related to the Mesozoic to Cenozoic deformation of Qiangtang terrane, hence it is also introduced briefly.

1.2.1 Songpan-Ganzi Flysch

The Songpan-Ganzi Flysch belt (SGF) is located in the northeastern part of the Tibetan plateau and west of the Sichuan basin (Fig. 1). It is bounded by the South China, North China, Kunlun–Qaidam and Qiangtang continental blocks (Fig. 1) (Nie et al., 1994).

The SGF, covered by Upper Triassic turbidites, has traditionally been interpreted to be floored by oceanic crust (e.g., Yin and Harrison, 2000; Roger et al., 2003). However, recent deep seismic data show the crustal structure (e.g., Wang et al., 2007). Geochemical and isotopic investigations on the magmatic rocks (e.g., Yuan et al., 2010), and tectonic modeling (Zhang, 2001b; 2002) also indicate that the terrane may currently be underlain by a Cathaysian-type continental basement, at least in its eastern part.

From the Late Permian to Early Jurassic, coeval subduction zones were active along Kunlun–Anyenagen to the north, Jinsha-Tethys to the south and Ganzi-Litang to the southeast (Fig. 1). Subsequent convergence of the South China, Kunlun-Qaidam and Qiangtang terranes induced the closure of the Songpan-Ganzi basin, a branch of the Paleo-Tethys Ocean (e.g. Roger et al., 2008; Pullen et al., 2008). The Middle to Late Triassic deep-water deposits that form the Songpan-Ganzi Flysch comprise an estimated $\sim 2.0 \times 10^6 \text{ km}^3$ of detrital material that accumulated in this triangular basin (Nie et al., 1994). These huge turbidites have diverse provenances, with major sources derived from the Qinling–Dabie orogen (Weislogel et al., 2010) and the central Qiangtang metamorphic belt (Zhang et al., 2006b). Especially in the western SGF, the Late Triassic turbidites were derived from nearby central Qiangtang Triassic collisional orogeny sources, rather than distant Dabie–Qinling sources (Zhang et al., 2008a).

Both northward subduction at the Kunlun–Anyenagen suture zone under the Kunlun arc and southward subduction at the Jinsha-Tethys underneath the Qiangtang terrane started during the Carboniferous (e.g., Li et al., 2002) and ceased in the Late Triassic (Pullen et al., 2011). The Late Triassic magmatism separated into two groups, high-K calc-alkaline rocks (221–212 Ma) and medium-to-high-K calc-alkaline

I-type granites (205–190 Ma) in the west of SGF. The magmatic source probably changed from the subducted Paleo-Tethys oceanic slab, including basalts and marine sediments, to the juvenile crust (Zhang et al., 2014). To the east, the Longmen Shan thrust–nappe belt separates the SGF from the Sichuan basin (Chen and Wilson, 1996; Reid et al., 2003). Westward subduction at the Ganzi–Litang suture zone separated SGF to the west of Yangtze Craton (Fig. 1) (Wang et al., 2013). Subduction related magma activity can also be separated into two groups, 228–210 Ma and 206–195 Ma, respectively (Zhang et al., 2014). The west-dipping Ganzi–Litang oceanic lithosphere was apparently bounded the Yidun Arc to the north from the SGF. The SGF was thus connected to, or collided with the northern part of the Yidun terrane during the Late Triassic (Wang et al., 2013). Arc volcanism developed in the eastern Yidun Arc during the Middle–Late Triassic, apparently in response to westwards subduction of the Ganzi–Litang back-arc.

Situations are more complex in the case of the Yidun Arc that was rifted from Kunlun arc during rollback of northward subduction of the Jinsha-Tethys (e.g. Pullen et al., 2008). The alternative opinion prefers that the Yidun Arc derived from the Yangtze Craton to the southeast, which was related to rollback of the eastward-subducted Yushu-Batang oceanic plate, which could be the eastern extension of the Jinsha-Tethys (Fig. 1). However, both theories agree that the Yidun arc is possibly underlain by Precambrian basement with Cathaysian affinity (e.g., Reid et al., 2007a) and covered by Paleozoic warm-water sediments and faunas (e.g., Metcalfe, 2013). This demonstrates that an unexposed Proterozoic basement exists beneath the Triassic sediments of the SGF (Zhang et al., 2006a). Inherited Neoproterozoic (880–740 Ma) zircon ages found in two samples from the SGF indicate either inheritance of zircon crystals from the surrounding SGF turbidite strata or possibly involvement of Yangtze Craton basement during crustal thickening and magma genesis (Weislogel, 2008).

The timing of suturing of the Qiangtang Block and Yidun Arc is constrained by the emplacement of post-tectonic plutons into deformed Paleozoic metasediments along the Yushu-Batang suture at 245 Ma. Subduction also occurred underneath the northern margin of the Qiangtang Block at the Yushu-Batang suture zone, resulting in arc volcanism that was synchronous with the deposition of extensive turbidites sequences across the region (Roger et al., 2003; Reid et al., 2005a). This is identified by the Early Triassic deformation that is documented in the western Yidun Arc (Yang et al., 2012). Because of closure of Yushu-Batang suture zone was earlier than closing of western JSS, the Jinsha suture may jump and connect with the Ganzi–Litang suture during Late Triassic. They represent the main branch of the Paleo-Tethys Ocean that closed by southward subduction (Yang et al., 2012).

Chapter1

The Ailaoshan suture zone, connected with the JSS suture zones, was interpreted as a back-arc basin branch of the Paleo-Tethys Ocean between the Simao and Linchang Blocks (Fig. 1) (Jian et al., 2009). Ophiolitic assemblages at the suture include meta-peridotite, gabbro, diabase and basalt capped by radiolarian-bearing siliceous rocks. N-MORB type ophiolites in the Ailaoshan suture have been dated as Middle-Late Devonian (ca. 387–374 Ma), and E-MORB type ophiolites dated as Lower Carboniferous (ca. 346–341 Ma) by Jian et al. (2009). Plagio-granite was dated as latest Devonian (ca. 362 Ma) by Jian et al. (1998) and the radiolarian siliceous rocks are Lower Carboniferous in age (e.g., Yumul Jr et al., 2008). Clasts in the olistostrome range in age from Silurian to early Permian. SHRIMP U–Pb analyses on collision-related Triassic volcanic rocks give ages of 247–246 Ma from rhyolites, and ca. 245–237 Ma from basaltic and intermediate-felsic volcanics (Zi et al., 2012). The Ailaoshan ocean basin is thus interpreted to have opened in the Late Devonian – Early Carboniferous and to have closed in the Middle Triassic.

One pluton (205 Ma) was emplaced simultaneously with a rapid uplift of the lithosphere, when surface deposits changed from deep-water turbidites to tidal flat sediments in the SGF. Therefore, it generated during decompression, probably related to the rapid removal of the overthickened lithospheric mantle (Yuan et al., 2010). This extension period is consistent with 225–200 Ma Ar–Ar cooling ages (Reid et al., 2005b). The sedimentary provenance data and magmatism history and deformation favor syn-convergent extensional tectonics. Marine strata of Jurassic age in the northwestern SGF unconformably overlie Upper Triassic turbidites, which also indicates extension during that period (Ding et al., 2013).

Generally, basement appears missing in the SGF and it may be mainly underlain by oceanic crust (Roger et al., 2010), but possibly have Cathaysian-type continental basement under the eastern edge. Concluding from the discussion above, the SGF experienced magmatism and basin development during Late Devonian (?) to 210 Ma at the ocean evolution stage, followed by extension at 205 Ma to 190 Ma. Its evolution includes a large arc collision event that was between the Yidun arc and the Qiangtang Terrane during early Triassic times (Pullen et al., 2008).

1.2.2 Lhasa terrane

The Lhasa terrane is bound to the north by the Banggong–Nujiang Suture (Meso-Tethys) and to the south by the Yarlung–Zangbo Suture (Ceno-Tethys) (Fig. 1). The oldest exposed rock on the Lhasa terrane is Precambrian crystalline basement. There are sporadic Paleozoic to Mesozoic strata that unconformably overlie the basement (Zhu et al., 2012). It collided with Qiangtang terrane (Eurasia continent) during the Cretaceous, just before the Eurasia-Indian continental collision (e.g. Zhang et al., 2012b). Some authors

Chapter 1

divided Lhasa into a north and south Lhasa two parts, with Paleozoic continental shelf-affinity sediments on north Lhasa, while the south Lhasa was occupied by a magmatic arc, the Gangdese arc that was active from the Late Mesozoic to the Cenozoic (England and Searle, 1986; Murphy et al., 1997; Miller et al., 2000).

The original position of Lhasa terrane within the Gondwana realm is still debated. Based on review of detrital zircon age mode and comparing Paleozoic faunas and floras, Metcalfe, (2013) proposed that the Lhasa terrane was connected to the Himalayan–Western Australian region during most of the Paleozoic era. The Qiangtang terrane drifted away from relatively cold water zone (northern Gondwana) to northern warm water before Middle Permian. However, the Lhasa terrane rifted later than the Qiangtang Block to the north according to Late Guadalupian (~260Ma) fusuline was still belonging to cold fauna (Zhang et al., 2010b). Missing of Upper Permian strata (Yin and Grant-Mackie, 2005) indicate northward drifting of Lhasa after the Middle Permian. Palaeomagnetic data show that the Lhasa terrane travelled from southern to northern hemisphere latitudes in the Late Triassic–Jurassic (Sun et al., 2010).

Eclogites aged 242 ± 15 to 292 ± 13 Ma (SHRIMP U–Pb) (Yang et al., 2009) and blueschist (Liu et al., 2009) enclosed within a Triassic metamorphic massif indicate a suture inside of Lhasa terrane. Together with ~260 Ma granite and the regional angular unconformity between the Middle and the Upper Permian would represent a Paleo-Tethys suture within the Lhasa block (e.g., Yang et al., 2009; Zhu et al., 2009a, b, 2011b). This suture thus separated Lhasa into south and north Lhasa two parts. However, an alternative explanation is that the entire Triassic massif was an overthrust sheet transported from the central Tibetan orogen (Zhang and Tang, 2009).

~205–174Ma magma along the southern margin of the Lhasa terrane (e.g., Ji et al., 2009; Zhang et al., 2007; Zhu et al., 2011a) is simultaneous with an early Jurassic (ca. 204–192 Ma) extension event (Weller et al., 2015). It is assumed here that this event is related to BNS opening. Subsequent syn-orogenic igneous activity at ~170–137 Ma represents a transition to compression of the Lhasa terrane at that time. This compression, which induced crustal thickening of the Lhasa block at 140–130 Ma, was related either to southward subduction of the Meso-Tethys or northward subduction of Ceno-Tethys under the Lhasa terrane in the middle Jurassic (Ding and Lai, 2003).

Exposure of Middle Cretaceous high-temperatures metamorphic rocks (134–105 Ma), associated with E–W-trending extensional faults in eastern Lhasa (Hu et al., 2004) and Cretaceous (135–100 Ma) post-orogenic bimodal magmatism (e.g. Zhu et al., 2009a) indicate that the Lhasa terrane was extended. Break-

off of southward subducting of Bangong–Nujiang ocean lithosphere may have caused elastic rebound of the upper crust (Zhu et al., 2009a; Zhu et al., 2010). Another delamination model has also been used to explain Middle Cretaceous magmatic rocks in the Lhasa block (Zhang et al., 2012a). This extension event would have caused an extensive marine transgression in northern Lhasa. Therefore, a tectonic transition from continental collision to extension in central Tibet occurred during Early Cretaceous times (ca. 120–95 Ma) (Zhang et al., 2012a). However, this extension model is in conflict with other models that envisage collision between the Lhasa and Qiangtang terranes during Aptian to Cenomanian (Kapp et al., 2007). Thrusting inside the Lhasa terrane began at ~90 Ma and lasted into Early Eocene times (~50Ma) (e.g., Kapp et al., 2007; Leier et al., 2007; DeCelles et al., 2007). This thrust event uplifted the Lhasa terrane and marked changing from shallow marine to non-marine depositional records (Volkmer et al., 2007).

1.2.3 Banggong-Nujiang suture zone

The ~1700 km Banggong–Nujiang suture (BNS) extends from Banggong Lake in the west to Nujiang in the east. It separated the Lhasa from South Qiangtang terranes (Dewey et al., 1988) and represents the former Meso-Tethys Ocean. Opening of this oceanic basin is recorded by rift-sediments (Schneider et al., 2003) and deep marine sediments, radiolarian cherts, are found ranging in age from the Carboniferous to the Early Cretaceous (Wang et al., 2002; Baxter et al., 2009).

Ophiolitic mélangé zones are found at the BNS, mainly in the Banggong Lake, Dong Tso and Lagkor Tso areas (Wang et al., 2008; Shi et al., 2008) and include MORB-type ophiolite, SSZ-type ophiolite (Shi, 2007; Shi et al., 2005), oceanic island-sea mountain basalt (Wang et al., 2005) and oceanic ridge plagiogranite (Zhang and Chen, 2007). Ages scatter from 221.6 ± 2.1 Ma to 167.0 ± 1.4 Ma (Wang et al., 2008; Shi, 2007), indicating that these ophiolites formed between the Lhasa and south Qiangtang terranes during the Late Triassic to Early Jurassic (She et al., 2009). The youngest ophiolitic gabbro from the suture zone is early Cretaceous in age (128 Ma) (Chen et al., 2006), which represents the BNS closure after 128Ma at its westernmost extent.

Closure of the BNS was due to divergent double subduction of BNS lithosphere, northward under the south Qiangtang terrane during the Mesozoic (Kapp et al., 2003a, 2007; Guynn et al., 2006) and southward under the Lhasa Terrane during the Permian–Early Cretaceous (Pan et al., 2006a; Zhu et al., 2009b; Zhu et al., 2009a; Zhu et al., 2011a), respectively. Early Jurassic–Middle Cretaceous (183–101 Ma) arc magmatic rocks, with calc-alkaline composition, are present on the southern margin of the Qiangtang block (Zhu et al., 2011a; Xu et al., 2014b). An unconformity between marine sediments and coarse clastic

Chapter1

sediments trends from Middle Jurassic in the east to Upper Cretaceous in the west along the BNS, indicating that the BNS was closed from east to west (Kapp et al., 2003a; Pan et al., 2006b; Nimaciren et al., 2005).

Commence of the Lower Cretaceous terrestrial sequence along with abundant volcanic rocks (131–110 Ma; Zhu et al., 2009a, 2011a) is interpreted to represent molasses sediments which derived from orogenic activity on the South Qiangtang terrane. This uplifting was caused by the collision between the Qiangtang and Lhasa blocks, but appears to precede uplift in the North Lhasa terrane by about 20 Myr.

A short-lived back-arc basin developed on the western part of the north Lhasa terrane in the early Cretaceous. Its existence is indicated by an extensive marine transgression and limestone unconformably overlying sandstones during the beginning of the Hauterivian (130 Ma) (Zhang et al., 2004). Along with coeval normal faulting and abundant volcanic rocks, back-arc extension was interpreted to relate to rollback of the northward-subducting Neo-Tethys during the Middle Cretaceous (ca. 120–95 Ma) (Zhang et al., 2004). Alternatively, this extension may relate to rollback of southward-subducting BNS lithosphere (Zhu et al., 2009a, b). All in all, a Cretaceous extension maybe occurred in response to a rollback of subducted oceanic slab.

Different from this back-arc theory, Kapp et al. (2005) proposed a foreland-basin mechanism to explain marine transgression. New geochemical data indicate that subduction of the BNS lithosphere continued until 96.1 ± 2.4 Ma (Li et al., 2014; Liu et al., 2012; Xu et al., 2014a) and a major magmatic event occurred in the middle Cretaceous (117–95 Ma) (Leloup et al., 2012). The Nima area on the South Qiangtang terrane records a transition from marine to non-marine sedimentation at 118–99 Ma (Kapp et al., 2007), which implicates that the South Qiangtang terrane underwent strong deformation and denudation in the Early to Middle Cretaceous (Kapp et al., 2007). This transformation from marine to non-marine deposits is coeval with shallow marine limestone deposited on the north Lhasa terrane (Kapp et al., 2005). Moreover, these marine sediments on northern Lhasa never extended into southern Qiangtang in central Tibet (Kapp et al., 2005). That let Kapp et al. (2003a) to explain the marine limestone as foreland basin deposits which formed when ophiolitic mélangé obducted southward onto the north margin of the Lhasa terrane in the Late Jurassic–Early Cretaceous (Kapp et al., 2003a).

1.2.4 Yarlung Zangbo suture zone

Yarlung–Zangbo suture zone (YZS) forms the boundary between the Indian continent and the Lhasa terrane in Tibet and represents remnants of Ceno-Tethys (Fig. 1).

The earliest oceanic sedimentary records is Late Permian seamount limestones within the western part of the YSZ in north of Burang (Xu et al., 2014c; Wang et al., 2010). The youngest cluster of detrital zircons ages from the Upper Triassic strata vary around 266–224 Ma (Li et al., 2010) which is consistent with an ocean that developed after the Triassic disaggregation of northern Gondwana (Bezard et al., 2011). The Lhasa terrane thus separated from India in the Late Permian.

Northward subduction of YZS beneath the Lhasa terrane is recorded by Late Cretaceous arc magmatic rocks in the Gangdese, south Lhasa terrane (Wen et al., 2008; Zhang et al., 2010a; Zhao et al., 2008; Zhu et al., 2011a). The subduction mélange was emplaced northward onto Gangdese Batholith at 95–80 Ma according to zircon U–Pb geochronological data mainly from central and eastern segments of the YZS (Li et al., 2010; Zhu et al., 2011a). Blueschist-facies metamorphism occurred during 132 to 80 Ma (e.g. Xu et al., 2014c). The HP rocks may have exhumed under oceanic basin hyper extension along the YZS (Maffione et al., 2015), which would be consistent with northern Lhasa also experiencing simultaneous extension.

1.3 Geological evolution within the Qiangtang Terrane

In this section, we will briefly introduce the geological background of the Qiangtang terrane. More detailed descriptions are found in Chapters 2–5. The Qiangtang Terrane is located in central Tibet (Fig. 1). It is bound by Songpan-Ganzi Flysch to the north and the Lhasa terrane to the south. Its central part is covered by subduction mélange and Late Triassic high-pressure rocks (e.g., Liu et al., 2011; Zhai et al., 2011b).

1.3.1 North Qiangtang terrane

The terms ‘North Qiangtang terrane’ (e.g., Bian et al., 2004; Jin, 2002) or ‘Eastern Qiangtang Block’ (Zhang et al., 2002) were proposed by Metcalfe (2002), based on the distribution of Early Permian warm Cathaysian affinity faunas and floras. Metcalfe (2002) regarded this block as a separate micro-terrane derived from South China–Indochina by back-arc spreading in the Carboniferous. The northern and southern flanks of the north Qiangtang block were involved in intensive arc magmatism during Permo-Triassic times, possibly related to the south-dipping subduction of the JSS (e.g., Kapp et al., 2003b), or alternatively N-dipping subduction of the LSS (Yang et al., 2011). The western boundary of this block is formed by the Altyn Tagh Fault (Fig. 1).

1.3.2 South Qiangtang terrane

The South Qiangtang terrane is bound to the north by the LSS and to the south by the BNS. Basement rocks are largely buried by an Ordovician to Jurassic cover sequence and obducted subduction mélangé (Wang and Wang, 2001; Zhao et al., 2014; Zhai et al., 2011b). Upper Carboniferous to Lower Permian glacial–marine deposits and cold-water faunas indicate it may still have been attached to Gondwana at that time (Li et al., 2007). These strata changed into Upper Permian warm-water Cathaysian faunas and floras which indicates that the South Qiangtang terrane had then separated from Gondwana and drifted to north, where it may have been connected to the Cimmerian continent by Late Permian times (Metcalf, 2011). Late Triassic limestone and Early Jurassic siliciclastics and carbonates unconformably overlie the older units (Zhao et al., 2015). Jurassic to Early Cretaceous marine sedimentary rocks were deformed and uplifted above sea level due to collision between Lhasa and Qiangtang terranes (Kapp et al., 2007). Deposition of non-marine that started at about 118 Ma (Li et al., 2014; Wu et al., 2014) is attributed to continued collision between the Lhasa and Qiangtang terranes and concomitantly shortening and uplift of the Qiangtang terranes.

1.3.3 Longmu Co-Shuanghu suture zone

The Longmu Co-Shuanghu suture zone (LSS) has been proposed as the main boundary between Eurasia and Gondwana (Li, 1987). It divides the Qiangtang terrane into a North and a South terrane (e.g., Li et al., 2009; Zhang et al., 2006c; Liu et al., 2011). The LSS is exposed around Gangmari, Gemuri, Jiaomuri, Mayigangri and Qiagelela areas (Zhai et al., 2011a). This suture is the geological relic of the Paleo-Tethys Ocean, which is the oldest Tethys oceanic crust relic currently recognized in the Qinghai-Tibet Plateau. The Paleozoic ophiolites within the LSS are composed mainly of Ordovician–Silurian ophiolite (e.g., Zhai et al., 2010), Permian ophiolite, Carboniferous–Permian oceanic island–ridge basalt, gabbro–diabase dykes, Devonian–Permian and Triassic radiolarian chert, and a Permian oceanic island–sea mountain accretionary complex (Zhai et al., 2006; Hu et al., 2014a). The oldest observed sedimentation ages indicate that the formation of the LSS can be traced back to at least the Middle Ordovician to Early Silurian.

This metamorphic belt possibly links eastward with the Ando (Zhang et al., 2010a), Jitang complex (Hu et al., 2014b) and Basu (Zhang et al., 2008b) metamorphic massifs, where (ultra) high-pressure rocks have been identified (Zhang and Tang, 2009). LSS may connect eastwards with the Changning–Menglian suture of SW China (Zhai et al., 2011a). The occurrence of Late Devonian and Permian pelagic radiolarian cherts in Changning–Menglian Suture in SW China supports this interpretation (Zhu et al., 2006b).

In the Qiangtang terrane, subduction related high-pressure rocks occur at Gangmari, Gemucuo, Hongjishan, Rongma and Duomuchaka as an EW striking belt (Li et al., 2006; Pullen et al., 2014; Zhai et al., 2001b). Blueschist exposed in Gangmari has glaucophane $^{40}\text{Ar}/^{39}\text{Ar}$ ages of 275.0 ± 0.9 Ma and 282.4 ± 0.8 Ma (Deng et al., 2001). Younger blueschists found in other locations have glaucophane and phengite $^{40}\text{Ar}/^{39}\text{Ar}$ ages that range from 236.8 ± 4.5 Ma to 217.2 ± 1.8 Ma (Li et al., 2006). The blueschist are of MORB- and OIB-type affinity. The base of the Upper Triassic sediments and volcanic sequence unconformably overlies all underlying strata, including blueschists, and marks the final closure of the LSS (Fu et al., 2010).

How the subduction related high-pressure (HP) rocks exhumation remains hotly debated. The “in situ exhumation model” proposed that the HP rocks exhumed in the northward subduction channel at the LSS, maybe related to break-off of subducted oceanic lithosphere (Li et al., 2009; Zhang et al., 2006c; Zhai et al., 2011a,b). However, the alternative “underthrust model” argued these HP rocks derived from >200 km southward subduction, underneath the Qiangtang terrane, at the Jinsha suture, and, exhumed due to extension of overlying crust that formed crustal-scale core complex (Kapp et al., 2000, 2003b).

1.4 Summary main points around and within Qiangtang terrane

1.4.1 Mainly geological evolution history around and within Qiangtang terrane

A very brief summary of the main events in and around the Qiangtang terrane is provided below.

- (1) Both the North Qiangtang terrane and Yidun arc are based on Cathayian basement. It remains unknown whether or not a crystalline basement is present underneath the Songpan-Ganzi Flysch belt because of the absence of any direct geological evidence. A Proterozoic crystalline basement must exist beneath the central Lhasa subterrane, the Amdo microcontinent and the south Qiangtang subterrane all of which experienced a Cambro-Ordovician magmatic event (530–490 Ma) and have Gondwana affinity. That indicates the main boundary of Eurasia and Gondwana is located in the centre of the Qiangtang terrane.
- (2) There are three branches of Paleo-Tethys Oceans in central Tibet, Kunlun-Anyenagen, Jinsa-Tethys (JSS) and Longmu Co-Shuanghu-Tethys (LSS). The earliest Paleo-Tethys realm evolution is recorded by Ordovician gabbro in the LSS. All these Paleo-Tethys branches vanished during the Late Triassic as the South Qiangtang terrane drifted to north and finally collided with Eurasia.
- (3) Amalgamation of the North and South Qiangtang terranes happened in the Late Triassic. Amalgamation mainly occurred by northward subduction of the Paleo Tethys underneath the North Qiangtang terrane, but minor southward subduction probably took place underneath the South

Qiangtang terrane. Exhumation and obduction of the (U)HP rocks is proposed to be related to closure of this divergent double subduction system.

- (4) Soon after closure of the Paleo-Tethys, the Lhasa Terrane rifted from the Qiangtang terrane. This extensional event is induced by intensive late Triassic to early Jurassic magmatism in the Paleo-Tethys realm which traversed from the South Qiangtang terrane to the Songpan-Ganzi belt. The Meso-Tethys opened due to this extensional event and finally formed the Bangong-Nujiang suture zones (BNS) in central Tibet.

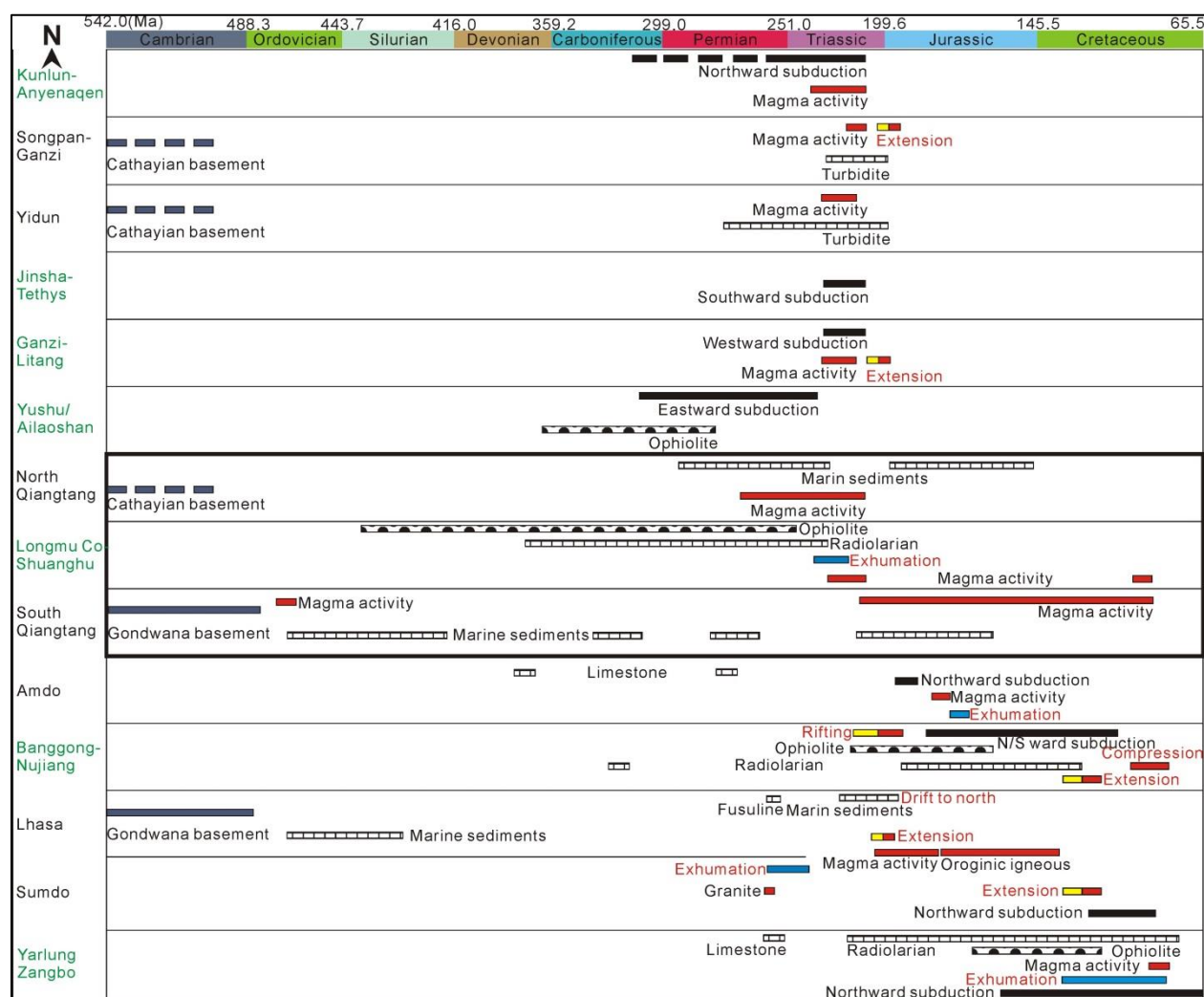


Fig. 2 Summary of tectonic, sedimentary and magmatic evolution of the Tibetan Plateau from Cambrian to Cretaceous times.

- (5) The BNS closed in a divergent double subduction setting, as indicated by arc magma on both the South Qiangtang and North Lhasa terranes. All observations and interpretations indicate that the northern Lhasa margin was under tectonic extension at Early Cretaceous times. This extension window around 140 Ma

was identified by Langshan formation and coeval intensive igneous activity. However, mainly compressional thrusts and uplifting occurred by the Lhasa-Qiangtang collision between 135 Ma and 90 Ma.

- (6) The Neo-Tethys (Yarlung-Zangbo) may have formed during the Triassic according to radiolarian records. It experienced long term evolution from Triassic until Cenozoic. Figure 2 is a summary sketch of these geological evolutions.

1.4.2 Main debates on the Qiangtang terranes

1. The presence or absence of basement in the Qiangtang terranes and its affinity has been debated for several decades (e.g. Dong et al., 2011). One problem is that large areas are covered by *mélange* and Paleo-Cenozoic sediments.
2. Questions are remaining on the subduction related high-pressure (HP) rocks found in the Qiangtang metamorphic belt (e.g. Liu et al., 2011). Currently, two contrasting models exist on the formation of the Qiangtang metamorphic belt. The first model suggests that the metamorphic rocks are part of the Songpan-Ganzi accretionary *mélange* that was underthrust during low-angle southward subduction of the Paleo-Tethyan oceanic lithosphere along the Jinsha suture (Kapp et al., 2000, 2003b; Yin and Harrison, 2000; Pullen et al., 2008, 2011). These high-P rocks were exhumed to shallow crustal levels as a result of rollback of the Songpan-Ganzi oceanic lithosphere along the Jinsha suture during the Late Triassic (Kapp et al., 2000, 2003b; Pullen et al., 2008, 2011). The second model suggests that the high-pressure metamorphic belt formed in situ along the LSS, which separates the Western Qiangtang with Gondwana affinity from the Eastern Qiangtang subterrane with Cathaysian affinity (e.g., Li, 1987; Li et al., 2009; Zhang et al., 2006d). In this model, the LSS formed from the northward subduction of the Longmu Co-Shuanghu Tethyan oceanic lithosphere (e.g., Li, 1987; Li et al., 2009; Zhai et al., 2011a), and the metamorphic rocks were exhumed in response to the slab breakoff of the subducted LSS lithosphere beneath the North Qiangtang subterrane (e.g., Zhang et al., 2011; Zhang et al., 2006d; Pullen and Kapp, 2014; Kapp et al., 2003b). However, the second model has so far not provided a satisfactory explanation for the HP rocks exhumation.
3. There appears to be relatively little deformation during Qiangtang and Lhasa collision because Mesozoic strata are only weakly deformed, a late Mesozoic mountain belt is missing (Schneider et al., 2003). This is in favor the underthrust model that proposed that the Lhasa terrane underthrust the south Qiangtang terrane during closure of BNS and thickened the Qiangtang terrane (Kapp et al., 2005). This implies that Qiangtang terrane was a rigid block after the North and South Qiangtang terranes reunited. Is that true or not? What is the evolution of Qiangtang

terrane during forming and closing of BNS to south? The pre-Cenozoic crustal structures must affect the Cenozoic Tibetan plateau formation.

1.5 Review of existing exhumation models

The controversy between in-situ and underthrust models for the Qiangtang terrane implicate different exhumation models for the (U)HP rocks that are found in the Qiangtang Metamorphic Belt (Kapp et al., 2000; Yin and Harrison, 2000; Zhang, 2001b; Kapp et al., 2003b; Zhang et al., 2006d). There is no simple and widely accepted mechanism for the burial of crustal rocks down to mantle depths and their exhumation to the surface (Philippon et al., 2011; Ring, 1999). Both field and laboratory work have been carried out to understand the mechanism of exhumation (Beaumont et al., 2009; Philippon et al., 2009; Platt et al., 2006). As this issue is importance for the interpretation of the Qiangtang Metamorphic Belt, hence the proposed (U)HP exhumation mechanisms are discussed here.

The common traits of exhumation are 1) exhumation characteristics change from earlier, faster, ductile to later, slower, brittle-ductile/brittle (Spencer et al., 2012; Warren et al., 2011; Philippon et al., 2009); 2) two stages of exhumation are suggested according to age distributions in Sulu-Dabie (Hacker et al., 2006) and detailed structural studies in the western Norway (Johnston et al., 2007) and the central Cyclades (Philippon et al., 2011). The general situation is that first fast exhumation stage controlled by buoyancy but the later slow exhumation dominated by erosion process; 3) the exhumation rate varies from 5 km/my to 80 km/my and is similar to the plate motion rate (e.g., Warren et al., 2008).

There are several proposed models to explain the (U)HP rocks exhumation, for examples channel flow, wedge extrusion and diapiric. In the channel flow model, the competition between Couette flow (caused by the drag of the subduction lithosphere) and Poiseuille flow (driven by the buoyancy of low-density subducted crustal material) control the exhumation process (Beaumont et al., 2009). The alternative wedge extrusion model suggest that the UHP slab rose coherently from mantle to crustal depths by buoyancy (Labrousse et al., 2004; Hacker et al., 2003; Young et al., 2007; Hacker, 2007). Diapiric flow envisages buoyant subducted material to be transported across the mantle wedge and eventually emplaced into the base of the overriding plate (Little et al., 2011). Other exhumation mechanisms include lithosphere-scale extension (resulting from plate divergence) (Malusà et al., 2011; Fossen, 2010), corner flow (Burov et al., 2001; Warren et al., 2011; Gerya and Stöckhert, 2002), and buoyancy-driven flexural rebound of unloaded continental lithosphere (Andersen et al., 1991), also termed ‘eduction’ (Duretz et al., 2012).

Chapter1

In the subduction channel (Cloos and Shreve, 1988), the strong buoyancy of serpentinites or hydrous continental rocks at the mantle depth was the most likely driving force for exhumation (Beltrando et al., 2010; Gerya and Stöckhert, 2002; Platt, 1993). Consequently, the thrust zone at the bottom and a detachment fault on the top of the channel assist the later exhumation (Rubatto and Hermann, 2001; Ganne et al., 2006; Bond et al., 2007; Johnston et al., 2007). Erosion (Baldwin et al., 2004) combined with forward normal faults allow material in the exhumation channel to move toward the surface as a wedge (Terry and Robinson, 2004).

Kapp et al. (2000) firstly proposed a dome-like core complex model to explain exhumation of blueschists in central Qiangtang. We not totally agree their model. Based on field evidences (Chapter 4) and numerical modeling (Chapter 6) we addressed a new exhumation mechanism for HP rocks in Qiangtang terrane.

1.6 Organization of the thesis

To address the questions that were listed above, an area around the town of Rongma in the centre of the Qiangtang terrane, and which includes *mélange*, was mapped. Based on that mapping, satellite image interpretation, 3D reconstructions and (thermo-) geochronology, the presence of basement in the South Qiangtang was confirmed (*Chapter2 and 3*), the structural relationships of different units in the area was determined (*Chapter2,3 and 4*), evidence for closure of an ocean between the North and South Qiangtang terranes was provided (*Chapter 4*), A mechanism for the exhumation and emplacement of the high-pressure rocks was proposed (*Chapter 4 and 6*), and the effect of opening and closure of the BNS on the South Qiangtang terrane was investigated (*Chapter5*).

The following five chapters are published papers (Chapters 2-4) and manuscripts in preparation for submission to peer-reviewed journals:

Chapter 2: Zhao, Z., Bons, P. D., Wang, G., Liu, Y., and Zheng, Y.: Origin and pre-Cenozoic evolution of the south Qiangtang basement, Central Tibet, *Tectonophysics*, 623, 52-66, <http://dx.doi.org/10.1016/j.tecto.2014.03.016>, 2014.

Chapter 3: Yang, Y., Zhao, Z. B., Yuan, T. Y., Liu, Y., and Li, C. Y.: Ordovician parallel unconformity in Qiangtang terrane, northern Tibet: Implications to Early Paleozoic evolution of northern Tibetan region. *Acta Petrologica Sinica*, 30, 2381-2392, 2014.

Chapter 3 was originally published in Chinese with an English abstract. Appendix A provides the original text in Chinese.

Chapter1

Chapter 4: Zhao, Z., Bons, P., Wang, G., Soesoo, A., and Liu, Y.: Tectonic evolution and high-pressure rock exhumation in the Qiangtang Terrane, Central Tibet, *Solid Earth*, 6, 457-473, 2015.

Chapter 5 Z. Zhao., P. D. Bons., K. Stübner., T. A. Ehlers and G. Wang.: Early Cretaceous exhumation of the Qiangtang Culmination and collision of the Qiangtang and Lhasa terranes, central Tibet (In preparation)

This chapter reports thermogeochronological work on the Rongma study area, carried out in Tübingen in collaboration with Stübner. It will form the base for a manuscript with the same title and as preliminary list of authors: Z. Zhao, P.D. Bons, K. Stübner, T.A. Ehlers and G. Wang. This chapter will be significantly shortened to meet the requirements for submission to the journal *Terra Nova*.

Chapter 6: Paul D. Bons., Evgene Burov., Enrique Gomez-Rivas., Alavar Soesoo., Douwe D.J. van Hinsbergen., Kun Wang., **Zhongbao Zhao** (preliminary list of authors in alphabetical order): Subduction reversal: an efficient mechanism for the exhumation of Ultra-high-pressure rocks. (In preparation)

This chapter is a preliminary draft for a manuscript to be submitted to the journal *Nature (Geoscience)* or *Geology*.

Appendix B contains the thermochronological data used in Chapter 5.

Appendix C includes the numerical modeling parameters for Chapter 6.

References

- Andersen, T. B., Jamtveit, B., Dewey, J. F., and Swensson, E.: Subduction and eduction of continental crust: major mechanisms during continent-continent collision and orogenic extensional collapse, a model based on the south Norwegian Caledonides, *Terra Nova*, 3, 303-310, 1991.
- Angiolini, L., Zanchi, A., Zanchetta, S., Nicora, A., and Vezzoli, G.: The Cimmerian geopuzzle: new data from South Pamir, *Terra Nova*, 25,352-360, 2013.
- Baldwin, S. L., Monteleone, B. D., Webb, L. E., Fitzgerald, P. G., Grove, M., and Hill, E. J.: Pliocene eclogite exhumation at plate tectonic rates in eastern Papua New Guinea, *Nature*, 431, 263-267, 2004.
- Baxter, A. T., Aitchison, J. C., and Zyabrev, S. V.: Radiolarian age constraints on Mesotethyan ocean evolution, and their implications for development of the Bangong–Nujiang suture, Tibet, *Journal of the Geological Society*, 166, 689-694, 2009.
- Beaumont, C., Jamieson, R., Butler, J., and Warren, C.: Crustal structure: A key constraint on the mechanism of ultra-high-pressure rock exhumation, *Earth and Planetary Science Letters*, 287, 116-129, 2009.
- Beltrando, M., Rubatto, D., and Manatschal, G.: From passive margins to orogens: The link between ocean-continent transition zones and (ultra) high-pressure metamorphism, *Geology*, 38, 559-562, 2010.
- Bezard, R., Hébert, R., Wang, C., Dostal, J., Dai, J., and Zhong, H.: Petrology and geochemistry of the Xiugugabu ophiolitic massif, western Yarlung Zangbo suture zone, Tibet, *Lithos*, 125, 347-367, 2011.

Chapter1

- Bian, Q. T., Li, D. H., Pospelov, I., Yin, L. M., Li, H. S., Zhao, D. S., Chang, C. F., Luo, X. Q., Gao, S. L., and Astrakhsantsev, O.: Age, geochemistry and tectonic setting of Buqingshan ophiolites, north Qinghai-Tibet Plateau, China, *Journal of Asian Earth Sciences*, 23, 577-596, 2004.
- Bond, C. E., Butler, R. W. H., and Dixon, J. E.: Co-axial horizontal stretching within extending orogens: the exhumation of HP rocks on Syros (Cyclades) revisited, *Geological Society, London, Special Publications*, 272, 203-222, 2007.
- Burov, E., Jolivet, L., Le Pourhiet, L., and Poliakov, A.: A thermomechanical model of exhumation of high pressure (HP) and ultra-high pressure (UHP) metamorphic rocks in Alpine-type collision belts, *Tectonophysics*, 342, 113-136, 2001.
- Sengor, A., and Natalin, B.: *Paleotectonics of Asia: fragments of a synthesis*, 1996.
- Şengör, A. C. I.: Plate tectonics and orogenic research after 25 years: a Tethyan perspective, *Earth-Science Reviews*, 27, 1-201, 1990.
- Chen, S. F., and Wilson, C. J.: Emplacement of the Longmen Shan Thrust—Nappe Belt along the eastern margin of the Tibetan Plateau, *Journal of Structural Geology*, 18, 413-430, 1996.
- Chen, Y., Zhang, K., Yang, Z., and Luo, T.: Discovery of a complete ophiolite section in the Juweng area, Nagqu County, in the central segment of the Bangong Co-Nujiang junction zone, Qinghai-Tibet Plateau, *Geological Bulletin of China*, 25, 694-699, 2006.
- Cloos, M., and Shreve, R. L.: Subduction-channel model of prism accretion, melange formation, sediment subduction, and subduction erosion at convergent plate margins: 1. Background and description, *Pure and Applied Geophysics*, 128, 455-500, 1988.
- DeCelles, P., Kapp, P., Ding, L., and Gehrels, G.: Late Cretaceous to middle Tertiary basin evolution in the central Tibetan Plateau: Changing environments in response to tectonic partitioning, aridification, and regional elevation gain, *Geological Society of America Bulletin*, 119, 654-680, 2007.
- Deng, X., Ding, L., Liu, X., and Zhou, Y.: Petrology and $40\text{ Ar}/^{39}\text{ Ar}$ isotopic ages of blueschists in Gangmar, central Qiangtang, northern Tibet, *Chinese Science Bulletin*, 46, 423-427, 2001.
- Dewey, J. F., Shackleton, R. M., Chengfa, C., and Yiyin, S.: The tectonic evolution of the Tibetan Plateau, *Philosophical Transactions of the Royal Society of London. Series A, Mathematical and Physical Sciences*, 327, 379-413, 1988.
- Dong, C. Y., Li, C., Wan, Y. S., Wang, W., Wu, Y. W., Xie, H. Q., and Liu, D. Y.: Detrital zircon age model of Ordovician Wenquan quartzite south of Lungmuco-Shuanghu Suture in the Qiangtang area, Tibet: Constraint on tectonic affinity and source regions, *SCIENCE CHINA Earth Sciences*, 54, 1034-1042, 2011.
- Ding, L., and Lai, Q.: New geological evidence of crustal thickening in the Gangdese block prior to the Indo-Asian collision, *Chinese Science Bulletin*, 48, 1604-1610, 2003.
- Ding, L., Yang, D., Cai, F., Pullen, A., Kapp, P., Gehrels, G., Zhang, L., Zhang, Q., Lai, Q., and Yue, Y.: Provenance analysis of the Mesozoic Hoh-Xil-Songpan-Ganzi turbidites in northern Tibet: Implications for the tectonic evolution of the eastern Paleo-Tethys Ocean, *Tectonics*, 32, 34-48, 2013.

Chapter1

- Duretz, T., Gerya, T., Kaus, B., and Andersen, T.: Thermomechanical modeling of slab eduction, *Journal of Geophysical Research: Solid Earth* (1978–2012), 117, 2012.
- England, P., and Searle, M.: The Cretaceous-tertiary deformation of the Lhasa Block and its implications for crustal thickening in Tibet, *Tectonics*, 5, 1-14, 1986.
- Fossen, H.: Extensional tectonics in the North Atlantic Caledonides: a regional view, Geological Society, London, Special Publications, 335, 767-793, 2010.
- Fu, X., Wang, J., Wu, T., and He, J.: Stratigraphy and paleoenvironment of the Quemo Co Formation in Shengli River area, northern Tibet, *Geology in China*, 37, 1305-1312, 2010.
- Ganne, J., Marquer, D., Rosenbaum, G., Bertrand, J. M., and Fudral, S.: Partitioning of deformation within a subduction channel during exhumation of high-pressure rocks: a case study from the Western Alps, *Journal of Structural Geology*, 28, 1193-1207, 2006.
- Gerya, T., and Stöckhert, B.: Exhumation rates of high pressure metamorphic rocks in subduction channels: the effect of rheology, *Geophysical research letters*, 29, 102-111, 2002.
- Guynn, J. H., Kapp, P., Pullen, A., Heizler, M., Gehrels, G., and Ding, L.: Tibetan basement rocks near Amdo reveal “missing” Mesozoic tectonism along the Bangong suture, central Tibet, *Geology*, 34, 505-508, 10.1130/g22453.1, 2006.
- Hacker, B., Andersen, T., Root, D., Mehl, L., Mattinson, J., and Wooden, J.: Exhumation of high-pressure rocks beneath the Solund Basin, western gneiss region of Norway, *Journal of Metamorphic Geology*, 21, 613-629, 2003.
- Hacker, B.: Ascent of the ultrahigh-pressure western gneiss region, Norway, *SPECIAL PAPERS-GEOLOGICAL SOCIETY OF AMERICA*, 419, 171-184, 2007.
- Hacker, B. R., Wallis, S. R., Ratschbacher, L., Grove, M., and Gehrels, G.: High-temperature geochronology constraints on the tectonic history and architecture of the ultrahigh-pressure Dabie-Sulu Orogen, *Tectonics*, 25, TC5006, 2006.
- Hu, J., Li, Q., Fang, N., Yang, J., and Ge, D.: Geochemistry characteristics of the Low Permian sedimentary rocks from central uplift zone, Qiangtang Basin, Tibet: insights into source-area weathering, provenance, recycling, and tectonic setting, *Arab J Geosci*, 1-16, 10.1007/s12517-014-1583-8, 2014a.
- Hu, R. Z., Burnard, P., Bi, X. W., Zhou, M. F., Pen, J. T., Su, W. C., and Wu, K. X.: Helium and argon isotope geochemistry of alkaline intrusion-associated gold and copper deposits along the Red River–Jinshajiang fault belt, SW China, *Chemical geology*, 203, 305-317, 2004.
- Hu, P., Li, C., Li, J., Wang, M., Xie, C., and Wu, Y.: Zircon U–Pb–Hf isotopes and whole-rock geochemistry of gneissic granites from the Jitang complex in Leiwuqi area, eastern Tibet, China: Record of the closure of the Paleo-Tethys Ocean, *Tectonophysics*, 623, 83-99, 2014b.
- Ji, W. Q., Wu, F. Y., Chung, S. L., Li, J. X., and Liu, C. Z.: Zircon U–Pb geochronology and Hf isotopic constraints on petrogenesis of the Gangdese batholith, southern Tibet, *Chemical Geology*, 262, 229-245, 2009.
- Jian, P., Wang, X., He, L., and Wang, C.: U–Pb zircon dating of the Shuanggou ophiolite from Xingping County, Yunnan Province, *Acta Petrologica Sinica*, 14, 207-211, 1998.

Chapter1

- Jian, P., Liu, D., Kröner, A., Zhang, Q., Wang, Y., Sun, X., and Zhang, W.: Devonian to Permian plate tectonic cycle of the Paleo-Tethys Orogen in southwest China (II): insights from zircon ages of ophiolites, arc/back-arc assemblages and within-plate igneous rocks and generation of the Emeishan CFB province, *Lithos*, 113, 767-784, 2009.
- Johnston, S. M., Hacker, B. R., and Andersen, T. B.: Exhuming Norwegian ultrahigh-pressure rocks: Overprinting extensional structures and the role of the Nordfjord–Sogn Detachment Zone, *Tectonics*, 26, TC5001, 2007.
- Kapp, P., Yin, A., Manning, C. E., Murphy, M., Harrison, T. M., Spurlin, M., Lin, D., Xi-Guang, D., and Cun-Ming, W.: Blueschist-bearing metamorphic core complexes in the Qiangtang block reveal deep crustal structure of northern Tibet, *Geology*, 28, 19-23, 2000.
- Kapp, P., Murphy, M. A., Yin, A., Harrison, T. M., Ding, L., and Guo, J.: Mesozoic and Cenozoic tectonic evolution of the Shiquanhe area of western Tibet, *Tectonics*, 22, TC1029, 2003a.
- Kapp, P., Yin, A., Manning, C. E., Harrison, T. M., Taylor, M. H., and Ding, L.: Tectonic evolution of the early Mesozoic blueschist-bearing Qiangtang metamorphic belt, central Tibet, *Tectonics*, 22, 1043-1068, 2003b.
- Kapp, P., Yin, A., Harrison, T. M., and Ding, L.: Cretaceous-Tertiary shortening, basin development, and volcanism in central Tibet, *Bulletin of the Geological Society of America*, 117, 865-878, 2005.
- Kapp, P., DeCelles, P. G., Gehrels, G. E., Heizler, M., and Ding, L.: Geological records of the Lhasa-Qiangtang and Indo-Asian collisions in the Nima area of central Tibet, *Geological Society of America Bulletin*, 119, 917-933, 2007.
- Labrousse, L., Jolivet, L., Andersen, T., Agard, P., Hébert, R., Maluski, H., and Scharer, U.: Pressure-temperature-time deformation history of the exhumation of ultra-high pressure rocks in the Western Gneiss Region, Norway, *SPECIAL PAPERS-GEOLOGICAL SOCIETY OF AMERICA*, 155-184, 2004.
- Leier, A. L., DeCelles, P. G., Kapp, P., and Ding, L.: The Takena Formation of the Lhasa terrane, southern Tibet: The record of a Late Cretaceous retroarc foreland basin, *Geological Society of America Bulletin*, 119, 31-48, 2007.
- Leloup, P. H., Arnaud, N. O., Mahéo, G., Paquette, J. L., Guillot, S., Valli, F., Li, H., Xu, Z., Lacassin, R., and Tapponnier, P.: Successive deformation episodes along the Lungmu Co zone, west-central Tibet, *Gondwana Research*, 21, 37-52, 10.1016/j.gr.2011.07.026, 2012.
- Li, C.: The Longmu Co-Shuanghu-Lancangjiang Suture as the northern boundary of the Gondwanaland in the Carboniferous and Permian, *Bull. Changcun Coll. Geol. Sci*, 17, 155-166, 1987.
- Li, G. W., Liu, X. H., Pullen, A., Wei, L. J., Liu, X. B., Huang, F. X., and Zhou, X. J.: In-situ detrital zircon geochronology and Hf isotopic analyses from Upper Triassic Tethys sequence strata, *Earth and Planetary Science Letters*, 297, 461-470, 2010.
- Li, C., Zhai, Q., Chen, W., Yu, J., Huang, X., and Zhang, Y.: Ar-Ar chronometry of the Eclogite from central Qiangtang area, Qinghai-Tibet Plateau., *Acta Petrologica Sinica*, 22, 2843-2849, 2006.
- Li, C., Zhai, Q., Dong, Y., Zeng, Q., and Huang, X.: Longmu Co-Shuanghu plate suture and evolution records of paleo-Tethyan oceanic in Qiangtang area, Qinghai-Tibet plateau, *Frontiers of Earth Science in China*, 1, 257-264, 2007.

Chapter1

- Li, C., Zhai, Q., Dong, Y., Liu, S., Xie, C., and Wu, Y.: High-pressure eclogite-blueschist metamorphic belt and closure of paleo-Tethys Ocean in Central Qiangtang, Qinghai-Tibet plateau, *Journal of Earth Science*, 20, 209-218, 2009.
- Li, Y., He, J., Wang, C., Han, Z., Ma, P., Xu, M., and Du, K.: Cretaceous volcanic rocks in south Qiangtang Terrane: Products of northward subduction of the Bangong–Nujiang Ocean?, *Journal of Asian Earth Sciences*, 2014 (in press).
- Little, T., Hacker, B., Gordon, S., Baldwin, S., Fitzgerald, P., Ellis, S., and Korchinski, M.: Diapiric exhumation of Earth's youngest (UHP) eclogites in the gneiss domes of the D'Entrecasteaux Islands, Papua New Guinea, *Tectonophysics*, 510, 39-68, 2011.
- Liu, S., Hu, R., Gao, S., Feng, C., Coulson, I. M., Feng, G., Qi, Y., Yang, Y., Yang, C., and Tang, L.: U–Pb zircon age, geochemical and Sr–Nd isotopic data as constraints on the petrogenesis and emplacement time of andesites from Gerze, southern Qiangtang Block, northern Tibet, *Journal of Asian Earth Sciences*, 45, 150-161, 10.1016/j.jseas.2011.09.025, 2012.
- Liu, Y., Liu, H., Theye, T., and Massonne, H. J.: Evidence for oceanic subduction at the NE Gondwana margin during Permo-Triassic times, *Terra Nova*, 21, 195-202, 2009.
- Liu, Y., Santosh, M., Zhao, Z. B., Niu, W. C., and Wang, G. H.: Evidence for palaeo-Tethyan oceanic subduction within central Qiangtang, northern Tibet, *Lithos*, 127, 39-53, 2011.
- Maffione, M., van Hinsbergen, D. J., Koornneef, L. M., Guilmette, C., Hodges, K., Borneman, N., Huang, W., Ding, L., and Kapp, P.: Forearc hyperextension dismembered the south Tibetan ophiolites, *Geology*, 2015 (In press).
- Malusà, M. G., Faccenna, C., Garzanti, E., and Polino, R.: Divergence in subduction zones and exhumation of high pressure rocks (Eocene Western Alps), *Earth and Planetary Science Letters*, 310, 21-32, 2011.
- Metcalf, I.: Permian tectonic framework and palaeogeography of SE Asia, *Journal of Asian Earth Sciences*, 20, 551-566, 2002.
- Metcalf, I.: Palaeozoic–Mesozoic history of SE Asia, Geological Society, London, Special Publications, 355, 7-35, 2011.
- Metcalf, I.: Gondwana dispersion and Asian accretion: Tectonic and palaeogeographic evolution of eastern Tethys, *Journal of Asian Earth Sciences*, 66, 1-33, 2013.
- Miller, C., Schuster, R., Klotzli, U., Frank, W., and Grasemann, B.: Late Cretaceous-Tertiary magmatic and tectonic events in the Transhimalaya batholith (Kailas area, SW Tibet), *Schweizerische Mineralogische und Petrographische Mitteilungen*, 80, 1-20, 2000.
- Murphy, M., Yin, A., Harrison, T., and Durr, S.: Did the Indo-Asian collision alone create the Tibetan plateau?, *Geology*, 25, 719-722, 1997.
- Nie, S., Yin, A., Rowley, D. B., and Jin, Y.: Exhumation of the Dabie Shan ultra-high-pressure rocks and accumulation of the Songpan-Ganzi flysch sequence, central China, *Geology*, 22, 999-1002, 1994.
- Najman, Y., Appel, E., Boudagher-Fadel, M., Bown, P., Carter, A., Garzanti, E., Godin, L., Han, J., Liebke, U., and Oliver, G.: Timing of India-Asia collision: Geological, biostratigraphic, and palaeomagnetic constraints, *Journal of Geophysical Research: Solid Earth* (1978–2012), 115, 2010.

Chapter1

- Nimaciren, X., and Qiangbazaxi, P.: Luosongzhandui, 2005. 1: 250, 000 geological report of Nagqu County with geological map, Xizang Institute of Geological Survey, Lhasa, 103-107,
- Pan, G., Mo, X., Hou, Z., Zhu, D., Wang, L., Li, G., Zhao, Z., Geng, Q., and Liao, Z.: Spatial-temporal framework of the Gangdese Orogenic Belt and its evolution, *Acta Petrologica Sinica*, 22, 521-533, 2006a.
- Pan, G., Wang, L., Li, R., Yuan, S., Ji, W., Yin, F., Zhang, W., and Wang, B.: Tectonic evolution of the Qinghai-Tibet plateau, *Journal of Asian Earth Sciences*, 53, 3-14, 2012.
- Pan, G. T., Mo, X., Hou, Z., Zhu, D., Wang, L., Li, G., Zhao, Z., Geng, Q., and Liao, Z.: Spatial-temporal framework of the Gangdese Orogenic Belt and its evolution, *Acta Petrologica Sinica*, 22, 521-533, 2006b.
- Philippon, M., Brun, J. P., and Gueydan, F.: Kinematic records of subduction and exhumation in the Ile de Groix blueschists (Hercynian belt; Western France), *Journal of Structural Geology*, 31, 1308-1321, 2009.
- Philippon, M., Brun, J. P., and Gueydan, F.: Tectonics of the Syros blueschists (Cyclades, Greece): From subduction to Aegean extension, *Tectonics*, 30, 4001-4016, 2011.
- Platt, J. P.: Exhumation of high-pressure rocks: a review of concepts and processes, *Terra Nova*, 5, 119-133, 1993.
- Platt, J. P., Anczkiewicz, R., Soto, J. I., Kelley, S. P., and Thirlwall, M.: Early Miocene continental subduction and rapid exhumation in the western Mediterranean, *Geology*, 34, 981-985, 2006.
- Pullen, A., Kapp, P., Gehrels, G. E., Vervoort, J. D., and Ding, L.: Triassic continental subduction in central Tibet and Mediterranean-style closure of the Paleo-Tethys Ocean, *Geology*, 36, 351-354, 10.1130/g24435a.1, 2008.
- Pullen, A., Kapp, P., Gehrels, G. E., Ding, L., and Zhang, Q.: Metamorphic rocks in central Tibet: Lateral variations and implications for crustal structure, *Bulletin of the Geological Society of America*, 123, 585-600, 2011.
- Pullen, A., and Kapp, P.: Mesozoic tectonic history and lithospheric structure of the Qiangtang terrane: Insights from the Qiangtang metamorphic belt, central Tibet, *Geological Society of America Special Papers*, 507, 507-504, 2014.
- Reid, A., Wilson, C. J. L., Shun, L., Pearson, N., and Belousova, E.: Mesozoic plutons of the Yidun Arc, SW China: U/Pb geochronology and Hf isotopic signature, *Ore Geology Reviews*, 31, 88-106, 2007.
- Reid, A. J., Wilson, C. J., and Liu, S.: Structural evidence for the Permo-Triassic tectonic evolution of the Yidun Arc, eastern Tibetan Plateau, *Journal of Structural Geology*, 27, 119-137, 2005a.
- Reid, A. J., Wilson, C. J., Phillips, D., and Liu, S.: Mesozoic cooling across the Yidun Arc, central-eastern Tibetan Plateau: A reconnaissance 40 Ar/39 Ar study, *Tectonophysics*, 398, 45-66, 2005b.
- Ring, U.: Exhumation processes: normal faulting, ductile flow and erosion, Geological Society Pub House, 1999.
- Roger, F., Arnaud, N., Gilder, S., Tapponnier, P., Jolivet, M., Brunel, M., Malavieille, J., Xu, Z., and Yang, J.: Geochronological and geochemical constraints on Mesozoic suturing in east central Tibet, *Tectonics*, 22, 1037, 2003.
- Roger, F., Jolivet, M., and Malavieille, J.: Tectonic evolution of the Triassic fold belts of Tibet, *Comptes Rendus Geoscience*, 340, 180-189, 2008.
- Roger, F., Jolivet, M., and Malavieille, J.: The tectonic evolution of the Songpan-Garzê (North Tibet) and adjacent areas from Proterozoic to Present: A synthesis, *Journal of Asian Earth Sciences*, 39, 254-269, 10.1016/j.jseaes.2010.03.008, 2010.

Chapter1

- Rubatto, D., and Hermann, J.: Exhumation as fast as subduction?, *Geology*, 29, 3-6, 2001.
- Schneider, W., Mattern, F., Wang, P. J., and Li, C.: Tectonic and sedimentary basin evolution of the eastern Bangong-Nujiang zone (Tibet): A Reading cycle, *International Journal of Earth Sciences*, 92, 228-254, 2003.
- She, H., Li, J., Ma, D., Li, G., Zhang, D., Feng, C., Qu, W., and Pan, G.: Molybdenite Re-Os and SHRIMP zircon U-Pb dating of Duobuza porphyry copper deposit in Tibet and its geological implications, *Mineral Deposits*, 28, 737-746, 2009.
- Shi, R., Yang, J., Xu, Z., and Qi, X.: Recognition of MOR-and SSZ-type ophiolites in the Bangong Lake ophiolite mélangé, western Tibet: evidence from two kinds of mantle peridotites, *Acta Petrologica et Mineralogica*, 24, 397-408, 2005.
- Shi, R.: SHRIMP dating of the Bangong Lake SSZ-type ophiolite: Constraints on the closure time of ocean in the Bangong Lake-Nujiang River, northwestern Tibet, *Chinese Science Bulletin*, 52, 936-941, 2007.
- Shi, R., Yang, J., Xu, Z., and Qi, X.: The Bangong Lake ophiolite (NW Tibet) and its bearing on the tectonic evolution of the Bangong–Nujiang suture zone, *Journal of Asian Earth Sciences*, 32, 438-457, 2008.
- Spencer, C. J., Harris, R. A., and Dorais, M. J.: The metamorphism and exhumation of the Himalayan metamorphic core, eastern Garhwal region, India, *Tectonics*, 31, TC1007, 10.1029/2010tc002853, 2012.
- Sun, Z., Jiang, W., Li, H., Pei, J., and Zhu, Z.: New paleomagnetic results of Paleocene volcanic rocks from the Lhasa block: tectonic implications for the collision of India and Asia, *Tectonophysics*, 490, 257-266, 2010.
- Terry, M. P., and Robinson, P.: Geometry of eclogite-facies structural features: Implications for production and exhumation of ultrahigh-pressure and high-pressure rocks, Western Gneiss Region, Norway, *Tectonics*, 23, TC2001, 2004.
- Volkmer, J. E., Kapp, P., Guynn, J. H., and Lai, Q.: Cretaceous-Tertiary structural evolution of the north central Lhasa terrane, Tibet, *Tectonics*, 26, TC6007, 2007.
- Wang, G., Wang, C.: Disintegration and age of basement metamorphic rocks in Qiangtang, Tibet, China. *Sci. China. Ser. D Earth Sci.* 44, 86–93, 2001.
- Wang, B. Q., Wang, W., Chen, W. T., Gao, J.-F., Zhao, X. F., Yan, D.-P., and Zhou, M. F.: Constraints of detrital zircon U-Pb ages and Hf isotopes on the provenance of the Triassic Yidun Group and tectonic evolution of the Yidun Terrane, Eastern Tibet, *Sedimentary Geology*, 289, 74-98, 2013.
- Wang, C. Y., Han, W. B., Wu, J. P., Lou, H., and Chan, W. W.: Crustal structure beneath the eastern margin of the Tibetan Plateau and its tectonic implications, *Journal of Geophysical Research: Solid Earth*, 112, 1978–2012, 2007.
- Wang, J., Liu, Y., Li, Q., Yue, G., and Pei, F.: Stratigraphic division and geological significance of the Jurassic cover sediments in the eastern sector of the Bangong Lake-Dengqen ophiolite belt in Tibet, *Geological Bulletin of China*, 21, 405-410, 2002.
- Wang, W. L., Aitchison, J., Lo, C. H., and Zeng, Q. G.: Geochemistry and geochronology of the amphibolite blocks in ophiolitic mélanges along Bangong-Nujiang suture, central Tibet, *Journal of Asian Earth Sciences*, 33, 122-138, 2008.

Chapter1

- Wang, Y., Zheng, Y., and Jin, Z.: Microstructures and Rheology of Harzburgite from Dongqiao, Northern Tibet, *Earth Science-Journal of China University of Geosciences*, 30, 52-60, 2005.
- Wang, Y., Ueno, K., Zhang, Y. c., and Cao, C. q.: The Changhsingian foraminiferal fauna of a Neotethyan seamount: the Gyanyima Limestone along the Yarlung-Zangbo Suture in southern Tibet, China, *Geological Journal*, 45, 308-318, 2010.
- Warren, C., Grujic, D., Kellett, D., Cottle, J., Jamieson, R., and Ghalley, K.: Probing the depths of the India-Asia collision: U-Th-Pb monazite chronology of granulites from NW Bhutan, *Tectonics*, 30, 1-24, 2011.
- Warren, C. J., Beaumont, C., and Jamieson, R. A.: Deep subduction and rapid exhumation: Role of crustal strength and strain weakening in continental subduction and ultrahigh-pressure rock exhumation, *Tectonics*, 27, 1-28, 2008.
- Weislogel, A. L.: Tectonostratigraphic and geochronologic constraints on evolution of the northeast Paleotethys from the Songpan-Ganzi complex, central China, *Tectonophysics*, 451, 331-345, 2008.
- Weislogel, A. L., Graham, S. A., Chang, E. Z., Wooden, J. L., and Gehrels, G. E.: Detrital zircon provenance from three turbidite depocenters of the Middle–Upper Triassic Songpan-Ganzi complex, central China: Record of collisional tectonics, erosional exhumation, and sediment production, *Geological Society of America Bulletin*, 122, 2041-2062, 10.1130/b26606.1, 2010.
- Weller, O., St-Onge, M., Searle, M., Waters, D., Rayner, N., Chen, S., Chung, S. L., and Palin, R.: Quantifying the P–T–t conditions of north–south Lhasa terrane accretion: new insight into the pre-Himalayan architecture of the Tibetan plateau, *Journal of Metamorphic Geology*, 33, 91-113, 2015.
- Wen, D. R., Liu, D., Chung, S. L., Chu, M. F., Ji, J., Zhang, Q., Song, B., Lee, T. Y., Yeh, M. W., and Lo, C. H.: Zircon SHRIMP U–Pb ages of the Gangdese Batholith and implications for Neotethyan subduction in southern Tibet, *Chemical Geology*, 252, 191-201, 2008.
- Jin, X. C.: Permo-Carboniferous sequences of Gondwana affinity in southwest China and their paleogeographic implications, *Journal of Asian Earth Sciences*, 20, 633-646, 2002.
- Wu, Z., Wu, X., Zhao, Z., Lu, L., Ye, P., and Zhang, Y.: SHRIMP U-Pb Isotopic Dating of the Late Cretaceous Volcanic Rocks and Its Chronological Constraint on the Red-beds in Southern Qiangtang Block, 35, 562-572, 2014.
- Xu, M., Li, C., Xu, W., Xie, C., Hu, P., and Wang, M.: Petrology, geochemistry and geochronology of gabbros from the Zhongcang ophiolitic mélangé, central Tibet: Implications for an intra-oceanic subduction zone within the Neo-Tethys Ocean, *Journal of Earth Science*, 25, 224-240, 2014a.
- Xu, M., Li, C., Zhang, X., and Wu, Y.: Nature and evolution of the Neo-Tethys in central Tibet: synthesis of ophiolitic petrology, geochemistry, and geochronology, *International Geology Review*, 1-25, 2014b.
- Xu, Z. Q., Dilek, Y., Yang, J.S., Liang, F. H., Liu, F., Ba, D. Z., Cai, Z. H., Li, G. W., Dong, H. W., and Ji, S. C.: Crustal structure of the Indus–Tsangpo suture zone and its ophiolites in southern Tibet, *Gondwana Research*, 27, 507-524, 2014c.
- Yang, J., Xu, Z., Li, Z., Xu, X., Li, T., Ren, Y., Li, H., Chen, S., and Robinson, P. T.: Discovery of an eclogite belt in the Lhasa block, Tibet: A new border for Paleo-Tethys?, *Journal of Asian Earth Sciences*, 34, 76-89, 2009.

Chapter1

- Yang, T. N., Hou, Z. Q., Wang, Y., Zhang, H. R., and Wang, Z. L.: Late Paleozoic to Early Mesozoic tectonic evolution of northeast Tibet: Evidence from the Triassic composite western Jinsha-Garzê-Litang suture, *Tectonics*, 31, TC4004, 2012.
- Yang, T. N., Zhang, H. R., Liu, Y. X., Wang, Z. L., Song, Y. C., Yang, Z. S., Tian, S. H., Xie, H. Q., and Hou, K. J.: Permo-Triassic arc magmatism in central Tibet: Evidence from zircon U–Pb geochronology, Hf isotopes, rare earth elements, and bulk geochemistry, *Chemical Geology*, 284, 270-282, 10.1016/j.chemgeo.2011.03.006, 2011.
- Yin, A., and Harrison, T. M.: Geologic evolution of the Himalayan-Tibetan orogen, *Annual Review of Earth and Planetary Sciences*, 28, 211-280, 2000.
- Yin, J., and Grant-Mackie, J.: Late Triassic-Jurassic bivalves from volcanic sediments of the Lhasa block, Tibet, *New Zealand Journal of Geology and Geophysics*, 48, 555-577, 2005.
- Young, D. J., Hacker, B. R., Andersen, T. B., and Corfu, F.: Prograde amphibolite facies to ultrahigh-pressure transition along Nordfjord, western Norway: Implications for exhumation tectonics, *Tectonics*, 26, TC1007, 2007.
- Yuan, C., Zhou, M. F., Sun, M., Zhao, Y., Wilde, S., Long, X., and Yan, D.: Triassic granitoids in the eastern Songpan Ganzi Fold Belt, SW China: Magmatic response to geodynamics of the deep lithosphere, *Earth and Planetary Science Letters*, 290, 481-492, 2010.
- Yumul Jr, G. P., Zhou, M. F., Wang, C. Y., Zhao, T. P., and Dimalanta, C. B.: Geology and geochemistry of the Shuanggou ophiolite (Ailao Shan ophiolitic belt), Yunnan Province, SW China: Evidence for a slow-spreading oceanic basin origin, *Journal of Asian Earth Sciences*, 32, 385-395, 2008.
- Zhai, Q., Li, C., and Huang, X. P.: Geochemistry of Permian basalt in the Jiamao area, central Qiangtang, Tibet, China, and its tectonic significance, *Geological Bulletin of China*, 25, 1419-1427, 2006.
- Zhai, Q. G., Wang, J., Li, C., and Su, L.: SHRIMP U-Pb dating and Hf isotopic analyses of Middle Ordovician meta-cumulate gabbro in central Qiangtang, northern Tibetan Plateau, *SCIENCE CHINA Earth Sciences*, 53, 657-664, 2010.
- Zhai, Q. G., Jahn, B. M., Zhang, R. Y., Wang, J., and Su, L.: Triassic Subduction of the Paleo-Tethys in northern Tibet, China: evidence from the geochemical and isotopic characteristics of eclogites and blueschists of the Qiangtang Block, *Journal of Asian Earth Sciences*, 42, 1356-1370, 2011a.
- Zhai, Q. G., Zhang, R. Y., Jahn, B. M., Li, C., Song, S. G., and Wang, J.: Triassic eclogites from central Qiangtang, northern Tibet, China: Petrology, geochronology and metamorphic PT path, *Lithos*, 125, 173-189, 2011b.
- Zhang, H., Xu, W., Guo, J., Zong, K., Cai, H., and Yuan, H.: Indosinian orogenesis of the Gangdese terrane: evidences from zircon U–Pb dating and petrogenesis of granitoids, *Earth Sci. J. China Univ. Geosci*, 32, 155-166, 2007.
- Zhang, H. F., Zhang, L., Harris, N., Jin, L. L., and Yuan, H.: U–Pb zircon ages, geochemical and isotopic compositions of granitoids in Songpan-Garze fold belt, eastern Tibetan Plateau: constraints on petrogenesis and tectonic evolution of the basement, *Contributions to Mineralogy and Petrology*, 152, 75-88, 2006a.

Chapter1

- Zhang, K. J., Xia, B. D., Wang, G. M., Li, Y. T., and Ye, H. F.: Early Cretaceous stratigraphy, depositional environments, sandstone provenance, and tectonic setting of central Tibet, western China, *Geological Society of America Bulletin*, 116, 1202-1222, 2004.
- Zhang, K.-J., Zhang, Y.-X., Xia, B.-D., and He, Y.-B.: Temporal variations of Mesozoic sandstone compositions in the Qiangtang block, northern Tibet (China): implications for provenance and tectonic setting, *Journal of Sedimentary Research*, 76, 1035-1048, 2006b.
- Zhang, K. J., Li, B., Wei, Q. G., Cai, J. X., and Zhang, Y. X.: Proximal provenance of the western Songpan–Ganzi turbidite complex (Late Triassic, eastern Tibetan plateau): Implications for the tectonic amalgamation of China, *Sedimentary Geology*, 208, 36-44, 2008a.
- Zhang, K. J., Zhang, Y. X., Tang, X. C., and Xia, B.: Late Mesozoic tectonic evolution and growth of the Tibetan plateau prior to the Indo-Asian collision, *Earth-Science Reviews*, 114, 236-249, <http://dx.doi.org/10.1016/j.earscirev.2012.06.001>, 2012a.
- Zhang, K.: Is the Songpan-Ganzi terrane (central China) really underlain by oceanic crust?, *JOURNAL-GEOLOGICAL SOCIETY OF INDIA*, 57, 223-230, 2001a.
- Zhang, K.: Escape hypothesis for North and South China collision and tectonic evolution of the Qinling orogen, eastern Asia, *Eclogae Geologicae Helvetiae*, 95, 237-247, 2002.
- Zhang, K., and Tang, X.: Eclogites in the interior of the Tibetan Plateau and their geodynamic implications, *Chinese Science Bulletin*, 54, 2556-2567, 2009.
- Zhang, K. J.: Blueschist-bearing metamorphic core complexes in the Qiangtang block reveal deep crustal structure of northern Tibet: Comment and Reply, *Geology*, 29, 90, 2001b.
- Zhang, K. J., Xia, B., and Liang, X.: Mesozoic–Paleogene sedimentary facies and paleogeography of Tibet, western China: tectonic implications, *Geological Journal*, 37, 217-246, 2002.
- Zhang, K. J., Cai, J. X., Zhang, Y. X., and Zhao, T. P.: Eclogites from central Qiangtang, northern Tibet (China) and tectonic implications, *Earth and Planetary Science Letters*, 245, 722-729, 2006c.
- Zhang, K. J., Zhang, Y. X., Li, B., Zhu, Y. T., and Wei, R. Z.: The blueschist-bearing Qiangtang metamorphic belt (northern Tibet, China) as an in situ suture zone: Evidence from geochemical comparison with the Jinsha suture, *Geology*, 34, 493-497, 2006d.
- Zhang, K. J., Zhang, Y. X., Tang, X. C., Xie, Y. W., Sha, S. L., and Peng, X. J.: First report of eclogites from central Tibet, China: evidence for ultradeep continental subduction prior to the Cenozoic India-Asian collision, *Terra Nova*, 20, 302-308, 2008b.
- Zhang, K. J., Tang, X. C., Wang, Y., and Zhang, Y. X.: Geochronology, geochemistry, and Nd isotopes of early Mesozoic bimodal volcanism in northern Tibet, western China: Constraints on the exhumation of the central Qiangtang metamorphic belt, *Lithos*, 121, 167-175, [10.1016/j.lithos.2010.10.015](http://dx.doi.org/10.1016/j.lithos.2010.10.015), 2011.
- Zhang, K. Z., and Chen, Y. L.: Plagiogranite in the Goicang ophiolites in Xizang, *Sedimentary Geology and Tethyan Geology*, 1, 005, 2007.

Chapter1

- Zhang, L. Y., Ding, L., Pullen, A., Xu, Q., Liu, D. L., Cai, F. L., Yue, Y. H., Lai, Q. Z., Shi, R. D., and Ducea, M. N.: Age and geochemistry of western Hoh-Xil–Songpan-Ganzi granitoids, northern Tibet: Implications for the Mesozoic closure of the Paleo-Tethys ocean, *Lithos*, 190, 328-348, 2014.
- Zhang, X., Shi, R., Huang, Q., Liu, D., Cidan, S., Yang, J., and Ding, L.: Finding of high-pressure mafic granulites in the Amdo basement, central Tibet, *Chinese Science Bulletin*, 55, 3694-3702, 2010a.
- Zhang, Y. C., Cheng, L. R., and Shen, S. Z.: Late Guadalupian (Middle Permian) Fusuline Fauna from the Xiala Formation in Xainza County, Central Tibet: Implication of the Rifting Time of the Lhasa Block, *Journal of Paleontology*, 84, 955-973, 2010b.
- Zhang, Z., Dong, X., Santosh, M., and Zhao, G.: Metamorphism and tectonic evolution of the Lhasa terrane, Central Tibet, *Gondwana Research*, 25, 170-189, 2012b.
- Zhao, T. P., Zhou, M. F., Zhao, J. H., Zhang, K. J., and Chen, W.: Geochronology and geochemistry of the c. 80 Ma Rutog granitic pluton, northwestern Tibet: implications for the tectonic evolution of the Lhasa Terrane, *Geological Magazine*, 145, 845-857, 2008.
- Zhao, Z., Bons, P. D., Wang, G., Liu, Y., and Zheng, Y.: Origin and pre-Cenozoic evolution of the south Qiangtang basement, Central Tibet, *Tectonophysics*, 623, 52-66, 2014.
- Zhao, Z., Bons, P., Wang, G., Soesoo, A., and Liu, Y.: Tectonic evolution and high-pressure rock exhumation in the Qiangtang Terrane, Central Tibet, *Solid Earth*, 6, 457-473, 2015.
- Zhu, D. C., Zhao, Z. D., Niu, Y., Mo, X. X., Chung, S. L., Hou, Z. Q., Wang, L. Q., and Wu, F. Y.: The Lhasa Terrane: Record of a microcontinent and its histories of drift and growth, *Earth and Planetary Science Letters*, 301, 241-255, 2011a.
- Zhu, D. C., Mo, X. X., Niu, Y., Zhao, Z. D., Wang, L. Q., Liu, Y. S., and Wu, F. Y.: Geochemical investigation of Early Cretaceous igneous rocks along an east-west traverse throughout the central Lhasa Terrane, Tibet, *Chemical Geology*, 268, 298-312, 2009a.
- Zhu, D. C., Zhao, Z. D., Pan, G. T., Lee, H. Y., Kang, Z. Q., Liao, Z. L., Wang, L. Q., Li, G. M., Dong, G. C., and Liu, B.: Early cretaceous subduction-related adakite-like rocks of the Gangdese Belt, southern Tibet: Products of slab melting and subsequent melt-peridotite interaction?, *Journal of Asian Earth Sciences*, 34, 298-309, 2009b.
- Zhu, D. C., Zhao, Z. D., Niu, Y., Mo, X. X., Chung, S. L., Hou, Z. Q., Wang, L. Q., and Wu, F. Y.: The Lhasa Terrane: Record of a microcontinent and its histories of drift and growth, *Earth and Planetary Science Letters*, 301, 241-255, 2010.
- Zhu, D. C., Zhao, Z. D., Niu, Y., Dilek, Y., and Mo, X. X.: Lhasa terrane in southern Tibet came from Australia, *Geology*, 39, 727-730, 2011b.
- Zhu, D. C., Zhao, Z. D., Niu, Y., Dilek, Y., Hou, Z. Q., and Mo, X. X.: The origin and pre-Cenozoic evolution of the Tibetan Plateau, *Gondwana Research*, 23, 1429-1454, 2012.
- Zhu, J., Du, Y., Liu, Z., Feng, Q., Tian, W., Li, J., and Wang, C.: Mesozoic radiolarian chert from the middle sector of the Yarlung Zangbo suture zone, Tibet and its tectonic implications, *Science in China Series D*, 49, 348-357, 2006a.

Chapter1

Zhu, T., Zhang, Q., Dong, H., Wang, Y., Yu, Y., and Feng, X.: Discovery of the Late Devonian and Late Permian radiolarian cherts in tectonic mélanges in the Cêdo Caka area, Shuanghu, northern Tibet, China, *Geological Bulletin of China*, 25, 1413-1418, 2006b.

Zi, J. W., Cawood, P. A., Fan, W. M., Wang, Y. J., Tohver, E., McCuaig, T. C., and Peng, T. P.: Triassic collision in the Paleo-Tethys Ocean constrained by volcanic activity in SW China, *Lithos*, 144, 145-160, 2012.

Chapter 2: Origin and pre-Cenozoic evolution of the south Qiangtang basement, Central Tibet

Zhongbao Zhao [a,b](#), Paul D. Bons [a](#), Genhou Wang [b](#), Yan Liu [c](#), Yilong Zheng [b](#)

a, Department of Geosciences, Eberhard Karls University Tübingen, Wilhelmstrasse 56, D-72074 Tübingen, Germany

b, School of Earth Science and Resources, China University of Geosciences, Beijing 100083, China

c, State Key Laboratory for Continental Tectonics and Dynamics, Institute of Geology, CAGS, Beijing 100037, China

Abstract

The Qiangtang terrane in Central Tibet, with its high-pressure rocks, is a key area to unravel the evolution of the Paleo-Tethys. We present a new 1:50,000 map of the Rongma area in the central Qiangtang terrane, of which relatively little is known so far. We show that the Qiangtang metamorphic belt can be separated in a Paleozoic autochthonous basement and an overlying allochthonous thrust stack of subduction mélangé that contains high-pressure rocks and Permian sediments. Detrital zircon ages (youngest peak at 591 Ma) and an ~ 470 Ma granite intrusion age constrain the age of the Qiangtang Basement to be between the Late Precambrian to Middle Ordovician. This is in agreement with the observed unconformity between basement and overlying Mid–Late Ordovician strata. This unconformity and the zircon age spectra are comparable to the Himalaya area. The Qiangtang terrane must thus have been part of the Gondwana supercontinent during the Early Paleozoic.

The occurrence of the Late Triassic eclogite and glaucophane-bearing schists in the Central Qiangtang terrane indicates the existence of a suture zone between the North and South Qiangtang terranes before the Late Triassic. This suture zone resulted from closure of the Paleo-Tethys between the North and South Qiangtang terranes. Late Triassic syn-collisional granites and rapidly exhumed high-pressure rocks resulted from the closure of this ocean and final amalgamation of the reunited Qiangtang terranes with Eurasia. Collision of the Lhasa and Qiangtang terranes is correlated with north dipping reverse faults in the south Qiangtang terrane, which were probably related to exhumation of the Qiangtang basement and formation of the Qiangtang Culmination.

Key words: Tibet, Qiangtang, high-pressure rocks, Paleo-Tethys, obduction, subduction mélangé

1. Introduction

The Tibetan Plateau, the largest orogenic feature on Earth, has been the focus of many recent geological and geophysical investigations (e.g. [Freymueller, 2011](#); [Gehrels et al., 2011](#); [Haines et al., 2003](#); [Tapponnier et al., 2001](#)). However, due to its high elevation, remoteness and complex geology, open questions remain on the pre-Cenozoic evolution of the plateau, particularly its interior, where the Qiangtang terrane is located in Central Tibet. From north to south, the Central Tibetan Plateau is formed by the Qaidam terrane, the Songpan–Ganzi Flysch Complex, and the Qiangtang and Lhasa terranes. These terranes are separated by EW striking suture zones of Paleozoic to Mesozoic age ([Fig. 1a](#)) ([Yin and Harrison, 2000](#)).

The Songpan–Ganzi Flysch Complex lies to the north of the Qiangtang terrane, with the Jinsha Suture Zone (JSZ) in between ([Yin and Harrison, 2000](#)) ([Fig. 1a](#)). This suture zone represents the Paleo-Tethys (or a branch of it) between Eurasia and the Qiangtang terrane that was consumed by southward subduction beneath the Qiangtang terrane in Late Triassic to Early Jurassic times ([Dewey et al., 1988](#); [Kapp et al., 2000](#); [Nie et al., 1994](#); [Yin and Nie, 1996](#)). The Bangong–Nujiang Suture Zone (BNSZ) separates the Qiangtang terrane from the Lhasa terrane in the south ([Fig. 1a](#)) ([Dewey et al., 1988](#); [Guynn et al., 2012](#); [Zhu et al., 2012](#)). It is defined by a broad and discontinuous belt of ophiolite fragments and mélangé. It is assumed to be the result of closure of the Meso-Tethys Ocean and subsequent collision of the Lhasa and Qiangtang terranes during the Early Cretaceous ([Dewey et al., 1988](#); [Guynn et al., 2006, 2012](#); [Kapp et al., 2003a, 2007](#)). Considering this complex setting, better knowledge of the geology of the Qiangtang terrane is important to understand the geological evolution of the Tibetan Plateau.

The Qiangtang terrane is traditionally divided into low-metamorphic grade Paleozoic (? Carboniferous–Permian) clastic metasediments and subduction related mélangé with high-pressure rocks, including eclogites ([Liu et al., 2011](#)), in the center of the terrane. Permian–Jurassic shallow-marine limestones, interbedded with minor sand-mudstones, overlie the southern and northern flanks of the Qiangtang terrane. Some authors subdivided the Qiangtang terrane into two parts, the North Qiangtang terrane and the South Qiangtang terrane (sometimes referred to as East and West Qiangtang, respectively), because the high-pressure rocks are found in the center of the Qiangtang terrane ([Fig. 1b](#)) ([Li et al., 2006](#); [Zhai et al., 2011](#)). The boundary between these two terranes is the Longmu Co–Shuanhu Suture Zone, situated north of the mélangé and high-pressure rocks.

The Qiangtang terrane is considered to have been a contiguous part of the Cimmerian super terrane along the Tethys margin of Gondwana ([Guynn et al., 2012](#)), because the terrane exposes Cambrian gneiss in

Amdo ([Guynn et al., 2006](#); [Kapp et al., 2000](#); [Xu et al., 1985](#)), extensive late Carboniferous–early Permian glaciomarine deposits in the central Qiangtang terrane ([Li et al., 1995](#)), and yields similar U–Pb detrital zircon age distributions for Upper Paleozoic strata within the south Qiangtang terrane ([Dong et al., 2011](#); [Gehrels et al., 2011](#); [Kapp et al., 2003b](#); [Leier et al., 2007](#); [Pullen et al., 2008](#)).

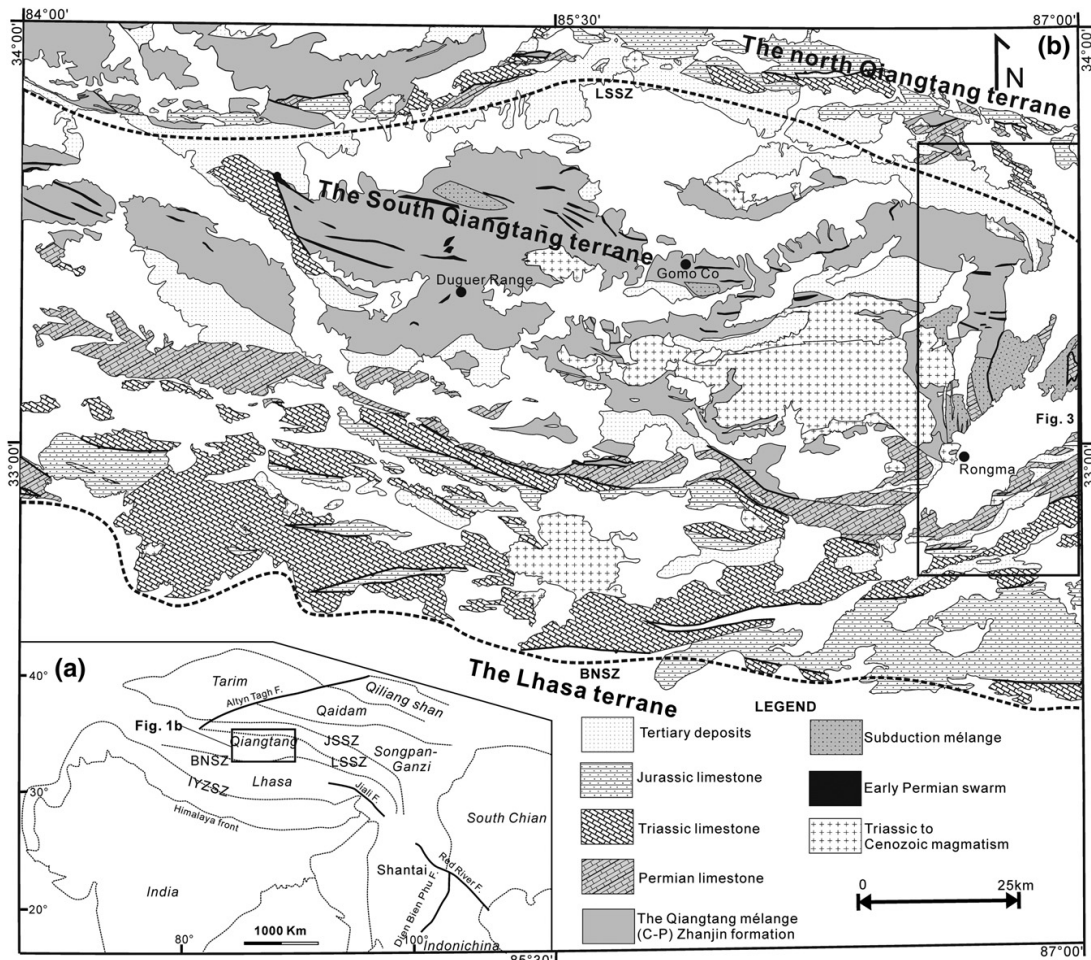


Fig. 1. Tectonic sketch of central Tibet, showing the several terranes and suture zones. (a) Structural sketch of Tibet. From north to south, the sutures are JSZ — Jinsha Suture Zone; LSSZ — Longmu Co–Shuanghu Suture Zone; BNSZ — Bangong–Nujiang Suture Zone; and IYSZ — Indus–Yarlung Suture Zone. (b) The main units of the Qiangtang terrane, central Tibet. The middle part is the Qiangtang culmination, with Mesozoic to Neozoic sediments mostly found on its the northern and southern flanks. Modified after [Deng et al. \(2005\)](#), [Kapp et al. \(2003b\)](#), [Li \(2006\)](#) and [Zeng et al. \(2002, 2006\)](#).

Within the Qiangtang terrane, eclogite-bearing blueschist-facies rocks have been found in Gangmu Co, Rongma etc., but their origin is under debate ([Kapp et al., 2000, 2003b](#); [Li et al., 2006](#); [Liang et al., 2012](#); [Liu et al., 2011](#); [Zhang et al., 2006a](#)). Two basic, but radically different models have been proposed for

the origin of these high- pressure rocks ([Fig. 2](#)). The “intra-Qiangtang suture model” envisages northward subduction of the Paleo-Tethys along the Longmu Co–Shuanhu Suture Zone (LSSZ) that separates the North and South Qiangtang terranes, and thrusting of the *mélange* over the South Qiangtang terrane ([Fig. 2a](#)) ([Li et al., 2009](#); [Zhai et al., 2011](#)). According to the alternative “underthrust model”, early Mesozoic *mélange* was thrust under the Qiangtang terrane from the Jinsha Suture Zone (JSZ) that bounds the Qiangtang terrane 200 km to the north ([Fig. 2b](#)) ([Kapp et al., 2000, 2003b](#); [Pullen et al., 2011](#)). In this model the *mélange* was underplated to the Qiangtang terrane and exhumed by detachment faulting. In the intra-Qiangtang suture model, allochthonous *mélange* is underlain by autochthonous Paleozoic basement, while the underthrust model predicts that the deeper crust in large parts of northern Tibet is *mélange*. Knowing the exact nature of the Paleozoic metamorphic rocks is therefore crucial to advance our understanding of the crustal structure of the Qiangtang terrane. The two very dissimilar models show that whether the Paleozoic low-grade metamorphic rocks are autochthonous basement or not has far-reaching consequences, not only for the pre-Cenozoic evolution of the Qiangtang terrane, but also for the whole Tibetan plateau and the Indo-Asian collision ([Kapp et al., 2003b](#)). Unfortunately, the presence of basement in the Qiangtang terrane ([Dong et al., 2011](#); [Pullen et al., 2011](#); [Wang and Wang, 2001](#)) and the origin of the high-pressure rocks ([Kapp et al., 2003b](#); [Li et al., 2009](#)) still remain controversial. The main aim of this paper is to clarify the relationship between the various units in the Qiangtang terrane, using detailed mapping and geochronology. We show that the low-grade metamorphic rocks are indeed autochthonous basement rocks of Early Paleozoic age and Gondwana affinity.

2. Geology of the Rongma area

Due to the remoteness and difficult field conditions, the Qiangtang terrane has not yet been mapped and studied in great detail. To gain better understanding of Paleozoic Tibet and the Paleo-Tethys, the Rongma area was mapped at a scale of 1:50,000 ([Fig. 3](#)). Paleozoic metamorphic rocks, subduction *mélange*, including eclogites, and Mesozoic strata are exposed in the area ([Liu et al., 2011](#); [Zhai et al., 2007](#)). Below we present and discuss the lithostratigraphy and structure separately.

2.1 Lithostratigraphy

Rocks that are exposed in the area vary greatly in their age, origin, metamorphic facies and deformation ([Kapp et al., 2000, 2003b](#)). Based on this, they can be divided into four main units. These are (1) Qiangtang basement (QB), consisting of greenschist-facies Paleozoic strata with pervasive folding and cleavage, (2) nautiloids-bearing Middle to Late Ordovician slate and ammonoid-bearing Carboniferous sandstone and siltstone (OC), (3) strongly deformed subduction *mélange* (SM) including high-pressure metamorphic rocks (HP) and (4) the uppermost cover unit that consists of Permian to Jurassic shallow

marine deposits (Fig. 3). Units 1–3 were intruded by the 210 ± 5 Ma Gangtang Co Granite, NW of the village of Rongma (Kapp et al. 2003b).

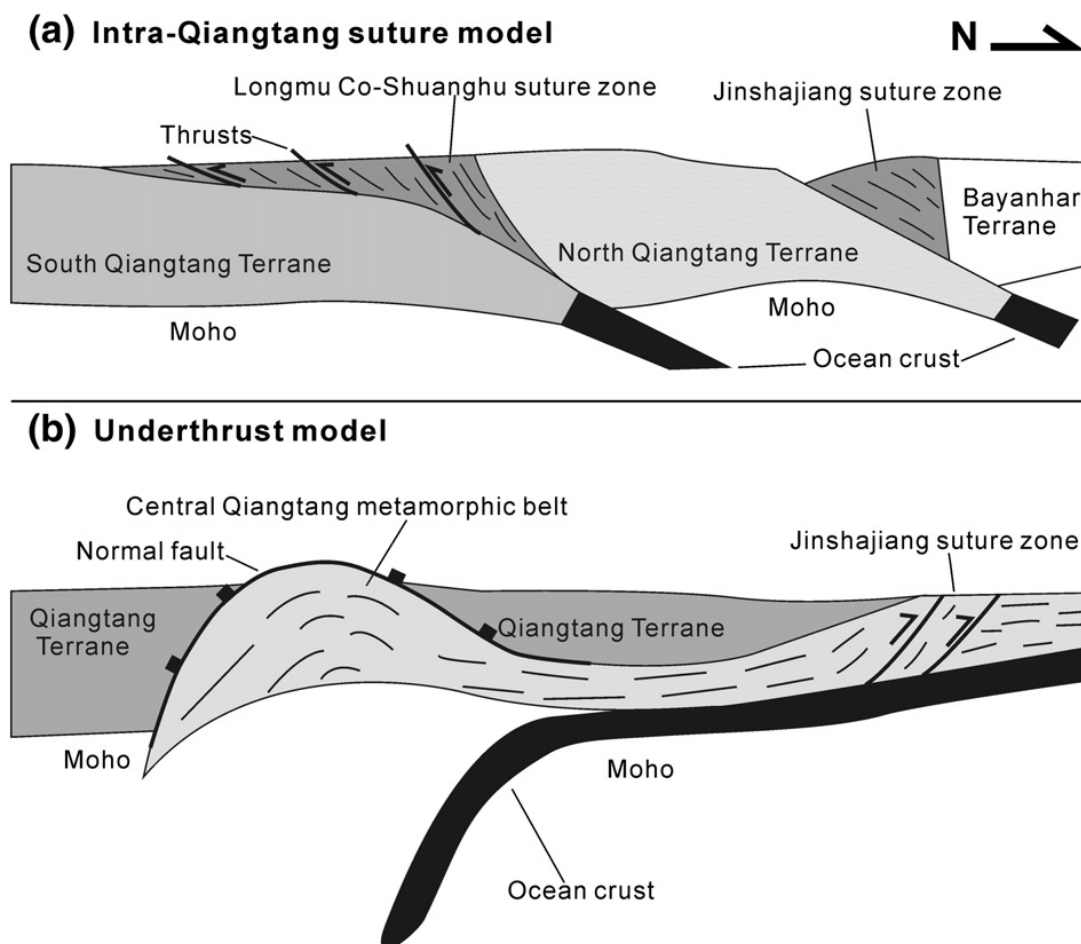


Fig. 2. Competing tectonic models for the central Qiangtang metamorphic belt in early Mesozoic times: (a) the intra-Qiangtang suture model (Li et al., 1995) and (b) the underthrust model (Kapp et al., 2003b).

As we will show below, the QB forms the structurally lowest unit and is exposed over large areas north of Rongma. Cheng and Xu (1986) and Kapp et al. (2003b) interpreted the fossil-free metamorphic rocks as Carboniferous in age, and assigned them to the Zhanjin Formation. In the mapping area, the unit is mainly of clastic sedimentary origin, metamorphosed to quartzite, phyllite, meta-arkose and minor marble (Li et al., 2006, 2007). Some mafic lenses are found, oriented parallel to the main foliation. The unit was intruded by Early Permian dyke swarms with gabbro, diabase and minor ultramafic rocks. The supposed Carboniferous age (Cheng and Xu, 1986) will be discussed and corrected below.

Chapter2

Middle to Late Ordovician strata of the Tashishan Formation are exposed at two locations, where they unconformably overlie the QB. One is ~ 20 km north of Gangtang Co and the other is near Rongma village ([Figs. 3, 4a](#)). The Tashishan formation is characterized by siltstone and slates, interbedded with volcanoclastics and calcareous slates that are rich in crinoids, nautiloids and graptolites. Previously, these outcrops of Ordovician strata were interpreted as klippen ([Li, 2006](#)). The Ordovician layers, however, unconformably overlie the QB. Where the unconformity is exposed, a basal conglomerate is found, consisting of cm–dm size quartzite and marble clasts in a calcareous matrix ([Fig. 5a, b](#)).

Carboniferous sediments, cm to 1 m thick sandstone and siltstone beds, are found a few kilometers west of the Ordovician outcrop near Rongma village ([Fig. 4a](#)). The beds form an open km-scale syncline bounded by a normal fault in the east. Carboniferous beds are not as strongly folded as the underlying basement rocks (QB) and beds are parallel to the contact with these underlying rocks. In the absence of any distinct faulting or shearing, the contact between QB and Carboniferous is interpreted as an unconformity.

The subduction mélangé (SM) is mainly found in the middle of the mapping area ([Fig. 3](#)). It is characterized by strongly deformed marine sedimentary rocks that contain less-deformed lenses. The marine sediment consists of pelites, siltstones, sandstones and minor limestones and cherts. These lithologies form the matrix of the mélangé, which contains blocks and lenses, tens of meters up to kilometers in size, of more competent rocks, such as pillow basalts, minor ultramafics, gabbros, diabase, etc. ([Cheng and Xu, 1986](#); [Kapp et al., 2003b](#)). Blueschist and eclogite-facies metamorphic slices (HP) are regarded as part of the subduction mélangé. They occur in roughly N–S trending belts and consist of eclogites, glaucophane-bearing schist, garnet-bearing phengite–quartz schist and marbles. The eclogites are generally found to be enclosed as lenses in garnet-bearing phengite–quartz schist. The protoliths of HP rocks have an oceanic affinity, and include basalt, gabbro and pelagic sediments ([Zhang et al., 2006b](#)). The subduction mélangé was interpreted as an accretionary mélangé formed at a convergent-plate margin ([Zhai et al., 2004](#)). Both the basement units (QB and OC) and the subduction mélangé are intruded by the Late Triassic Gangtang Co granite ([Figs. 3, 4b](#)).

The Late Permian to Jurassic shallow-marine deposits are divided into three types. In the north, Late Permian to Late Triassic shallow-marine limestones, interbedded with minor siltstone and coral layers, contain Eurasian warm-water faunas (Cathaysian affinity; similar to the South China block) ([Li et al., 1995](#)). In the middle part of the mapping area, Permian shallow-marine limestones of the Longge group

structurally overlie both the Qiangtang basement and the subduction mélangé (Fig. 3). Fossils in these limestones include bivalves, gastropods, echinoderms, foraminifera and tetracorals.

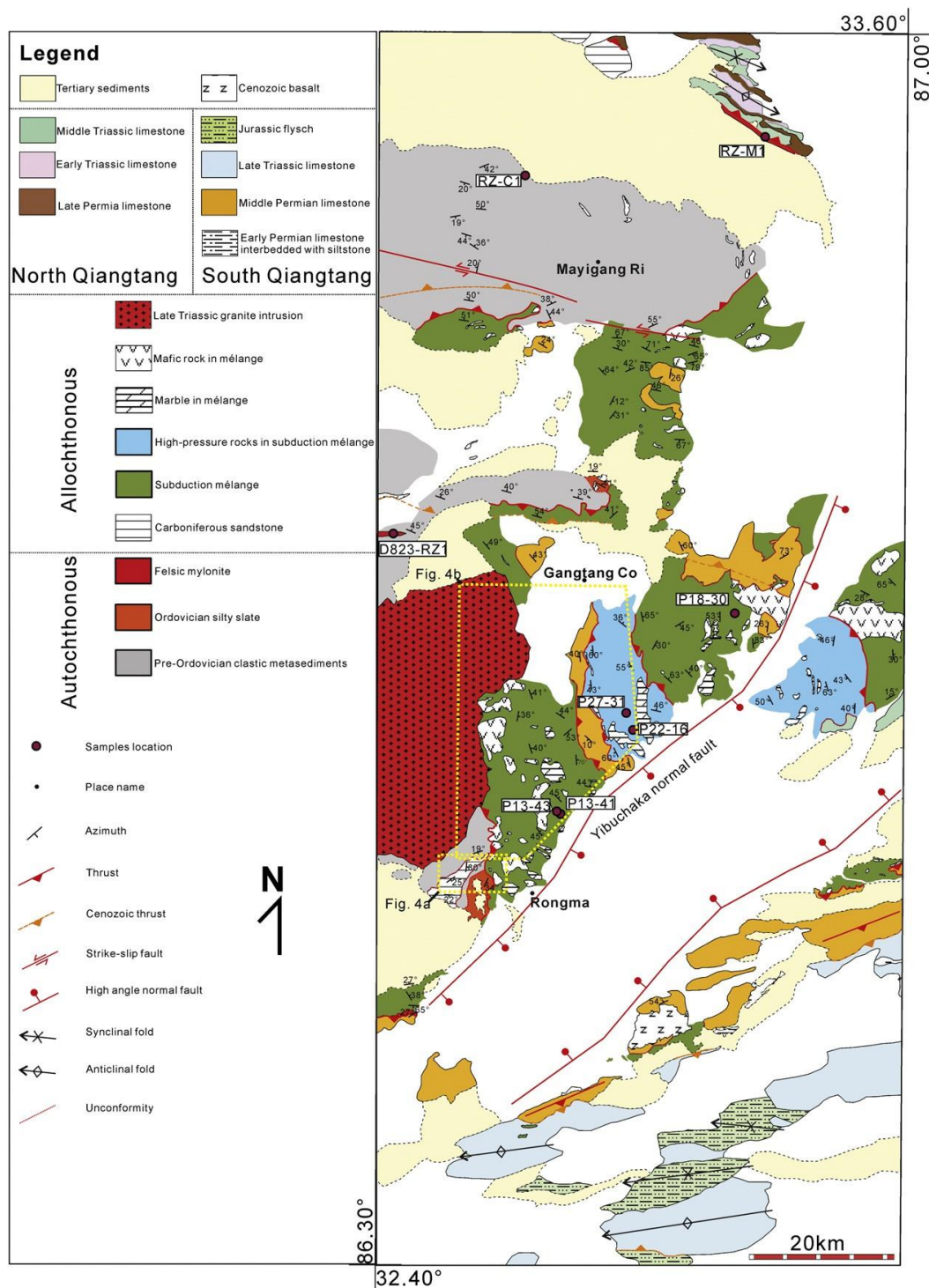


Fig. 3. (a) Detailed geological map of the Qiangtang basement, subduction mélangé and overlying sediments of the Rongma area based on our mapping. Locations of samples discussed in this paper are shown. Locations of Fig. 4a and b are shown by the yellow frames.

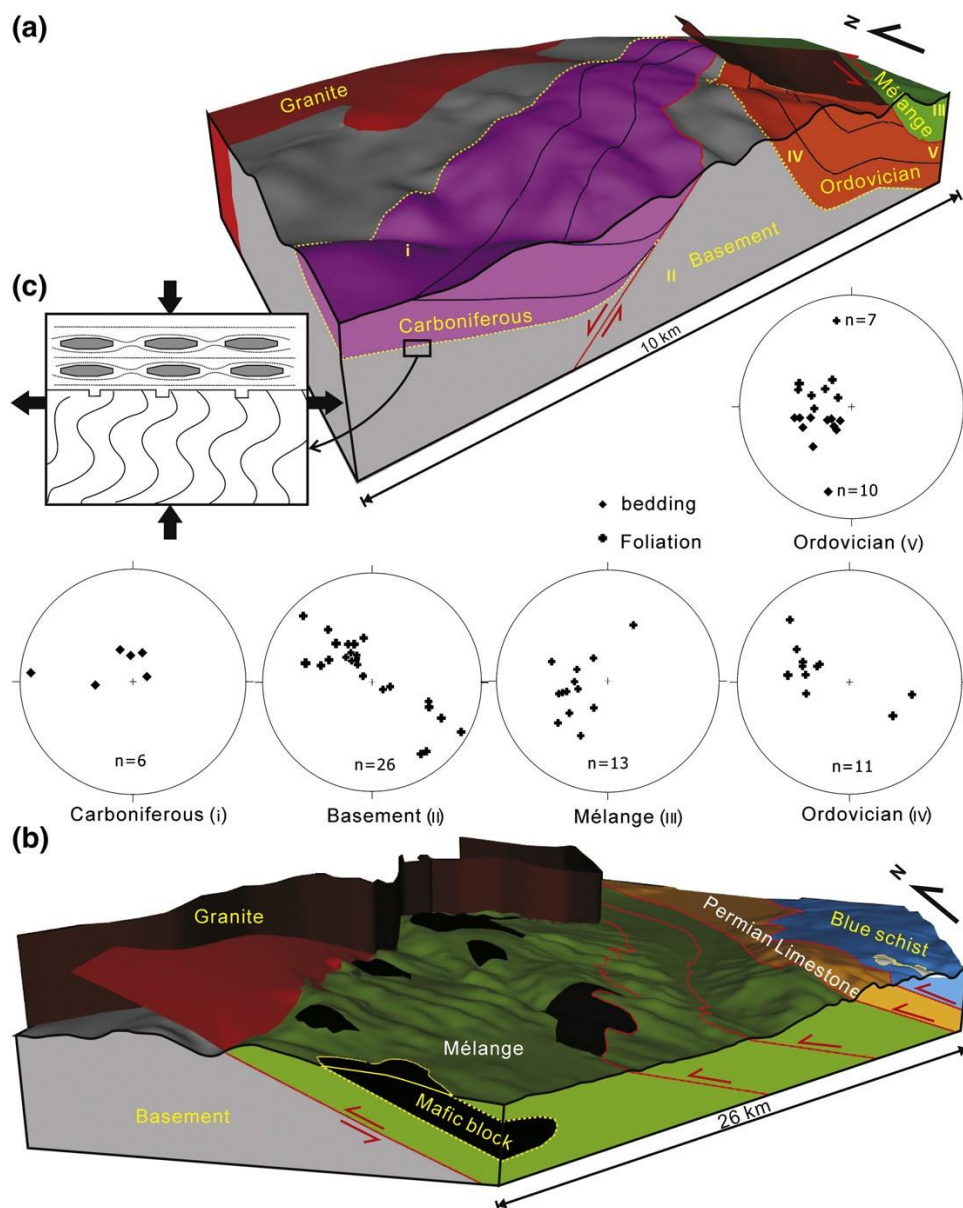


Fig. 4. (a) 3-D reconstruction of relationships between basement (QB), Ordovician slates, Carboniferous sandstones (OC) and subduction mélangé (SM) near Rongma village. The Ordovician slates and Carboniferous sandstone unconformably overlie the basement, while the subduction mélangé is thrust onto the other three units. Poles to bedding and main foliation are shown in lower-hemisphere, equal area stereoplots for five locations (I to V) in the block diagram. (b) Larger-scale 3D reconstruction of the Rongma area showing how the low-grade mélangé, the Permian sediments and high-pressure rocks form an allochthonous stack of thrusts on top of the Paleozoic autochthonous rocks. Thrusts are cut by the Late Triassic Gangtang Co granite. Locations of diagrams are shown in [Fig. 3](#). Reconstructions were made with Move™ by Midland Valley. (c) Sketch showing the different response to the same deformation event (Db2): bedding in QB at a small angle to the shortening direction is folded, while bedding in the overlying Carboniferous and Ordovician is oriented closer to the extension direction and therefore stretched.

Chapter2

Based on this fossil content, [Zhang et al. \(2012\)](#) determined an Early Permian age. Some of these Permian rocks were mapped as Carboniferous by [Kapp et al. \(2003b\)](#). Below it will be shown that the reclassification of these rocks as Permian has significant implications for the structural interpretation of the area. Early Permian sandstones and minor siltstones that stratigraphically underlie the Longge group are found in the south of the area. These are cold-water deposits with glaciomarine faunas ([Li et al., 1995](#)). Late Triassic limestones with minor sandstones and conglomerate at the base overlie the early Permian sandstone further south in the area. Jurassic flysch deposits uncomfortably overlie the south flank of the Qiangtang culmination.

Finally terrestrial sediments, possibly as old as Cretaceous, but mostly Tertiary and Cenozoic ([Kapp et al., 2005](#)), were deposited on top of all previous lithologies.

2.2 Structural relationships

2.2.1 Deformation of the basement (QB) and Ordovician-Carboniferous strata (OC)

Deformation of the basement (QB) and Ordovician–Carboniferous strata (OC) Layers and main foliation in the clastic meta-sediments of the basement generally dip about 40–50° to the NE–NW in the north of the area and turn to ~ 30° to the SE in the southern part of the culmination. The large-scale structure is thus an open anticlinorium, the Qiangtang Culmination, with a fold axis that plunges to the east. Several steep EW-striking reverse faults are found at Mayigang Ri Mountain and south of it ([Fig. 3](#)), and may be associated with the formation of the culmination.

In outcrop and thin section, two tectonic foliations can be observed ([Fig. 5c, d, e](#)). The oldest one (Sb1) is formed by a fine tectonic layering ([Fig. 5c, d, e](#)) (Turner et al., 1994). Bedding and Sb1 are overprinted by a second and main folding event (Fb2), which produced an axial planar cleavage (Sb2). Fb2 folds are the dominant folds in outcrop. Fb2 folding around a NE–SW trending fold axis is clearly visible in the orientation distribution of bedding and Sb1 near Rongma village ([Fig. 4](#)). Folds are similar and range from open to tight and from the cm to m scale, depending on lithology. Psammitic units tend to have larger scale folds. Sb2 is a crenulations cleavage formed by microfolding of Sb0/1 and new growth of aligned sericite and biotite.

A >5 km long and up to 200 m wide EW-striking felsicmylonite zone separates North Qiangtang terrane rocks in the hanging wall from South Qiangtang basement to the south. Unfortunately, the outcrop of the mylonite zone is limited as most of the area is covered by recent sediments. The strong foliation and

stretching lineation indicates high strain. Porphyroclasts (Fig. 5g) show a dextral sense of shear (north moving east). A second, EW-striking, felsic mylonite zone is found west of Gangtang Co in the center of the area. This steep mylonite with a steep stretching lineation shows a north-side-up movement (Fig. 5h). Both felsic mylonites contain quartz, feldspar, garnet and tourmaline and are interpreted to be sheared granites or granitic dykes/sills. Gabbro dykes that intruded the basement in the north are undeformed and have been dated as Early Permian in age (Zhai et al., 2009).

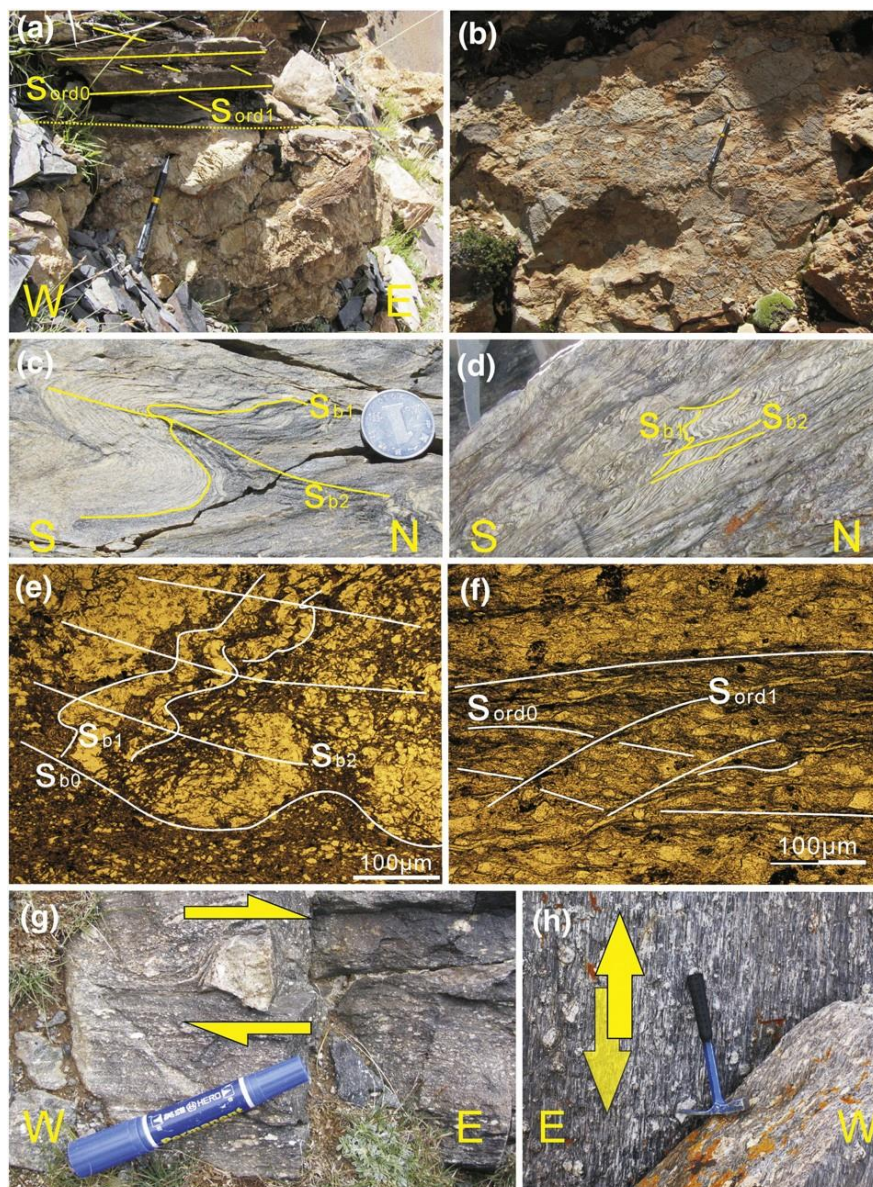


Fig. 5. Field images of the South Qiangtang basement (QB) and Ordovician strata. (a) Bedding (Sord0) and foliation (Sord1) of Ordovician strata overlying the basal conglomerate. (b) The basal conglomerate with limestone pebbles in a silty matrix, approximately 20 m above the unconformity. (c–d) Main foliation in the basement. Sb2 developed with variable intensity axial planar to folds in Sb1. (e) Micrograph showing the relationship between bedding (Sb0), (f) Micrograph showing the relationship between bedding (Sord0) and foliation (Sord1). (g) Field image showing a dextral sense of shear with yellow arrows indicating north moving east. (h) Field image showing a north-side-up movement with yellow arrows indicating north moving up.

Sb1 and Sb2 in a basement pelite. (f) Micrograph showing bedding (Sord0) and cleavage (Sord1) in an Ordovician pelite. Whereas the basement has two distinct foliations, only one (Sord1) could be observed in outcrop and thin section in Ordovician rocks. (g) Felsic mylonite with a dextral sense of shear at the northern edge of the south Qiangtang terrane. Looking down parallel to the mylonitic foliation. (h) An E–W striking felsic mylonite found to the west of Gangtang Co, looking south onto the mylonitic foliation with a steep stretching lineation. North block moves up.

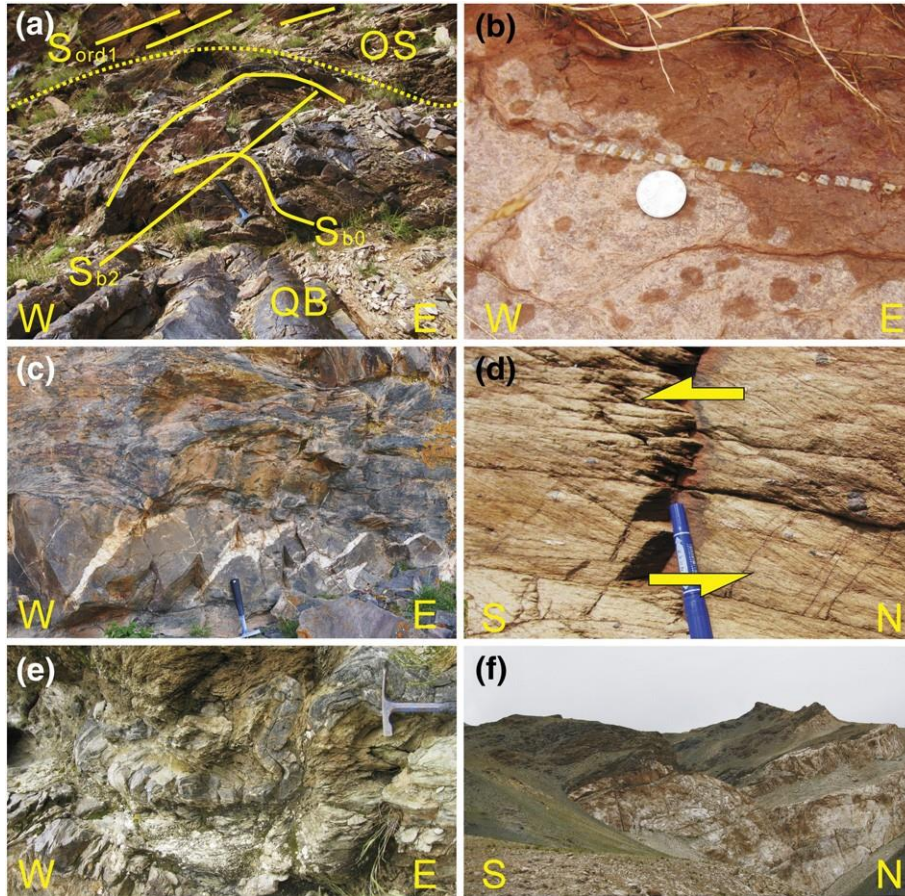


Fig. 6. (a) Relationship between deformation structures in Qiangtang Basement (QB) rocks and overlying Ordovician Strata (OS). In the basement, bedding (Sb0) and Sb1 are folded with Sb2 as axial planar cleavage. Sb2 is roughly parallel to Sord1 above the unconformity, and is therefore assumed to result from the same post-Ordovician deformation event. (b) The post-Ordovician deformation event produced folds in basement bedding and first foliation (Sb1), but stretching of Ordovician layers, as is indicated by this stretched *Sinoceras* nautiloid. (c) Competent sandstone layers in the Carboniferous are boudinaged, indicating the Carboniferous strata experienced the same layer-parallel stretching as the Ordovician layers. (d) Deformation in the subduction mélangé is intense with the development of a strong foliation in the mudstone and pressure shadows around quartzite clasts. These indicate a top to the south shearing here. (e) Strong and multiply deformed high-pressure rocks. Competent garnet-bearing phengite schist layers alternate with less competent muscovite schists. (f) Shallowly dipping marble lenses included in blueschists.

The Qiangtang Basement and overlying Middle to Late Ordovician and Carboniferous beds are separated by faulted unconformities (Figs. 4a, 6a). The Ordovician and Carboniferous layers lie parallel to the unconformity and are not folded, contrary to the underlying basement bedding (Fig. 4a). However, boudinage of nautiloids (Fig. 6b) and a strong cleavage (Fig. 5f) indicate that the Ordovician strata were deformed as well. The same holds for the Carboniferous layers where boudinage of competent sandstone layers also indicates stretching of these layers (Fig. 6c). Bedding in the basement is oriented at a high angle to the unconformity, while Sb2 only makes a small angle and is approximately parallel to the cleavage in the Ordovician rocks. We interpret the difference in folding of beds below and above the unconformities to result from the different orientation relative to the folding event that produced Sb2. Whereas bedding and Sb1 in the basement were oriented in the shortening field of this deformation, Ordovician and Carboniferous layers were in the stretching field and therefore did not fold, but stretch (Fig. 4c). Both units thus experienced the same deformation event, which therefore post-dates the Carboniferous. No evidence for a foliation equivalent to Sb1 could be found in the Ordovician and Carboniferous rocks and the deformation that produced this foliation thus probably preceded the Ordovician unconformity.

2.2.2 Deformation of the subduction mélange

Deformation of the Permian to Middle Triassic subduction mélange is much stronger than in the underlying basement and the Ordovician– Carboniferous rocks. The mélange has a strong main foliation (Sm1) (Fig. 6d), which is chaotic in orientation, but is on average flat lying, approximately parallel to the contact with the underlying basement rocks. The mélange is tightly folded with fold axes trending N–S to NW–SE. The foliation wraps around inclusions, lenses and boudins of relatively competent lithologies, such as metabasalt, gabbro, metasediment, etc. Clasts range from centimeters to hundreds of meters in size. These competent inclusions have sigma shapes, with quartz or calcite in the pressure shadows (Fig. 6d). Less competent lithologies, such as chert and sandstone, form strongly stretched layers, where complex deformation structures can be found in the tails of large sigma-clasts. These observations all indicate intense shearing of the mélange, with a top to the S to SW shearing indicated by the σ -clasts (Fig. 6d).

High-pressure rocks in the mélange also show intense deformation, with tight similar folds (Fig. 6e, f). The high-pressure rocks are separated from the lower-grade mélange by faults. High-pressure rocks, low metamorphic-grade mélange and Permian rocks form alternating N–S trending belts in the center of the

area. Marbles and mafics are found in all units. Glaucophane-bearing blueschists exhibit tight similar folds, while garnet-bearing quartz schists may even develop sheath folds. Deformation within the high-pressure rocks thus appears the most intense of all rocks in the area, even more than the low-grade *mélange*. This strong shearing probably resulted from subduction and exhumation at the subduction zone that separated the South and North Qiangtang terranes.

2.2. 3 Deformation of the Permian to Jurassic strata

In the northern part of the area, the Late Permian–Late Triassic shallow marine limestones are gently folded with hinges that plunge to the SE and $\sim 35^\circ$ dipping limbs ([Fig. 7a](#)). In the center of the area, only Permian limestones are found, which are in contact with *mélange* belts (including HP rocks) that lie structurally both above and below the Permian rocks. Layering in the limestones is preserved and is mostly east dipping, parallel to the contacts to adjacent units. Folded veins show an increase in deformation towards the contacts.

The structures are more complex in the south of the mapping area. The Early Permian sandstone and siltstone layers form south-directed recumbent isoclinal folds. Both the Middle Permian and Late Triassic limestones form open folds. All fold hinges in these strata strike EW in the west, and turn to NE–SW striking in the east of the mapping area ([Fig. 7b, c](#)). The Jurassic flysch is relatively undeformed and shows a gentle dip to the south ([Fig. 7d](#)).

The Permian strata overlie the subduction *mélange* that is younger than the Middle Triassic ([Fig. 3](#)). A fault (thrust) must thus lie between these two units. Differences in fold intensity and style suggest the presence of an unconformity between the Early Permian sand and siltstones and the overlying Late Permian limestones ([Fig. 7b](#)). Due to the lack of Early Triassic sediments, the Late Triassic limestones are assumed to unconformably overlie the Permian limestones. In the south of the mapping area, the Late Triassic strata are thrust onto the Jurassic flysch along north-dipping thrusts ([Fig. 3](#)).

2.2.4 Nature of contacts between units

To show the structural relationships between the various units we use the area north of Rongma village ([Fig. 4](#)), where [Kapp et al. \(2003b\)](#) provide an E–W profile. Here, boundaries between units could be determined in the field, as well as using ASTER satellite images. The high topography makes it possible to determine the orientation of contacts and map units by using the interaction between these and

Chapter2

topography, which was done with Move™ by Midland Valley. This provides orientations on the map scale, which is preferable to using outcrop-scale observations and measurements, due to the often chaotic deformation on the small scale, and the potential overprinting of multiple deformation phases.

From west to east the following rocks crop out: (a) Pre-Ordovician rocks (QB), unconformably overlain by Ordovician and Carboniferous sediments (OC), (b) *mélange* with abundant lenticular mafic inclusions, (c) a NS-trending band of Permian layers, (d) blueschists, and finally (e) *mélange* that is structurally overlain by (f) a second occurrence of Permian rocks. Note that the western band of Permian rocks (c) and part of the eastern occurrence of Permian (f) were classified as Carboniferous by [Kapp et al. \(2003b\)](#).

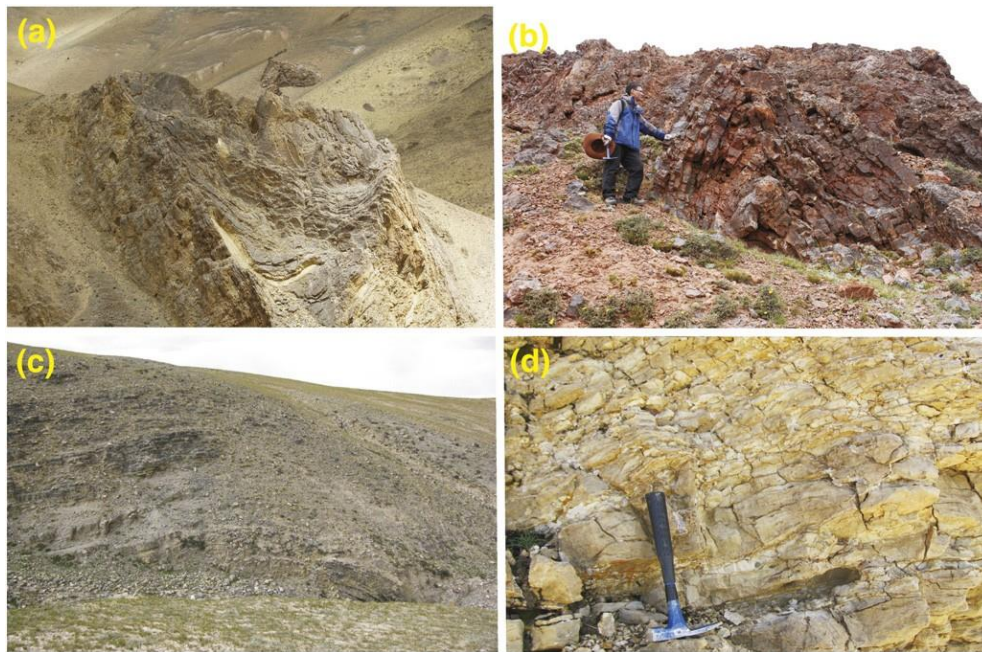


Fig. 7. Outcrop images of upper Permian to Jurassic strata, showing differences in folding intensity. (a) Strong folding, with SE-plunging fold axes, in Middle Triassic limestone in the northern part of the area. Looking to the NW. (b) Folded Middle Permian shallow-marine limestones from the SE of the area. (c) Late Triassic limestones in the south of the area only show gentle folding with shallowly E or W plunging hinges. (d) Jurassic flysch, only found in the south of the area, is virtually undeformed.

The Pre-Ordovician to Carboniferous rocks are bound to the east by an $\sim 35^\circ$, E-dipping fault ([Fig. 4a](#)). In accordance with [Kapp et al. \(2003b\)](#) we interpret this fault to be a thrust. East of this fault contacts between units, bedding, lenses and transposed foliations generally dip to the east and northeast, with a dip of $\sim 35^\circ$ that gradually decreases towards the east. The Permian (c) is thus a sheet between *mélange* and overlying blueschist. We could not recognize consistent sense-of-shear indicators on contact zones.

Chapter2

However, we interpret the contacts as thrusts because of parallelism between the unit contacts and foliations within units, as well as top to the S and SW shear indicators within the *mélange*. In our interpretation, thrusting would have stacked the various units (together the “allochthonous”), with highly different metamorphic grade and internal deformation onto the autochthonous basement of Pre-Ordovician to Carboniferous rocks in the west.

The large Gangtang Co Granite truncates the contacts between the various units and is itself undeformed. Intrusion of the granite at 210 ± 5 Ma must, therefore, have post-dated thrusting of the allochthonous units on top of the autochthonous basement.

2.2.5 Deformation of the Tertiary and Cenozoic strata

Terrestrial sediments lie unconformably on all previously mentioned units. Ages range from possibly Cretaceous to Cenozoic ([Kapp et al., 2005](#)). Orientations of the gently folded beds roughly follow the shape of the Qiangtang Culmination, suggesting it grew further during and after the Tertiary red bed deposition. The Tertiary strata are cut by recent normal faults that have a minor sinistral component. These faults are steep and approximately NE-striking. These transtensional faults locally form scarps in Quaternary deposits. One major structure of this generation is the S-shaped, ~ 340 km long Yibuchaca Fault, which extends across the whole area ([Taylor et al., 2003](#)).

3. Geochronology work in central Qiangtang terrane

U–Pb zircon geochronology of three samples of the Qiangtang basement, three samples of the subduction *mélange* and two samples for the high pressure metamorphic rocks were analyzed to determine their provenance and maximum sedimentary ages. Felsic mylonites (RZ-M1 and D823-RZ) and phyllite (RZ-C1) are from the basement. Pelites constituted by quartz, mica and matrix (P13-41), diorite (P13-43) and quartzite (P18-30) belong to the subduction *mélange*. Garnet-bearing mica-quartz schists with intense foliation (P22-16 and P27-31) were sampled from the high-pressure unit. Sample locations are shown in [Fig. 3](#).

3.1 Analytical Methods

U, Th and Pb of all samples except D823-RZ were measured at the LA-ICP-MS Zircon U-Pb Geochronology Experimental Center of China University of Geosciences (Beijing). Samples were processed using conventional magnetic and density techniques to concentrate the non-magnetic, heavy

Chapter 2

minerals before zircons were finally handpicked at the Langfang Geological Experiment Center. Zircon crystals were mounted and then polished to section the crystals for analysis. All zircons were imaged using transmitted and reflected light microscopy, as well as cathodoluminescence (CL) to reveal their internal structure. Before zircon LA-ICP-MS U–Pb isotopic analysis and prior to carbon coating, the surface of the mounts was acid-washed in dilute HNO₃ and pure alcohol to remove any lead contamination.

The instrument couples a quadrupole ICP-MS (Agilent 7500a) and a UP-193 Solid-State laser (193 nm, New Wave Research Inc.) with an automatic positioning system. Laser spot size was set to ~36 µm for analyses, laser energy density at 8.5 J/cm² and repetition rate at 10 Hz. The procedure of laser sampling is 5-s pre-ablation, 20-s sample-chamber flushing and 40-s sampling ablation. The ablated material is carried into the ICP-MS by a high-purity Helium gas stream with a flux of 0.8 L/min. The whole laser path was fluxed with N₂ (15 L/min) and Ar (1.15 L/min) in order to increase energy stability. The counting time for U, Th, ²⁰⁴Pb, ²⁰⁶Pb, ²⁰⁷Pb and ²⁰⁸Pb was 20 ms, and 15 ms for other elements. Calibrations for the zircon analyses were carried out using NIST 610 glass as an external standard and Si as internal standard. U–Pb isotope fractionation effects were corrected using zircon 91500 (Wiedenbeck et al., 1995) as external standard. The ratio of the number of standard zircons to analyzed zircons was 1:10 during the test. Zircon standard TEMORA (417 Ma) from Australia (Black et al., 2003) was also used as a secondary standard to supervise the deviation of age measurement/calculation. Isotopic ratios and element concentrations of zircons were calculated using GLITTER (ver. 4.4, Macquarie University). Concordia ages and diagrams were obtained using Isoplot/Ex (3.0) (Ludwig, 2003). Common lead was corrected using LA-ICP-MS Common Lead Correction (ver. 3.15), following the method of Andersen (2002). The analytical data are given in supplementary data.

The zircon grains of sample D823-RZ were analysed for U, Th and Pb using SHRIMP II at the Beijing SHRIMP Center, Institute of Geology, Chinese Academy of Geological Sciences. Analytical procedures followed those of Williams (1998), and data were processed using the Excel-based Squid and Isoplot programs (Ludwig, 2003). Mass resolution during the analytical sessions was ~5000 (1% definition). Spot sizes were 25–30 µm, and the intensity of the primary O₂[−] ion beam was 4–6 nA. Each spot was rastered for 120–180 s prior to analysis. Data were determined by taking 5 scans on ⁹⁰Zr¹⁶O⁺, ²⁰⁴Pb⁺, background, ²⁰⁶Pb⁺, ²⁰⁷Pb⁺, ²⁰⁸Pb⁺, ²³⁸U⁺, ²³²Th¹⁶O⁺, ²³⁸U¹⁶O⁺. Common Pb corrections were made using the measured ²⁰⁴Pb; uncertainties quoted in the supplementary data are at 1σ, whereas weighted mean ages of individual samples are quoted at the 95% confidence level (2σ).

Low concentration of ^{235}U relative to ^{238}U result in low concentrations of ^{207}Pb in younger zircons, and in substantially larger measurement uncertainty for $^{206}\text{Pb}/^{207}\text{Pb}$. Consequently, the $^{206}\text{Pb}/^{207}\text{Pb}$ ages for younger grains are less precise than the $^{206}\text{Pb}/^{238}\text{U}$ ages. As the expected ages from the basement are <1000 Ma, we preferred to use the $^{206}\text{Pb}/^{238}\text{U}$ ages. Reported crystallization ages of younger (~ 500 Ma) magmatism is generally based on a weighted average of $^{206}\text{Pb}/^{238}\text{U}$ ages for a cluster of concordant analyses. All analytical results are listed in the supplementary data. Random and systematic errors are included in the supplementary data.

3.2 Analytical results

3.2.1 Samples from the Qiangtang basement

RZ-M1 is a felsic mylonite composed of quartz, plagioclase and muscovite with minor biotite from the northern edge of the basement, about 20 km from the Myyigang Ri ([Fig. 3](#)). Excluding five discordia ages, the remaining 35 zircons give a peak age of 464 Ma ([Fig. 8](#)). The average age of the ten youngest zircons is 468 ± 17 Ma ([Fig. 9a](#)). The youngest age from this sample is 468 Ma. Hence, the protolith age of this felsic mylonite is 468 ± 17 Ma. The age of mylonitization is unknown.

Quartzite sample RZ-C1 from alternating phyllites and quartzites has a well-developed foliation defined by sericite and stretched quartz grains. It was collected ~ 10 km north of the Myyigang Ri ([Fig. 3](#)). The age of the youngest zircon, from a population of 83, is 534 Ma, while the mean age of the youngest population is 591 Ma ([Fig. 8](#)), which is taken as the maximum depositional age of the meta-sediment ([Dickinson and Gehrels, 2009](#)).

Sample D823-RZ is from a mylonitic orthogneiss of granitic composition from the central part of the Qiangtang basement ([Fig. 3](#)). It contains stretched quartz grains, feldspar porphyroclasts, and fine-grained muscovite that define the foliation. Minor garnet and tourmaline porphyroclasts are also found. The majority of zircon analyses in this sample are well concordant although there are two discordant analyses of Precambrian age ([Fig. 9b](#)). Thirteen concordant analyses give an average age of 472 ± 3.4 Ma, which is assumed to represent the protolith age.

3.2.2 Samples from the subduction mélange

Argillite sample P18-30 comes from an extensive exposure of subduction mélange near the northern edge of the mélange area ([Fig. 3](#)). All 72 zircon grains analyzed from this sample are of sufficient quality to be

included in the age spectrum. This sample yielded a spectrum with many different peaks in the Neoproterozoic and early Paleozoic, including strong peaks at 535 Ma, 903 Ma and ~ 1487 Ma (Fig. 8). There is a group of ages at ~ 2500 Ma and the oldest age is 3278 Ma. The mean age, 535 Ma, of the youngest population is taken as the maximum depositional age of this sample.

Sandstone sample P13-41 is from a layer located 10 km north of Rongma (Fig. 3). A total of 26 zircons from this sandstone were analyzed and 19 of these passed the minimum requirements to be used in the age spectrum. The age spectrum for this sample has two prominent peaks at 621 Ma and 976 Ma, with another peak at 1622 Ma (Fig. 8). There is a small peak at 742 Ma and a scattering of ages between 1800 Ma and 2300 Ma. There is only one Archean age at 2850 Ma. The youngest zircon population gives a maximum depositional age of 621 Ma.

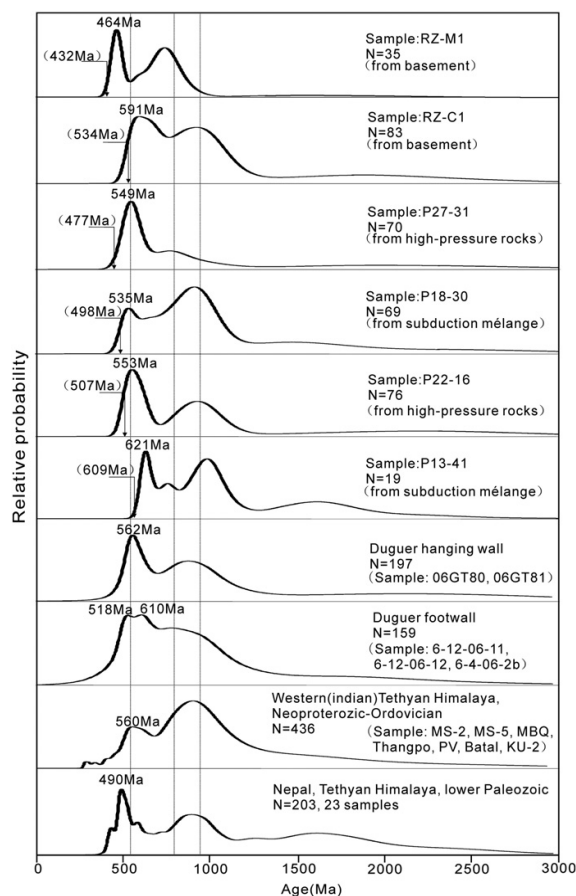


Fig. 8. Detrital zircon U-Pb age spectra for Qiangtang basement, high-pressure rocks and subduction mélange, compared with the spectra from other Himalayan-Tibetan terranes, namely Lower Paleozoic Tethyan Himalaya from Myrow et al. (2010), Neoproterozoic to Ordovician Western Tethyan Himalaya from DeCelles et al. (2000), and the South Qiangtang Duguer Range from Pullen et al. (2011). Age spectra are plotted as relative probability curves, which were made by fitting normal distributions to the zircon apparent ages and their corresponding 2σ errors. The same procedure was applied to the original data provided by Myrow et al. (2010), DeCelles et al. (2000) and Pullen et al. (2011). The ages of the youngest peaks are provided, as well as the age of the youngest zircon apparent ages were used, as our main interest is in Phanerozoic ages. When multiple spot analyses were obtained on a single zircon (from Qiangtang meta-sandstones), only the most concordant result was plotted. “N” is the number of individual zircon analyses. The arrow shows the youngest zircon age in each sample.

Sample P13-43 is a diorite located near P13-41 (Fig. 3). It is composed largely of plagioclase, K-feldspar and biotite with minor quartz and amphibole. The analyses from 18 zircons for this sample yielded a crystallization age of 280 ± 15 Ma. Four ~500 Ma ages are interpreted as inherited zircon ages (Fig. 9c).

Samples P22-16 and P27-31 are from high-pressure units in the center of the mapping area ([Fig. 3](#)). They are largely composed of quartz, muscovite and garnets. They have a well-developed banding defined by layers of quartz and aligned muscovite and garnet-rich layers. There were a total of 146 valid analyses that were used in the age spectrum (supplementary data). The resulting age spectrum has two broad, overlapping peaks at ~ 550 Ma and ~ 990 Ma (P22-16 only). The maximum depositional age of these high-metamorphic grade rocks is estimated as less than ~ 550 Ma.

4. Discussion

The Qiangtang terrane, one of the largest units of the Tibetan plateau, forms the largest exposure of metamorphic rocks, including eclogites, in the interior of the Tibet. Understanding the character and origin of these rocks is crucial to constrain the tectonic evolution of Central Tibet. Of particular interest is the controversial question whether autochthonous basement is exposed in the area ([Li et al., 1995, 2006](#)) or that *mélange* was thrust underneath Paleozoic crust and now exposed by subsequent doming under a flat-lying detachment ([Kapp et al., 2000](#)). In the following, we discuss the evidence for the presence of basement in the South Qiangtang terrane and its relationship to other terranes. Recognition of autochthonous basement and its relationship with the overlying subduction *mélange* helps to clarify the formation and origin of this *mélange*.

4.1 The existence of the Qiangtang basement

The large area of exposed metamorphic rocks with different lithologies, metamorphic grades and deformation characteristics has led to ongoing debate on the question whether there is basement, or not, in the Qiangtang terrane. The central Qiangtang metamorphic rocks were initially interpreted to be Paleozoic basement of the Qiangtang terrane, as it was mapped to be unconformably overlain by Devonian and younger strata ([Cheng and Xu, 1986](#)) and as indicated by geochronology by [Dong et al. \(2011\)](#) and [Wang and Wang \(2001\)](#). However, the central Qiangtang metamorphic *mélange* must be younger than early Paleozoic, because it includes metasedimentary strata with Carboniferous to Late Triassic fossils ([Kapp et al., 2003b; Li and Zheng, 1993](#)).

Our detailed mapping provides evidence for the presence of basement in the south Qiangtang terrane. Four distinct units, the Qiangtang basement, the Ordovician slate and the Carboniferous sandstone, the subduction *mélange* and the upper most Paleo-Mesozoic sediments could be defined in the central Qiangtang metamorphic belt ([Fig. 3](#)). Evidence for the existence of the Qiangtang basement includes: (1) the basement is composed mainly of quartzite, phyllite and minor mylonite, which is distinctly different

from the subduction mélangé that includes abundant mafic lenses and limestone, although both units show similar metamorphic grade, except for the high-pressure units in the mélangé. (2) The foliation Sb2 overprints cleavage Sb1 (Fig. 5c, d, e) and is pervasive throughout the whole area (Fig. 3). However, no correlation could be found between the strong Sm1 in the subduction mélangé and Sb2. Contrary to the basement, the subduction mélangé experienced intensive non-coaxial shear with structures such as sigma clasts and boudinage. (3) The Mid–Late Ordovician and Carboniferous strata are found to unconformably overlie the basement. These units only share the second basement deformation event (Sb2) (Figs. 5a, b, 6a, c). (4) The basement was intruded by a 472 ± 3.4 Ma granite, which is older than the Permian to Late Triassic mélangé.

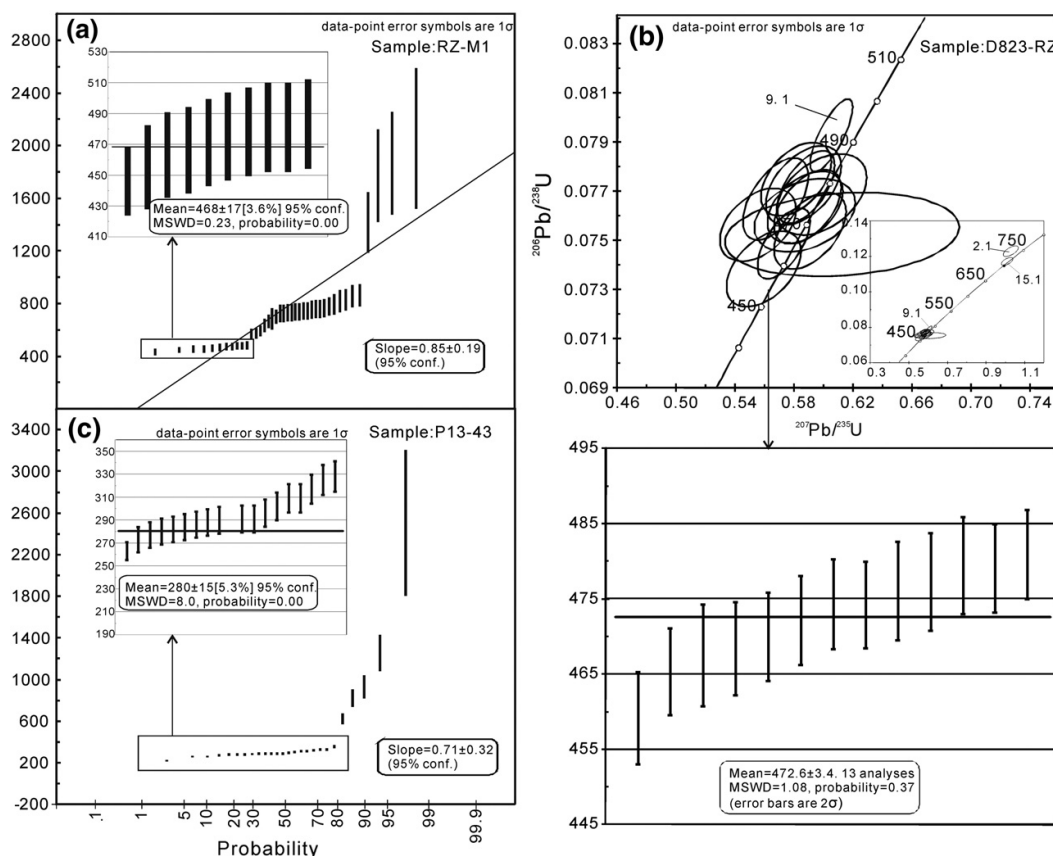


Fig. 9. Concordia plots of U–Pb ion microprobe single spot analyses (error ellipses are 1σ) of zircon from mylonites RZ-M1 (a) and D823-RZ (b) and diorite P13-43 (c). The minimum average ages of the three samples are 468 ± 17 Ma, 472.6 ± 3.4 Ma and 280 ± 15 Ma, respectively.

4.2 Age of the Qiangtang basement

Fossils were not found within the basement. The age of the basement is thus determined with geochronology and the relationship with the overlying Ordovician slates. The youngest zircon from a

basement quartzite (sample RZ-C1) is 534 Ma and the mean of the youngest age population of this sample 591 Ma ([Fig. 8](#)), so the maximum deposition age of basement is Cambrian or Late Precambrian. Two ~ 470 Ma felsic orthogneiss samples ([Fig. 9a, b](#)) show that the basement was intruded by felsic magma before the Middle Ordovician. This pre- 470 Ma age of the basement is also consistent with the unconformity between the basement and the Middle to Late Ordovician strata.

Two other exposures of basement in Qiangtang terrane are the Gangma Co Gneiss ([Kapp et al., 2000](#)) and the Duguer Range ([Pullen et al., 2011](#)). U–Pb ages of zircons from the Gangma Co Gneiss range from 419 to 556 Ma ([Kapp et al., 2000](#)) and from 476 to 471 Ma in the Duguer orthogneisses, which is similar to our results ([Fig. 8](#)). Other basement rocks of the Tibetan Plateau have been documented in many papers ([Zhu et al., 2012](#), and reference therein). To the south of the Qiangtang terrane, the younger suite of the Amdo Orthogneiss intruded the older basement between 540 and 460 Ma ([Guynn et al., 2012](#)). One granite in the central Lhasa terrane ([Fig. 1](#)), which is unconformably overlain by low-grade Paleozoic strata, yielded a U–Pb zircon age of 509 Ma ([Gehrels et al., 2011](#)). In the Himalayan Orogen, south of the Indus–Yarlung Suture ([Fig. 1](#)), orthogneisses of the Greater Himalayan zone have yielded ages ranging from ca. 500 to 480 Ma ([DeCelles et al., 2000](#)), whereas granites intruding this lithotectonic zone have ages of 480–472 Ma ([Gehrels et al., 2003](#)). All these data suggest the prevalence of Cambrian–Ordovician basement underlying vast areas of the Tibetan Orogen.

4.3 The origin of the south Qiangtang Early Paleozoic basement

[Pullen et al. \(2011\)](#) show that detrital zircons from the North and South Qiangtang terranes and the Duguer Range, ca. 100 km west of our study area, all have similar age spectra, with primary peaks at ca 550, 800 and 950 Ma, which is comparable with our sample RZ-C1 ([Fig. 8](#)). These age spectra are also similar to those from the Lhasa and the Himalaya terranes ([Fig. 8](#)). This similarity in zircon age spectra implies that the Qiangtang terrane was contiguous with the Lhasa and Himalayan terranes along the northern margin of Gondwana during early Paleozoic times ([Gehrels et al., 2006](#); [Kapp et al., 2003b](#); [Pullen et al., 2011](#)). Most Gondwana reconstructions place the Lhasa and Qiangtang terranes at the northern edge of India ([Guynn et al., 2012](#); [Metcalf, 1996](#); [Torsvik and Smethurst, 1999](#)), although some authors place the Lhasa terrane adjacent to the northern margin of Australia ([Zhu et al., 2011](#)). The unconformity between the Ordovician strata and the basement is also observed in the Himalaya ([Gehrels et al., 2003](#)) and Lhasa terrane ([Zhu et al., 2012](#)), which confirms that the Qiangtang terrane was part of the Gondwana supercontinent at least until Late Ordovician times. The Qiangtang terrane must thus have separated from Gondwana later than the Late Ordovician.

[Cawood et al. \(2007\)](#) proposed the Bhimphedian Orogeny, which can be related to Andean-style orogenesis in response to the final assembly of Gondwana at the northern margin of the Indian continent in the Early Paleozoic. This orogenic event is not related to the Pan- African Orogeny, which is driven by continent–continent collision during Gondwana assembly, but rather occurs on the margin of Gondwana. After their >591 Ma deposition, the Qiangtang basement rock experienced Db1 and formed Sb1, which may be in response to the southward subduction of the Proto-Tethys ([Gehrels et al., 2006](#)). In the Himalaya area, metamorphism occurred around 490–480 Ma, soon after the end of deposition at 510–500 Ma. Granite formation and emplacement were largely post-tectonic and occurred at 480–470 Ma ([Cawood et al., 2007](#)). We envisage that our granite intruded at ~470 Ma in a similar setting. This was followed by erosion and renewed sedimentation in a passive margin setting in the Ordovician ([Gehrels et al., 2006](#)).

4.4 Origin of the subduction mélangé

Detrital zircons from the garnet-bearing phengite schist (samples P22-16 and P27-31) and from the low-grade mélangé (P18-30 and P13-41) have age spectra similar to those of the Early Paleozoic basement ([Fig. 8](#)). The provenance of these rocks is thus inferred to be this basement, in accordance with [Pullen et al. \(2011\)](#). Tectonic erosion of the Qiangtang basement would have been the main source for material in the subduction mélangé, which itself is younger. The 280 ± 15 Ma gabbro sample P13-43 shows this, as well as fossil evidence ([Li and Zheng, 1993](#)). These younger ages are consistent with Late Triassic exhumation of the mélangé as already proposed by [Zhai et al. \(2011\)](#).

[Kapp et al. \(2000, 2003b\)](#) argued that the mélangé was underthrust southward beneath the entire Gondwana-affinity Qiangtang terrane by low-angle subduction of Paleo-Tethys oceanic lithosphere along the Jinsha suture in the north ([Fig. 2b](#)) during Paleozoic–Mesozoic closure of the Paleo-Tethys ocean. The mélangé, initially below the basement, was subsequently exhumed as metamorphic core complexes. This model is contrary to our mapping, which shows that the mélangé overlies the Paleozoic basement and Ordovician to Carboniferous slates ([Fig. 4a,b](#)), which are exposed to the west of the Rongma village ([Fig. 3](#)). In the intra-Qiangtang suture model ([Li, 1987; Zhai et al., 2011](#)), the Longmu Co–Shuanghu Suture Zone divides the Qiangtang terrane into a northern and southern part ([Fig. 1](#)). In this scenario, the subduction mélangé is derived, probably by tectonic erosion, from the overriding North Qiangtang terrane. The North and South Qiangtang terranes were connected until Carboniferous times ([Zhai et al., 2009](#)). Zircon age spectra in both terranes are therefore the same ([Pullen et al., 2011](#)) and the similarity with spectra in the mélangé can therefore not be used to distinguish between southward subduction below a

Chapter 2

single Qiangtang terrane or northward subduction beneath the Northern Qiangtang terrane, as proposed here.

Our observations are in support of the model where the subduction mélangé was thrust over Paleozoic crustal rocks of Gondwana affinity. The large scale, 3D model of the central area ([Fig. 4b](#)) shows that mélangé and Permian rocks form a stack of east-dipping sheets, contrary to the interpretation of [Kapp et al. \(2000, 2003b\)](#) that the late Paleozoic rocks are on top of a flat-lying detachment. Furthermore, the detachment model ([Fig. 6a of Kapp et al., 2003b](#)) is based on the rocks above the detachment west and east of Rongma village to all be of the same (Carboniferous) age. Our mapping shows this not to be the case, which casts further doubt on the existence of the detachment and underthrusting of the mélangé. Finally, the underthrusting model requires exhumation of the mélangé from >35 km ([Kapp et al., 2003b](#)). Although the mélangé contains blueschist and even eclogite-facies rocks, large parts of the mélangé are of low metamorphic grade. Based on our observations, we summarize the geological history of the area in the discussion that follows ([Fig. 10](#)).

The age of the Paleozoic basement (QB) is at the most the very latest Precambrian. Db1 deformation produced the first tectonic foliation (Sb1) and the basement was intruded by granites around 472 Ma. Middle to Late Ordovician slates and Carboniferous sand-siltstones (OC) unconformably overlie the basement. All three units experienced Db2 deformation and were intruded by the Middle Permian gabbro swarms. These units together form the Paleozoic autochthonous basement.

Permian sediments were deposited on the margins of the North and South Qiangtang terranes, which were separated by the Paleo-Tethys since no later than Carboniferous times ([Zhai et al., 2013](#)). Closure of this ocean by northward subduction ([Li et al., 2006](#)) led to the formation of the subduction mélangé and high-pressure rocks, which were exhumed during the Late Triassic ([Zhai et al., 2011](#)). Details of the exhumation mechanism are beyond the scope of this paper, but in accordance with [Beaumont et al. \(2009\)](#), [Warren et al. \(2008\)](#) and others we suggest that this may have occurred in the subduction channel between the subducting oceanic plate and the overlying North Qiangtang continental crust. This is consistent with the mélangé containing rocks with a continental-crust and oceanic-plate affinity. Upon closure of the suture, Permian sediments, low-pressure mélangé and high-pressure rocks were thrust towards the south to southwest to form an allochthonous thrust stack on top of the South Qiangtang Paleozoic autochthonous basement. Intrusion of the ~ 210 Ma Gangtang Co granite postdates thrusting and is thus set in a late- to post-tectonic environment. Most Late Triassic intrusions and volcanics are found north of the Longmu Co–Shuanghu Suture Zone, consistent with northward subduction ([Zhai et al., 2012](#); [Zhang](#)

et al., 2011). That the Gangtang Co granite intruded into South Qiangtang crust could be related to slab break-off (Zhang et al., 2011). At the time of intrusion of the Gangtang Co granite, sedimentation commenced again in the south of the study area, possibly in a flexural foreland basin related to the thrust stack north of it.

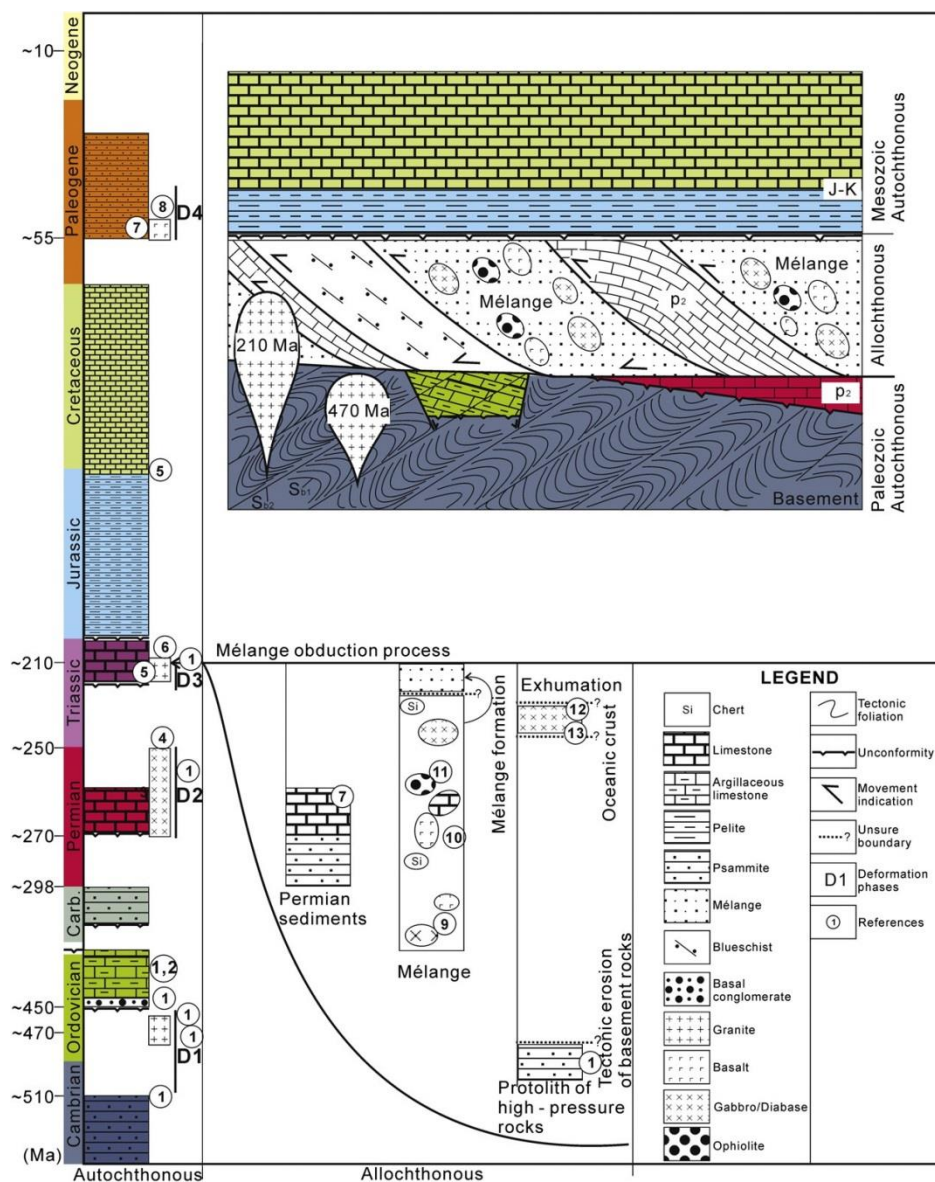


Fig. 10. Summary of the Paleozoic to early Mesozoic tectonic evolution of the South Qiangtang terrane. Left column: stratigraphic column of autochthonous units. Allochthonous units (Permian sediments, subduction mélangé and high-pressure rocks) were obducted onto the Paleozoic autochthonous in Late Triassic times. Early Ordovician D1 represents the earliest granodiorite found in the South Qiangtang terrane, approximately coeval with the first deformation event that formed Sb1. Permian gabbro (D2) records the rifting between the North and South Qiangtang terranes. Magmatic activity (granite intrusions, D3) marks the latest stages of the subduction and following collision

between the North and South Qiangtang terranes. Early Paleogene basalts (D4) formed during convergence between the Indian and Eurasian continents. The simplified tectonic-evolution sketch of the south Qiangtang basement shows that the allochthonous Triassic subduction mélangé, including high-pressure rocks and overlying Permian sediments, was obducted southwards onto the South Qiangtang basement. Post-collisional Jurassic to Cretaceous sediments form a second, Mesozoic autochthonous series. Numbers refer to references: (1) this paper; (2) [Li \(2006\)](#); (3) [Zhang et al. \(2012\)](#); (4) [Zhai et al. \(2009\)](#); (5) [Zeng et al. \(2002\)](#); (6) [Kapp et al. \(2003a,b\)](#); (7) [Dai et al. \(2012\)](#); (8) Unpublished data; (9) [Zhai et al. \(2010\)](#); (10) [Zhai et al. \(2013\)](#); (11) [Zhai et al. \(2006\)](#); (12) [Zhai et al. \(2011\)](#); (13) [Zhang et al. \(2006a,b\)](#).

After collision between the South and North Qiangtang terranes, the entire Qiangtang terrane became more stable. Jurassic and Cretaceous sediments were deposited on top of the allochthonous after closure of the suture, forming the Mesozoic autochthonous. North dipping reverse faults in the south Qiangtang terrane may represent the collision stage between the Lhasa and amalgamated Qiangtang terranes and may have caused exhumation of the Qiangtang basement in the Qiangtang culmination.

5. Conclusions

Detailed lithological and structural mapping in the South Qiangtang terrane allowed the definition of three main units in the area: (1) the Paleozoic autochthonous basement of the Qiangtang terrane, (2) the Mesozoic allochthonous with subduction mélangé, from low- to eclogite-facies metamorphic grade, and thrust sheets of Permian sediments, and (3) the overlying Mesozoic autochthonous of Jurassic to Cretaceous sediments.

Detrital zircons and dating of orthogneisses constrain the age of the basement between ~ 591 and 470 Ma. The basement is unconformably overlain by Ordovician slates with a basal conglomerate and Carboniferous sand- and siltstones. Similarity with the Lhasa and Himalaya areas suggests that the Paleozoic autochthonous basement was part of the northern margin of Gondwana during the Early Paleozoic ([Cawood et al., 2007](#); [Pullen et al., 2011](#); [Zhu et al., 2012](#)).

Two radically different models have been proposed for the Mesozoic tectonics of the Qiangtang area: the intra-Qiangtang suture model with northward subduction ([Li, 1987](#); [Zhai et al., 2011](#)) and the underthrust model with southward subduction ([Kapp et al., 2000, 2003b](#); [Pullen et al., 2011](#)). A crucial difference between the two models is that basement should structurally underlie the mélangé in the first model, and overlie it in the second. According to our mapping, the subduction mélangé and thrust sheets of Permian sediments overlie the Paleozoic autochthonous basement, which provides strong new evidence for the

Chapter2

intra-Qiangtang suture model. In this model, the Paleo-Tethys subduction mélange and Permian sediments were thrust (~100 km) onto the south Qiangtang terrane during convergence between the South and North Qiangtang terranes in the Late Triassic. Our findings in a small part of the Qiangtang terrane will not end the controversy on the Mesozoic evolution of the area. More detailed stratigraphic and structural mapping of the whole area will be needed to settle the debate and answer the question how the high-pressure rocks were exhumed.

Acknowledgement

This research was funded by the China Geological Survey (CGS) through the 1:50,000 regional geological surveys in the Qomo Ri, Gangmari, and Rongma areas of Tibet as well as project 1212011121271, entitled “Tectonic attributes of the South Qiangtang Mesozoic–Cenozoic basin, based on deformation and metamorphic character”. It was also supported by the project named “Tectonic framework and orogeny of Qiangtang–East Tibet terrane in central Tibetan plateau”. Meanwhile, we appreciate the Program for Changjiang Scholars and Innovative Research Team in University (IRT1083). Z.Z. thanks the Chinese Scholarship Council for financial support (2011640017). We thank A. Soesoo and M.A. Elburg for their advice and P. Kapp for a critical, but helpful review.

Appendix A. Supplementary data to this article can be found online at <http://dx.doi.org/10.1016/j.tecto.2014.03.016>.

References

- Andersen, T., 2002. Correction of common lead in U–Pb analyses that do not report ²⁰⁴Pb. *Chem. Geol.* 192, 59–79.
- Beaumont, C., Jamieson, R., Butler, J., Warren, C., 2009. Crustal structure: a key constraint on the mechanism of ultra-high-pressure rock exhumation. *Earth Planet. Sci. Lett.* 287, 116–129.
- Black, L.P., Kamo, S.L., Allen, C.M., Aleinikoff, J.N., Davis, D.W., Korsch, R.J., Foudoulis, C., 2003. TEMORA 1: a new zircon standard for Phanerozoic U–Pb geochronology. *Chem. Geol.* 200, 155–170.
- Cawood, P.A., Johnson, M.R., Nemchin, A.A., 2007. Early Palaeozoic orogenesis along the Indian margin of Gondwana: tectonic response to Gondwana assembly. *Earth Planet. Sci. Lett.* 255, 70–84.
- Cheng, J., Xu, G., 1986. Geologic map of the Gaize region with report: Tibetan Bureau of Geology and Mineral Resources. 369 pp. Chinese .
- Dai, J., Zhao, X., Wang, C., Zhu, L., Li, Y., Finn, D., 2012. The vast proto-Tibetan Plateau: new constraints from Paleogene Hoh Xil Basin. *Gondwana Res.* 22, 434–446.
- DeCelles, P., Gehrels, G., Quade, J., LaReau, B., Spurlin, M., 2000. Tectonic implications of U–Pb zircon ages of the Himalayan orogenic belt in Nepal. *Science* 288, 497–499.

Chapter2

- Deng, X.W., Tao, P., Mou, S.Y., 2005. Geological map of the Dinggu area (Scale at 1: 250,000): Guizhou Institute of Geological Survey.
- Dewey, J.F., Shackleton, R.M., Chengfa, C., Yiyin, S., 1988. [The tectonic evolution of the Tibetan Plateau. Philosophical Transactions of the Royal Society of London. Series A. Math. Phys. Sci. 327, 379–413.](#)
- Dickinson, W.R., Gehrels, G.E., 2009. [Use of U–Pb ages of detrital zircons to infer maximum depositional ages of strata: a test against a Colorado Plateau Mesozoic database. Earth Planet. Sci. Lett. 288, 115–125.](#)
- Dong, C.Y., Li, C., Wan, Y.S., Wang, W., Wu, Y.W., Xie, H.Q., Liu, D.Y., 2011. [Detrital zircon age model of Ordovician Wenquan quartzite south of Lungmuco–Shuanghu Suture in the Qiangtang area, Tibet: constraint on tectonic affinity and source regions. Sci. China. Earth Sci. 54, 1034–1042.](#)
- Freymueller, J.T., 2011. [Earth science: a new mechanical model for Tibet. Nature 472, 48–49.](#)
- Gehrels, G., DeCelles, P., Martin, A., Ojha, T., Pinhassi, G., Upreti, B., 2003. [Initiation of the Himalayan orogen as an early Paleozoic thin-skinned thrust belt. GSA Today 13, 4–9.](#)
- Gehrels, G., DeCelles, P., Ojha, T., Upreti, B., 2006. [Geologic and U–Th–Pb geochronologic evidence for early Paleozoic tectonism in the Kathmandu thrust sheet, central Nepal Himalaya. Geol. Soc. Am. Bull. 118, 185–198.](#)
- Gehrels, G., Kapp, P., DeCelles, P., Pullen, A., Blakey, R., Weislogel, A., Ding, L., Guynn, J., Martin, A., McQuarrie, N., 2011. [Detrital zircon geochronology of pre-Tertiary strata in the Tibetan–Himalayan orogen. Tectonics 30, TC5016.](#)
- Guynn, J.H., Kapp, P., Pullen, A., Heizler, M., Gehrels, G., Ding, L., 2006. [Tibetan basement rocks near Amdo reveal “missing” Mesozoic tectonism along the Bangong suture, central Tibet. Geology 34, 505–508.](#)
- Guynn, J., Kapp, P., Gehrels, G.E., Ding, L., 2012. [U–Pb geochronology of basement rocks in central Tibet and paleogeographic implications. J. Asian Earth Sci. 43, 23–50.](#)
- Haines, S.S., Klemperer, S.L., Brown, L., Jingru, G., Mechie, J., Meissner, R., Ross, A., Wenjin, Z., 2003. [INDEPTH III seismic data: from surface observations to deep crustal processes in Tibet. Tectonics 22, 1001.](#)
- Kapp, P., Yin, A., Manning, C.E., Murphy, M., Harrison, T.M., Spurlin, M., Lin, D., Xi-Guang, D., Cun-Ming, W., 2000. [Blueschist-bearing metamorphic core complexes in the Qiangtang block reveal deep crustal structure of northern Tibet. Geology 28, 19–23.](#)
- Kapp, P., Murphy, M.A., Yin, A., Harrison, T.M., Ding, L., Guo, J., 2003a. [Mesozoic and Cenozoic tectonic evolution of the Shiquanhe area of western Tibet. Tectonics 22, TC1029.](#)
- Kapp, P., Yin, A., Manning, C.E., Harrison, T.M., Taylor, M.H., Ding, L., 2003b. [Tectonic evolution of the early Mesozoic blueschist-bearing Qiangtang metamorphic belt, central Tibet. Tectonics 22, 1043–1068.](#)
- Kapp, P., Yin, A., Harrison, T.M., Ding, L., 2005. [Cretaceous–Tertiary shortening, basin development, and volcanism in central Tibet. Bull. Geol. Soc. Am. 117, 865–878.](#)
- Kapp, P., DeCelles, P.G., Gehrels, G.E., Heizler, M., Ding, L., 2007. [Geological records of the Lhasa–Qiangtang and Indo-Asian collisions in the Nima area of central Tibet. Geol. Soc. Am. Bull. 119, 917–932.](#)
- Leier, A.L., Kapp, P., Gehrels, G.E., DeCelles, P.G., 2007. [Detrital zircon geochronology of Carboniferous–Cretaceous strata in the Lhasa terrane, Southern Tibet. Basin Res. 19, 361–378.](#)

Chapter2

- Li, C., 1987. [The Longmu Co-Shuanghu–Lancangjiang Suture as the northern boundary of the Gondwanaland in the Carboniferous and Permian. Bull. Changchun Coll. Geol. Sci. 17, 155–166.](#)
- Li, C., 2006. Geological map of the Myyi Gang Ri area (Scale at 1:250,000): University of Jilin Region Institute of Geological Survey.
- Li, C., Zheng, A., 1993. [Paleozoic stratigraphy in the Qiangtang region of Tibet: relations of the Gondwana and Yangtze continents and ocean closure near the end of the Carboniferous. Int. Geol. Rev. 35, 797–804.](#)
- Li, C., Cheng, L., Hu, K., Yang, Z., Hong, Y., 1995. [Study on the Paleo-Tethys suture zone of Lungmu Co-Shuanghu. Tibet. Geol. Publ. House, Beijing.](#)
- Li, C., Zhai, Q., Dong, Y., Huang, X., 2006. Discovery of eclogite and its geological significance in Qiangtang area, central Tibet. [Chin. Sci. Bull. 51, 1095–1100.](#)
- Li, C., Zhai, Q., Dong, Y., Zeng, Q., Huang, X., 2007. [Longmu Co–Shuanghu plate suture and evolution records of Paleo-Tethyan oceanic in Qiangtang area, Qinghai–Tibet plateau. Front Earth Sci. Chin. 1, 257–264.](#)
- Li, C., Zhai, Q., Dong, Y., Liu, S., Xie, C., Wu, Y., 2009. [High-pressure eclogite–blueschist metamorphic belt and closure of Paleo-Tethys Ocean in Central Qiangtang, Qinghai–Tibet plateau. J. Earth Sci. 20, 209–218.](#)
- Liang, X., Wang, G., Yuan, G., Liu, Y., 2012. [Structural sequence and geochronology of the Qomo Ri accretionary complex, Central Qiangtang, Tibet: implications for the Late Triassic subduction of the Paleo-Tethys Ocean. Gondwana Res. 22, 470–481.](#)
- Liu, Y., Santosh, M., Zhao, Z.B., Niu, W.C., Wang, G.H., 2011. [Evidence for palaeo-Tethyan oceanic subduction within central Qiangtang, northern Tibet. Lithos 127, 39–53.](#)
- Ludwig, K., 2003. [User's Manual for Isoplot 3.00: A Geochronological Toolkit for Microsoft Excel. Kenneth R. Ludwig.](#)
- Metcalf, I., 1996. [Gondwanaland dispersion, Asian accretion and evolution of eastern Tethys. Aust. J. Earth Sci. 43, 605–623.](#)
- Myrow, P.M., Hughes, N.C., Goodge, J.W., Fanning, C.M., Williams, I.S., Peng, S., Bhargava, O.N., Parcha, S.K., Pogue, K.R., 2010. [Extraordinary transport and mixing of sediment across Himalayan central Gondwana during the Cambrian–Ordovician. Geol. Soc. Am. Bull. 122, 1660–1670.](#)
- Nie, S., Yin, A., Rowley, D.B., Jin, Y., 1994. [Exhumation of the Dabie Shan ultra-high-pressure rocks and accumulation of the Songpan–Ganzi flysch sequence, central China. Geology 22, 999–1002.](#)
- Pullen, A., Kapp, P., Gehrels, G.E., Vervoort, J.D., Ding, L., 2008. [Triassic continental subduction in central Tibet and Mediterranean-style closure of the Paleo-Tethys Ocean. Geology 36, 351–354.](#)
- Pullen, A., Kapp, P., Gehrels, G.E., Ding, L., Zhang, Q., 2011. [Metamorphic rocks in central Tibet: lateral variations and implications for crustal structure. Bull. Geol. Soc. Am. 123, 585–600.](#)
- Tapponnier, P., Zhiqin, X., Roger, F., Meyer, B., Arnaud, N., Wittlinger, G., Jingsui, Y., 2001. [Oblique stepwise rise and growth of the Tibet Plateau. Science 294, 1671–1677.](#)
- Taylor, M., Yin, A., Ryerson, F.J., Kapp, P., Ding, L., 2003. [Conjugate strike-slip faulting along the Bangong–Nujiang suture zone accommodates coeval east–west extension and north–south shortening in the interior of the Tibetan Plateau. Tectonics 22, 1044.](#)

Chapter2

- Torsvik, T.H., Smethurst, M.A., 1999. [Plate tectonic modelling: virtual reality with GMAP](#). *Comput. Geosci.* 25, 395–402.
- Turner, S., Sandiford, M., Flöttmann, T., Foden, J., 1994. [Rb/Sr dating of differentiated cleavage from the upper Adelaidean metasediments at Hallett Cove, southern Adelaide fold belt](#). *J. Struct. Geol.* 16, 1233–1241.
- Wang, G., Wang, C., 2001. [Disintegration and age of basement metamorphic rocks in Qiangtang, Tibet, China](#). *Sci. China. Ser. D Earth Sci.* 44, 86–93.
- Warren, C.J., Beaumont, C., Jamieson, R.A., 2008. [Deep subduction and rapid exhumation: role of crustal strength and strain weakening in continental subduction and ultrahigh-pressure rock exhumation](#). *Tectonics* 27, 1–28.
- Wiedenbeck, M., Alle, P., Corfu, F., Griffin, W., Meier, M., Oberli, F., Quadt, A., Roddick, J., Spiegel, W., 1995. [Three natural zircon standards for U–Th–Pb, Lu–Hf, trace element and REE analyses](#). *Geostand. Newslett.* 19, 1–23.
- Williams, I., 1998. [U–Th–Pb geochronology by ion microprobe](#). *Rev. Econ. Geol.* 7, 1–35.
- Xu, R.H., Schärer, U., Allègre, C.J., 1985. [Magmatism and metamorphism in the Lhasa block \(Tibet\): a geochronological study](#). *J. Geol.* 93, 41–57.
- Yin, A., Harrison, T.M., 2000. [Geologic evolution of the Himalayan–Tibetan orogen](#). *Annu. Rev. Earth Planet. Sci.* 28, 211–280.
- Yin, A., Nie, S., 1996. [A Phanerozoic palinspastic reconstruction of China and its neighboring regions](#). In: Yin, Harrison, T.M. (Eds.), *World and Regional Geology*. Cambridge Univ. Press, New York, pp. 442–485.
- Zeng, Q.G., Mao, G.Z., Chen, G.R., 2002. Geological map of the Ri Gang Pei Co area (Scale at 1:250,000): Tibet Autonomous Region Institute of Geological Survey.
- Zeng, Q.G., Mao, G.Z., Chen, G.R., 2006. Geological map of the Gai Ze area (Scale at 1: 250,000): Tibet Autonomous Region Institute of Geological Survey.
- Zhai, Q.G., Li, C., Cheng, L., Zhang, Y., 2004. [Geological features of Permian ophiolite in the Jiaomuri area, Qiangtang, Tibet, and its tectonic significance](#). *Reg. Geol. China* 23, 1228–1229.
- Zhai, Q.G., Li, C., Huang, X.p., 2006. [Geochemistry of Permian basalt in the Jiaomuri area, central Qiangtang, Tibet, China, and its tectonic significance](#). *Geol. Bull. China* 25, 1419–1427.
- Zhai, Q.G., Li, C., Huang, X.P., 2007. [The fragment of Paleo-Tethys ophiolite from central Qiangtang, Tibet: geochemical evidence of metabasites in Guoganjianian](#). *Sci. China Ser. D Earth Sci.* 50, 1302–1309.
- Zhai, Q.G., Li, C., Wang, J., Ji, Z.S., Wang, Y., 2009. [SHRIMP U–Pb dating and Hf isotopic analyses of zircons from the mafic dyke swarms in central Qiangtang area, Northern Tibet](#). *Chin. Sci. Bull.* 54, 2279–2285.
- Zhai, Q.G., Wang, J., Li, C., Su, L., 2010. [SHRIMP U–Pb dating and Hf isotopic analyses of Middle Ordovician meta-cumulate gabbro in central Qiangtang, northern Tibetan Plateau](#). *Sci. China. Earth Sci.* 53, 657–664.
- Zhai, Q.G., Jahn, B.M., Zhang, R.Y., Wang, J., Su, L., 2011. [Triassic subduction of the Paleo-Tethys in northern Tibet, China: evidence from the geochemical and isotopic characteristics of eclogites and blueschists of the Qiangtang Block](#). *J. Asian Earth Sci.* 42, 1356–1370.

Chapter2

- Zhai, Q.G., Jahn, B., Su, L., Wang, J., Mo, X.X., Lee, H., Wang, K., Tang, S., 2012. [Triassic arc magmatism in the Qiangtang area, northern Tibet: Zircon U–Pb ages, geochemical and Sr–Nd–Hf isotopic characteristics, and tectonic implications. J. Asian Earth Sci. 63, 162–178.](#)
- Zhai, Q.G., Jahn, B.M., Wang, J., Su, L., Mo, X.X., Wang, K.L., Suohan, T., Lee, H.Y., 2013. [The Carboniferous ophiolite in the middle of the Qiangtang terrane, Northern Tibet: SHRIMP U–Pb dating, geochemical and Sr–Nd–Hf isotopic characteristics. Lithos 168, 186–199.](#)
- Zhang, K.J., Cai, J.X., Zhang, Y.X., Zhao, T.P., 2006a. [Eclogites from central Qiangtang, northern Tibet \(China\) and tectonic implications. Earth Planet. Sci. Lett. 245, 722–729.](#)
- Zhang, K.J., Zhang, Y.X., Li, B., Zhu, Y.T., Wei, R.Z., 2006b. [The blueschist-bearing Qiangtang metamorphic belt \(northern Tibet, China\) as an in situ suture zone: evidence from geochemical comparison with the Jinsa suture. Geology 34, 493–497.](#)
- Zhang, K.J., Tang, X.C., Wang, Y., Zhang, Y.X., 2011. [Geochronology, geochemistry, and Nd isotopes of early Mesozoic bimodal volcanism in northern Tibet, western China: constraints on the exhumation of the central Qiangtang metamorphic belt. Lithos 121, 167–175.](#)
- Zhang, Y., Shen, S., Shi, G., Wang, Y., Yuan, D., 2012. [Tectonic evolution of the Qiangtang Block, northern Tibet during Late Cisuralian \(Late Early Permian\): evidence from fusuline fossil records. Palaeogeogr. Palaeoclimatol. Palaeoecol. 350, 139–148.](#)
- Zhu, D.C., Zhao, Z.D., Niu, Y., Dilek, Y., Mo, X.X., 2011. [Lhasa terrane in southern Tibet came from Australia. Geology 39, 727–730.](#)
- Zhu, D.C., Zhao, Z.D., Niu, Y., Dilek, Y., Hou, Z.Q., Mo, X.X., 2012. [The origin and pre-Cenozoic evolution of the Tibetan Plateau. Gondwana Res. 23, 1429–1454.](#)

**Chapter 3: Ordovician parallel unconformity in Qiangtang terrane, northern Tibet:
Implications to Early Paleozoic evolution of northern Tibet regions**

Yang Yao^{1,2}, Zhao Zhongbao ^{3,4}, Yuan Tingyuan ^{2,3}, Liu Yan², Li Congying⁵

1, College of Earth Sciences, Chengdu University of Technology, Chengdu 610059, China

2, State Key Laboratory of Continental Tectonics and Dynamics, Institute of Geology, Chinese Academy of
Geological Sciences, Beijing 100037, China

3, China University of Geosciences, Beijing 100083, China

4, Department of Geosciences, Eberhard Karls University Tübingen, Tübingen D-72074, Germany

5, Guangzhou Institute of Geochemistry, Chinese Academy of Sciences, Guangzhou 510604, China

This paper was originally published in Chinese in *Acta Petrologica Sinica*, 30, 2381-2392, 2014. The original paper is included in Appendix A. The English translation is given below.

Abstract

Several issues have been disputed for a long time in Qiangtang terrane, northern Tibet, such as whether it has the metamorphic basement, as well as the pre-Cenozoic history. Here we report the Tashishan Formation, which located in the northern position of southern Qiangtang terrane, of Middle and Late Ordovician is parallel unconformity on thick-bedded fossil-free low-grade metamorphic quartz sandstones which has been interbedded by thin layer of marl. Nearly 600 detrital zircons dating results indicates that the maximum sedimentary age of the free low-grade metamorphic quartz-sandstone is 527 ± 7 Ma. And more than 300 detrital zircons dating results indicate that maximum sedimentary age of the quartz sandstone at the bottom of Tashishan Formation is 471 ± 6 Ma. The age gap between the quartz sandstones above the unconformity and the underlying low-grade metamorphic quartz sandstone is up to 56 Myr, indicative of an obvious depositional hiatus between two quartz sandstones. This further confirms that the unconformity between the two quartz sandstones is Early Ordovician. An independent piece of evidence is that fossil-free low-grade quartz sandstone was intruded by Early Ordovician granitoids (471-477 Ma). The sedimentary rock underlying the unconformity is, therefore, named as Rongma Formation and classified in Late Cambrian era in this study. Cathodoluminescence images and geochronological studies indicate that the detrital zircons of quartz sandstones above the unconformity were mainly from crystalline rocks which formed in the late period of the Pan-African event and close to their provenance. This imply that the Late Pan-African crystalline rocks had exhumed in Early Ordovician, and then, underwent denudation, providing material sources for the Middle and Late Ordovician sedimentary rocks.

The discovery of the parallel unconformity of Ordovician reflects that the south Qiangtang terrane is one portion of the Gondwana supercontinent, as Himalayan and Lhasa terranes. The distinctive difference in Paleozoic strata between South Qiangtang and North Qiangtang terranes shows that there is an ancient ocean basin between the two terranes in the Early Ordovician at least, and the two terranes evolved independently.

Key words: Detrital zircon; Ordovician parallel unconformity; Pan-African event; South Qiangtang, northern Tibet; Gondwana supercontinent

1. Introduction

A >500 km long EW-striking orogeny is located in central Qiangtang and nominated as Qiangtang Culmination (Wu et al., 1986) which separated Qiangtang into north and south Qiangtang terranes (Fig. 1). The tectonic characters of Qiangtang Culmination have been debated for decades. Wu et al. (1986) assigned these metamorphic mélanges as Amugang Group, which is located in the central Qiangtang Culmination. From base to top, they are gneiss, quartzite, greenschists and cherts and belong to pre-Devonian Qiangtang basement. Moreover, the Qiangtang basement separated into two layers, crystalline base and metamorphic softer cover (Huang et al., 2001). The Guogangjia Group (~1111 Ma) and Gemu Ri Group (>1111 Ma), which separated from assigned basement, belong to the Proterozoic metamorphic basement (Wang and Wang, 2001). However, Li et al., (1997) argued that the metamorphic rocks belong to Late Triassic mélange instead of basement of Qiangtang terrane (Li et al., 2003). The metamorphic unit includes ultramafic blocks, mafic blocks and low-temperature eclogites and blueschists (Li et al., 2006; Kapp et al., 2000; 2003; Zhang et al., 2006; Liu et al., 2011) which were assigned as greenschists before by Wu et al, (1986). Furthermore, large divergence of sedimentary characters and lithostratigraphy on both sides of the culmination show that the Qiangtang Culmination represents an important boundary, which is an in situ suture zone (Li, 1987; Zhang et al., 2001). North Qiangtang belongs to the Cathaysian domain, while, South Qiangtang has Gondwana affinity. This model was argued by Kapp et al, (2000; 2003) who proposed that the Qiangtang Culmination is a metamorphic core complex like structure. It formed by diapiring of deep subducted material during southward low-angle subduction of Jinsha suture, ~200 km to north. It is similar with back arc extension during subducted slab rollback. Recently, Pullen et al, (2008) modified this underthrust model to island arc collision with Qiangtang which induced core complex structures within Qiangtang terrane. They are not focused on long-distance low-angle subduction of Jinsha suture. Core complex model assumes that the Qiangtang has not been separated by a suture and that the main boundary of Eurasia and Gondwana is located in Jinsha suture (Gehrels et al., 2011; Pullen et al., 2011). Some authors attribute the metamorphic belts as relics of ophiolite, and there is no basement underneath it (Pan et al., 2012a, b). These mélange together with mélange from the Bangong Hu-Nujiang suture zone to the south form the largest and spectacular relics of

Tethys Ocean in Tibetan Plateau. In their view, the Longmu Co-Shuanghu suture and Bangong Hu-Nujiang suture belong to one suture, which separate Gondwana from Eurasia, but different branches. This manuscript reports parallel unconformity on the north edge of the South Qiangtang terrane and identified the underlying quartz sandstone as pre-Cambrian in age, we assign it as Rongma Group. Our conclusion tries to offer more evidences of geological evolution of Qiangtang terrane.

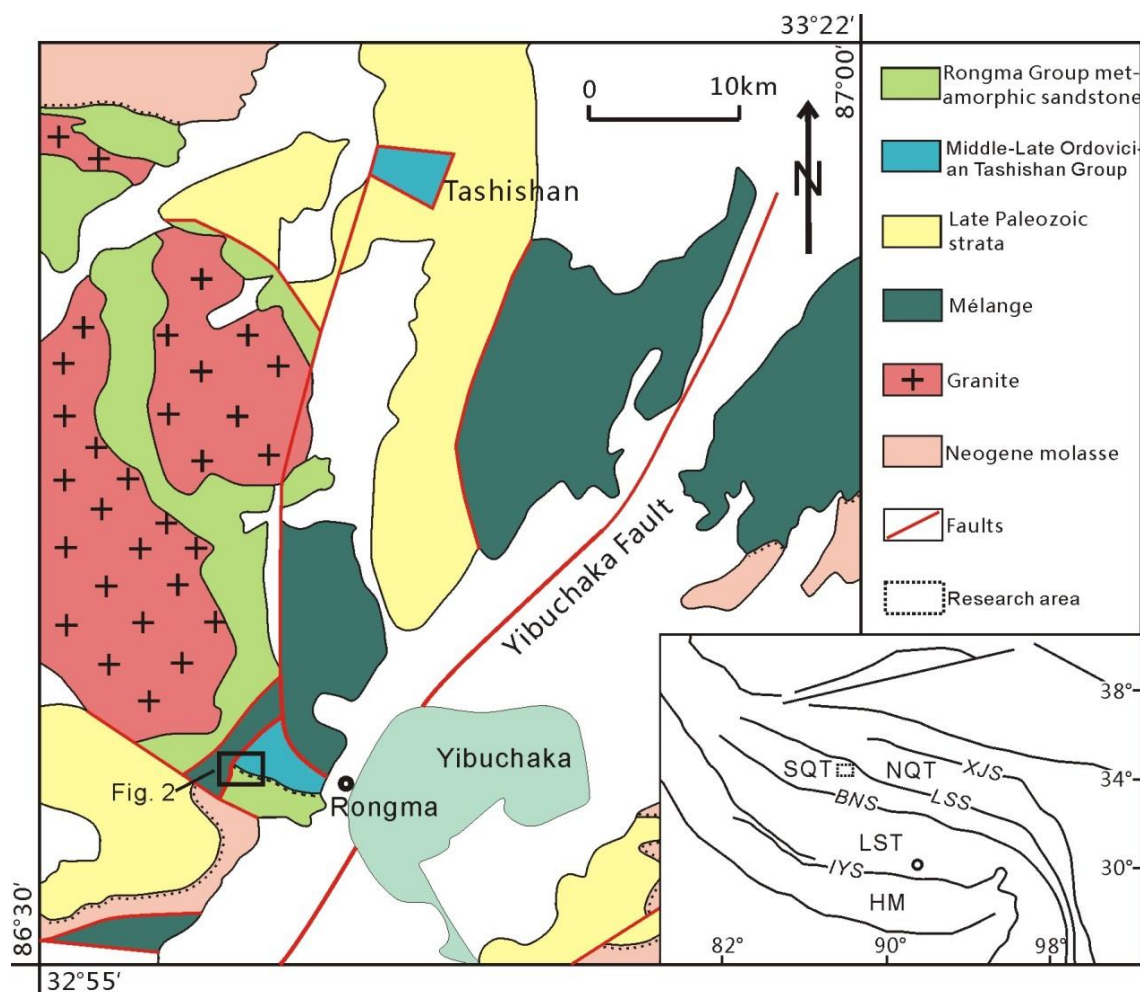


Fig. 1 Simplified geological map of Rongma, northern Tibet (Modified after Liu et al., 2011 and Zhao et al., 2014). LST-Lhasa terrane; SQT-south Qiangtang terrane; NQT-north Qiangtang terrane; HM-Himalaya Block; IYS-Indus-Yalongzangbu suture zone; BNS-Bangong Hu-Nujiang suture zone; LSS-Longmu Co-Shuanghu suture zone; XJS-Xijinwulan-Jinsha suture zone.

2. Geological background

The research area is located in Rongma, northern Tibetan Plateau (Fig. 1). Accretion mélangé, low-metamorphic grade Rongma Group (RG) quartz sandstone, Middle-Late Ordovician Tashishan Group quartz sandstone intercalated with marlstone, Late Paleozoic siltstone and Neogene purple-red molasse

cropped out in the research area (Fig. 1). Indosinian porphyritic granite intruded the low metamorphic grade Rongma Group (Zhao et al., 2014). Accretion *mélange* is not in sequence and includes mafic blocks, ultramafic blocks (e.g. pillow basalt, gabbro, serpentinite) and high-pressure, low-temperature metamorphic rocks (such as, garnet-bearing and glaucophane-bearing blueschists) (Li et al., 2006; Pullen et al., 2008; Liu et al., 2011). Other rock units, which are composed of greenschists, dark-gray micaceous quartzite, chlorite-bearing micaceous quartzite and marble, also occur in the *mélange*. In the field, the greenschists are spread over a large area and was nominated as Amugang Group (Wu et al., 1986). The greenschists are strongly deformed and developed tight folds and non-root folds. It contacts with Rongma quartz sandstone and Ordovician Tashishan Group by faults (Fig. 2, 3). The temporary named Rongma Group is mainly consisting of middle to thick-layered metamorphic quartz sandstone intercalated with thin layers of marl. The Middle-Late Ordovician Tashishan Group directly overlies the Rongma Group (Fig. 2, 4). The Rongma Group quartz sandstone crops out extensively, from Shuanghu (east) to Gaize (west), ~500 km long and ~50 km in width, which was nominated as the Amugang Group (quartzite section) before (Wu et al., 1986).

Quartz sandstone (RG) is always middle to thick-layered and experienced strong deformation, but the primary sedimentary bedding can still be recognized by composition differences in Rongma (Fig. 2). The Tashishan Group was assigned by the geological survey group of Jilin University (2005), with the group named after the location name ‘Tashishan’ (Fig. 1). About 20 km² Tashishan Group raft contacted with Paleozoic strata in Tashishan area (Fig. 1), however, the base of this unit does not crop out. Abundant *Sinoceras* was found in the upper siltstone or carbonate section, so it dated as Middle-Late Ordovician age (Jilin University, 2005). Basal conglomerate (~20 m thick) based under Tashishan Group exhibit a better outcrop near Rongma village (Fig. 1, 2). The fossil-bearing calcareous siltstone is conformably overlying the basal conglomerate (Fig. 5) and gradually changes to quartz sandstone intercalated with thin layer marls towards up. There are *Sinoceras* in the marls and calcareous siltstone which are the same as in the Tashishan Group (Fig. 5). Although the Tashishan Group is strongly deformed, with S-C fabric development and sheared *Sinoceras*, its sedimentary layering is still recognizable by intercalation of sandstone and marl. The original sedimentary layering seems parallel to the underlying basal conglomerate (Fig. 5). Carboniferous strata are missing in the research area. Ordovician rocks contact with Permian *mélange* by faults (Fig. 2). Neogene Kangtuo Group molasse unconformably overlies all the older units (Fig. 2).

3. Unconformity between Rongma Group and Tashishan Group

The unconformity is located 3 km west of Rongma village, Nima County (Fig. 1, 2). From top to bottom, the profile includes (Fig. 4) the Tashishan Group, basal conglomerate and the Rongma Group. Overlying

the basal conglomerate, > 50m and 10°-20° SW dipping. the Tashishan Group is composed of middle-thick-bedded quartz siltstone and fine sandstone interbedded with marl and shale. In thin section, quartz sandstone consists mainly of quartz (0.1-0.2mm) and minor muscovite, fine-grained zircon, tourmaline and so on (Fig. 6). White-gray calcareous siltstone (~30m), intercalated with white arenaceous shale and marl, is situated between quartz sandstone and the basal conglomerate. Fossils were not found in the calcareous siltstone.

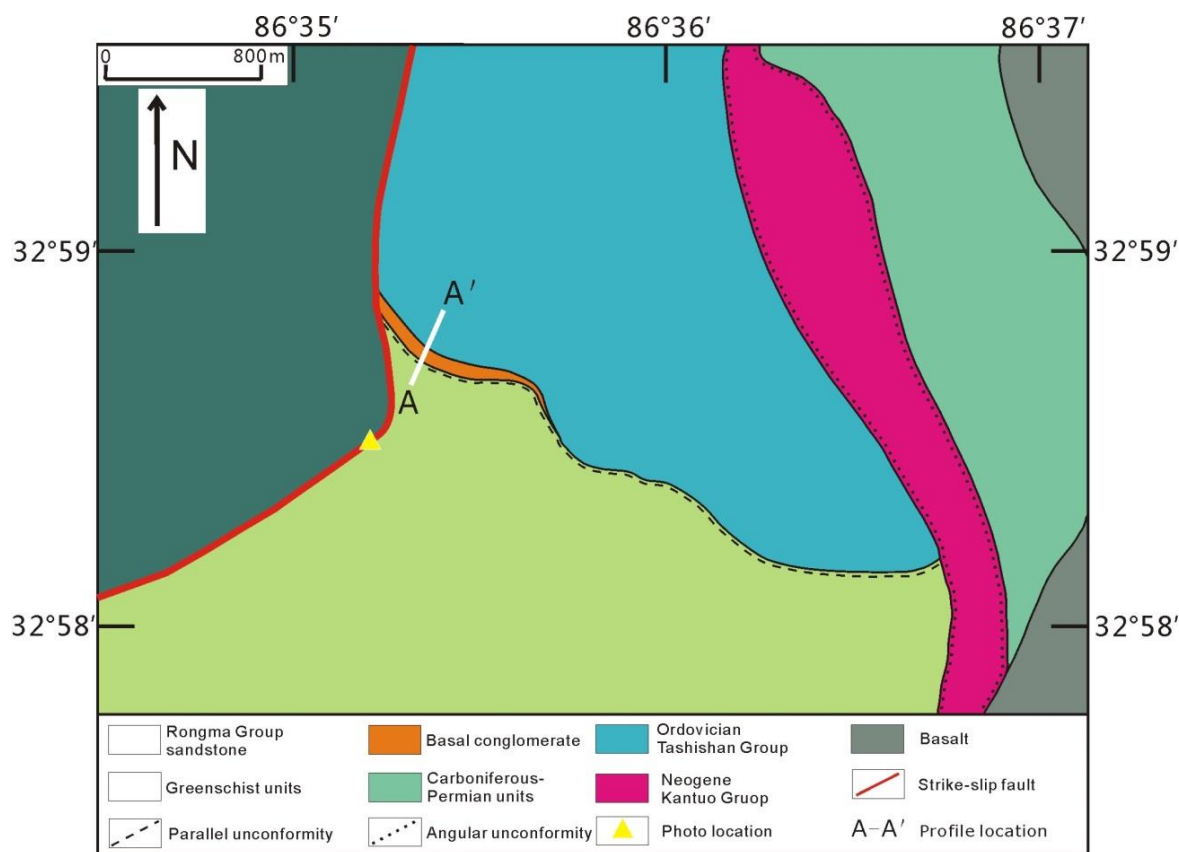


Fig. 2 Geological sketch map of Rongma area, northern Tibet (location sees Fig. 1)

The basal conglomerate (~20m thick) contains homogeneous pebbles, such as white-gray metamorphic quartz sandstone (Fig. 5), which mainly derived from bottom units. The oval-shaped or subangular pebbles are rounded and well sorted. Diameters of pebbles are approximately 3-12 cm and the largest may be as long as 20 cm (Fig. 5d). The sedimentary layering is illustrated by diameter gradient, which decreases towards the top (Fig. 5d, 6b). These graded layers are parallel with original layering in both the overlying and underlying units, which indicates that the conglomerate is a sedimentary breccia and not a tectonic breccia (Fig. 5a).

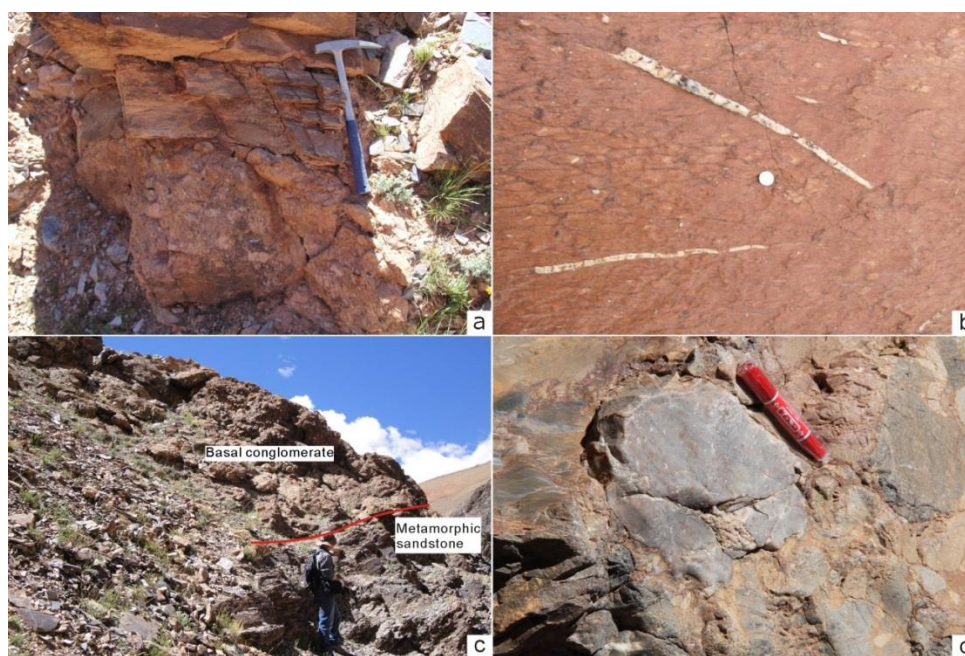
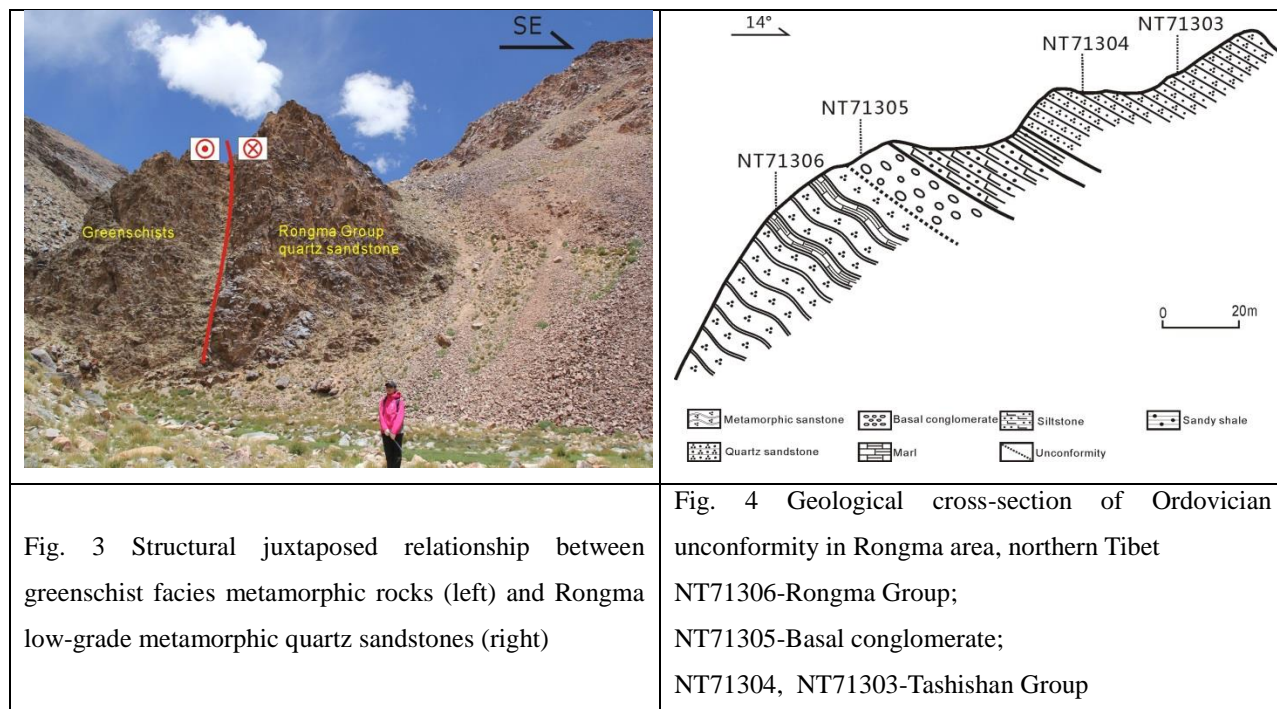
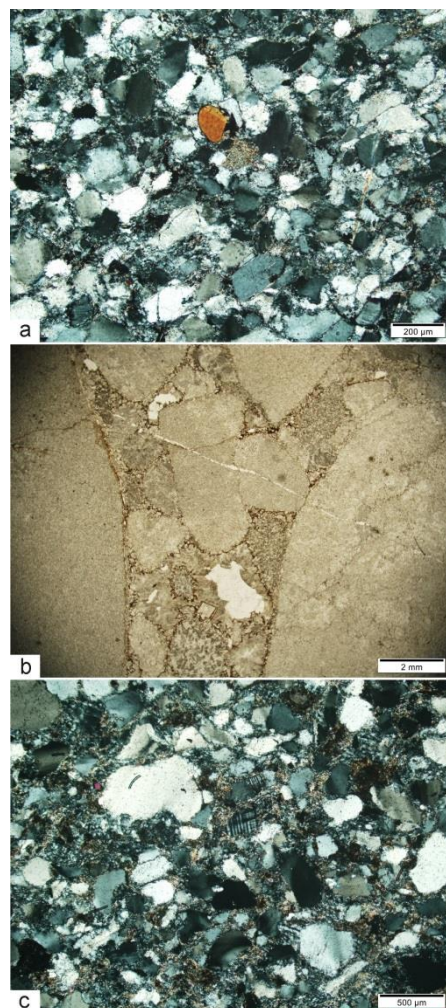


Fig. 5 Field photos of Cambrian-Ordovician strata in the Rongma area, northern Tibet. a, basal conglomerate and conformably overlying sandstone; b, fossil-bearing Ordovician marl; c, basal conglomerate and conformably underlying Rongma Group quartz sandstone; d, pebbles in basal conglomerate.

The base of the Rongma Group consists of grey or pale-yellow metamorphic quartz sandstone and conformably underlies the basal conglomerate (Fig. 2, 4, 5). The outcrop of the Rongma Group does not show its base or any fossils. Under the microscope, metamorphic quartz sandstone shows an equigranular texture and massive structure. Contents include quartz, feldspar and a small amount of mica (Fig. 6c). ~0.05-0.5 mm quartz grains account for a proportion of about 75% and commonly have undulatory extinction under orthogonal polarized light. The feldspar content is about 5%-10% and contains both plagioclase and microcline (Fig. 6c). ~0.1 mm plagioclase and ~0.25 mm microcline may indicate near provenance deposits. The argillaceous or calcareous cements are characterized by fine-grained sericite, chlorite and other metamorphic minerals (Fig. 6c). Minor euhedral zircons have been found in thin section.

Fig. 6 Photomicrographs of rocks above and beneath the unconformity in the Rongma area, northern Tibet, respectively. a, Tashishan Group sandstone (cross-polarized); b, basal conglomerate (single-polarized) ; c, Rongma Group metamorphic sandstone (cross-polarized), part of matrix contains sericite and chlorite.



4. Analysis methods

A total of 4 samples has been analyzed in this paper. They derived from underlying Rongma Group metamorphic quartz sandstone (NT71306), middle basal conglomerate (NT71305) and overlying sandstone (NT71303, NT71304) (Fig. 4). The sample location is 32°58'40" N; 86°35'20" E. Zircons were separated using conventional heavy-liquid and magnetic techniques. Representative grains were handpicked under a binocular microscope, mounted in epoxy resin disks, and then polished and gold coated. Zircons were examined under transmitted and reflected light, and then imaged by cathodoluminescence (CL) at the Beijing Sensitive High Resolution Ion Microprobe (SHRIMP) Centre to reveal their internal structures and decide laser positions.

Measurements of U, Th, and Pb concentrations of zircons were carried out by means of LA-ICP-MS at the Key Laboratory of Isotope Geochronology and Geochemistry, Guangzhou Institute of Geochemistry, CAS. A Resolution M-50 laser-ablation system was used in conjunction with an Agilent 7500 ICP-MS. The clearest, least fractured rims of the zircon crystals were selected as suitable targets for laser ablation

analyses. Sample mounts were placed in the two-volume sample cell flushed with Ar and He. Laser ablation was operated at a constant energy 80 mJ and at 8 Hz, with a spot diameter of 31 μm . The ablated material was carried by the He gas to the Agilent 7500 ICP-MS. Element corrections were made for mass bias drift, which was evaluated by reference to standard glass NIST 610 (Y.S. Liu et al., 2008). The data processing was conducted using the Ludwig SQUID1.0 and the ISOPLOT/Ex program (v. 3.0) of Ludwig (2003). The detailed results are shown in table 1.

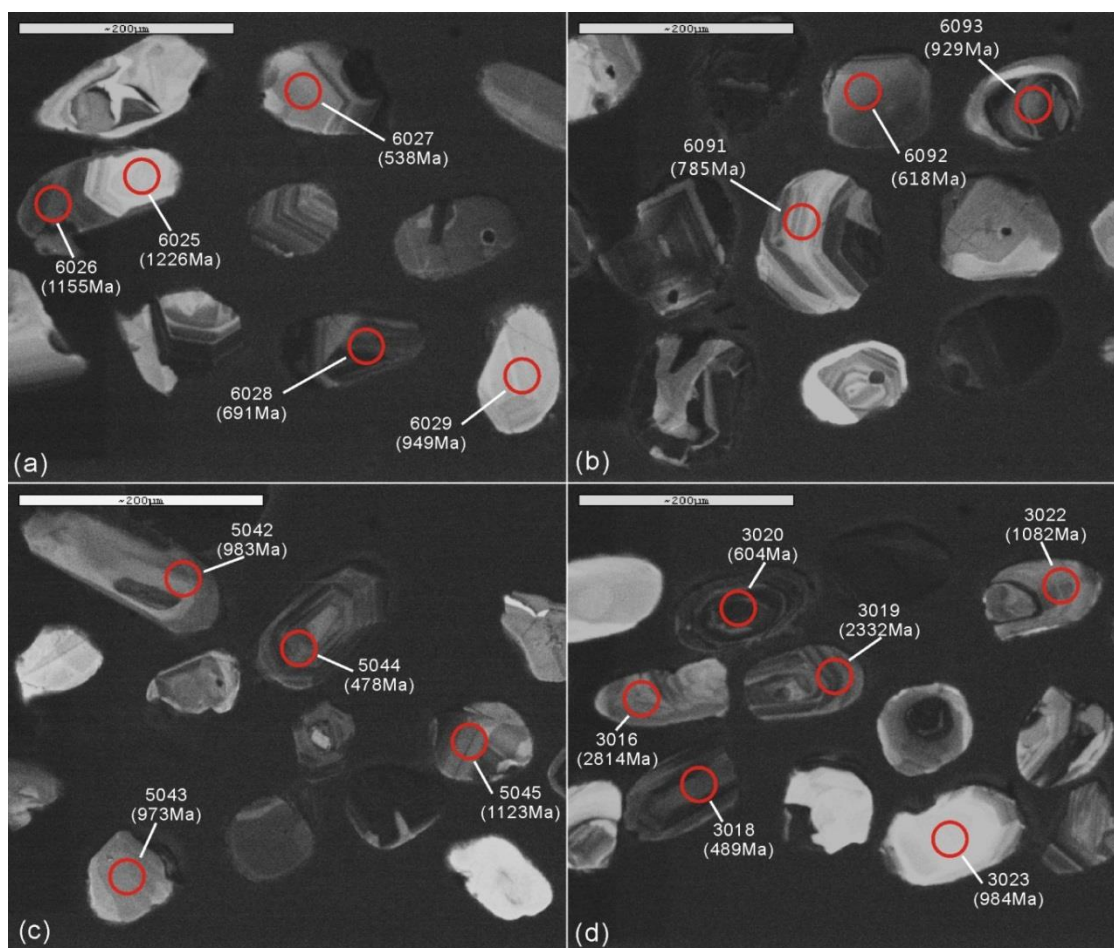


Fig. 7 Cathodoluminescence images of detrital zircons from the rocks under and above unconformity in Rongma area, northern Tibet, respectively. a, b CL images of detrital zircon from Rongma Group; c, d CL images of detrital zircons from Tashishan Group. Oscillatory zoning is common. Minor zircons occur accretion rim and get rounded. Red circle indicates laser beam location. Both dating numbers and individual ages are shown.

5. Analysis results

~80-180 μm zircons, derived from Rongma Group metamorphic quartz sandstone, are mostly elongate and minor equiaxed or oval-shaped with oscillatory zoning (Fig. 7a, b). In CL images, crystal traits reflect a magmatic character. Some of the zircons were rimmed by a dark accretion edge (Fig. 7a). Sample

NT71306 was analyzed with 123 zircons and 128 laser spots which five more zircons tested both in the cores and dark rims. The analysis results show a large variation in Th content (0.6×10^{-6} - 674×10^{-6}), U (23.9×10^{-6} - 856.8×10^{-6}) and Th/U (0.01 - 2.42). Most of Th/U value are larger than 0.1 (Table 1). The detrital zircons from metamorphic quartz sandstone yielded a wide range of ages from 527 to 3340 Ma (Fig. 8a). The youngest zircon age is 527 ± 7 Ma with 4% discordant and the oldest age is 3340 ± 33 Ma with 96% harmony (Fig. 8a).

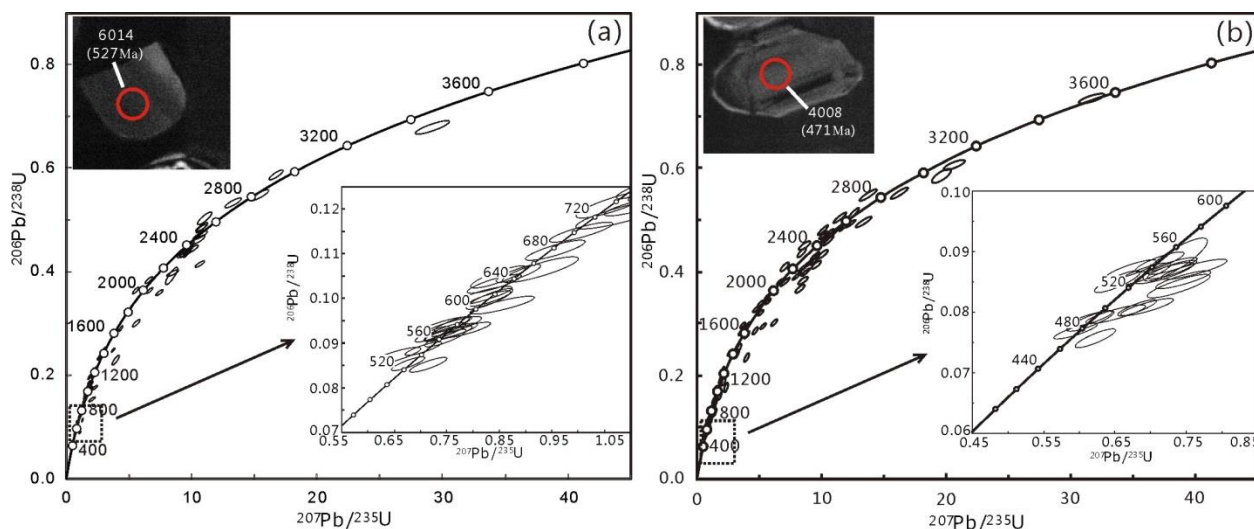


Fig. 8 Detrital zircon concordant diagrams for clastic rocks under and above the unconformity in Rongma area, northern Tibet, respectively.

Overlying the unconformity, detrital zircons from Tashishan Group and basal conglomerate are mostly columnar in shape with minor oval-shaped grains. Zircon grains range from $60\mu\text{m}$ to $200\mu\text{m}$ in size and also developed oscillatory zoning under CL image (Fig. 7c, d). Some of the zircons grew with dark accretion rim (Fig. 7d). About 302 detrital zircon grains and 311 laser spots from three samples (NT71303; NT71304 and NT71305) were analyzed. Nine were grains analyzed both in core and newly grown rim. Analysis results indicate a large range of Th, U and Th/U, 1.2×10^{-6} - 281.5×10^{-6} , 28×10^{-6} - 1391.7×10^{-6} and 0.01 - 3.32, respectively (Table 1). The ages fall between 471 Ma and 3552 Ma populations (Fig. 8b) with the youngest age 471 ± 6 Ma (95% concordant) and the oldest age 3552 ± 26 Ma (99% concordant). The chronological difference between the Rongma Group and the Tashishan Group is that 470-480 Ma ages only occur in the overlying Tashishan group and basal conglomerate (Fig. 8b). Furthermore, the zircon CL image of 470-480 Ma show a crystalline character which is distinct from other detrital zircons (Fig. 7c, d).

6. Discussion

Pullen et al, (2008) and Dong et al, (2011) proposed three main detrital age ranges, 500-700 Ma, 885-1100 Ma and 2350-2580Ma, which peaked at 615 Ma, 980 Ma and 2485 Ma, respectively (Fig. 9). Overlying unconformity, more than 300 detrital zircons dated around 470-520 Ma, 580-800 Ma and 950-1100 Ma, with three main frequencies with largest peak ages at 500 Ma, 585 Ma, 800 Ma and 985 Ma. But there are large age frequencies differences between the overlying and underlying units. The detrital zircons from underlying units are all older than 525Ma and have different age accumulative traits which are younger than 620 Ma. That indicates that the two units were deposited at different times and non in sequence. In CL images, most of zircons crystallized with euhedral or semi-euhedral (except a few rounded ones) shape (Fig. 7) and maintained magmatic oscillatory zoning, demonstrated that they sourced from crystalline rocks and close provenance. Moreover, both CL images and age frequency from the overlying Tashishan Group are similar with results from neighbor regions, located 100 km to the west (Pullen et al., 2011) and 50 km to the northwest (Hu et al., 2010) (Fig. 11). These results illustrate that quartz sandstone of the Tashishan Group derived from nearby Pan-African crystalline rocks. Hence, the crystalline rocks must be exhumed to the surface during the Early Ordovician and eroded into the nearby basin which offered material to Ordovician sandstone in Rongma. Therefore, there was an orogeny or culmination (similar to Qiangtang Culmination) in the Ordovician.

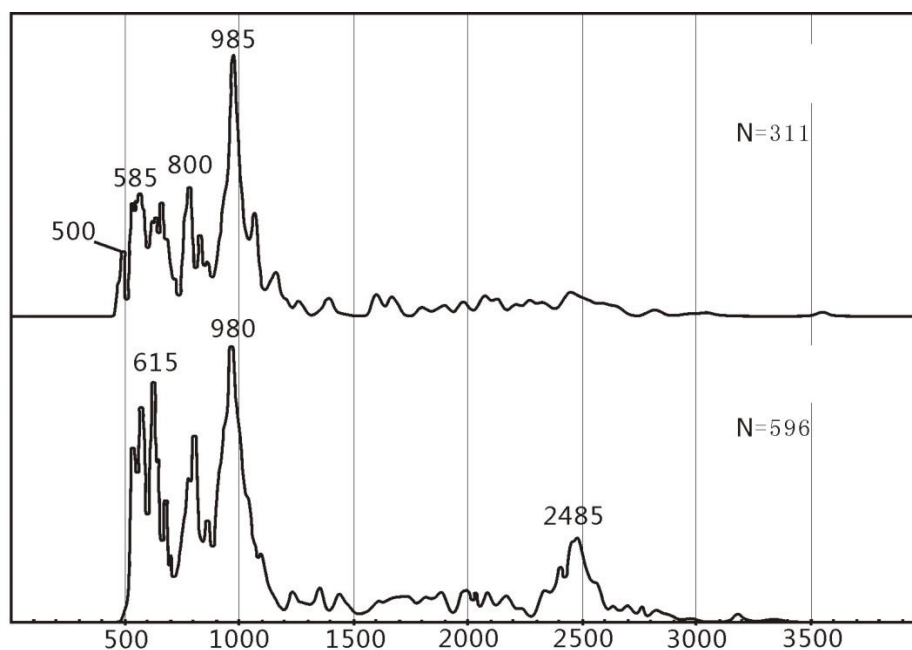


Fig. 9 Detrital zircon age frequency diagram for clastic rocks under and above the unconformity in the Rongma area, northern Tibet, respectively. The total of 311 zircons, which are derived from the Tashishan Group, are all our data.

Chapter3

The underlying unit ages include our 128 data, 323 data from Pullen et al, (2008) and 145 zircon ages from Dong et al, (2011). When individual ages are <1200Ma, we use $^{206}\text{Pb}/^{238}\text{U}$, otherwise, $^{207}\text{Pb}/^{238}\text{Pb}$ were used.

Due to the absence of fossils in the metamorphic quartz sandstone of the Rongma Group, there are debates about its age (Li, 2003) that hinders our understanding of the Qiangtang basement. Our work attempts to reveal the age of this fossil-free unit, as well as the Qiangtang basement. A total of ~600 zircons, both from our results and the literature, shows that the maximum depositional age of the Rongma Group is 527 ± 7 Ma which is older than overlying Tashishan Group (471 ± 6 Ma). According to this difference, we conclude that the Rongma Group deposited during 527 ± 7 Ma and 471 ± 6 Ma. A strongly deformed two-mica granite (100 km to west) was dated as 471-476 Ma (Pullen et al., 2011), which coincides with our unpublished data. Our field observation found that this granite intruded the Rongma Group. Zhao et al. (2014) documented another strongly deformed granite (471Ma) that intruded the Rongma Group about 30 km NW of our research area. These evidences confirm that the Rongma Group quartz sandstone deposited during 527 ± 7 Ma and 476 Ma. Considering the sandstone must have experienced burial diagenesis before it was intruded by granite at a certain depth, the Rongma Group hence formed in the Middle-Late Cambrian in the north of the South Qiangtang terrane. Field relationships show that this sedimentary discontinuity is parallel to the unconformity between Rongma Group and Tashishan Group.

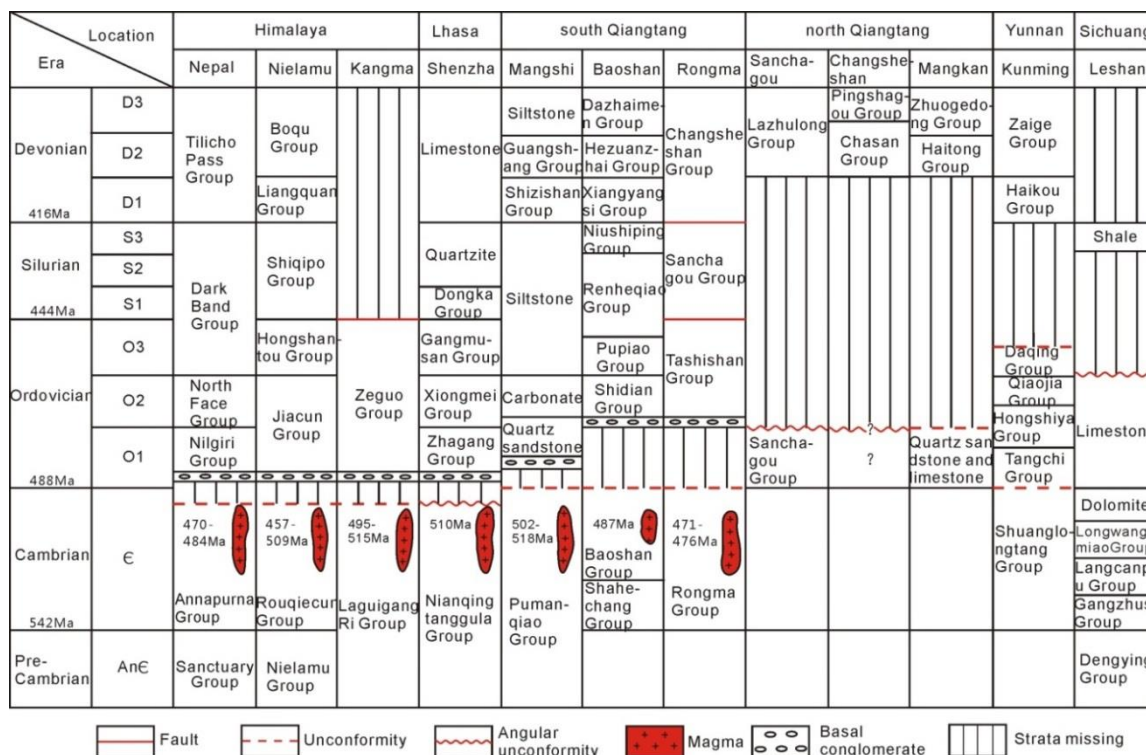


Fig. 10 Stratigraphic correlation in Tibetan regions. Nepal strata-Gehrels et al, (2003; 2011), granite age-Schärer and Allegre, (1983); Johnson et al, (2001). Nielamu strata-Zhu et al, (2003), Magma age-Xu et al, (2005); Liu et al, (2007a). Kangma strata-Zhou et al, (2004), granite age-Xu et al, (2005); Lee et al, (2000). Shenzha strata-Ji et al, (2009), Magma age-Gehrels et al, (2011); Ji et al, (2009). Mangshi-Cai et al, (2013). Baoshan strata-Huang et al, (2012); Tang et al, (1982), granite-Song et al, (2007). Rongma strata-Jilin University, (2005); this paper, granite-Pullen et al, (2011); Hu et al, (2010). Sanchakou strata-Xia et al, (2006). Changsheshan strata- Jilin University, (2005); this paper. Mankang strata-China Geological Survey, (1984). Kunming strata-Fang et al, (2000); Zhang et al, (2013). Leshan strata-Xu et al, (2012). Detailed locations are shown in Figure 11.

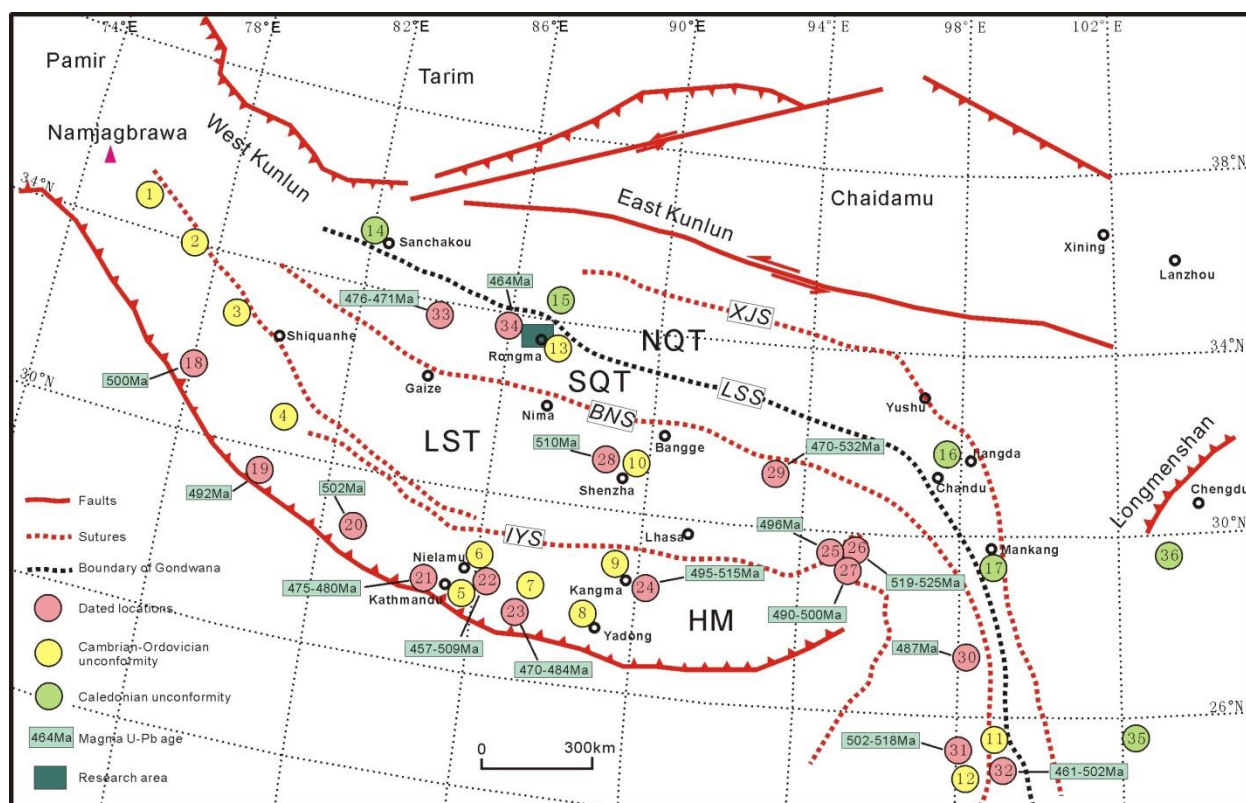


Fig. 11 Tectonic units and records of the Early Paleozoic orogenic events in the Tibet region. 1-Baig et al., 1988; 2-Garyanti et al., 1986; 3-Miller et al., 2007; 4-Valdiya et al., 1995; 5; 21-Gehrels et al., 2003; 6-Zhu et al., 2003; 7-Yin et al., 1974; 8, 9- Zhou et al., 2004; 10, 28, 33-Gehrels et al., 2011; 11-Huang et al., 2012; 12-Cai et al., 2013; 13-Xia et al., 2006; 14-Jilin University, 2005 and this paper; 16, 17-China Geological survey, 1984; 18-Miller et al., 2001 and Spencer et al., 2012; 19- Decelles et al., 1998; 20-Godin et al., 2001; 22-Xu et al., 2005 and Liu et al., 2007a; 23-Schärer et al., 1983 and Johnson et al., 2001; 24-Lee et al., 2000; 25-Dong et al., 2009; 26 -Liu et al., 2007b; 27-Zhang et al., 2008; 29-Xie et al., 2010 and Guynn et al., 2012; 30-Sun et al., 2007 ; 31-Cai et al., 2013; 32- Dong et al., 2012 and Liu et al., 2012; 34-Hu et al., 2010; 35-Fang et al., 2000 and Zhang et al., 2013; 36-Xu et al., 2012.

LST-Lhasa terrane; SQT-south Qiangtang terrane; NQT-north Qiangtang terrane; HM-Himalaya Block; IYS-Indus-Yalongzangbu suture zone; BNS-Bangong Hu-Nujiang suture zone; LSS-Longmu Co-Shuanghu suture zone; XJS-Xijinwulan-Jinsha suture zone.

According to the comparison of Early Paleozoic strata (Fig. 10, 11) within and around the Tibetan Plateau, we conclude that 1) the central Qiangtang Culmination separates northern Eurasia from southern Gondwana by geological records, 2) the Early Ordovician unconformity developed from south Himalaya to South Qiangtang and extending to the east, such as the Baoshan Block in Yunnan, China, 3) the unconformities are mainly parallel, although local angular unconformities formed occasionally (Tan et al., 1982; Zhu et al., 2003; Zhou et al., 2004; Jilin University, 2005; Ji et al., 2009; Huang et al., 2012; Cai et al., 2013; Gehrels et al., 2003; 2011). Intensive 460-510 Ma magmatic activity occurred in the southern Qiangtang Culmination and always intruded Cambrian strata (Fig. 10, 11) (Xu et al., 2005; Song et al., 2007; Ji et al., 2009; Hu et al., 2010; Cai et al., 2013; Schärer et al., 1983; Johnson et al., 2001; Liu et al., 2007a, b; Pullen et al., 2011; Gehrels et al., 2011). During the Middle-Late Ordovician, these regions experienced continued deposition and weak magma intrusion activity. However, the eastern Tibetan Plateau (Yunnan and Sichuan Basin) experienced a continued sedimentary event during the Cambrian to Ordovician without obvious interruptions (Fig. 10) (Fang et al., 2000; Xu et al., 2012; Zhang et al., 2013). Nonetheless, the unconformity formed after the Early Ordovician and upper Ordovician to lower Devonian strata are absent (Fang et al., 2000; Jilin University, 2005; Xia et al., 2006; Xu et al., 2012; Zhang et al., 2013). The overlying Devonian molasses cover Early Ordovician strata with large unconformable angles (Fig. 10) and 460-510 Ma magmas are absent which is instead of developing younger Caledonian orogeny (Fig. 10, 11).

Differences between north and south Qiangtang terranes developed as early as the Cambrian-Ordovician (Fig. 10, 11). The south Qiangtang terrane connected with Lhasa and Himalaya terranes to the south and the Baoshan block to the southeast. All these terranes experienced ~500 Ma Pan-African movement and assembled together during formation of the Gondwana supercontinent. At Middle-Late Ordovician times, break-up of the Gondwana supercontinent contributed a marine transgression and led to Middle-Late Ordovician strata unconformably overlying Cambrian basement. However, the north Qiangtang terrane has Yangtze affinity and experienced strong Caledonian fold affects, which indicates that an old ocean separated the south and north Qiangtang terranes in the Cambrian-Ordovician.

7. Conclusion

1. The Rongma Group metamorphic quartz sandstone is unconformably underlying Middle-Late Ordovician Tashishan Group on south Qiangtang terrane.
2. Provenance of the Middle-Late Ordovician Tashishan Group is local crystalline rocks, which recorded

Chapter3

the Pan-African orogeny event. The Rongma Group exhumed to surface at Early Ordovician times, before later intensive erosion. That means an ancient culmination was forming and delivering sediments to nearby basins.

3. The north and south Qiangtang were separated as early as the Cambrian-Ordovician by an ocean and started their independent evolution.

Chapter 4: Tectonic evolution and high-pressure rock exhumation in the Qiangtang terrane, central Tibet

Z. Zhao^{1,2}, P. D. Bons¹, G. Wang², A. Soesoo³, and Y. Liu⁴

1 Department of Geosciences, Eberhard Karls University Tübingen, Wilhelmstrasse 56, 72074 Tübingen, Germany

2 School of Earth Science and Resources, China University of Geosciences, Beijing 100083, China

3 Institute of Geology, Tallinn University of Technology, Ehitajate tee 5, Tallinn 19086, Estonia

4 State Key Laboratory for Continental Tectonics and Dynamics, Institute of Geology, CAGS, Beijing 100037, China

Abstract

Conflicting interpretations of the > 500 km long, east–west-trending Qiangtang metamorphic belt have led to very different and contradicting models for the Permo-Triassic tectonic evolution of central Tibet. We define two metamorphic events, one that only affected pre-Ordovician basement rocks and one subduction-related Triassic high-pressure metamorphism event. Detailed mapping and structural analysis allowed us to define three main units that were juxtaposed due to collision of the north and south Qiangtang terranes after closure of the Ordovician–Triassic ocean that separated them. The base is formed by the Precambrian–Carboniferous basement, followed by non-metamorphic ophiolitic mélangé containing mafic rocks that range in age from the Ordovician to Middle Triassic. The top of the sequence is formed by strongly deformed sedimentary mélangé that contains up to > 10 km size rafts of both unmetamorphosed Permian sediments and high-pressure blueschists. We propose that the high-pressure rocks were exhumed from underneath the south Qiangtang terrane in an extensional setting caused by the pull of the northward subducting slab of the Shuanghu–Tethys. High-pressure rocks, sedimentary mélangé and margin sediments were thrust on top of the ophiolitic mélangé that was scraped off the subducting plate. Both units were subsequently thrust on top of the south Qiangtang terrane continental basement. Onset of Late Triassic sedimentation marked the end of the amalgamation of both Qiangtang terranes and the beginning of spreading between Qiangtang and north Lhasa to the south, leading to the deposition of thick flysch deposits in the Jurassic.

Keywords: Qiangtang Terrane, Tibet, exhumation, high-pressure metamorphism, subduction

1. Introduction

The Tibetan plateau is an amalgamation of terranes that were accreted to the southern margin of Eurasia during Phanerozoic times (Yin and Harrison, 2000). From north to south, these terranes are the Qilian Shan, Qaidam, Songpan–Ganzi flysch complex, Qiangtang and Lhasa terranes (Fig. 1a). Terrane boundaries are defined by widely scattered belts of ophiolitic fragments and mélanges with high-pressure rocks (Zhu et al., 2012). These represent the opening and closure of several oceans. However, which ocean subducted where, when and in which direction is still subject of ongoing controversy. For example, Triassic subduction mélange and high-pressure rocks that are exposed in the Qiangtang metamorphic belt in central Tibet are interpreted in radically different ways (Kapp et al., 2003b; Li et al., 2006; Zhai et al., 2011a; Liang et al., 2012; Zhao et al., 2014).

Li et al. (1987) interpreted the blueschists and subduction mélange as the remnants of a Late Triassic suture zone. They proposed that the Qiangtang terrane was separated into a northern and a southern terrane by the Paleo-Tethys Ocean. As a result of northward subduction of this Paleo-Tethys underneath the north Qiangtang terrane (NQT), high-pressure rocks and subduction mélange were thrust southward onto the south Qiangtang terrane (SQT) (Zhang et al., 2006b; Zhai et al., 2011b; Zhao et al., 2014). The inferred suture between the two terranes is called the Longmu Co–Shuang Hu suture (short “Shuanghu” suture). The alternative to this “overthrust” model is the “underthrust” model of Kapp et al. (2000, 2003b) and Pullen and Kapp (2014), in which the Paleo-Tethys separated a single Qiangtang terrane in the south and the Songpan–Ganzi flysch complex in the north. The Paleo-Tethys subducted to the south underneath the Qiangtang terrane along the Jinsha suture (JSS). High-pressure rocks and mélange were subsequently exhumed by core-complex-like normal faulting and doming in the middle of the Qiangtang terrane. To avoid confusion of the names of the various oceans, we use the term “Shuanghu–Tethys” for the ocean that is proposed to have separated the SQT and NQT and subducted at the Shuanghu suture.

The two different models thus predict totally different tectonic histories of central Tibet and, therefore, the initial boundary conditions for Cenozoic growth of the Tibetan plateau. Here we present the results of detailed mapping and structural reconstruction of the Rongma area in the centre of the Qiangtang metamorphic belt. These results support the overthrust model and thus indicate that the north and south of the Qiangtang terrane were once separated by an ocean that closed in the Late Triassic.

2. Regional setting

The Qiangtang terrane is located in the centre of the Tibetan plateau (Fig. 1a). It extends for more than 1200 km from east to west and reaches a maximum width of ~ 500 km. South-east of the Tibetan plateau it connects with the Sibumasu terrane (Metcalf, 2009). The Songpan–Ganzi flysch complex lies to the north of it, with the Jinsha Suture Zone (JSS) in-between (Yin and Harrison, 2000).

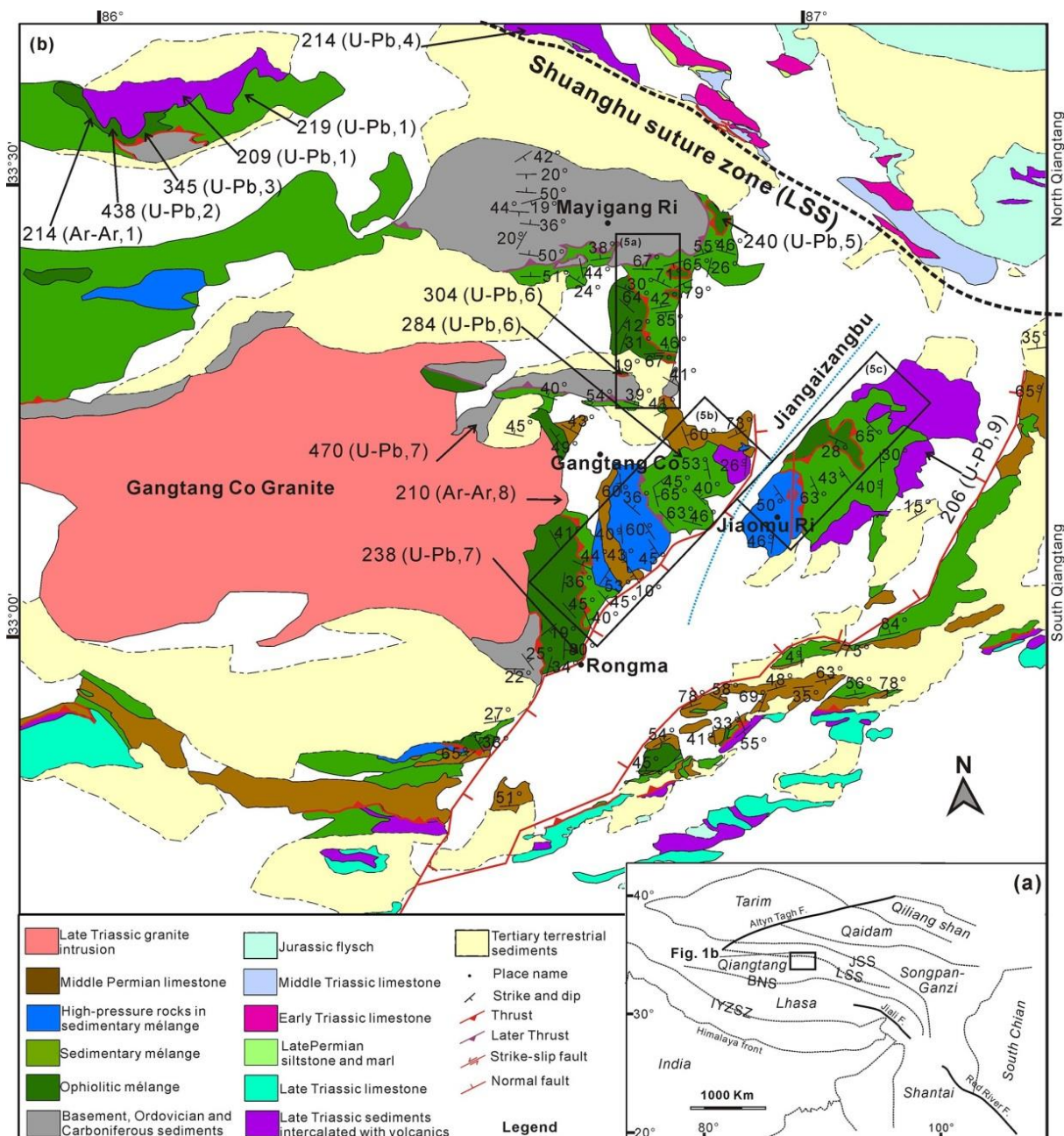


Figure 1. (a) Structural sketch of Tibet. From north to south, the sutures are Jinsha suture zone (JSS); Longmu Co–Shuanghu suture zone (LSS); Bangong–Nujiang suture zone (BNS); and Indus–Yarlung suture zone (IYSZ). (b) Geological map of the study area (rectangle in (a)) around Rongma on the

northern margin of the south Qiangtang terrane. The LSS zone separates the south Qiangtang from the north Qiangtang terrane in the northeast of the area. Strikes and dips are the properties of main tectonic foliation in strongly deformed rocks, while bedding is the property of less deformed rocks. Rectangles show the locations of structural reconstructions in Fig. 5. Numbers in parentheses refer to the following references: (1) Li et al. (2007); (2) Zhai et al. (2010); (3) Zhai et al. (2013b); (4) Wang et al. (2008a); (5) unpublished data; (6) Zhai et al. (2009); (7) Zhao et al. (2014); (8) Kapp et al. (2003b); (9) Zhu (2005).

This suture zone represents the Paleo-Tethys (or a branch of it) between Eurasia and the Qiangtang terrane that was consumed by southward subduction beneath the Qiangtang terrane in Late Triassic to Early Jurassic times (Dewey et al., 1988; Nie et al., 1994; Yin and Nie, 1996; Kapp et al., 2003b). The Bangong–Nujiang suture zone (BNS) separates the Qiangtang terrane from the Lhasa terrane to the south. It is characterized by an > 1200 km long EW-trending belt of widely scattered ophiolitic fragments that are associated with a thick sequence of mainly Jurassic flysch, mélangé and volcanic rocks (Wang et al., 1983). The belt exhibits an anomalously large across-strike width, especially in far western Tibet between Rutog and Shiquanhe and northwest of Lhasa between Xainza and Amdo (Kapp et al., 2003a).

Some regard the Qiangtang terrane as a single terrane (Kapp et al., 2003b; Pullen et al., 2011) that, together with the Sibumasu terrane, separated from Gondwana in Paleozoic times (Metcalf, 2009). Others divided the terrane into a north Qiangtang and a south Qiangtang terrane (Li et al., 2009; Liu et al., 2011). In this model, the two terranes were separated by the Shuanghu suture that closed in Late Triassic times by northward subduction of ocean underneath the NQT. This north–south division will be used throughout this paper. It should be noted that the SQT and NQT are equivalent to the east and west Qiangtang terranes of Zhu et al. (2012) respectively.

In the SQT, the autochthonous units consist of low metamorphic grade pre-Ordovician basement, unconformably overlain by Middle Ordovician siltstone and Carboniferous flysch and sandstone, including glaciomarine deposits, all with Gondwana affinity (Zhao et al., 2014). Only Late Devonian limestones and Early Carboniferous limestone intercalated with siltstone are exposed on the southern margin of the NQT. Permian sediments are different in the NQT and SQT. In the SQT, only Middle Permian limestones are exposed, characterized by cold-water fauna (Li et al., 1995; Zhang and Tang, 2009). In the NQT, only Late Permian sedimentary rocks are found, comprising sandstone, mudstone and limestone with abundant warm water fusulinid and coral fossils of Cathaysian affinity (Li et al., 1995; Zhang and Tang, 2009). Lower to Middle Triassic sediments are only found on the southern margin of the

NQT (Fig. 1b). These are bathyal sediments including fossiliferous limestone, massive limestone, oolitic limestone and minor intercalated sandstone and siltstone layers.

Late Triassic terrestrial sediments, limestones and volcanics are the first post-collisional deposits in both the SQT and NQT. Magmatic arc volcanics dominate on the southern margin of the NQT (Zhai and Li, 2007; Zhai et al., 2013a), whereas the occurrence of limestone increases towards the south. During the Jurassic, marine sediments were deposited on both the SQT and NQT, while Cretaceous limestones are only found on the SQT (Kapp et al., 2005). Tertiary, and possibly also late Cretaceous, conglomerates unconformably overlie all above rocks in intramontane, fault-bounded basins (Kapp et al., 2005).

High-pressure rocks, including blueschists and eclogites, as well as subduction *mélange* with ophiolitic fragments are found scattered over an > 500 km long, EW-striking belt in the middle of the Qiangtang terrane: the central Qiangtang metamorphic belt (Kapp et al., 2003b; Zhang et al., 2006a; Liu et al., 2011). Ar-Ar analyses on synkinematic phengite, zircon U-Pb and Lu-Hf isotopic ages from high-pressure units yielded ages from 244 to 214 Ma (Pullen et al., 2008; Zhai et al., 2011b), which is interpreted to provide an estimate for the age of suture zone closing (Li et al., 2009) as well as exhumation of the high-pressure rocks. These ages coincide with those of granitoids in the Qiangtang terrane, which range in age from 234 to 177 Ma (Zhang et al., 2011). Only one Late Triassic granite, the $\sim 210 \pm 4$ Ma Gangtang Co granite (Kapp et al., 2003b) is found in the SQT within the study area. This large, undeformed granite intruded both *mélange* and basement rocks (Kapp et al., 2003b; Zhao et al., 2014). This granite thus marks the end of collisional activity and is approximately coeval with volcanic deposits in the NQT and the SQT.

Based on the brief overview above, the rocks in the Qiangtang terrane can be divided into three groups. The first consists of autochthonous continental crustal rocks older than the Late Triassic ocean closure, including pre-Ordovician basement rocks and overlying Ordovician to Triassic units. Units deposited after closure, including the Gangtang Co granite, form the second autochthonous series. These range from Late Triassic sediments and volcanics to recent terrestrial deposits. The third group is formed by the *mélange* and high-pressure rocks and also includes blocks and rafts of the older autochthonous series rocks. The two conflicting models make testable predictions on stratigraphy, metamorphic grade and structural relationships between the different rock units in the study area. These are briefly discussed here. This is followed by a more detailed overview of the stratigraphy in the critical period from the Permian to the Triassic and a structural geological analysis. The observations are then compared with the predictions of the different models.

2.1. Cold- vs. warm-water fauna

In the underthrust model, the Qiangtang terrane formed one single block that drifted northwards from the Gondwana margin. Permian to Middle Triassic sediments are expected to reflect this northward drift by showing a trend from cold- to warm-water faunas. Contemporaneous sediments on the NQT and SQT should not show a significant difference in paleolatitude (Pullen and Kapp, 2014). In the overthrust model, the NQT and SQT were separated by an ocean of unknown width. Contemporaneous Permo-Triassic sediments would then be deposited on terranes with potentially significantly different latitude, and cold-water fauna is to be expected in the SQT but not in the NQT (e.g. Li et al., 1995).

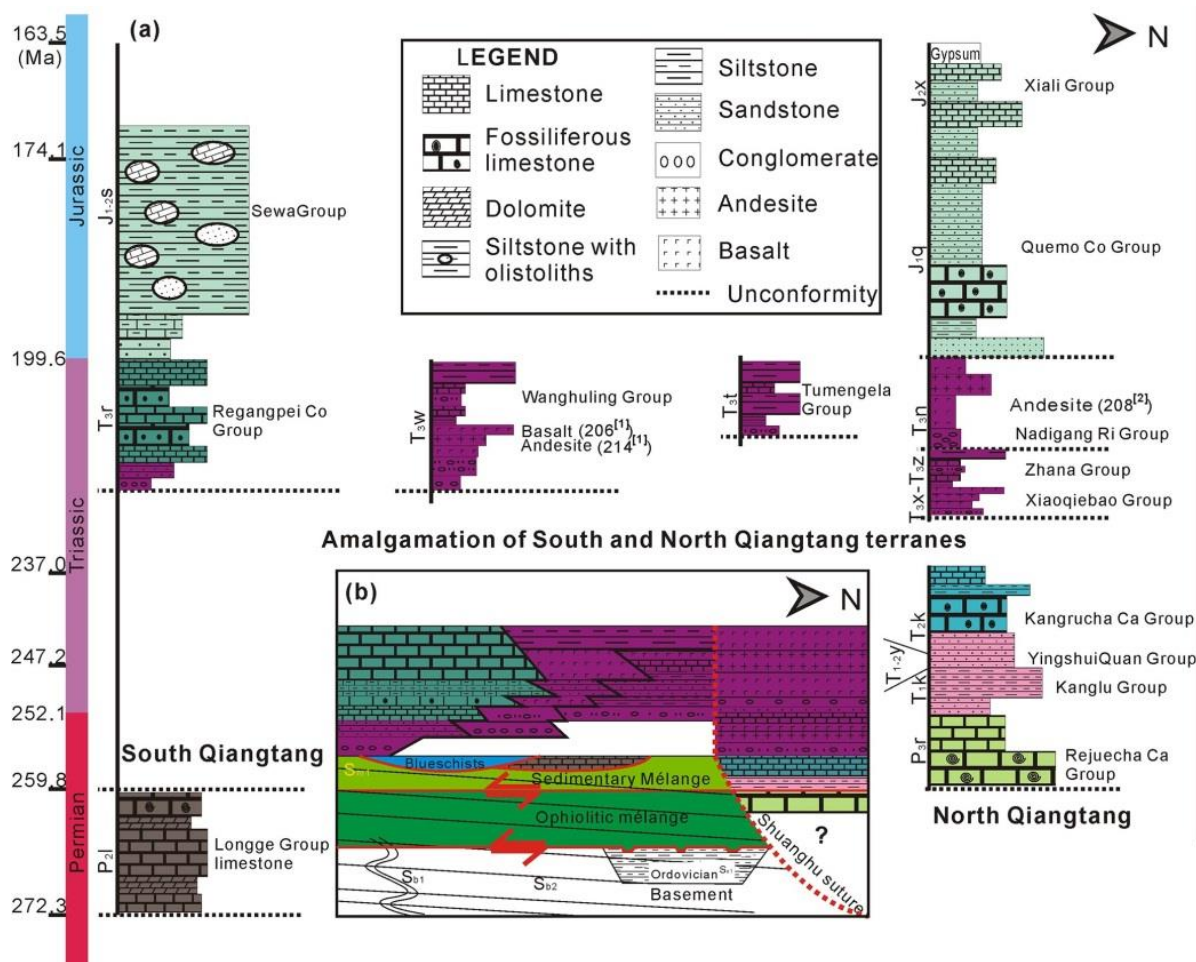


Figure 2. (a) Permian to Jurassic lithostratigraphic columns for the Qiangtang area, from south (left) to north (right); (b) structural and stratigraphic relationships. Basement, ophiolitic mélangé and sedimentary mélangé with blueschists and Permian sediments form a stack of thrust-bounded sheets. These are unconformably overlain by Late Triassic sediments and volcanics. Sources: (1) Li et al. (2007) and (2) Wang et al. (2008a).

2.2. Metamorphic grade

In the underthrust model, the *mélange* is formed between the Qiangtang terrane continental crust and the subducting oceanic plate, which is thought to subduct southward at a shallow angle. This implies that all *mélange* rocks were once buried below the Qiangtang continental crust, down to a depth of at least 35 km (Kapp et al., 2003b). In the overthrust model, the *mélange*, including high-pressure rocks, derives from the Shuanghu suture in the north of the study area. This *mélange* may include high-pressure rocks but not necessarily exclusively, such as in the case of the Franciscan complex (e.g. Agard et al., 2009). The distribution of metamorphic grade in the allochthonous units is thus an important criterion to distinguish between the two models.

2.3. Structural position of the *mélange*

In the underthrust model, the *mélange* is exhumed by normal faulting that produced metamorphic core-complex-like domes south of the JSS suture zone. This occurred due to rollback of the subducting slab (Kapp et al., 2000, 2003b; Pullen et al., 2011) or later during Jurassic extension (Fu et al., 2010a). Continental crust should thus lie structurally above the *mélange*, separated by normal faults. The opposite is to be expected in the overthrust model, which envisages the *mélange* to be thrust over the SQT. *Mélange* should then structurally overlie autochthonous crustal rocks, separated by thrusts (Zhao et al., 2014).

3. The basic stratigraphic and lithological frame in the Qiangtang terrane

Here we review the Permian to Jurassic stratigraphy of the study area (Fig. 2a), including lithofacies, paleontology and paleogeography, with particular attention to the Late Triassic unconformity. Stratigraphic age assignments were made by correlating lithostratigraphy with biostratigraphic sections within or near the study area.

3.1. Pre-collision stratigraphy and lithologies

Pre-Ordovician basement rocks crop out in the SQT in the Rongma area around the Gangtang Co granite and as a thrust sheet at Mount Mayigang Ri. These rocks are dominantly quartzite and phyllite, experienced greenschist-facies metamorphism and were deformed twice (Zhao et al., 2014). Detrital zircons show that the basement was pre-Ordovician in age and has a Gondwana affinity (Dong et al., 2011). It is unconformably overlain by slates of the Tashishan formation, dated as Middle to Late Ordovician with *Sinoceras*–*Michelinoceras* fossils (Li et al., 2004; Zhao et al., 2014). Within the area, Ordovician rocks are only found in two small areas near Rongma Village. The Devonian is only represented in the NQT; in the NQT, Carboniferous limestones are found just northeast of the study area

(Li, 2006). Carboniferous sandstones with cephalopod fossils also unconformably overlie pre-Ordovician basement rocks west of Rongma. Fossiliferous Carboniferous siltstones in the NQT were dated as Late Carboniferous (Wu et al., 2009). Ordovician to Carboniferous sediments are not metamorphosed and only one deformation phase can be recognised by folding, boudinage and cleavage development (Zhao et al., 2014). The first deformation phase observed in the basement is thus pre-Ordovician, whereas the second must be post-Carboniferous.

Only the Middle Permian Longge Group (P2l) is found in the SQT. This unit comprises massive, poorly bedded reef or platform limestones including micritic bioclastic limestone, sparry oolitic limestone, dolomicrite, and brecciated dolomite. Fossils are abundant, including stromatopores, crinoids, brachiopods, gastropods, corals, benthic foraminifera and fusuline, constraining the age to the Middle Permian. This fusuline fauna is characterised by the presence of the distinctive bitemperate fossils (Zhang et al., 2014). These strata occur as large fault-bounded rafts within the *mélange*, with a maximum thickness of ~ 5000 m. Early to Middle Permian strata are absent in the NQT, where only the Upper Permian Rejuechaca Group (P3r) occurs. It consists of grey to light-grey massive bioclastic limestone and dark-green layered micritic limestone with brachiopods and gastropods. These platform limestones reach > 500 m in thickness and contain marine faunas of typically Cathaysian provenance (Wu and Lang, 1990; Chen et al., 2009; Zhang et al., 2012b).

Late Permian to Middle Triassic strata are missing in the SQT. However, in the NQT, the Lower Triassic Kanglu Group (T1k) conformably overlies the P3r. Its thickness can reach ~ 950 m. This unit consists mainly of cyclically alternating purple, yellow or grey fine-grained sandstones, siltstones and marls. The Lower Triassic age is confirmed by the presence of *Claraia* fossils. The overlying > 1500 m thick Yingshuiquan Group (T1–2y) consists of light-grey, massive oolitic limestone intercalated with thinly layered quartz and feldspathic sandstone. The limestones are sandy and contain abundant bivalves and brachiopods. The Lower Triassic sequence is topped by the Kangnan Group (T2k) (< 310 m), which consists of grey-green, fine-grained marls at the base and a bivalve-rich limestone at the top.

3.2. Syn- to post-collision stratigraphy and lithologies

The terrane-wide, Late Triassic unconformity marks the end of subduction activity (Zhai et al., 2011a) and the beginning of a new cycle of sedimentation that continued through most of the Mesozoic.

In the NQT, the base of the Late Triassic sequence is formed by T3x and T3z. Polymictic conglomerates, pebbly siltstone and mudstone are found at the base of the Xiaoqiebao Group (T3x). Overlying the basal

Chapter 4

conglomerate are pillow basalt, basaltic lavas, andesite, rhyolite, tuffites, intraformational breccias and mass flow deposits. These, in turn, are overlain by several tens of metres of coral-bearing limestones and plant-debris-bearing sandstone with some conglomerate. The upper unit is the Zhana Group (T3z) that mainly consists of fine-grained lithic sandstone, tuffaceous sandstone and siltstone (Zhang et al., 2005). The total thickness of these units is more than 2000 m. The Late Triassic Nadigang Ri Group (T3n) in the NQT starts with a set of fluvial conglomerates (Zhu et al., 2013), followed by mainly basaltic volcanic breccia, basalt and layered quartz andesite. Minor terrestrial intervals occur in the predominantly volcanic succession. A rhyolite in this sequence was dated at 208 Ma (Wang et al., 2007). The total thickness of the Nadigang Ri Group is about 800 m.

Sediments of the Late Triassic Tumengela Group (T3t), Jiaomuchaca Group (T3j) and Wanghuling Group (T3w) are found in the middle of the study area, unconformably overlying the *mélange*. The Tumengela Group is characterized by thick-bedded, coarse to pebbly lithic sandstone and fine-grained feldspar-quartz sandstone at base. The middle unit is occupied by a dark-grey, rhythmic sequence of layered carbonaceous shale, silty shale or greyish-yellow calcareous silt. The uppermost part is composed of grey micrite and dark-grey calcareous mudstone (Zhu et al., 2013). The lower part of the T3j consists of conglomerates and platform-facies limestone, while the upper part is formed by reefal limestone with corals, brachiopods, sponges and crinoids (Zhu et al., 2013). Components of the conglomerate include poorly sorted volcanic debris, limestone and chert. The Wanghuling Group commences with a conglomerate with highly variable clasts that include limestone, basalt, sandstone and high-pressure rocks. Upwards, the conglomerate grades into sandstone intercalated with siltstone, followed by ~ 300 m of tuffaceous sand- and siltstone, rhyolite and limestone intercalations. One rhyolite layer was dated as 214 ± 4 Ma and actinolite from the underlying units gave an Ar-Ar age of 219.7 ± 6.5 Ma (Li et al., 2007; Wang et al., 2008a).

On the SQT, Late Triassic sedimentation commenced with conglomerates to sandstones (Li and Wen, 2007) unconformably overlying Permian sediments, as well as *mélange*. In the south of the area, the basal clastic sediments are overlain by medium- to thick-bedded clastic sediments and carbonates of the Riganpei Co Group (T3r) (> 3000 m). This fossiliferous group mostly consists of grey micritic limestone and oolitic limestone, intercalated with breccia, calcarenite and shell-clastic limestone, deposited in a marginal sea or carbonate platform (Zhu et al., 2013).

From south to north the Late Triassic shows a transition from shallow marine, carbonate dominated sediments towards terrestrial fluvial sediments and an increasing amount of bimodal volcanic deposits

that dominate the sequence in the NQT (Fig. 2b). Onset of sedimentation progresses from ~ 220 Ma in the south to ~ 206 Ma in the north.

3.3. Post-collision stratigraphy and lithologies

The Early Jurassic Quemo Co Group (J1q, ~ 1700 m thick) unconformably overlies the T3n on the NQT. The base of this unit is characterized by coarse clastic rocks deposited in a river-delta environment. This unit grade upwards into several cycles of mud limestone, oolitic limestone, mudstone, argillaceous siltstone and sandstone, representing an overall transgression (Fu et al., 2010b). This is followed by the Middle Jurassic Xiali Group (J2x) that shows a regressive sequence throughout the north Qiangtang basin. The lower part of this unit is composed of mudstone interbedded with sparry oolitic limestone, while the upper part consists of mudstone, micritic limestone and gypsum intercalations (Zhang et al., 2006c).

In the southern part of the area, < 1000 m thick Jurassic strata of the Sewa Group (J1–2s) conformably overlie the Triassic (T3r). The group consists of dark shales, siltstones, fine- to medium-grained sandstones with olistoliths, limestone lenses and quartzite. The whole sequence of sandy foreshore or shore facies sediments is possibly related to the earliest stages of basin subsidence in the southern Qiangtang realm during Early Jurassic extension (Duan et al., 2009; Schneider et al., 2003) and Mesotethys formation (Baxter et al., 2009). Tertiary (possible even Late Cretaceous) to recent terrestrial sediments, mostly conglomerates, covers the area in scattered, usually fault-bounded basins (Kapp et al., 2005).

3.4. Lithologies and metamorphism of the mélangé in the Qiangtang terrane

The subduction mélangé, only found on the SQT, is divided into three lithologies: (1) ophiolitic mélangé (Zhai et al., 2007, 2010), (2) sedimentary mélangé consisting of deep-water clastic sediments together with blocks and rafts of high-pressure rocks and (3) Permian limestones (Zhang et al., 2012a; Fig. 1b).

The ophiolitic mélangé consists of gabbro, diabase and basalt blocks and lenses, intercalated with deep-water siltstone, with minor chert, mudstone, sandstone and limestone. The mafic rocks have ocean-island or MORB affinities (Zhai et al., 2004; 2007) and range in age from the Ordovician to Triassic. Ordovician to Carboniferous gabbro ages were reported from rocks in the NW of the study area (Fig. 1b), which were interpreted as Paleozoic ophiolitic segments (Zhai et al., 2009, 2010, 2013b). Permian ophiolitic mélangé was first documented by Zhai et al. (2007) in the Jiaomu Ri area. Northwest of Rongma village, mélangé of gabbro blocks, pillow basalt and minor ultramafic blocks embedded in siltstone have Permian and Triassic ages (Li et al., 2009; Zhang et al., 2012a). Most of these mafic rocks preserved their original

structures such as amygdules in basalt (Fig. 3a). In a thin section, the gabbros show no signs of strong deformation or of metamorphism (Fig. 3b). That means that the ophiolitic *mélange* was never buried to significant depths.

The sedimentary *mélange* is mainly found south of Mayigang Ri, north and east of Jiaomu Ri and in an east–west- to southwest–northeast-trending belt in the southern part of the study area (Fig. 1b). Its composition is highly variable and includes sandstone, siltstone, mudstone, chert, thinly bedded limestone and minor mafic blocks. Competent lithologies are embedded as lenses in a strongly foliated matrix (Fig. 3c). Various sedimentary structures are preserved, such as Bouma sequences, graded bedding, load casts (Fig. 3d) and flute marks. Sections of the stratigraphy are preserved but disturbed by folds and faults (Fig. 3e). The sediments are not metamorphosed, as can be seen from a lack of recrystallisation in a fine-grained siltstone (Fig. 3f). Fossils show that occasional limestone blocks are of Permian age (Zhang et al., 2012a). Preservation of fossils and primary sedimentary microstructures show that the sedimentary *mélange* was not metamorphosed. However, the Permian limestones in contact with blueschists NE of Rongma trend towards strongly deformed marbles at that contact. The marbles contain assemblages of calcite + tremolitic amphibole \pm epidote \pm garnet \pm quartz, which indicates elevated temperatures (up to ~ 500 °C) but relatively low pressure (Bucher and Frey, 2002). Microstructures indicate strong ductile deformation of the calcite (twinning, dynamic recrystallisation) after at least growth of tremolitic amphibole (Fig. 4a). The garnet, however, appears to have grown post-tectonically, implying a syn- to post-tectonic thermal event (Fig. 4b).

High-pressure rocks are found in association with the clastic sediments and Permian limestones of the sedimentary *mélange*. Main outcrops of high-pressure rocks are located in Jiaomu Ri and south of Gangtang Co (Fig. 1b). They consist of phengite-quartz schists, blueschists and eclogites (Kapp et al., 2003b; Liu et al., 2011; Zhai et al., 2011b; Zhang et al., 2006a). Peak metamorphic age is ~ 244 Ma and exhumation occurred around 220–214 Ma (Zhai et al., 2011b; Pullen et al., 2011). Maximum temperature and pressure ranges are 410–460 °C and 2.0–2.5 GPa. All authors agree that the exhumation was related to subduction, although the mechanism and plate tectonic setting remains under debate (Kapp et al., 2003b; Zhang et al., 2006b; Li et al., 2009; Pullen and Kapp, 2014).

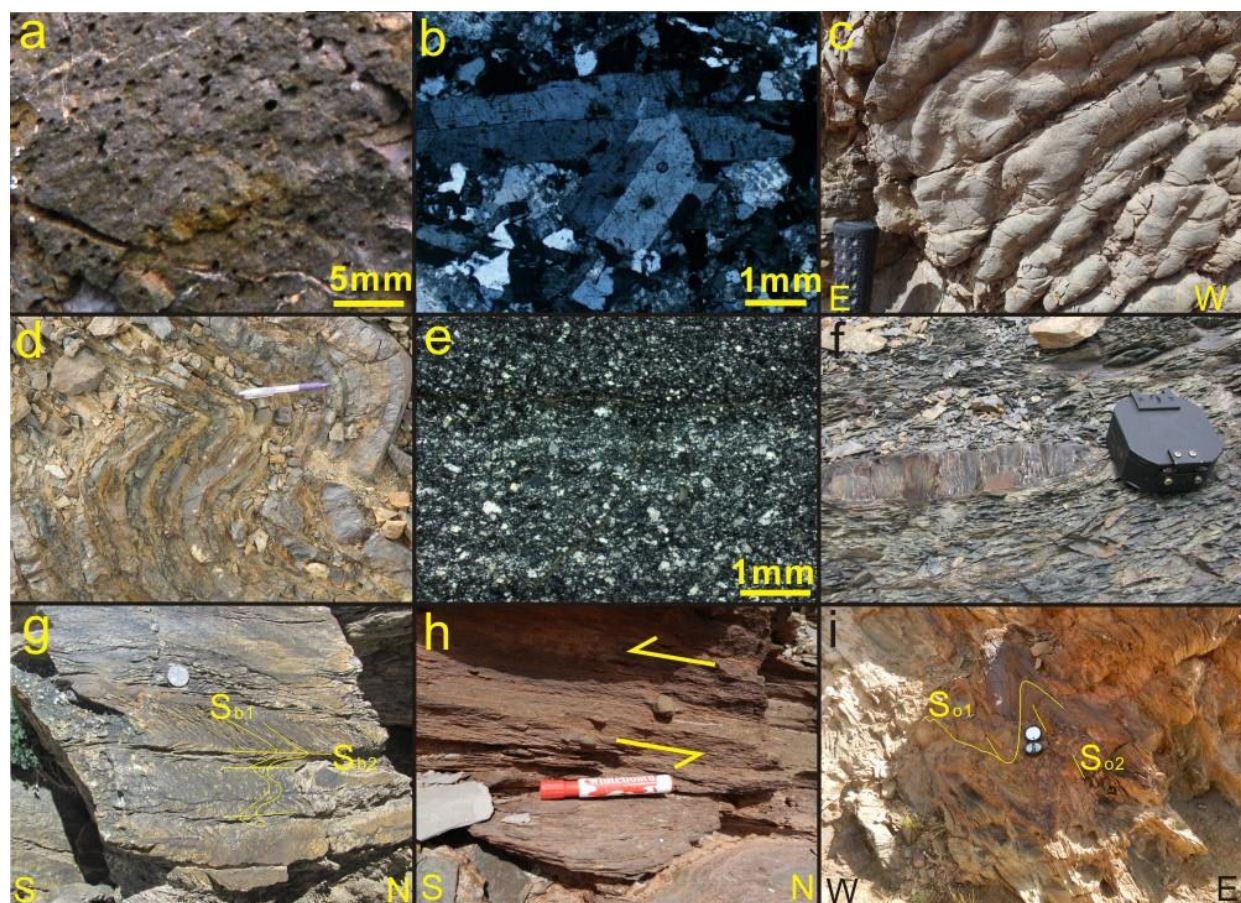


Figure 3. Field photographs and micrographs showing metamorphism and deformation in the different units: (a) amygdules in basalt from the ophiolitic *mélange*, west of Rongma; (b) thin sections of gabbro, west of Rongma; (c) load cast in mudstone from the southern part of the sedimentary *mélange*; (d) folded chert from the sedimentary *mélange* west of Jiangaizangbu River; (e) thin sections of siltstone, west of Rongma, which show that the ophiolitic and sedimentary *mélanges* did not experience any significant metamorphism; (f) typical main foliation in the sedimentary *mélange* wrapping around competent blocks, here sandstone; (g) outcrop view of basement deformation: Sb1 is folded, during which a second, crenulation cleavage Sb2 developed. (h) Pressure shadow around pebbles in the Ordovician siltstone indicate top-to-south shearing. (i) Near the thrust where ophiolitic *mélange* is thrust over Ordovician sediments (Fig. 6b), their deformation is more intense, with the local development of an axial planar So2.

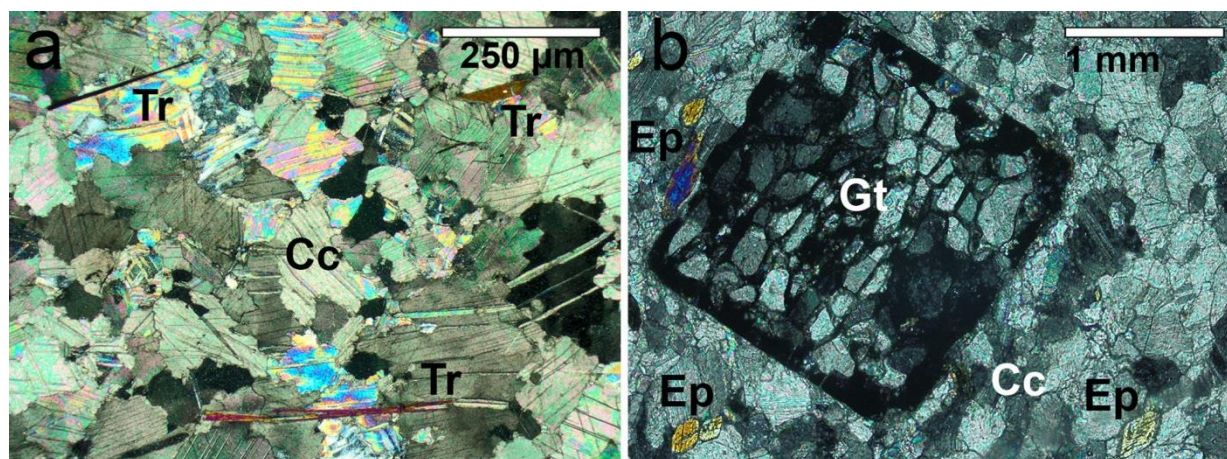


Figure 4. Micrographs (crossed polars) of marbles at the contact between Permian limestone and blueschist, northeast of Rongma; deformed and dynamically recrystallised calcite (Cc) with aligned needles of tremolitic amphibole (Tr); (b) calcite marble with epidote (Ep) and post-tectonic poikiloblastic garnet (Gt).

At this stage it is useful to compare the stratigraphy described here with that of the detailed map of the Rongma and Jiaomu Ri area of Kapp et al. (2003). These authors define two types of *mélange*: blueschist and greenschist-facies *mélange*. The blueschist, which is readily identified in the field and on satellite images, corresponds to the high-pressure rocks described above. According to Kapp et al. (2003), greenschist *mélange* only occurs west of the Jiangaizangbu valley in areas that we classified as ophiolitic or sedimentary *mélange*. Large areas that we mapped as *mélange*, because of the chaotic nature and strong deformation of the rocks, were assigned to an autochthonous Carboniferous (C1-2) to Permian (P1-4) series that overlies the *mélange* in the interpretation of Kapp et al. (2003). The Carboniferous sandstone, siltstone phyllite and slate (C1) west of Rongma are equivalent to the pre-Ordovician basement and overlying Ordovician and Carboniferous metasediments (Zhao et al., 2014). C1 northeast of Rongma is part of the sedimentary *mélange*. Fossil evidences show that the C2 sandy limestone interbedded with siliciclastics actually belongs to the Middle Permian Longge Group (P2l; Zhang et al., 2012a, 2014).

The Permian sequence of Kapp et al. (2003b) begins with turbiditic fine-grained volcanoclastic greywacke, sandstone, siltstone, and slate (P1) and thinly bedded dark-grey limestone (P2), both of which are part of the sedimentary *mélange* in our interpretation. Part of the basalts, as well as volcano-sedimentary sandstones to conglomerate/breccia (P3), corresponds to the Late Triassic Tumengela Group (T3t) and Wanghuling Group (T3w), the latter dated at 214 ± 4 (SHRIMP) to 206 ± 4 (Ar-Ar) Ma on rhyolite and basalt of the Wanghuling Group (Zhu et al., 2005; Li et al., 2007). Other outcrops of P3 we assigned to either ophiolitic *mélange* (dominated by mafic rocks) or the sedimentary *mélange* (dominated by

sediments and breccias). The limestone and subordinate sandstone (P4) corresponds to the sediments of the top of the Wanghuling Group in areas where P3 corresponds to its base. In the remainder of the area northeast of Jiaomu Ri, P3 is mapped as sedimentary *mélange*.

As pointed out by Zhang et al. (2012b), the differences in stratigraphic and lithological classification clearly have major consequences for the inferred tectonic history of the Qiangtang area. In the map of Kapp et al. (2003b) the area of *mélange* is less than half that shown in Fig. 1. Furthermore, all *mélange* is at least greenschist facies, derived from depths of ~ 35 km. Greenschist-facies rocks can indeed be found in the ophiolitic and sedimentary *mélange*, but these occur together with non-metamorphic rocks. The whole *mélange* unit is therefore non-metamorphic, but includes metamorphic rocks from various origins, such as the Qiangtang basement (Zhao et al., 2014).

3.5. Igneous activity in the Qiangtang terrane

Apart from the ophiolites, the Qiangtang area records Carboniferous to Jurassic igneous activity. EW-striking diabase dykes intrude basement rocks and were dated at 284 ± 3 and 302 ± 4 Ma by Zhai et al. (2009). Mostly felsic magmatic activity is dated between about 275 and 248 Ma in the NQT east of the study area and interpreted as related to northward subduction underneath the NQT (Yang et al., 2011; Zhang et al., 2013). This is followed by bimodal activity that continued into the Jurassic (Zhang et al., 2011). Triassic (236–219 Ma) adakites and magnesian andesites from the Tuotuohe area, central NQT, are interpreted as subduction related but indicate that the mantle source was metasomatised by slab melting (Wang et al., 2008b). Some basalts show continental arc affinities, the source most likely being a mixture of MORB- and within-plate basaltic source. This suggests the lithospheric mantle may be slightly to moderately enriched, most likely by a previous subduction process (Zhai et al., 2004). Whereas abundant arc-related Permo-Triassic activity is documented in the NQT, relatively little evidence for such activity is documented in the SQT. Wu and Lang (1990) reported Late Permian andesites and dacites in the SQT, which led Liu et al. (2011) to propose not only subduction to the north underneath the NQT but also to the south underneath the SQT.

Along the southern margin of the NQT the Nadigang Ri group is mainly composed of acid tuff, dacite, rhyolite and minor basaltic volcanic rocks ranging in age from 223 to 205 Ma (Zhai and Li, 2007; Fu et al., 2008). These rocks show a trend from melt generated by melting of subducted slab (ca. 223–219 Ma) to melting of Proterozoic oceanic crust (ca. 215–205 Ma; Zhai et al., 2013a). Bimodal activity continued to ~ 177 Ma (Zhang et al., 2011) and includes the intrusion of the Gangtang Co granite at ~ 210 Ma (Kapp et al., 2003b; Hu et al., 2012). Granite samples from Gangtang Co granite (unpublished data) show

a deep Eu anomaly as normalised to EMORB or OIB and show REE contents similar to OIB-derived melts. Some trace element concentrations, such as Ta, Yb, Nb, Y and Rb, suggest granite formation in a syn-collisional volcanic arc environment. The mafic lavas were probably derived from the mantle, whereas the felsic lavas were probably derived from partial melting of the continental crust in response to the asthenospheric upwelling (Zhang et al., 2011).

4. Structures and tectonics of the *mélange* in mapping area

Although there are abundant data on stratigraphy and igneous activity in the area, only a few (and contradicting) structural analyses have been published so far (e.g. Kapp et al., 2003; Pullen et al., 2011; Liang et al., 2012; Zhao et al., 2014). Below we present the results of detailed mapping in conjunction with 3-D modelling using satellite images and the program 3-D Move™ by Midland Valley. The falsecolour ASTER images proved to be very useful, as different units can be recognised clearly and mapped in inaccessible areas after ground-truthing in mapped areas. The high topography also allows orienting the main structures and faults on the large scale.

The large-scale structure was modelled for three areas: SE of Mayigang Ri, NW of Rongma and NE of Jiaomu Ri (Fig. 5; see Fig. 1a for locations). The block diagrams show that the various units form a large-scale fold-and-thrust belt. Precambrian basement, exposed at Mayigang Ri, forms a flat-lying, N-dipping sheet that overlies a sheet of sedimentary *mélange*, separated by a $\sim 5\text{--}20^\circ$ NE-dipping fault gouge (Fig. 6a). The upper few tens of metres of the underlying sedimentary *mélange* are strongly sheared with a top-to-the-south sense of shear. The sedimentary *mélange* is itself underlain by ophiolitic *mélange*. Lithologies and main foliations are approximately parallel and follow the contacts between the various units, interpreted as thrusts. All units and main foliation are folded with shallowly plunging, EW- striking fold axes (Fig. 5). To the south, north of Gangtang Co, the ophiolitic *mélange* is thrust over N-dipping Precambrian basement and slivers of Ordovician slate (Figs. 5, 6c). Unfortunately, most of this area is covered by Tertiary sediments.

West of Rongma, NE-dipping ophiolitic *mélange* overlies Precambrian basement and Ordovician and Carboniferous sediments (Fig. 6b). The main and only foliation in these latter units, as well as the second foliation (Sb2) in the underlying basement rocks, dips to the NE and increases in intensity towards the contact. The contact itself was initially a ductile shear zone that was overprinted by brittle deformation, as mylonitic rocks are found as clasts in brittle breccias. Sigmoidal clasts in Ordovician sediments indicate a top-to-the-south shearing (Fig. 3g). To the east, the ophiolitic *mélange* is overlain by a sheet of sedimentary *mélange* followed by a sheet of blueschists that contains marble lenses. The blueschists are

gently folded around NS-striking fold axes. The strongly deformed high-pressure rocks are overlain by a sheet of non-metamorphic and relatively undeformed Permian limestones. The sequence of ophiolitic mélange, sedimentary mélange and blueschists is repeated again towards Jiaomo Ri. The shallow-dipping blueschists clearly overlie the sedimentary mélange (Fig. 6d).

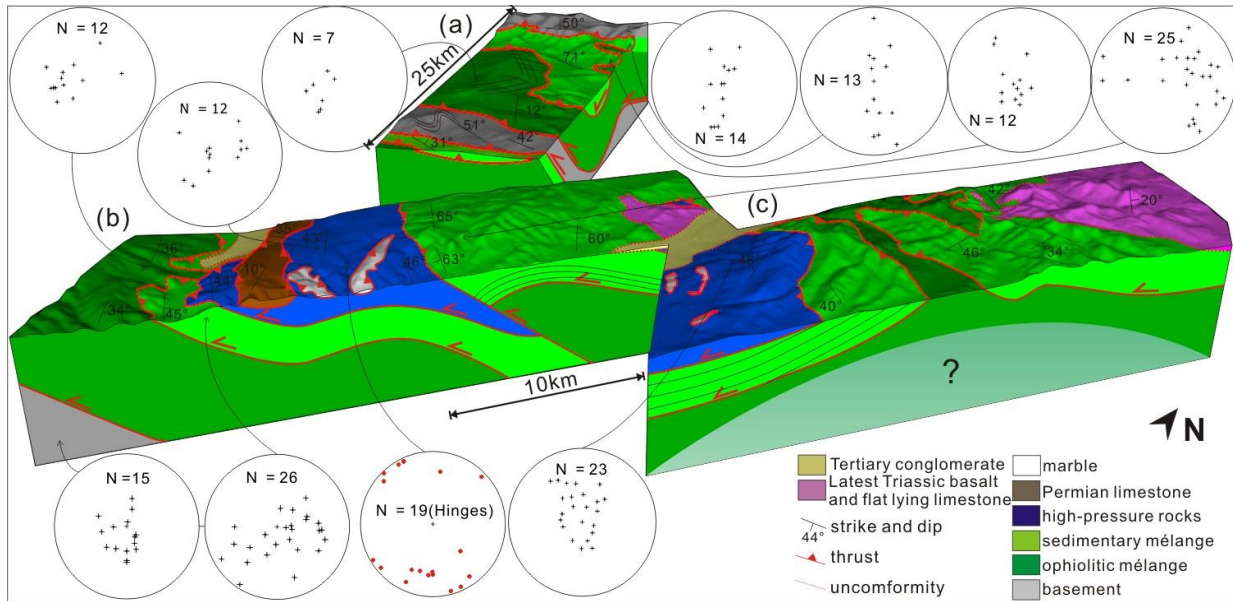


Figure 5. Three-dimensional reconstruction of selected areas near Rongma in the centre of the area showing the fold-and-thrust geometry of the three main sheets: basement, ophiolitic mélange and sedimentary mélange together with high-pressure rocks and rafts of (Permian) sediments. These are unconformably overlain by Late Triassic sediments: (a) south of Maignag Ri, (b) northeast of Rongma and (c) northeast of Jiaomo Ri (see Fig. 1b). Lower-hemisphere equal-area stereoplots show the distribution of the main foliations (black crosses), as well as orientations of fold axes (red dots).

The large-scale structure of the area is thus a fold-and-thrust belt of, from bottom to top, Qiangtang basement (Pre-Cambrian to Carboniferous), ophiolitic mélange and finally juxtaposed sedimentary mélange, blueschists and rafts of Permian sediments. All these units have a dominant tectonic foliation that is approximately parallel to the main lithological boundaries. This foliation is the second foliation (Sb2) in the Precambrian basement (Fig. 3h), the first in the Carboniferous and Ordovician sediments (So1, Fig. 3g) and the main one (Sm1) in the mélanges, which wraps around lenses and clasts. The parallelism of these foliations between the different units and with the main sheets indicates that they all formed during the thrusting event that created the stack of sheets. This is confirmed by So2 west of Rongma, which is approximately parallel to bedding, causing boudinage and locally south-vergent isoclinal folding (Fig. 3i). It increases in intensity towards the mylonitic/breccia contact with the over-

lying ophiolitic mélange, as is to be expected if So₂ had been formed during thrusting of that mélange over the basement.

The ~ 8 km thick stack of sheets is folded and thrust on the > 10 km scale. The thickness of the stack, here derived from mapping and structural reconstructions, is confirmed by seismic data of Lu et al. (2013) and Li et al. (2013). The strike of the thrusts rotates from EW in the north towards NS in the east. In the southern part of the area folding and thrusting is south-vergent again (Fig. 5). This variation in trends is interpreted as the result of later doming of the central Qiangtang Culmination, which may have occurred as late as the Jurassic (Kapp et al., 2003a). Late Triassic limestones and overlying basalts discordantly overlie the sedimentary mélange and blueschists. These Triassic units are almost undisturbed and undeformed and shallowly dip to the east. The absence of equivalent Late Triassic sediments further west may be because these were never deposited here or because of the aforementioned doming, with the upper units now removed by erosion. The discordant contact between Late Triassic layers and underlying mélange and blueschists, as well as the lack of deformation in the Late Triassic layers, is evidence that sheet-parallel thrusting happened before the ~ 210 Ma Triassic sedimentation.

Further evidence is the fact that the undeformed 210 Ma Gangtang Co granite is in intrusive contact with basement rocks and ophiolitic mélange and clearly cuts the contact between these two units (Fig. 1b; Zhao et al., 2014). Formation of the sheet stack can thus be constrained to have occurred between about 220 Ma (Ar-Ar age of blueschists; Zhai et al., 2011a, b) and 210 Ma, which is the age of the granite intrusion and onset of Late Triassic sedimentation.

Timing of the folding and thrusting of the sheet stack is less clear. Folding of Late Triassic and Jurassic units in the south of the area and even occasional folding of Tertiary conglomerates are clear evidence for Mesozoic to Tertiary tectonic activity (Kapp et al., 2005). Late Triassic sedimentation commenced earlier in the south than in the north of the SQT terrane. This suggests the presence of a foreland basin or depression in front of the thrust belt (Fig. 6e), with sedimentation progressively extending to the north as erosion flattened the topography. It cannot be excluded that the fold and thrust belt, at least in part, occurred in the Late Triassic.

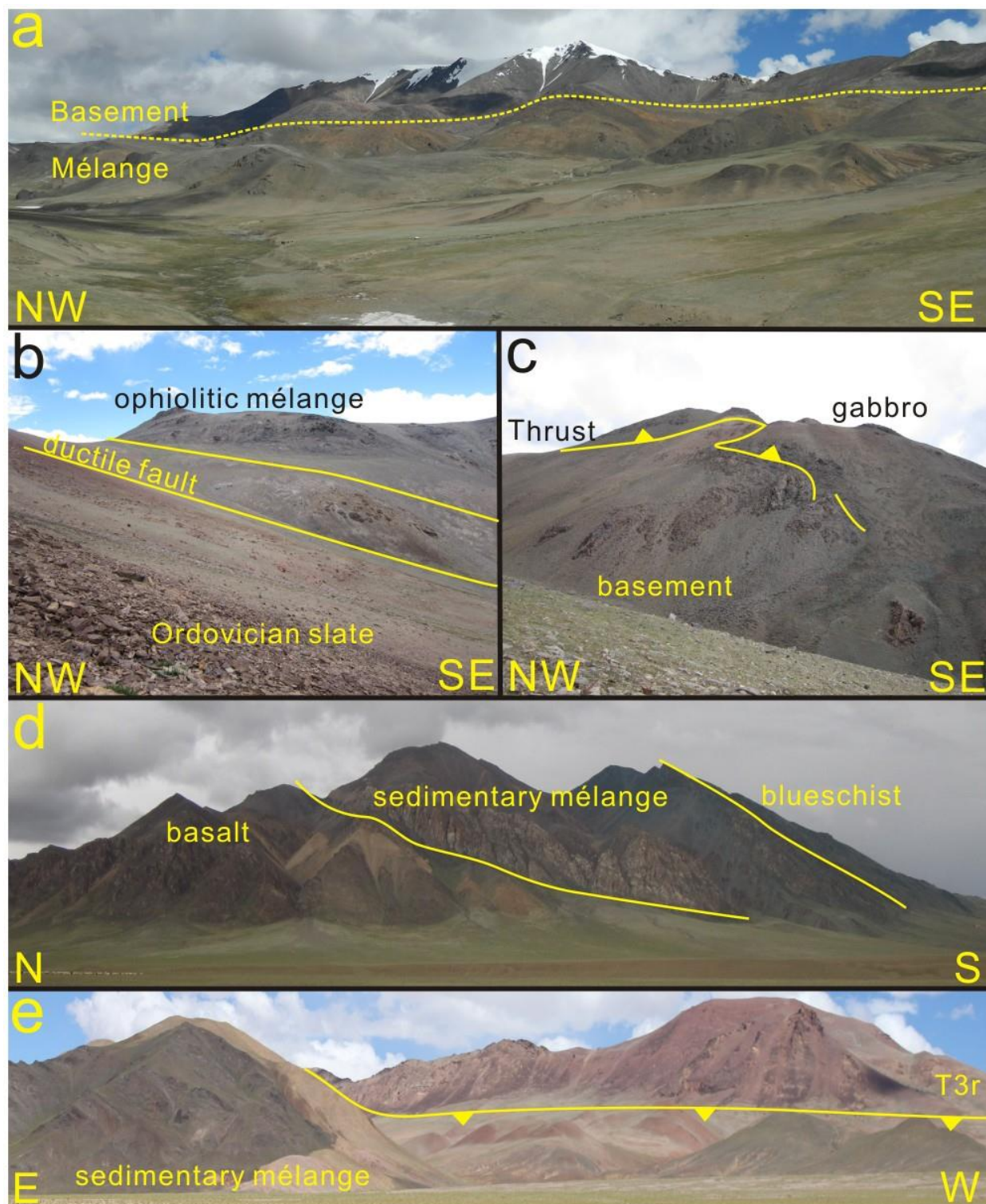


Figure 6. Field relationships of the main units. (a) View to the NW towards the Mayigang Ri Thrust, which thrusts basement on top of sedimentary mélangé. (b) West of Rongma, ophiolitic mélangé is thrusts on top of basement and Ordovician sediments, now separated by a wide fault zone. (c) Folded thrust that placed gabbros of the ophiolitic mélangé on top the basement, north of Gangtang Co. (d) View

from the north towards Jiaomu Ri, clearly showing that blueschists lie above the sedimentary *mélange*, which in turn overlies basalts of the ophiolitic *mélange*. (e) North-dipping thrust places subduction *mélange* over Late Triassic limestone (T3r) in the south of the study area, showing that at least part of the thrusting postdated the Late Triassic.

5. Discussion

5.1. Summary of main events and structures

Any model for the tectonic evolution of the Qiangtang terrane(s) must take the following observations into account:

1. The SQT is a continental terrane with Gondwana affinity (Dong et al., 2011; Zhao et al., 2014) that comprises a Precambrian basement that is unconformably overlain by Ordovician to Middle Permian sediments.
2. Subduction-related igneous activity in the NQT ranges in age from 275 to 248 Ma (Yang et al., 2011; Zhang et al., 2013) and is attributed to subduction of the Paleo-Tethys to the north at the Shuanghu suture (Yang et al., 2011) or alternatively to southward subduction of the Paleo-Tethys towards the south at the JSS suture (Wang et al., 2008b). Equivalent igneous activity is rare in the SQT. Both the NQT and SQT saw bimodal igneous activity, ranging in age from 236 to 177 Ma, with signatures indicating mafic underplating and ensuing crustal melting (Zhang et al., 2011). Most authors attribute this to some form of slab break-off (Zhai and Li, 2007; Zhang et al., 2011; Peng et al., 2014).
3. Although all workers agree that high-pressure rocks and subduction-related *mélange* crop out in the centre of the Qiangtang terrane, there is no agreement on the extent and classification of the various rocks. According to some authors, most of the area under consideration is a single “metamorphic belt” (e.g. Zhang et al., 2011), which ignores the fact that many rocks in this area are not metamorphic. Furthermore, metamorphism in the Precambrian rocks is pre-Ordovician (Zhao et al., 2014) and is unrelated to the Triassic high-pressure metamorphism of the blueschists. An opposite view is taken by Kapp et al. (2003b), who restrict the *mélange* to greenschist- to blueschist-facies rocks and classify the other, non-metamorphic rocks as part of the overlying Qiangtang continental crust. However, in our view this restricts the definition of *mélange* in the area too much, as large areas are *mélange* but not metamorphic. Based on our mapping, we define three main *mélange* lithologies: an ophiolitic and a sedimentary *mélange*, both not-metamorphosed (but carrying metamorphic inclusions), and a high-pressure unit.
4. The ophiolitic *mélange* consists of a range of sediments and abundant gabbros and basalts. A coherent oceanic crust sequence is, however, not observed. Ages of the mafic rocks range from Ordovician to Triassic.

5. The high-pressure rocks experienced peak metamorphic conditions at ~ 240 Ma and exhumed between 220 and 210 Ma, giving a minimum exhumation rate of $> 1 \text{ cm yr}^{-1}$ (Zhai et al., 2011b).
6. In the Rongma area, the main units form a stack of sheets with Precambrian to Carboniferous basement at the base, ophiolitic *mélange* in the middle and sedimentary *mélange* with large rafts of blueschists and non- metamorphic Permian sediments towards the top.
7. Formation of the sheet stack by S- to SW-thrusting took place between about 220 and 210 Ma. It was postdated by intrusion of the undeformed, 210 Ma Gangtang Co granite and onset of Late Triassic sediment deposition and volcanic activity.
8. The sheet stack was folded and thrust, again in an S to SW direction. Timing is uncertain and can range from the Late Triassic to the Mesozoic.

5.2. Existence of a Paleo-Tethys ocean and direction of subduction

The first question that needs to be addressed is whether the north and south Qiangtang are individual terranes that were separated by an ocean or not. One argument for the presence of this ocean is that glacial deposits and cold-water fauna indicate that the south Qiangtang terrane remained at high southern latitudes until the Middle Permian. However, only Upper Permian warm-water sediments are found in north Qiangtang terrane. It is thus possible that the north and south Qiangtang terranes moved into warmer regions together between the Middle and Late Permian. As was discussed by Pullen et al. (2014), cold- and warm-water faunas in the NQT and SQT neither prove nor disprove a separation of the two terranes.

Most authors invoke Permo-Triassic arc-related igneous activity, mainly in the NQT, as evidence for the former existence of the Shuanghu–Tethys between the NQT and SQT (Yang et al., 2011; Zhai et al., 2011a; Zhang et al., 2013; Peng et al., 2014). With few exceptions (Wang et al., 2008b), these authors interpret the igneous activity to result from northward subduction of this ocean underneath the NQT. Further indications for a former ocean between the NQT and SQT are the ophiolitic *mélange* and high-pressure rocks with oceanic affinity (Zhai et al., 2007; 2013a) in the SQT. However, Pullen and Kapp (2014) favour a southward subduction of the JSS–Tethys underneath a single Qiangtang terrane. The main argument for this is that in their structural interpretation, the subduction *mélange* in the Qiangtang terrane lies underneath the continental crust and was later exhumed by doming and normal faulting. The question is thus whether the *mélange* lies below or above continental crustal rocks. Several arguments are in favour of the latter. If the *mélange* was below the crust, it came from a depth of at least 35 km (Kapp et al., 2003b) and all *mélange* rocks must be metamorphic. This is not the case. Even with the restrictive definition of *mélange* in the map of Kapp et al. (2003b), areas mapped as greenschist are not all

metamorphosed (Fig. 3a–e). As not all *mélange* rocks are metamorphic, they cannot all have come from a depth of tens of kilometres, as required in the underthrust model. Furthermore, this model requires a very shallow subduction angle for the subduction *mélange* to be at a relatively shallow depth 200 km south of the suture. This cannot explain the subduction-related igneous activity only in the north, close to the postulated suture. Finally, our mapping and structural interpretation clearly favours emplacement of the *mélange* on top of the continental crust (Fig. 5). If, as argued here, the *mélange* and high-pressure rocks were not exhumed by core-complex-like doming, their presence within the SQT is difficult to reconcile with any model other than the former presence of an ocean between the NQT and SQT.

5.3. Models for exhumation of high-pressure rocks

The presence of high-pressure rocks is one of the arguments to invoke subduction to the south or north of the NQT. The southward underthrust model of Kapp et al. (2003b) provides a clear mechanism of exhumation of the high-pressure rocks: metamorphic core-complex-like doming. This requires all *mélange* to have experienced high-pressure conditions, which contradicts our findings. The sequence of basement rocks at the base, overlain by ophiolitic *mélange* and high-pressure rocks, sedimentary *mélange* and sediments, cannot be reconciled with the proposed exhumation in a core complex, in which the autochthonous basement rocks should lie above the *mélange*.

Proponents of the northward subduction of a Shuanghu–Tethys underneath the NQT do not provide detailed mechanisms on the exhumation of the high-pressure rocks. Most authors propose high-pressure metamorphism at the downgoing slab, with subsequent exhumation in the orogenic wedge, possibly related to slab break-off (e.g. Zhang, 2006a; Li et al., 2009; Liu et al., 2011; Yang et al., 2011; Zhai et al., 2011a, b, 2012; Tang and Zhang, 2013). One problem with this exhumation in a convergent setting is that it should be related to extensive erosion during exhumation, which appears inconsistent with the regional sedimentary record (Pullen and Kapp, 2014). Exhumation of high-pressure rocks in the orogenic wedge also does not explain how the high-pressure rocks are brought into contact with non-metamorphic sediments and sedimentary *mélange* as is observed in the Rongma area.

5.4. Proposed tectonic evolution

Below we provide an overview of the sequence of tectonic events that affected the Qiangtang area. The model we propose aims to explain our observations made in the study area and those published in the literature. Of particular relevance are the following: (1) the NQT and SQT were separated by an ocean of unknown width; (2) the high-pressure rocks and tectonic *mélange* are found in a fold-and-thrust belt of a stack of three sheets-basement rocks, ophiolitic *mélange* and sedimentary *mélange*-together with HP

rocks and undeformed Permian sediments; (3) mafic rocks in the ophiolitic mélangé range in age from the Ordovician to the Triassic. A key observation that needs to be explained is that the exhumed high-pressure rocks were brought into direct contact with originally overlying non-metamorphic sediments and mélangé.

5.4.1. Pre-Ordovician (> 470 Ma)

The pre-Ordovician clastic metasediments form the oldest and structurally lowest unit of the Qiangtang basement. These rocks experienced low-grade metamorphism and one stage of deformation, leading to folding and the formation of the first cleavage (Sb1). This event is tentatively attributed to the Bhimphedian Orogeny (Cawood, 2007), when the basement rocks still formed part of (assembling) Gondwana (Zhao et al., 2014).

5.4.2. Ordovician to Permian (470–270 Ma)

Opening of the Shuanghu–Tethys between the NQT and the SQT probably commenced in the (Late) Ordovician. The SQT formed the passive northern margin of Gondwana on which sediments were deposited at various stages from the Ordovician to the Permian. Exposures of the Sumdo eclogites in the Lhasa terrane may indicate that the SQT and north Lhasa terrane together separated from Gondwana as early as the Carboniferous (Yang et al., 2009). Initial rifting and subsequent ocean spreading produced mafic rocks with ages ranging from the Ordovician to the Permian in central Qiangtang (Zhai et al., 2010, 2012, 2013).

5.4.3. Upper Permian to Lower Triassic (270–240 Ma)

Northward subduction of the Paleo-Tethys underneath the NQT commenced at ~ 275 Ma, as is indicated by arc activity in the NQT (Yang et al., 2012; Fig. 7a). The youngest known passive margin sediments (P21) were deposited on the SQT, but no known sedimentation occurred at the active southern margin of the NQT where arc volcanism occurred instead. Ocean-floor sediments and mafics from the oceanic crust were accreted to the NQT: the future ophiolitic mélangé (Zhai et al., 2010, 2012, 2013). Although igneous activity indicates that most of the subduction occurred on the northern margin of the Shuanghu–Tethys, the southern margin, with cold, > 100-million-year-old oceanic crust, would probably also have started to subduct (Fig. 7b; Liu et al., 2011). This would have brought oceanic crust and material from lower crust of the overriding SQT plate down to > 100 km by ~ 240 Ma, which is the age of peak metamorphism in the high-pressure rocks (Pullen et al., 2011).

5.4.4. Middle Triassic (240–220 Ma)

With (minor) subduction to the south as well, the Shuanghu–Tethys plate would have formed a divergent double subduction zone (Gray and Foster, 2004; Soesoo et al., 1997; Zhao, 2015) with a long slab subducting to the north and a short one to the south. A divergent double subduction zone was proposed for the Shuanghu–Tethys by Liu et al. (2011). As long as the two sutures are far enough apart, each

operates independently from the other. In the absence of spreading in-between, the two sutures must converge by rollback. This inevitably leads to the two sutures converging to the point where the slab pull of one subduction zone starts to affect the other. At some point in this scenario, the slab pull of the long (northern) slab will override the opposite pull of the short (southern) slab, which results in the short one being pulled up and towards the north (Fig. 7c). This scenario is similar to the current situation of the Adria plate, which subducts underneath Italy (short slab) and the Dinarides (long slab; Gvirtzman and Nur, 2001; Di Stefano et al., 2009; Giacomuzzi et al., 2012). The Adria plate now moves as a whole towards the Dinarides, causing rapid extension east of the Apennines (Devoti et al., 2008; Weber et al., 2010). The proposed model for exhumation of high-pressure rocks in a divergent double subduction zone is novel but bears some similarities with models for exhumation by slab rotation (Hacker et al. 2000; Webb et al., 2013) or slab eduction (Andersen et al., 1991; Duretz et al., 2012; Brueckner and Cuthbert, 2013). The main difference is that we suggest that the pull of the longer slab is the driving force for slab extraction and resulting exhumation of high-pressure rocks. Extraction of the slab from underneath the SQT causes extension of its margin, while high-pressure rocks exhume. Trench and Permian margin sediments are dragged off the margin and brought in contact with the exhumed high-pressure rocks from below to form the observed association of sedimentary *mélange*, rafts of Permian sediments and blueschists. All these rocks, as well as the SQT Precambrian to Carboniferous basement are expected to experience strong flattening strain due to the extension, as well as a top-to-south shearing. This is consistent with the D2 deformation in basement rocks (Sb2, So1) and main foliation in the sedimentary *mélange* (Sm1). It should be noted that this core-complex-like extension is to some extent similar to that proposed by Kapp et al. (2003b) with the difference being that we propose the whole oceanic slab, not only the *mélange*, to form the core of the complex. The structural relationships are in part similar as described by these authors: low-grade rocks juxtaposed onto high-pressure rocks in a strongly extensional setting.

A second effect of the extraction of the short slab is rising of the asthenosphere, with resulting mafic igneous activity, as well as melting of the crust, producing felsic melts. In the SQT, bimodal activity is documented from ~ 236 Ma (Zhang et al., 2011). Liu et al. (2011) showed that exhumation of the high-pressure rocks was approximately isothermal (~ 500 °C) down to at least ~ 7 kbar, suggesting rapid exhumation that is in accordance with the proposed model. Juxtaposition of the still relatively hot exhuming blueschists and non-metamorphic sedimentary *mélange* and sediments can explain the formation of epidote, tremolitic amphibole and garnet-bearing marbles at the contact (Fig. 4). Additional heating may have been related to mantle upwelling and concomitant igneous activity.

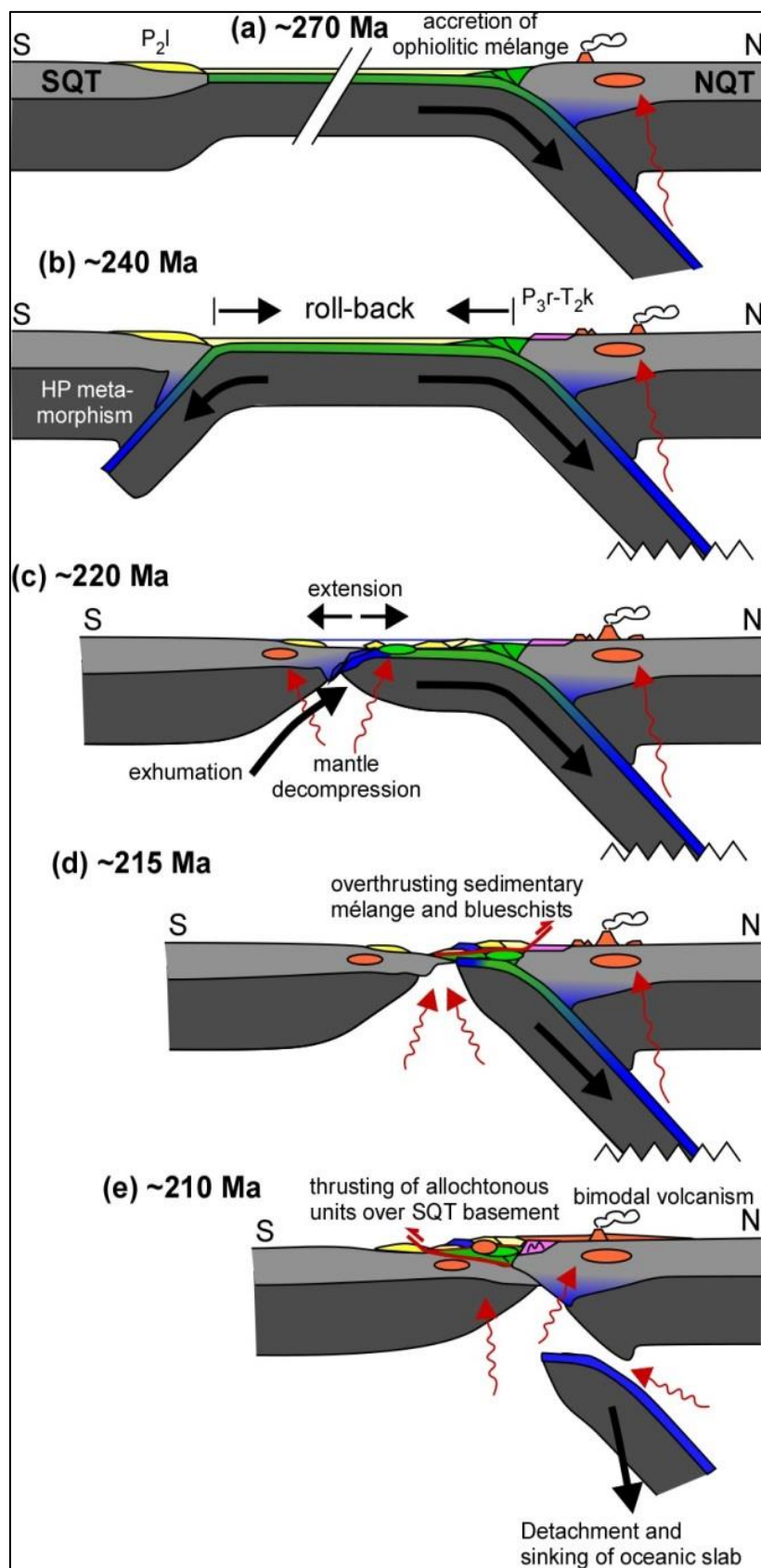


Figure 7. Schematic drawings of the Permian to Early Jurassic geological evolution of the Shuanghu–Tethys. Ages shown in the drawings are approximate only. (a) Northward subduction of the Shuanghu–Tethys underneath the NQT started at about 275 Ma. Minor southward subduction would have commenced in the Early Triassic, necessitating rollback and convergence of the NQT and SQT. (c) Interaction between the converging subduction zones led to extraction of the short southern slab and concomitant exhumation of high-pressure rocks. These are brought in contact with surface-derived margin sediments and basement in a strongly extensional setting. (d) With ongoing convergence of the NQT and SQT, the sedimentary mélangé (with high-pressure rocks) is thrust on top of the ophiolitic mélangé at the LSS suture. (e) Ophiolitic and sedimentary mélangé are ultimately thrust onto the SQT upon final collision of the two terranes. Asthenospheric upwelling leads to bimodal igneous activity on both sides of the Shuanghu–Tethys suture zone.

5.4.5. Middle–Upper Triassic (220–200 Ma)

Northward movement of the Shuanghu–Tethys plate, during convergence of the NQT and SQT, carried the mix of sedimentary mélangé and high-pressure rocks northward, towards and in the end on top of the accreted material at the northern suture, the ophiolitic mélangé (Fig. 7d). As the two terranes collided, all these rocks were thrust onto the SQT, producing the sheet stack as is now observed. At this stage, the Shuanghu–Tethys slab finally slid down into the mantle, giving rise to a last stage of asthenosphere upwelling and resulting bimodal igneous activity, including the 210 Ma Gangtang Co granite and Upper Triassic rhyolites and basalts, mostly in the north but also extending south onto the (former) SQT (Fig. 7e). Post-collisional sediments, intercalated with volcanics, cover the amalgamated Qiangtang terrane. From south to north, these Upper Triassic deposits show two trends: from shallow marine, carbonate-dominated sediments towards terrestrial fluvial sediments and an increasing amount of bimodal volcanic deposits. This can be interpreted as a foreland basin that developed in the south in front of the thrust belt in the north. Southward propagation of thrusting finally thrust mélangé and P21 in the hanging wall against latest Triassic sediments in the footwall (Fig. 6e).

5.4.6. Jurassic (200–170 Ma)

Following the closure of Longmu Co–Shuanghu suture zone, the Bangong–Nujiang suture zone opened between the amalgamated Qiangtang terrane and the north Lhasa terrane. Jurassic shallow marine deposits unconformably overlie Late Triassic T3n sediments and volcanics on the NQT. Jurassic the deep-water flysch sediments (J1–2s) cover all the older units in the southern SQT. These are thought to represent the opening of the Bangong–Nujiang suture zone (Schneider et al., 2003; Baxter et al., 2009). It is not known whether Jurassic sediments once covered the whole Qiangtang terrane or they were never deposited there. Jurassic sediments, if once present, could have been removed during formation of the central Qiangtang Culmination. This domal structure may have formed as early as the Jurassic (Kapp et al., 2005) or during compressional stages resulting from the closure of the Meso- and Neo-Tethys during the Cretaceous and Paleogene respectively (Kapp et al., 2007; Xu et al., 2014). Minor terrestrial sediments, mostly conglomerates in fault-bounded basins, were deposited during the Cretaceous and Tertiary.

6. Conclusions

Subduction mélangé and high-pressure rocks in the Qiangtang terrane record an important stage in the evolution and formation of the Tibetan Plateau, which has consequences for the location of different former oceans. Our mapping and structural analysis of the Rongma area in the centre of the metamorphic belt leads to the following main conclusions:

Chapter 4

1. The north and south Qiangtang terranes were formerly separated by an Ordovician–Triassic ocean.
2. Metamorphism in the central Qiangtang metamorphic belt occurred in two unrelated stages. The first, a lower greenschist-facies event, occurred in pre-/early-Ordovician times and affected the Precambrian basement. A second event produced the high-pressure rocks that exhumed in the Triassic as a result of the closure at the Longmu Co–Shuang Hu suture zone between the north and south Qiangtang terranes.
3. The pre- to syn-collision lithologies (> 210 Ma) can be grouped into three main units: (1) carboniferous and older basement, (2) non-metamorphic ophiolitic *mélange* and (3) non-metamorphic sedimentary *mélange* with large rafts and sheets of non-metamorphic Permian sediments and high-pressure rocks (mostly blueschists).
4. To explain the current structural relationships of the units, we propose that the high-pressure rocks were exhumed by extraction of a short, south-dipping slab from underneath the south Qiangtang terrane, bringing them in contact with the sedimentary *mélange* and Permian margin sediments. This unit was subsequently thrust on top of the ophiolitic *mélange*. Upon final collision of the north and south Qiangtang terranes, both units were placed on top of the Paleozoic south Qiangtang basement. The whole tripartite stack was subsequently further shortened into a south-verging fold and thrust belt. This may have been a consequence of the amalgamation of the two terranes or later (Jurassic–Paleogene) events.
5. After closure of the Longmu Co–Shuanghu suture zone, Upper Triassic sedimentation commenced in the south in a foreland setting and progressively extended to the north where extensive bimodal volcanic activity occurred, which is interpreted as the result of mantle upwelling due to the final sinking of the Paleo-Tethys slab.

This study is based on a large study area in the centre of the Qiangtang terrane, which extends over almost 2000 km. We hope that this study encourages more work, including detailed mapping and structural analysis, in the whole terrane to confirm or reject the former presence of an ocean between the north and south Qiangtang terranes as well as investigate the consequences in terms of presence and size of other oceans between the various terranes that form the Tibetan Plateau.

Author contributions.

Fieldwork was carried out by G. Wang and his team, including Y. Liu and Z. Zhao. Structural interpretations, modelling and thin section analyses were carried out by Z. Zhao and P. D. Bons. A. Soesoo scrutinized the geochemical data. The paper was written by all authors.

Acknowledgements.

This research was funded by the China Geological Survey (CGS) through the 1 : 50 000 regional geological surveys in the Qomo Ri, Gangmari and Rongma areas of Tibet as well as project 1212011121271, titled “Tectonic attributes of the south Qiangtang Mesozoic-Cenozoic basin, based on deformation and metamorphic character”. Additionally, we appreciate the Program for Changjiang University Scholars and Innovative Research Teams (IRT1083). Z. Zhao thanks the Chinese Scholarship Council for financial support. We thank the whole mapping team of the China University of Geosciences, Beijing. We appreciate the helpful comments and criticism of two anonymous reviewers. We also thank Thomas Wenzel for his advice on petrology.

References

- Agard, P., Yamato, P., Jolivet, L., and Burov, E.: Exhumation of oceanic blueschists and eclogites in subduction zones: timing and mechanisms, *Earth-Sci. Rev.*, 92, 53–79, 2009.
- Andersen, T. B., Jamveit, B., Dewey, J. F., and Swenson, E.: Subduction and exhumation of continental crust: major mechanism during continent–continent collision and orogenic extensional collapse, a model based on the south Caledonides, *Terra Nova*, 3, 303–310, 1991.
- Baxter, A. T., Aitchison, J. C., and Ziyabrev, S. V.: Radiolarian age constraints on Mesotethyan ocean evolution, and their implications for development of the Bangong-Nujiang suture, Tibet, *J. Geol. Soc. London*, 166, 689–694, 2009.
- Brueckner, H. K. and Cuthbert, S. J.: Extension, disruption, and translation of an orogenic wedge by exhumation of large ultrahigh-pressure terranes: Examples from the Norwegian Caledonides, *Lithosphere*, 5, 277–289, 2013.
- Bucher, K. and Frey, M.: Petrogenesis of metamorphic rocks, 7th Edn., Springer, Berlin-Heidelberg, Germany, 259–277, 2002.
- Cawood, P. A., Johnson, M. R., and Nemchin, A. A.: Early Palaeozoic orogenesis along the Indian margin of Gondwana: Tectonic response to Gondwana assembly, *Earth Planet. Sc. Lett.*, 255, 70–84, 2007.
- Chen, S., Cheng, L., Wu, S., and Zhu, Y.: Late Permian fusulines from the Raggyorcaka Formation, northern Qiangtang, Tibet, China, *Geological Bulletin of China*, 28, 1725–1729, 2009.
- Devoti, R., Riguzzi, F., Cuffaro, M., and Doglioni, C.: New GPS constraints on the kinematics of the Apennines subduction, *Earth Planet. Sc. Lett.*, 273, 163–174, 2008.
- Dewey, J. F., Shackleton, R. M., Chengfa, C., and Yiyin, S.: The tectonic evolution of the Tibetan Plateau, *Philos. T. R. Soc. A*, 327, 379–413, 1988.
- Di Stefano, R., Kissling, E., Chiarabba, C., Amato, A., and Giardini, D.: Shallow subduction beneath Italy: Three-dimensional images of the Adriatic-European-Tyrrhenian lithosphere system based on high-quality P wave arrival times, *J. Geophys. Res.-Sol. Ea.*, 114, 1978–2012, 2009.
- Dong, C., Li, C., Wan, Y., Wang, W., Wu, Y., Xie, H., and Liu, D.: Detrital zircon age model of Ordovician Wenquan quartzite south of Lungmuco-Shuanghu Suture in the Qiangtang area, Tibet: Constraint on tectonic affinity and source regions, *Sci. China Ser. D*, 54, 1034–1042, 2011.

- Duan, Z., Zhong, C., Zhu, H., Cheng, J., Li, Z., and Wang, Z.: Sedimentary characteristics of Middle Jurassic Sewa and Buqu Formations from Qiangzi Well-2, southern Qiangtang basin, Tibet, *Geology in China*, 36, 355–365, 2009.
- Duret, T., Gerya, T. V., Kaus, B. J. P., and Andersen, T. B.: Thermomechanical modelling of slab eduction, *J. Geophys. Res.-Sol. Ea.*, 117, 1978–2012, [doi:10.1029/2012JB009137](https://doi.org/10.1029/2012JB009137), 2012.
- Fu, X., Wang, J., Wang, Z., and Chen, W.: U-Pb Zircon Age and Geochemical Characteristics of Volcanic 5 Rocks from the Juhua Mountain Area in the northern Qiangtang Basin, northern Xizang (Tibet), *Geological Review*, 54, 232–242, 2008.
- Fu, X., Wang, J., Tan, F., Chen, M., and Chen, W.: The Late Triassic rift-related volcanic rocks from eastern Qiangtang, northern Tibet (China): Age and tectonic implications, *Gondwana Res.*, 17, 135–144, 2010a.
- Fu, X., Wang, J., Wu, T., and He, J.: Stratigraphy and paleoenvironment of the Quemo Co Formation in Shengli River area, northern Tibet, *Geology in China*, 37, 1305–1312, 2010b.
- Giacomuzzi, G., Civalleri, M., De Gori, P., and Chiarabba, C.: A 3-D vs. model of the upper mantle beneath Italy: Insight on the geodynamics of central Mediterranean, *Earth Planet. Sc. Lett.*, 335, 105–120, 2012.
- Gray, D. and Foster, D.: Tectonic evolution of the Lachlan Orogen, southeast Australia: historical review, data synthesis and modern perspectives, *Aust. J. Earth Sci.*, 51, 773–817, 2004.
- Gvirtzman, Z. and Nur, A.: Residual topography, lithospheric structure and sunken slabs in the central Mediterranean, *Earth Planet. Sc. Lett.*, 187, 117–130, 2001.
- Hacker, B. R., Ratschbacher, L., Webb, L. E., McWilliams, M., Ireland, T. R., Calvert, A., Dong, S., Wenk, H.-R., and Chateigner, D.: Exhumation of ultrahigh-pressure continental crust in east-central China: Late Triassic – Early Jurassic tectonic unroofing, *J. Geophys. Res.*, 105, 13339–13364, 2000.
- Hu, P., Li, C., Su, L., and Zhang, H.: Geochemical and ⁴⁰Ar-³⁹Ar isotope chronological characteristics of Wugongshan Indo-Chinese granites in central Qiangtang, Tibetan Plateau, *Geological Bulletin of China*, 31, 843–851, 2012.
- Kapp, P., Yin, A., Manning, C. E., Murphy, M., Harrison, T. M., Spurlin, M., Lin, D., Xi-Guang, D., and Cun-Ming, W.: Blueschist-bearing metamorphic core complexes in the Qiangtang block reveal deep crustal structure of northern Tibet, *Geology*, 28, 19–23, 2000.
- Kapp, P., Murphy, M. A., Yin, A., Harrison, T. M., Ding, L., and Guo, J.: Mesozoic and Cenozoic tectonic evolution of the Shiquanhe area of western Tibet, *Tectonics*, 22, TC1029, [doi:10.1029/2001TC001332](https://doi.org/10.1029/2001TC001332), 2003a.
- Kapp, P., Yin, A., Manning, C. E., Harrison, T. M., Taylor, M. H., and Ding, L.: Tectonic evolution of the early Mesozoic blueschist-bearing Qiangtang metamorphic belt, central Tibet, *Tectonics*, 22, 1043–1068, 2003b.
- Kapp, P., Yin, A., Harrison, T. M., and Ding, L.: Cretaceous-Tertiary shortening, basin development, and volcanism in central Tibet, *Bull. Geol. Soc. Am.*, 117, 865–878, 2005.
- Kapp, P., DeCelles, P. G., Gehrels, G. E., Heizler, M., and Ding, L.: Geological records of the Lhasa-Qiangtang and Indo-Asian collisions in the Nima area of central Tibet, *Bull. Geol. Soc. Am.*, 119, 917–932, 2007.
- Li, C.: The Longmu Co-Shuanghu-Lancangjiang Suture as the northern boundary of the Gondwana land in the Carboniferous and Permian, *Bull. Changchun Coll. Geol. Sci.*, 17, 155–166, 1987.

- Li, C.: Geological map of the Myyi Gang Ri area (Scale at 1 : 250 000), University of Jilin Region Institute of geological survey, China, 2006.
- Li, X. and Wen, F.: Discovery of the Late Triassic Rigain Peico Formation and the unconformity between it and its under lying strata in eastern Rutog, Tibet, China, *Geological Bulletin of China*, 26, 1009–1013, 2007.
- Li, C., Cheng, L., Hu, K., Yang, Z., and Hong, Y.: Study on the paleo-Tethys suture zone of Lungmu Co-Shuanghu, Tibet, *Geol. Publ. House, Beijing, China*, 131 pp., 1995.
- Li, C., Cheng, L., Zhang, Y., and Zhai, Q.: Discovery of Ordovician- Devonian strat in the south of the Qiangtang area, Tibet, *Geological Bulletin of China*, 23, 602–604, 2004.
- Li, C., Zhai, Q., Dong, Y., and Huang, X.: Discovery of eclogite and its geological significance in Qiangtang area, central Tibet, *Chinese Sci. Bull.*, 51, 1095–1100, 2006.
- Li, C., Zhai, Q., Dong, Y., Zeng, Q., and Huang, X.: Longmu Co- Shuanghu plate suture and evolution records of paleo-Tethyan oceanic in Qiangtang area, Qinghai-Tibet plateau, *Frontiers of Earth Science in China*, 1, 257–264, 2007.
- Li, C., Zhai, Q., Dong, Y., Liu, S., Xie, C., and Wu, Y.: High-pressure eclogite-blueschist metamorphic belt and closure of paleo-Tethys Ocean in Central Qiangtang, Qinghai-Tibet plateau, *J. Earth Sci.*, 20, 209–218, 2009.
- Li, Q., Gao, R., Feng, X., Lu, Z., Hou, H., Ye, G., Li, P., Wang, H., Ye, Z., and Xiong, X.: Structural Characteristics of the Basement beneath Qiangtang Basin in Qinghai-Tibet Plateau: Results of Interaction Interpretation from Seismic Reflection/Refraction Data, *Acta Geol. Sin.-Engl.*, 87, 358–377, 2013.
- Liang, X., Wang, G., Yuan, G., and Liu, Y.: Structural sequence and geochronology of the Qomo Ri accretionary complex, Central Qiangtang, Tibet: Implications for the Late Triassic subduction of the Paleo-Tethys Ocean, *Gondwana Res.*, 22, 470–481, 2012.
- Liu, Y., Santosh, M., Zhao, Z. B., Niu, W. C., and Wang, G. H.: Evidence for palaeo-Tethyan oceanic subduction within central Qiangtang, northern Tibet, *Lithos*, 127, 39–53, 2011.
- Lu, Z., Gao, R., Li, Y., Xue, A., Li, Q., Wang, H., Kuang, C., and Xiong, X.: The upper crustal structure of the Qiangtang Basin revealed by seismic reflection data, *Tectonophysics*, 606, 171–177, 2013.
- Metcalf, I.: Late Palaeozoic and Mesozoic tectonic and palaeogeo-graphical evolution of SE Asia, *Geol. Soc. SP*, London, UK, 315, 7–23, 2009.
- Nie, S., Yin, A., Rowley, D. B., and Jin, Y.: Exhumation of the Dabie Shan ultra-high-pressure rocks and accumulation of the Songpan-Ganzi flysch sequence, central China, *Geology*, 22, 999–1002, 1994.
- Peng, T., Zhao, G., Fan, W., Peng, B., and Mao, Y.: Late Triassic granitic magmatism in the Eastern Qiangtang, Eastern Tibetan Plateau: Geochronology, petrogenesis and implications for the tectonic evolution of the Paleo-Tethys, *Gondwana Res.*, [doi:10.1016/j.gr.2014.01.009](https://doi.org/10.1016/j.gr.2014.01.009), 27, 1494–1508, 2014.
- Pullen, A. and Kapp, P.: Mesozoic tectonic history and lithospheric structure of the Qiangtang terrane: Insights from the Qiangtang metamorphic belt, central Tibet, *Geol. S. Am. S.*, 507, 507–504, 2014.
- Pullen, A., Kapp, P., Gehrels, G. E., Vervoort, J. D., and Ding, L.: Triassic continental subduction in central Tibet and Mediterranean-style closure of the Paleo-Tethys Ocean, *Geology*, 36, 351–354, 2008.

- Pullen, A., Kapp, P., Gehrels, G. E., Ding, L., and Zhang, Q.: Metamorphic rocks in central Tibet: Lateral variations and implications for crustal structure, *Bull. Geol. Soc. Am.*, 123, 585–600, 2011.
- Schneider, W., Mattern, F., Wang, P. J., and Li, C.: Tectonic and sedimentary basin evolution of the eastern Bangong-Nujiang zone (Tibet): A Reading cycle, *Int. J. Earth Sci.*, 92, 228–254, 2003.
- Sengör, A., Altınır, D., Cin, A., Ustaömer, T., and Hsü, K.: Origin and assembly of the Tethyside orogenic collage at the expense of Gondwana Land, *Geol. Soc. Eng. Geol. Sp.*, 37, 119–181, 1988.
- Soesoo, A., Bons, P. D., Gray, D. R., and Foster, D. A.: Divergent double subduction: tectonic and petrologic consequences, *Geology*, 25, 755–758, 1997.
- Tang, X. and Zhang, K.: Lawsonite-and glaucophane-bearing blueschists from NW Qiangtang, northern Tibet, China: mineralogy, geochemistry, geochronology, and tectonic implications, *Int. Geol. Rev.*, 56, 150–166, 2013.
- Wang, J., Fu, X., Chen, W., and Wang, Z.: The Late Triassic Paleo-weathering Crust in the Qiangtang Basin Northern Tibet: geology, geochemistry and significance, *Acta Geol. Sin.-Engl.*, 25, 487–494, 2007.
- Wang, J., Fu, X. G., Chen, W. X., Wang, Z. J., Tan, F. W., Chen, M., and Zhuo, J. W.: Chronology and geochemistry of the volcanic rocks in Woruo Mountain region, northern Qiangtang depression: Implications to the Late Triassic volcanic-sedimentary events, *Sci. China Ser. D*, 51, 194–205, 2008a.
- Wang, Q., Wyman, D. A., Xu, J., 5 Wan, Y., Li, C., Zi, F., Jiang, Z., Qiu, H., Chu, Z., and Zhao, Z.: Triassic Nb-enriched basalts, magnesian andesites, and adakites of the Qiangtang terrane (Central Tibet): evidence for metasomatism by slab-derived melts in the mantle wedge, *Contrib. Mineral. Petr.*, 155, 473–490, 2008b.
- Wang, S., Li, Z., and Qiangba, X.: Geologic map and geologic report of the Xigaze area, Tibetan Bur. of Geol. and Miner. Resour., Lhasa, China, 1983.
- Webb, L. E., Baldwin, S. L., Little, T. A., and Fitzgerald, P. G.: Can microplate rotation drive subduction inversion?, *Geology*, 36, 823–826, 2008.
- Weber, J., Vrabec, M., Pavlovic-Precceren, P., Dixon, T., Jiang, Y., and Stopar, B.: GPS-derived motion of the Adriatic microplate from Istria Peninsula and Po Plain sites, and geodynamic implications, *Tectonophysics*, 483, 214–222, 2010.
- Wu, G., Yao, J., and Ji, Z.: The Late Carboniferous Fusulinids in the central part of northern Qiangtang, Tibet, China, *Geological Bulletin of China*, 28, 1276–1280, 2009.
- Wu, R. Z. and Lang, B. L.: The new strata data of the Late Permian in northwest Tibet, *Journal of Stratigraphy* (in Chinese with English abstract), 14, 216–221, 1990.
- Xu, M., Li, C., Zhang, X., and Wu, Y.: Nature and evolution of the Neo-Tethys in central Tibet: synthesis of ophiolitic petrology, geochemistry, and geochronology, *Int. Geol. Rev.*, 56, 1–25, 2014.
- Yang, J., Xu, Z., Li, Z., Xu, X., Li, T., Ren, Y., Li, H., Chen, S., and Robinson, P. T.: Discovery of an eclogite belt in the Lhasa block, Tibet: A new border for Paleo-Tethys?, *J. Asian Earth Sci.*, 34, 76–89, 2009.
- Yang, T., Zhang, H., Liu, Y., Wang, Z., Song, Y., Yang, Z., Tian, S., Xie, H., and Hou, K.: Permo-Triassic arc magmatism in central Tibet: Evidence from zircon U-Pb geochronology, Hf isotopes, rare earth elements, and bulk geochemistry, *Chem. Geol.*, 284, 270–282, 2011.

Chapter4

- Yin, A. and Harrison, T. M.: Geologic evolution of the Himalayan-Tibetan orogen, *Annu. Rev. Earth Pl. Sc.*, 28, 211–280, 2000.
- Yin, A. and Nie, S.: A Phanerozoic palinspastic reconstruction of China and its neighboring regions, *The Tectonics of Asia*, Cambridge Univ. Press, New York, USA, 442–485, 1996.
- Zhai, Q. and Li, C.: Zircon SHRIMP dating of volcanic rock from Nadigangri Formation in Juhuaashan, Qiangtang, Northern Tibet and its geological significance, *Acta Geol. Sin.-Engl.*, 81, 795–800, 2007.
- Zhai, Q., Li, C., and Huang, X.: The fragment of Paleo-Tethys ophiolite from central Qiangtang, Tibet: Geochemical evidence of metabasites in Guoganjianian, *Sci. China Ser. D*, 50, 1302–1309, 2007.
- Zhai, Q., Li, C., Cheng, L., and Zhang, Y.: Geological features of Permian ophiolite in the Jiaomuri area, Qiangtang, Tibet, and its tectonic significance, *Regional Geology of China*, 23, 1228–1229, 2004.
- Zhai, Q., Li, C., Wang, J., Ji, Z., and Wang, Y.: SHRIMP U-Pb dating and Hf isotopic analyses of zircons from the mafic dyke swarms in central Qiangtang area, Northern Tibet, *Chinese Sci. Bull.*, 54, 2279–2285, 2009.
- Zhai, Q., Wang, J., Li, C., and Su, L.: SHRIMP U-Pb dating and Hf isotopic analyses of Middle Ordovician meta-cumulate gabbro in central Qiangtang, northern Tibetan Plateau, *Sci. China Ser. D*, 53, 657–664, 2010.
- Zhai, Q., Jahn, B. M., Zhang, R., Wang, J., and Su, L.: Triassic Subduction of the Paleo-Tethys in northern Tibet, China: evidence from the geochemical and isotopic characteristics of eclogites and blueschists of the Qiangtang Block, *J. Asian Earth Sci.*, 42, 1356–1370, 2011a.
- Zhai, Q., Zhang, R., Jahn, B. M., Li, C., Song, S., and Wang, J.: Triassic eclogites from central Qiangtang, northern Tibet, China: Petrology, geochronology and metamorphic PT path, *Lithos*, 125, 173–189, 2011b.
- Zhai, Q.-G., Jahn, B.-M., Su, L., Wang, J., Mo, X.-X., Lee, H.-Y., Wang, K.-L., and Tang, S.: Triassic arc magmatism in the Qiangtang area, northern Tibet: Zircon U-Pb ages, geochemical and Sr-Nd-Hf isotopic characteristics, and tectonic implications, *J. Asian Earth Sci.*, 63, 162–178, 2013a.
- Zhai, Q., Jahn, B., Wang, J., Su, L., Mo, X., Wang, K., Suohan, T., and Lee, H.: The Carboniferous ophiolite in the middle of the Qiangtang terrane, Northern Tibet: SHRIMP U-Pb dating, geochemical and Sr-Nd-Hf isotopic characteristics, *Lithos*, 168, 186–199, 2013b.
- Zhang, K. J.: Blueschist-bearing metamorphic core complexes in the Qiangtang block reveal deep crustal structure of northern Tibet: Comment, *Geology*, 29, p. 90, 2001.
- Zhang, K. and Tang, X.: Eclogites in the interior of the Tibetan Plateau and their geodynamic implications, *Chinese Sci. Bull.*, 54, 2556–2567, 2009.
- Zhang, S., Wang, H., Feng, D., Jiang, X., Li, X., and Li, Q.: The Xi-aochaka Group and Riganpeicuo Group stratigraphic sequence and correlation in the Qiangtang area, Tibet – question the validity of the boundary between Qiangnan and Qiangbei strata, *Jilin Geology*, 24, 16–20, 2005.
- Zhang, K., Cai, J., Zhang, Y., and Zhao, T.: Eclogites from central Qiangtang, northern Tibet (China) and tectonic implications, *Earth Planet. Sc. Lett.*, 245, 722–729, 2006a.
- Zhang, K., Zhang, Y., Li, B., Zhu, Y., and Wei, R.: The blueschist-bearing Qiangtang metamorphic belt (northern Tibet, China) as an in situ suture zone: Evidence from geochemical comparison with the Jinsa suture, *Geology*, 34, 493–497, 2006b.

- Zhang, K., Zhang, Y., Xia, B., and He, Y.: Temporal variations of Mesozoic sandstone compositions in the Qiangtang block, north- ern Tibet (China): implications for provenance and tectonic set- ting, *J. Sediment. Res.*, 76, 1035–1048, 2006c.
- Zhang, K. J. and Tang, X. C.: Eclogites in the interior of the Tibetan Plateau and their geodynamic implications, *Chinese Sci. Bull.*, 54, 2556–2567, 2009.
- Zhang, K., Tang, X., Wang, Y., and Zhang, Y.: Geochronology, geochemistry, and Nd isotopes of early Mesozoic bimodal volcanism in northern Tibet, western China: Constraints on the exhumation of the central Qiangtang metamorphic belt, *Lithos*, 121, 167– 175, 2011.
- Zhang, Y., Shen, S., Shi, G., Wang, Y., and Yuan, D.: Tectonic evolution of the Qiangtang Block, northern Tibet during Late Cisuralian (Late Early Permian): Evidence from fusuline fossil records, *Palaeogeogr. Palaeoclimatol.*, 350, 139–148, 2012a.
- Zhang, Y., Shi, G., and Shen, S.: A review of Permian stratigraphy, palaeobiogeography and palaeogeography of the Qinghai-Tibet Plateau, *Gondwana Res.*, 24, 55–76, 2012b.
- Zhang, H., Yang, T., Hou, Z., Song, Y., Ding, Y., and Cheng, X.: Petrogenesis and tectonics of late Permian felsic volcanic rocks, eastern Qiangtang block, north-central Tibet: Sr and Nd isotopic evidence, *Int. Geol. Rev.*, 1–12, 2013.
- Zhang, Y., Shi, G., Shen, S., and Yuan, D.: Permian Fusuline Fauna from the Lower Part of the Lugu Formation in the Central Qiang- tang Block and its Geological Implications, *Acta Geol. Sin.- Engl.*, 88, 365–379, 2014.
- Zhao, G.: Jiangnan Orogen in South China: Developing from divergent double subduction, *Gondwana Res.*, 27, 1173–1180, [doi:10.1016/j.gr.2014.09.004](https://doi.org/10.1016/j.gr.2014.09.004), 2015.
- Zhao, Z., Bons, P. D., Wang, G., Liu, Y., and Zheng, Y.: Origin and pre-Cenozoic evolution of the south Qiangtang basement, Central Tibet, *Tectonophysics*, 623, 52–66, 2014.
- Zhu, T.: Geological map of the Jiangaida Ri area (Scale at 1 : 250 000): Geology and Resource Institute of Chengdu, China, 2005.
- Zhu, D., Zhao, Z., Niu, Y., Dilek, Y., Hou, Z., and Mo, X.: The origin and pre-Cenozoic evolution of the Tibetan Plateau, *Gond- wana Res.*, 23, 1429–1454, 2012.
- Zhu, T., Feng, X., Wang, X., and Zhou, M.: Reconstruction of the Triassic Tectonic Lithofacies Paleogeography in Qiangtang Re- gion, Northern Qinghai, Tibet Plateau, China, *Acta Geol. Sin.- Engl.*, 87, 378–394, 2013.

Chapter 5: Early Cretaceous exhumation of the Qiangtang Culmination and collision of the Qiangtang and Lhasa terranes, central Tibet

Z. Zhao, P.D. Bons, K. Stübner, T.A. Ehlers and G. Wang

This chapter reports thermogeochronological work on the Rongma study area, carried out in Tübingen in collaboration with Stübner. It will form the base for a manuscript with the same title and as preliminary list of authors: Z. Zhao, P.D. Bons, K. Stübner, T.A. Ehlers and G. Wang. This chapter will be significantly shortened to meet the requirements for the intended submission to the journal *Terra Nova*.

Abstract

The Qiangtang Culmination in central Tibet is characterized by early Mesozoic blueschist-bearing mélangé and upper Paleozoic strata in the core and mainly Triassic–Jurassic strata along the limbs. In the Rongma area, the culmination is unconformably overlain by weakly deformed mid-Cretaceous conglomerate and volcanics. This relationship demonstrates that the Qiangtang terrane was above sea level and experienced significant denudation prior to mid-Cretaceous times. We use zircon (U-Th)/He ages to constrain the exhumation history of the Qiangtang terrane. From 210 to 140 Ma, the South Qiangtang terrane experienced slow exhumation with maximum exhumation rate ~ 0.06 mm/y. Collision between the Lhasa and Qiangtang terranes led to faster exhumation of South Qiangtang terrane during ~ 140 –90 Ma, with exhumation rates in the range of 0.12–0.3 mm/y. A passive oceanic margin developed due to the opening at the Bangong Hu–Nujiang suture (BNS) between the Lhasa and Qiangtang terranes during the Jurassic, that response to slow uplifting rate of Qiangtang. This increased exhumation rate in the Lower Cretaceous was caused, when closure of BNS and Lhasa–Qiangtang collision by thick-skinned folding and thrusting of the South Qiangtang terrane.

1. Introduction

The Tibetan Plateau consists of several terranes, from north to south, the Songpan–Ganzi, the North and South Qiangtang terranes, the Lhasa terrane and the Himalaya terrane (Fig.1), which were accreted onto the Asian continent during Mesozoic to Cenozoic times (e.g., Yin and Harrison, 2000; Zhu et al., 2012). This study focuses on the closure of the Bangong Hu–Nujiang suture (BNS), which is located between Lhasa and South Qiangtang terranes (e.g. Kapp et al., 2003b; Zhang et al., 2004). Collision of the two terranes left its traces near the suture, but is expected to also be recorded further inward in the Tibetan

Plateau, such as in the Qiangtang and Songpan-Ganzi terranes (e.g. Ratschbacher et al., 2003; Vassallo et al., 2007; Tian et al., 2014). Understanding the accretion mechanism and timing may shed light on the development of the Tibetan crustal structure.

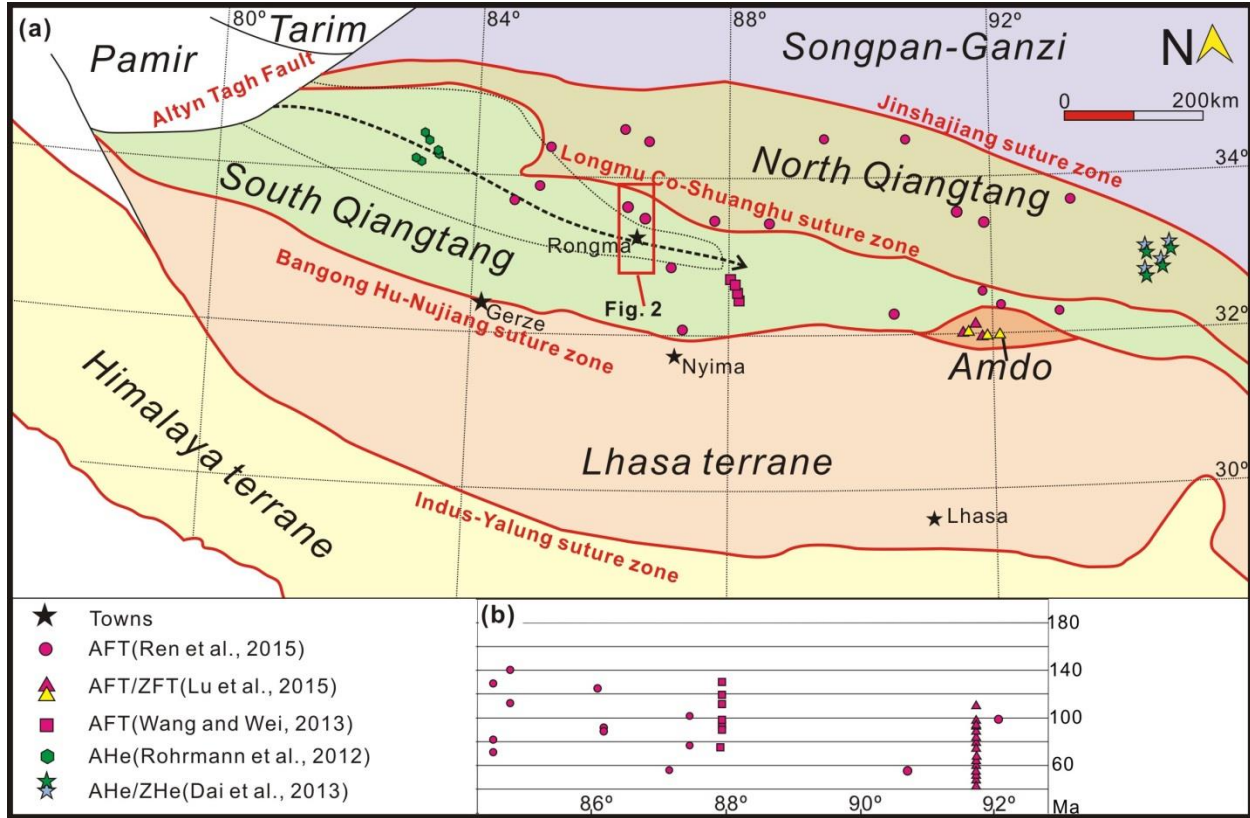


Fig. 1 (a) Tectonic map of central Tibet (modified from Zhu et al., 2012). Main terranes and sutures are shown. Available thermochronological data locations are plotted in the Qiangtang terranes. The rectangle indicates the study area and location of Figure 2. (b) Apatite fission track ages of the Qiangtang terranes plotted as function of longitude.

The EW striking Bangong Hu-Nujiang suture (BNS) experienced Jurassic to Middle Cretaceous oceanic evolution (e.g., Liu et al., 2015; Xu et al., 2014). A wide belt of Early Jurassic–Middle Cretaceous arc magmatic rocks on South Qiangtang (Zhang et al., 2014; Zeng et al., 2015) indicates that the BNS lithosphere was subducted beneath the South Qiangtang terrane (Li et al., 2014; Liu et al., 2015; Fan et al., 2014; Xu et al., 2014). Kapp et al. (2003a) argued that the BNS closed at ~145Ma, based on stratigraphic arguments. Recent geochemical data of Early Cretaceous magma indicate that most magma is A-type granite (Qu et al., 2012) and formed due to thickening of the crust (Sui et al., 2013). These observations are in favour of the BNS closing before ~140 Ma, followed by continental collision between the Lhasa and South Qiangtang terranes (Zhu et al., 2013). The Lower Cretaceous molasse along the BNS represents that collision between the Qiangtang and Lhasa terranes, which happened during the Early Cretaceous (131–120 Ma; Zhu et al., 2009b; Zhu et al., 2009a).

Zircon fission track ages are 108.7-69.8 Ma in the North Qiangtang terrane (Ren et al., 2015), 120-80 Ma in the northern part (Wang and Wei, 2013) and 117-78 Ma in southern part of the South Qiangtang terrane (Lu et al., 2015). All these data indicate Qiangtang terrane experienced exhumation due to the collision of Lhasa-Qiangtang during the Cretaceous. Apatite fission-track ages range between 140 and 50 Ma and show a trend towards younger ages in the east (Fig. 1b). Exhumation rates subsequently dropped from the beginning of the Paleocene (Lu et al., 2015).

The north-western part of the South Qiangtang terrane is occupied by a large domal structure (Yin and Harrison, 2000; Kapp et al., 2005), the Qiangtang Culmination, which exposes basement rocks and Permo-Triassic sediments and *mélange*, including (U)HP rocks (Zhai et al., 2011; Zhao et al., 2015). The subduction-related rocks are interpreted to have been emplaced during late Triassic collision of the North and South Qiangtang terranes (Zhai et al., 2011; Zhao et al., 2015). Alternatively, these rocks derive from southward subduction at the Jinshajian suture and subsequent core complex-style doming (Kapp et al., 2003b; Pullen et al., 2014). Zhao et al. (2015) favoured the first interpretation and showed that the Late Triassic collision event was followed by north-south directed folding and thrusting, and formation of the Qiangtang Culmination of undetermined age. Here we present structural data from the Qiangtang Culmination near the town of Rongma together with new zircon (U-Th)/He (ZHe) ages. The data show a change from slow to fast exhumation at ~140 Ma, coinciding with a change from marine to terrestrial sedimentation. The results are in accordance with early Cretaceous closure of the BNS ocean, followed by shortening and thickening of the crust in the Qiangtang terrane, leading to rapid exhumation around ~100 Ma.

2. Geological setting

The Qiangtang terrane lies between the Songpan-Ganzi belt to the north and the Lhasa terrane to the south. Whether the Qiangtang is a single terrane (e.g. Kapp et al., 2003b) or consists of a North and South Qiangtang terrane that amalgamated along the Longmu Co-Shuang Hu suture zone (LSS) in the Late Triassic (Zhai et al., 2011) is strongly debated. We favour the interpretation that the Qiangtang terranes were separated from Ordovician until Late Triassic times (e.g., Li et al., 2009; Zhai et al., 2011) because of tectonic relationships among different units. Marginal sediments and *mélange*, including (U)HP rocks, were thrust southward on top of the South Qiangtang basement, forming an ~8 km thick stack of thrust sheets that extends up to 100 km south of the LSS (Zhao et al., 2014; 2015). A foreland basin subsequently formed on the South Qiangtang terrane, with latest Triassic sediments and volcanics unconformably overlying basement rocks, pre-closure sediments on south Qiangtang terrane and *mélange*

(Wang and Yi, 2001; Zhao et al., 2015). >5 km thick Jurassic flysch on the northern passive margin of the BNS comfortably overlies the Triassic sediments (Schneider et al., 2003; Ren et al., 2015; Wang et al., 2005). Jurassic strata were involved in south-vergent folding and thrusting and formation of the Qiangtang Culmination, which much therefore have formed later than the Jurassic (Zhang et al., 2006).

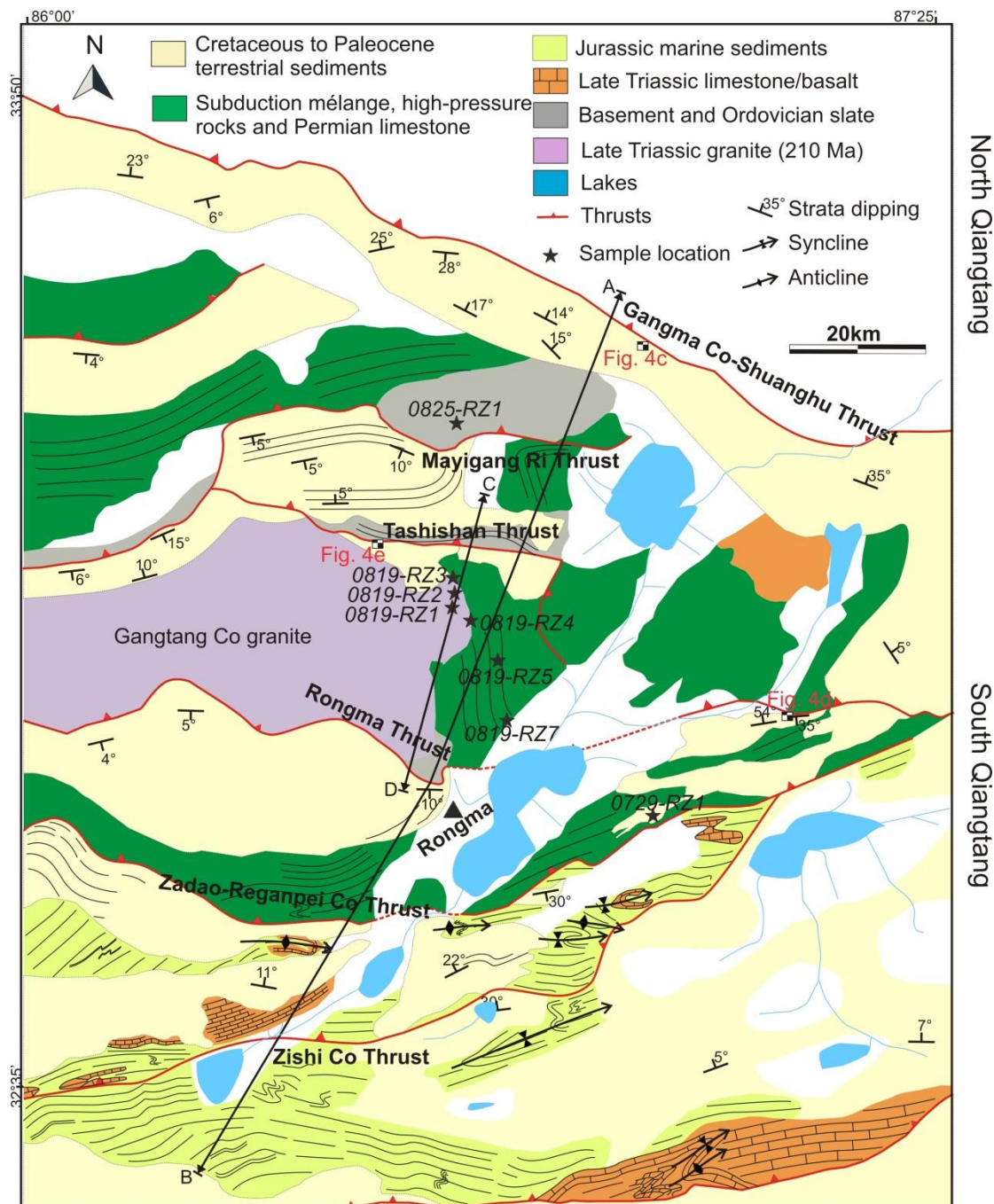


Fig. 2 Simplified geologic map of the Rongma region, based on the Chinese geological map (Wang et al., 2013; 2014), unpublished 1:50,000-scale mapping and Zhao et al. (2015). Samples and photo locations are also shown.

All aforementioned units are unconformably overlain by Cretaceous to Cenozoic terrestrial sediments, mostly conglomerates, and minor basalts (Kapp et al., 2003a). In the study area, basalts just above the unconformity near the town of Rongma (Fig. 4a) were dated at ~102-75 Ma (Li et al., 2014; Wu et al., 2014). The terrestrial sediments are gently folded or tilted, but have been involved in thrusting as will be described below.

3. Mesozoic tectonics of the Rongma area

The study area is located in the Qiangtang Culmination near the town of Rongma (Fig. 1a). The area is bound by the LSS suture zone to the north and spans the entire north-south width of the subduction mélangé belt (Fig. 2). It also extends south into Jurassic flysch. This region is one of high elevation but moderate relief, with elevations ranging from ~4500 to ~6200 m, and is characterized by approximately east-west-trending thrust fault-bound ranges that expose Paleozoic basement, subduction mélangé and Late Triassic to Jurassic sedimentary strata (Pullen et al., 2014; Zhao et al. 2014; 2015). Cretaceous to Cenozoic fluvial-lacustrine sediments are found in east-west trending intramontane basins, (Fig. 2).

3.1 Lithological units

Rocks ranging in age from the Cambrian to Neogene are exposed in the South Qiangtang terrane and in the study area. The Paleozoic basement consists of mainly greenschist-facies quartzite, Ordovician slate and Carboniferous sandstone (Zhao et al., 2014; 2015). The basement is structurally overlain by mélangé, which includes ophiolitic and sedimentary mélangé, (U)HP rocks and rafts of Permian sediments. Basement and mélangé are intruded by the ~210 Ma Gangtang Co granite (Kapp et al., 2003b), evidence that closure of the LSS suture and thrusting of the mélangé on top of the basement occurred before (Zhao et al., 2015). Total thickness of the mélangé is estimated at ~8 km, based on seismic data (Li et al., 2013) and structural reconstructions (Zhao et al., 2015).

The post-collisional sequence commences with Late Triassic foreland-basin sediments with conglomerates at the base, followed by volcanics and carbonates of the >3 km thick Riganpei Co Group (T_{3r}) (Li and Wen, 2007; Zhu et al., 2013). Late Triassic strata are found unconformably overlying the mélangé unit in the northeast of the study area, and as the lowest exposed unit south of the Zadao-Reganpei Co thrust (Figure 2). Jurassic sediments conformably overlie the Triassic strata and are only exposed south of this thrust. The Jurassic here consists of the Quse (J_{1q}), Sewa (J_{1-2s}), Buqu (J_{2b}), Xiali (J_{2x}) and Suowa Group (J_{3s}) from bottom to top. Jurassic, marine sediments consist of shales, siltstones, sandstones, olistolithic clastic sediments and several limestone units (Liu et al., 2007; Li et al., 2010). The

shallow-water carbonate platform sediments of the youngest Suowa Group indicate a regression towards the end of the Jurassic, with sedimentation reaching just into the Cretaceous (Berriasian-Barremian) (Li et al., 2010). Total thickness of the Jurassic is ~6 km.

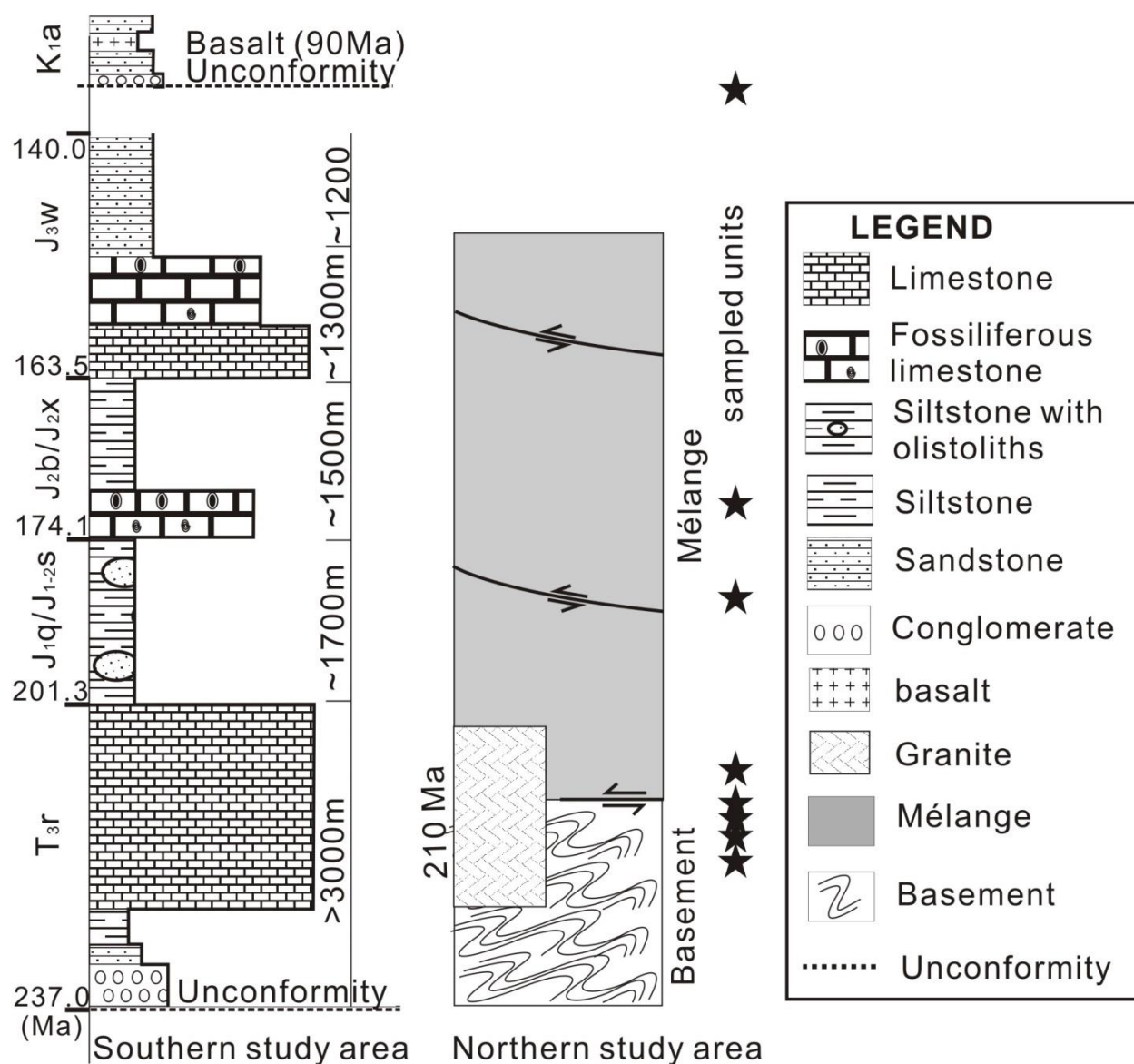


Fig. 3 Schematic stratigraphic column of the Rongma area, showing the litho-stratigraphic position of the ZHe-samples. See text for details.

Sedimentation commenced again with the deposition of the middle Cretaceous, terrestrial Abushan Group (K_{1a}) (Fig. 3) that mainly consists of red molasse intercalated with trachyte andesite, dated at ~102-75 Ma (Li et al., 2014; Wu et al., 2014). Fossil evidence indicates that sedimentation may have continued until ~30Ma (Li et al., 2006). The Abushan Group may reach a thickness of up to ~1 km. Neogene sediments and lakes now cover part of the area.

3.2 Main thrusts in the Rongma area

The major, approximately east-west–striking thrusts in the Rongma area are shown in Figure. 2. All dip to the north as is shown by seismic profiles (Lu et al., 2014) and our 3D structural reconstruction (Zhao et al., 2015).

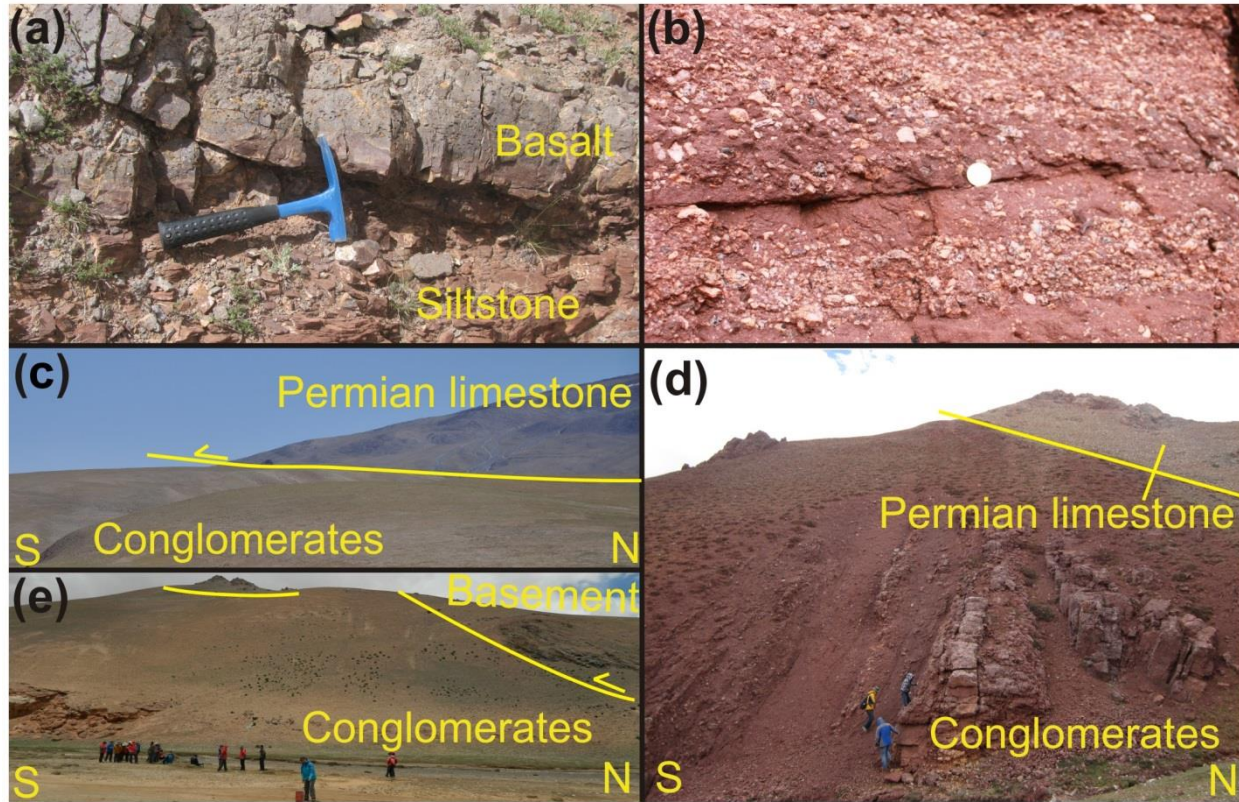


Fig. 4 Field photos showing the main relationships between conglomerate and other units. (a) Cretaceous basalt unconformably overlying siltstones of the sedimentary mélangé. (b) Close-up of Cretaceous conglomerates with large feldspar clasts, probably derived from the nearby Gangtang Co granite. (c) Permian limestone thrust southward onto Cretaceous and younger terrestrial sediments. (d) Permian limestone thrust over folded conglomerate. (e) Flat lying terrestrial conglomerate overthrust by basement rocks.

The Gangma Co-Shuanghu thrust is a reactivation of the LSS and separates the North and South Qiangtang terranes (Kapp et al., 2005) (Fig. 2). It places folded Late Permian limestone in the north over Cretaceous to Tertiary, flat-laying conglomerates (Fig. 4c). The Mayigang Ri and Tashishan thrust place strongly deformed basement southward in contact with Cretaceous footwall rocks (Fig. 4e). Of particular interesting to this study is the Rongma thrust, which uplifts the Gangtang Co granite (~210 Ma, Kapp et al., 2003b) together with basement to the surface during deposition of intramontane conglomerate in its front (Fig. 2). The base of the conglomerate contains coarse feldspar clasts (as large as several

centimeters sizes), which probably derived from the nearby Gangtang Co granite (Fig. 4b). The nature of the contact between *mélange* and Late Triassic foreland sediments is clearly seen at the Zadao-Regangpei Co thrust (Kapp et al., 2005). The Zadao-Regangpei Co Thrust carries *mélange* units in its hanging wall, which are thrust onto conglomerates and Late Triassic limestone.

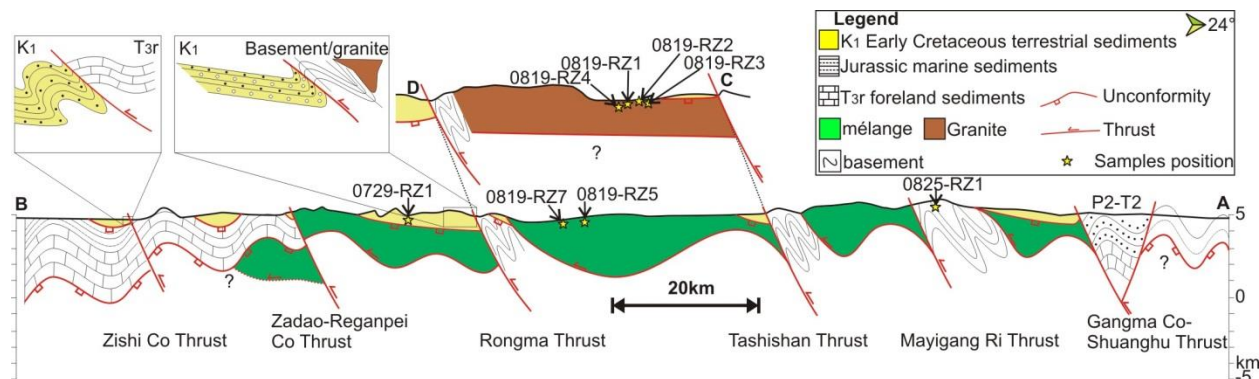


Fig. 5 N-S profile through the South Qiangtang terrane (location in Figure 2). Several thrusts accommodated the south-directed shortening and exhumation of the basement and *mélange* units. Two insets show the structural relationships near the thrusts in detail.

Figure 5 shows the geological cross section through the Rongma area, which transverses all the major thrusts and sample locations. The section shows the configuration after the main phase of shortening and exhumation of the Gangtang Co granite and basement in the Qiangtang Culmination. The Jurassic flysch as well as the Late Triassic limestone are folded which indicate Jurassic or younger deformation. The conglomerate unit is only gently folded, except near thrusts, such as at the Zishi Co and Rongma thrust (Fig. 4d). Clasts in the conglomerate are derived from hanging-wall lithologies, such as large feldspars from the Gangtang Co granite in case of the Rongma thrust and Triassic limestone in case of the Zishi Co thrust. We thus conclude that the conglomerates formed towards the end of the fold and thrust movement, after most of the exhumation in the core of the Qiangtang Culmination had taken place.

4. U-Th/He dating

4.1 Sampling

Seven samples from different structural levels were selected for zircon (U-Th)/He (ZHe) analysis. Six samples (0819-RZ1-7) are located in between the Tashishan Thrust Rongma Thrust (Fig. 2). 0819-RZ1-4 are from the Late Triassic Gangtang Co granite. 0819-RZ5 and 0819-RZ7 are derived from *mélange* rocks that the granite intruded into. One sample (0825-RZ1) is located in the hanging wall of the Mayigang Ri

Thrust and derived from basement rocks (Fig. 2). In addition, one sample from Cretaceous sandstone above the Zadao-Reganpei Co Thrust was used for detrital ZHe analysis.

4.2. Method

Idiomorphic zircon grains were selected based on suitable grain shape and size. Grain dimensions were measured for the calculation of the alpha-correction factor (Hourigan et al., 2005). Single grains were packed in Nb-tubes for U-Th/He analysis. In general we analysed 3-5 aliquots per sample. Helium was measured in the Patterson Helium-extraction line at the University of Tübingen, which is equipped with a 960 nm diode laser. Heating schedule was 10 min at 20 A. Each grain was re-heated and analysed to make sure that the grain was degassed entirely in the first step.

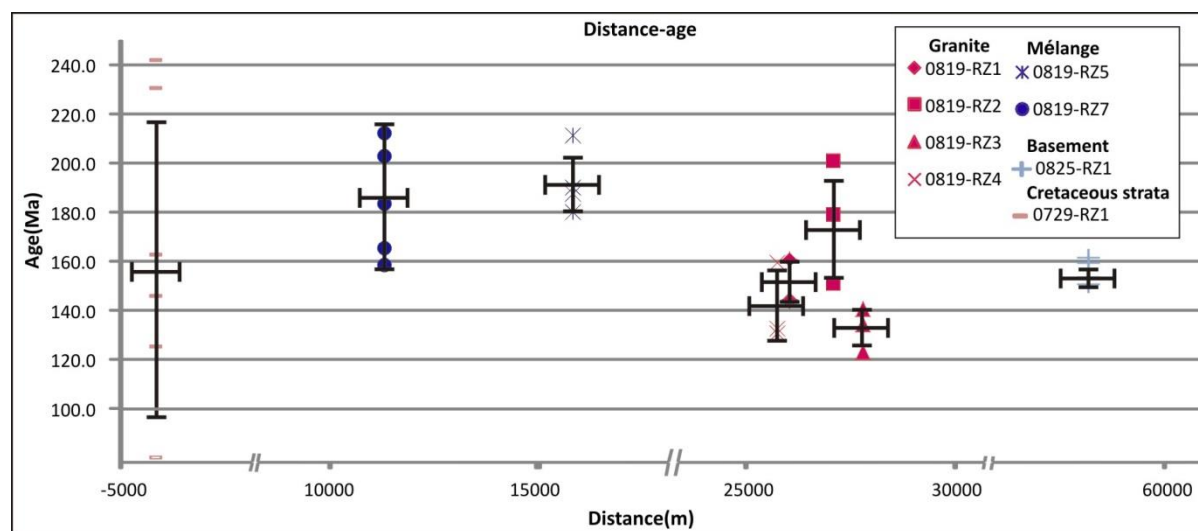


Fig. 6 Plotting of all individual zircon (U-Th)/He data against with samples relative distances to Rongma Thrust.

Concentrations of U and Th were determined by isotope dilution using the Thermo Fisher iCAP ICP-MS at University Tübingen equipped with an all-PFA sample introduction system. Zircon samples and Nb-tubes were spiked with a calibrated mixed spike of ^{233}U + ^{230}Th and dissolved in Berghof pressure digestion bombs in a $\text{HF}+\text{HNO}_3$ mixture at 200 °C for 5 days. Zircons were analysed in a final solution of 5% HNO_3 + 0.5% HF . Grain mass was estimated from measured ^{91}Zr concentrations assuming 49.77 wt-% Zr in zircon. The analytical error of ICP measurements is reported as 2 relative standard deviations (%). For Helium measurements the analytical error is generally <2% and not included in the data report.

In contrast to the analytical uncertainty, the reproducibility of the sample age constitutes a much larger error. We therefore report the mean U-Th/He age and the standard deviation of the measured aliquots as

the sample error. For single grain ages we apply a 5% 2-sigma error based on the reproducibility of standard measurements in the lab.

4.3 Results

Three samples from the Late Triassic Granite (0819-RZ1, 3, 4) produced similar cooling age from 131 ± 0.7 Ma to 149 ± 8 Ma (Table 1). Granite sample 0819-RZ2 yielded older ages (201- 156 Ma) and has a higher spread in single grain ages, and we interpret this sample as an outlier. Two mélangé samples 0819-RZ5 and RZ7 yielded broad ranges of single grain ZHe ages from 158.5 to 271.5 Ma (Fig. 6, Table 1). Four single-grain ages of basement-quartzite sample 0825-RZ1 yield an average age of 148 ± 3.8 Ma. The detrital ages from Cretaceous sandstone 0729-RZ1 range from 81.9 to 241.9 Ma.

5. Discussions

5.1 Exhumation stages in south Qiangtang terrane

According to our thermochronological results and published data (Fig. 7), we separate exhumation process of south Qiangtang terrane into three stages.

Stage 1: Jurassic-Cretaceous slow cooling

ZHe ages of the two mélangé samples range from 158.5 to 271.5 Ma. The large spread in single-grain ages may result from extremely slow cooling (Guenther et al., 2013). A Middle to Late Triassic deposition age of the mélangé constrained by fossils and dating of enclosed gabbros (Zhao et al., 2015). We thus suggest that the samples were not heated sufficiently to fully reset the ZHe system since deposition, and some or all single grain ages may therefore reflect detrital cooling ages or geologically meaningless mixed (partially reset) ages. In contrast, basement sample (quartzite, 0825-RZ1) from the Mayigang Ri thrust sheet and all granite samples except 0819-RZ2 yield well reproducible single-grain ages suggesting that the ZHe data reflect cooling through the ZHe closure temperature of 180 °C (Reiners, 2005). Thermal resetting of these samples may indicate that these samples were exhumed in the Late Jurassic to earliest Cretaceous from greater depth compared to the mélangé samples. Cooling ages from the Gangma Co granite may result from continuous slow cooling from emplacement to ambient temperatures, but the >60 Ma time span from crystallization of the pluton (210 Ma, Kapp et al., 2003b) to cooling through the ZHe closure temperature suggests that the 150-133 Ma cooling ages correspond to a tectonically or erosionally controlled episode of exhumation and cooling. This interpretation is corroborated by the identical cooling age of the quartzite sample (148 ± 3.8 Ma). Suggesting that both thrust sheets were exhumed in the latest Jurassic/earliest Cretaceous.

Chapter 5

The field relationships and the structural reconstruction indicate that the *mélange* is ~8 km thick and overlying basement. The Gantang Co granite mostly intruded the basement, but also the overlying *mélange*. The *mélange* was overlain by an unknown amount of Late Triassic to Jurassic sediments. For a typical continental geothermal gradient of 25 °C/km, the 180 °C ZHe closure temperature corresponds to a depth of ~7 km. Consistent ZHe cooling ages indicate that the granite and basement samples derive from depths >7 km, while the structurally higher *mélange* samples were buried <7 km and therefore not fully reset. This suggests that the total thickness of the Late Triassic to Jurassic sequence in the present Qiangtang Culmination never reached the full ~7.5 km as is found further south (Fig. 3).

The range of cooling ages (133-150 Ma) and an estimated thickness of the ZHe partial retention zone of >1 km yields a first-order estimate of a cooling rate of ≥ 0.06 mm/yr. Apatite fission track ages from South Qiangtang (Lu et al., 2015) yield an Early Cretaceous cooling rate of ~9 °C/Ma or, using a 25 °C/km geothermal gradient, an exhumation rate of 0.06 mm/yr. We therefore suggest that ZHe and AFT cooling ages can be attributed to slow continuous exhumation and cooling at erosion of the South Qiangtang terrane at rates <0.1 mm/yr.

Stage 2: Thrusting and rapid exhumation in the Cretaceous

By the mid Cretaceous the basement and granite were exhumed to the surface and covered by Cretaceous clastic sediments, intercalated with minor basalts (102-75 Ma, Li et al., 2014; Wu et al., 2014). Using the youngest detrital ZHe age of 82 Ma (sample 0729Z) found in these sediments as a minimum constraint for the depositional age of this sample we propose that thrusting in the Early Cretaceous resulted in the formation of the thrust belt in the Rongma area, syn-kinematic erosion and exhumation and finally formation of the intramontane basins. Exhumation rates are poorly constrained and range from 0.15 mm/yr (based on new ZHe ages only) to 0.3 mm/yr (based on AFT ages from Lu et al, 2015; Figure 7).

Stage 3: Cenozoic slow exhumation

Cenozoic (≤ 70 Ma; Lu et al., 2015) apatite He ages are reported from Ando and thermal modelling suggest slow exhumation at 0.04-0.07 mm/yr as a result of very low erosion rates throughout the Cenozoic. The exhumation rate thus slowed down by one order of magnitude.

5.2 Cause for crustal shortening and exhumation in the early Cretaceous

The Bangong Hu-Nujiang Ocean (BNS) opened and developed between Lhasa and south Qiangtang terranes from the Late Triassic onwards (Schneider et al., 2003, Liu et al., 2015). During the Jurassic,

thick (~6 km) sediments were deposited on the southern margin of the South Qiangtang terrane. The sequence of sandy foreshore or shore facies sediments is probably related to Jurassic extension and opening of the BNS ocean (Duan et al., 2009; Schneider et al., 2003; Baxter et al., 2009). Sediments were derived from the centre of the amalgamated South and North Qiangtang terranes (Schneider et al., 2003, Liu et al., 2015). Late Jurassic (155 ± 3 Ma) granodiorite and 162–143 Ma (40Ar-39Ar, mica) metamorphic rocks found in the Duguer Range on South Qiangtang (Pullen et al., 2011), interpreted as resulting from a Late Jurassic detachment further indicate Late Jurassic extension (Wang et al., 2008). We assign the first slow exhumation to this extensional stage.

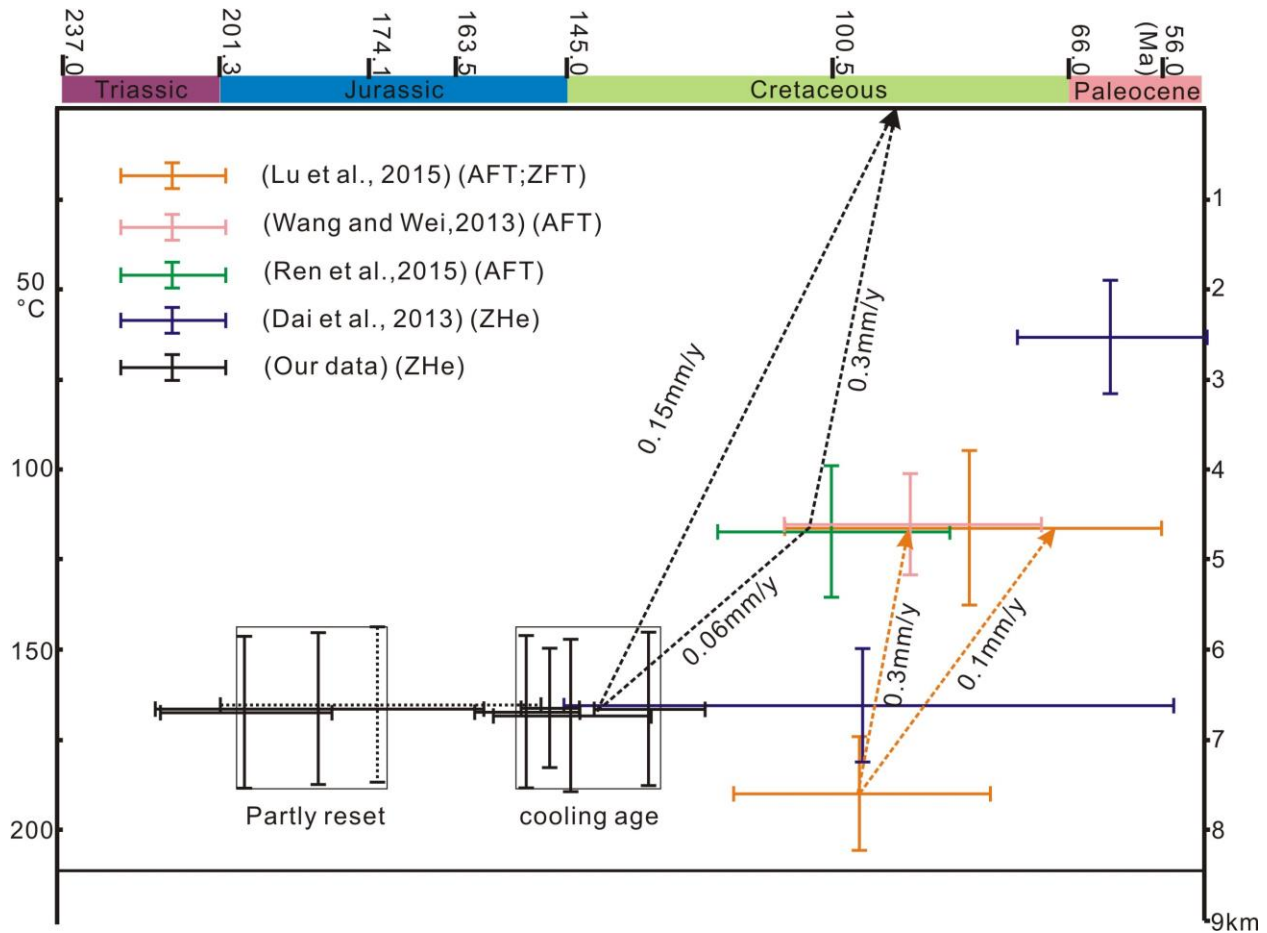


Fig. 7 Thermochronologic data from both literatures and our results show a change of the exhumation rate between ~140 Ma and ~90 Ma.

The basement and intruded granite arise cross the zircon (U-Th)/He cooling threshold between 149 and 131 Ma. During or soon after this cooling event, fast exhumation rate brought the basement and Late Triassic granite to the surface, where it was unconformably overlain by Middle Cretaceous terrestrial conglomerate (Fig. 7). Cessation of marine sedimentation in the Early Cretaceous (Li et al., 2001; Chen et

al., 2012; Cai, 2014; Duan et al., 2009; Liu et al., 2007), as well as igneous activity during 120-95 Ma indicate collision between the South Qiangtang and Lhasa terranes (e.g., Kapp et al., 2005; Kapp et al., 2007; Leloup et al., 2012; Lu et al., 2015; Liu et al., 2015). This collision phase can be attributed to the observed accelerated exhumation within the Qiangtang Culmination, leading to folding of Late Triassic-Jurassic strata, and kilometers offsets along south-verging thrusts. Most of this shortening had ceased by the time of Mid-Cretaceous conglomerate deposition, as these sediments are mostly only moderately deformed or tilted.

Our conclusion are in accordance with other apatite/zircon fission-track ages results which also show fast Middle Cretaceous (120-75 Ma) cooling rates in the order of 0.31-0.1 mm/y (Wang and Wei, 2013; Lu et al., 2015). Similar Early-Middle Cretaceous rapid uplift and denudation is also observed in the Songpan-Ganzi area, which is likely to be a response of Lhasa-South Qiangtang collision as well (e.g., Dai et al., 2013; Ratschbacher et al., 2011; Li et al., 2014; Tian et al., 2014). We thus conclude that the Qiangtang Culmination formed by south-vergent folding and thrusting in the Early Cretaceous, ending around the time of Mid Cretaceous volcanism. Major thrusts controlled depocenters of the basins during the Late Cretaceous (Wu et al., 2014). Mid-Cretaceous red beds around Rongma may have been deposited in basins that developed along the main faults (wedge-top basins, Kapp et al., 2005). This model implies substantial crustal thickening and perhaps plateau formation in central Tibet prior to the Indo-Asian collision. After 90Ma, central Tibet experienced ongoing, but slow exhumation (Lu et al., 2015), which that the effect of the India-Eurasia collision did not reach far into central Tibet.

6. Conclusions

Our ZHe results indicate that the Qiangtang Culmination experienced slow exhumation with a maximum exhumation rate of ~0.06 mm/y from 210 to 140 Ma. During Early Cretaceous, exhumation accelerated to 0.15-0.3 mm/y, forming the culmination. Exhumation was caused by north-south shortening resulting in south-verging, thick-skinned folding and thrusting. Mid Cretaceous terrestrial conglomerates and minor volcanics mark the waning stages of this crustal-thickening stage.

After foreland basin evolution during the Late Triassic (Zhao et al., 2015), the South Qiangtang terrane became the passive margin of the developing Bangong Hu-Nujiang ocean between the Lhasa and South Qiangtang terranes in the Jurassic. Early Cretaceous closure of this ocean and collision between the Lhasa and South Qiangtang terranes led to shortening and fast exhumation of South Qiangtang terrane. Preservation of a gently dipping angular unconformity beneath mid-Cretaceous conglomerate and tuffs in the Qiangtang terrane demonstrates that parts of central Tibet were above sea level at the middle

Cretaceous (>90Ma). Thickening of the crust in central Tibet may have occurred or at least commenced in the early to middle Cretaceous, well before final collision of India against Eurasia.

Acknowledgement

This research was supported by the projects issued by China Geological Survey (CGS), including the 1:50,000 regional geological surveys in the Qomo Ri, Gangmari, and Rongma areas of Tibet as well as the project titled “Tectonic attributes of the South Qiangtang Mesozoic-Cenozoic basin, based on deformation and metamorphic character”. Additionally, we appreciate the Program for Changjiang University Scholars and Innovative Research Teams (IRT1083). Z. Zhao thanks the Chinese Scholarship Council for financial support. We thank the whole mapping team of the China University of Geosciences, Beijing.

References

- Baxter, A. T., Aitchison, J. C., and Zyabrev, S. V.: Radiolarian age constraints on Mesotethyan ocean evolution, and their implications for development of the Bangong–Nujiang suture, Tibet, *Journal of the Geological Society*, 166, 689-694, 2009.
- Cai, Z.: Jurassic stratigraphic characteristics and sedimentary environment analysis in South qiangtang region of Tibet, Master thesis, P618.13, 2014.
- Chen, W., He, Y., Zhan, W., Xiong, X., Wu, T., Li, W., and Chen, J.: The discovery of Dicheiropollis in Esima area of southern Qiangtang Basin, Tibet, and its geological significance, *Geological Bulletin of China*, 31, 1602-1607, 2012.
- Dai, J., Wang, C., Hourigan, J., and Santosh, M.: Insights into the early Tibetan Plateau from (U–Th)/He thermochronology, *Journal of the Geological Society*, 170, 917-927, 2013.
- Dodson, M.: Theory of cooling ages, in: *Lectures in isotope geology*, Springer, 194-202, 1979.
- Duan, Z., Zhong, C., Zhu, H., Cheng, J., Li, Z., and Wang, Z.: Sedimentary characteristics of Middle Jurassic Sewa and Buqu Formations from Qiangzi Well-2, southern Qiangtang basin, Tibet, *Geology in China*, 36, 355-365, 2009.
- Fan, J. J., Li, C., Xu, J. X., and Wang, M.: Petrology, geochemistry, and geological significance of the Nadong ocean island, Banggongco–Nujiang suture, Tibetan plateau, *International Geology Review*, 1-14, 2014.
- Guenther, W. R., Reiners, P. W., Ketcham, R. A., Nasdala, L., and Giester, G.: Helium diffusion in natural zircon: Radiation damage, anisotropy, and the interpretation of zircon (U-Th)/He thermochronology, *American Journal of Science*, 313, 145-198, 2013.
- Hourigan, J. K., Reiners, P. W., and Brandon, M. T.: U-Th zonation-dependent alpha-ejection in (U-Th)/He chronometry, *Geochimica et Cosmochimica Acta*, 69, 3349-3365, 2005.
- Kapp, P., Murphy, M. A., Yin, A., Harrison, T. M., Ding, L., and Guo, J.: Mesozoic and Cenozoic tectonic evolution of the Shiquanhe area of western Tibet, *Tectonics*, 22, TC1029, 2003a.

- Kapp, P., Yin, A., Manning, C. E., Harrison, T. M., Taylor, M. H., and Ding, L.: Tectonic evolution of the early Mesozoic blueschist-bearing Qiangtang metamorphic belt, central Tibet, *Tectonics*, 22, 1043-1068, 2003b.
- Kapp, P., Yin, A., Harrison, T. M., and Ding, L.: Cretaceous-Tertiary shortening, basin development, and volcanism in central Tibet, *Bulletin of the Geological Society of America*, 117, 865-878, 2005.
- Kapp, P., DeCelles, P. G., Gehrels, G. E., Heizler, M., and Ding, L.: Geological records of the Lhasa-Qiangtang and Indo-Asian collisions in the Nima area of central Tibet, *Geological Society of America Bulletin*, 119, 917-933, 2007.
- Leloup, P. H., Arnaud, N. O., Mahéo, G., Paquette, J. L., Guillot, S., Valli, F., Li, H., Xu, Z., Lacassin, R., and Tapponnier, P.: Successive deformation episodes along the Lungmu Co zone, west-central Tibet, *Gondwana Research*, 21, 37-52, 10.1016/j.gr.2011.07.026, 2012.
- Li, C., Huang, X. p., Mou, S., and Chi, X.: Age dating of the Zougouyouchacuo volcanic rocks and age determination of the Kangtuo Formation in southern Qiangtang, northern Tibet, China, *Geological Bulletin of China*, 25, 226-228, 2006.
- Li, C., Zhai, Q., Dong, Y., Liu, S., Xie, C., and Wu, Y.: High-pressure eclogite-blueschist metamorphic belt and closure of paleo-Tethys Ocean in Central Qiangtang, Qinghai-Tibet plateau, *Journal of Earth Science*, 20, 209-218, 2009.
- Li, Q., Gao, R., Fang, S., Lu, Z., Han, H., Guo, Y., Li, P., Wang, H., Yang, Z., and Xie, X.: Structural Characteristics of the Basement beneath Qiangtang Basin in Qinghai - Tibet Plateau: Results of Interaction Interpretation from Seismic Reflection/Refraction Data, *Acta Geologica Sinica - English Edition*, 87, 358-377, 2013.
- Li, X., Wang, C., Yi, H., and Li, Y.: Middle Cretaceous and Eocene lithofacies and paleogeography in Tibet, *Regional Geology of China*, 20, 82-89, 2001.
- Li, X., and wen, F.: Discovery of the Late Triassic Rigain Pünco Formation and the unconformity between it and its underlying strata in eastern Rutog, Tibet, China, *Geological Bulletin of China*, 26, 1009-1013, 2007.
- Li, Y., Wang, C., Li, Y., Ma, C., Wang, L., and Peng, S.: The Cretaceous tectonic event in the Qiangtang Basin and its implications for hydrocarbon accumulation, *Petroleum Science*, 7, 466-471, 2010.
- Li, Y., He, J., Wang, C., Han, Z., Ma, P., Xu, M., and Du, K.: Cretaceous volcanic rocks in south Qiangtang Terrane: Products of northward subduction of the Bangong-Nujiang Ocean?, *Journal of Asian Earth Sciences*, 2014 (in press).
- Liu, J., Yang, P., Chen, W., Chen, W., and Fu, X.: Discovery of silicified wood in the Middle Jurassic Gyar i Formation in the southern Qiangtang depression, Tibet, China, and its significance, *Geological Bulletin of China*, 26, 1692-1696, 2007.
- Liu, D., Shi, R., Ding, L., Huang, Q., Zhang, X., Yue, Y., and Zhang, L.: Zircon U-Pb age and Hf isotopic compositions of Mesozoic granitoids in southern Qiangtang, Tibet: Implications for the subduction of the Bangong-Nujiang Tethyan Ocean, *Gondwana Research*, 2015 (in press).

- Lu, L., Zhen, Z., Zhenhan, W., Cheng, Q., and Peisheng, Y.: Fission Track Thermochronology Evidence for the Cretaceous and Paleogene Tectonic Event of Nyainrong Microcontinent, Tibet, *Acta Geologica Sinica (English Edition)*, 89, 133-144, 2015.
- Qu, X., Wang, R., Dai, J., Li, Y., Qi, X., Xin, H., Song, Y., and Du, D.: Discovery of Xiongmei porphyry copper deposit in middle segment of Bangonghu–Nujiang suture zone and its significance, *Mineral Deposits*, 31, 1-12, 2012.
- Pullen, A., Kapp, P., Gehrels, G. E., Ding, L., and Zhang, Q.: Metamorphic rocks in central Tibet: Lateral variations and implications for crustal structure, *Bulletin of the Geological Society of America*, 123, 585-600, 2011.
- Pullen, A., and Kapp, P.: Mesozoic tectonic history and lithospheric structure of the Qiangtang terrane: Insights from the Qiangtang metamorphic belt, central Tibet, *Geological Society of America Special Papers*, 507, 507-504, 2014.
- Ratschbacher, L., Hacker, B. R., Calvert, A., Webb, L. E., Grimmer, J. C., McWilliams, M. O., Ireland, T., Dong, S., and Hu, J.: Tectonics of the Qinling (Central China): tectonostratigraphy, geochronology, and deformation history, *Tectonophysics*, 366, 1-53, 2003.
- Ratschbacher, L., Krumrei, I., Blumenwitz, M., Staiger, M., Gloaguen, R., Miller, B. V., Samson, S. D., Edwards, M. A., and Appel, E.: Rifting and strike-slip shear in central Tibet and the geometry, age and kinematics of upper crustal extension in Tibet, *Geological Society, London, Special Publications*, 353, 127-163, 2011.
- Ren, Z., Cui, J., Liu, C., Li, T., Cheng, G., Dou, S., Tian, T., and Luo, Y.: Apatite Fission Track Evidence of Uplift Cooling in the Qiangtang Basin and Constraints on the Tibetan Plateau Uplift, *Acta Geologica Sinica (English Edition)*, 89, 467-484, 2015.
- Reiners, P. W.: Zircon (U-Th)/He thermochronometry, *Reviews in Mineralogy and Geochemistry*, 58, 151-179, 2005.
- Rohrmann, A., Kapp, P., Carrapa, B., Reiners, P. W., Guynn, J., Ding, L., and Heizler, M.: Thermochronologic evidence for plateau formation in central Tibet by 45 Ma, *Geology*, 40, 187-190, 2012.
- Schneider, W., Mattern, F., Wang, P. J., and Li, C.: Tectonic and sedimentary basin evolution of the eastern Bangong-Nujiang zone (Tibet): A Reading cycle, *International Journal of Earth Sciences*, 92, 228-254, 2003.
- Sui, Q.-L., Wang, Q., Zhu, D.-C., Zhao, Z.-D., Chen, Y., Santosh, M., Hu, Z.-C., Yuan, H.-L., and Mo, X.-X.: Compositional diversity of ca. 110Ma magmatism in the northern Lhasa Terrane, Tibet: Implications for the magmatic origin and crustal growth in a continent–continent collision zone, *Lithos*, 168, 144-159, 2013.
- Tian, Y., Kohn, B. P., Hu, S., and Gleadow, A. J.: Postorogenic rigid behavior of the eastern Songpan-Ganze terrane: Insights from low-temperature thermochronology and implications for intracontinental deformation in central Asia, *Geochemistry, Geophysics, Geosystems*, 15, 453-474, 2014.
- Vassallo, R., Jolivet, M., Ritz, J.-F., Braucher, R., Larroque, C., Sue, C., Todt, M., and Javkhlanbold, D.: Uplift age and rates of the Gurvan Bogd system (Gobi-Altay) by apatite fission track analysis, *Earth and Planetary Science Letters*, 259, 333-346, 2007.
- Wang, C. S., and Yi, H. S.: *Geology Evolution and Oil and Gas Prospect Evaluation of Qiangtang Basin in Tibet*. Beijing: Geological Publishing House. 1-215 (in Chinese), 2001.

- Wang, G., Zhang, W., Zhou, X., Jia, J., and Yu, H.: Middle Jurassic high-pressure shearing revealed by phengite in Jiazuqiao metamorphic complex, eastern Tibet, *Acta Petrologica Sinica*, 24, 395-400, 2008.
- Wang, J., Tan, F. W., Li, Y. L.: The Potential of the Oil and Gas Resources in the Major Sedimentary Basin on the Qinghai-Xizang (Tibet) Plateau. Beijing: Geological Publishing House. 1-317 (in Chinese), 2005.
- Wang, L., and Wei, Y.: Apatite fission track thermochronology evidence for the Mid-Cretaceous tectonic event in the Qiangtang Basin, Tibet, *Acta Petrologica Sinica*, 29, 1039-1047, 2013.
- Wu, Z., Ye, P., and Yin, C.: The Early Cenozoic Gerze Thrust System in Northern Tibet, *Acta Geoscientica Sinica*, 34, 31-38, 2013.
- Wu, Z., Wu, X., Zhao, Z., Lu, L., Ye, P., and Zhang, Y.: SHRIMP U-Pb Isotopic Dating of the Late Cretaceous Volcanic Rocks and Its Chronological Constraint on the Red-beds in Southern Qiangtang Block, 35, 562-572, 2014.
- Xu, M., Li, C., Zhang, X., and Wu, Y.: Nature and evolution of the Neo-Tethys in central Tibet: synthesis of ophiolitic petrology, geochemistry, and geochronology, *International Geology Review*, 1-25, 2014.
- Yin, A., and Harrison, T. M.: Geologic evolution of the Himalayan-Tibetan orogen, *Annual Review of Earth and Planetary Sciences*, 28, 211-280, 2000.
- Zeng, M., Zhang, X., Cao, H., Effensohn, F. R., Cheng, W., and Lang, X.: Late Triassic initial subduction of the Bangong-Nujiang Ocean beneath Qiangtang revealed: stratigraphic and geochronological evidence from Gaize, Tibet, *Basin Research*, 2015 (in press).
- Zhai, Q. G., Jahn, B. M., Zhang, R. Y., Wang, J., and Su, L.: Triassic Subduction of the Paleo-Tethys in northern Tibet, China: evidence from the geochemical and isotopic characteristics of eclogites and blueschists of the Qiangtang Block, *Journal of Asian Earth Sciences*, 42, 1356-1370, 2011.
- Zhang, K. J., Xia, B., Zhang, Y. X., Liu, W. L., Zeng, L., Li, J. F., and Xu, L. F.: Central Tibetan Meso-Tethyan oceanic plateau, *Lithos*, 210, 278-288, 2014.
- Zhang, K. J., Xia, B. D., Wang, G. M., Li, Y. T., and Ye, H. F.: Early Cretaceous stratigraphy, depositional environments, sandstone provenance, and tectonic setting of central Tibet, western China, *Bulletin of the Geological Society of America*, 116, 1202-1222, 2004.
- Zhang, K. J., Zhang, Y. X., Xia, B. D., and He, Y. B.: Temporal variations of Mesozoic sandstone compositions in the Qiangtang block, northern Tibet (China): implications for provenance and tectonic setting, *Journal of Sedimentary Research*, 76, 1035-1048, 2006.
- Zhao, Z., Bons, P. D., Wang, G., Liu, Y., and Zheng, Y.: Origin and pre-Cenozoic evolution of the south Qiangtang basement, Central Tibet, *Tectonophysics*, 623, 52-66, 2014.
- Zhao, Z., Bons, P., Wang, G., Soesoo, A., and Liu, Y.: Tectonic evolution and high-pressure rock exhumation in the Qiangtang Terrane, Central Tibet, *Solid Earth*, 6, 457-473, 2015.
- Zhu, D. C., Mo, X. X., Niu, Y., Zhao, Z. D., Wang, L. Q., Liu, Y. S., and Wu, F. Y.: Geochemical investigation of Early Cretaceous igneous rocks along an east-west traverse throughout the central Lhasa Terrane, Tibet, *Chemical Geology*, 268, 298-312, 2009a.

Chapter5

- Zhu, D. C., Zhao, Z. D., Pan, G. T., Lee, H. Y., Kang, Z. Q., Liao, Z. L., Wang, L. Q., Li, G. M., Dong, G. C., and Liu, B.: Early cretaceous subduction-related adakite-like rocks of the Gangdese Belt, southern Tibet: Products of slab melting and subsequent melt-peridotite interaction?, *Journal of Asian Earth Sciences*, 34, 298-309, 2009b.
- Zhu, D. C., Zhao, Z. D., Niu, Y., Dilek, Y., Hou, Z. Q., and Mo, X. X.: The origin and pre-Cenozoic evolution of the Tibetan Plateau, *Gondwana Research*, 23, 1429-1454, 2012.
- Zhu, T., Feng, X., Wang, X., and Zhou, M.: Reconstruction of the Triassic Tectonic Lithofacies Paleogeography in Qiangtang Re- gion, Northern Qinghai, Tibet Plateau, China, *Acta Geol. Sin.- Engl.*, 87, 378–394, 2013.

Chapter 6: Subduction reversal: an efficient mechanism for the exhumation of ultra-high-pressure rocks

Paul D. Bons¹, Evgene Burov², Enrique Gomez-Rivas³, Alavar Soesoo⁴, Douwe D.J. van Hinsbergen⁵, Kun Wang² and Zhongbao Zhao¹

(1) Department of Geosciences, Eberhard Karls University Tübingen, Germany.

(2) iSTeP - Institut des Sciences de la Terre de Paris - UMR 7193 UPMC-CNRS, Université P. & M. Curie (Paris VI), Paris, France.

(3) Department of Geology and Petroleum Geology, University of Aberdeen, Scotland, UK.

(4) Institute of Geology, Tallinn University of Technology, Tallinn, Estonia.

(5) Department of Earth Sciences, University of Utrecht, Utrecht, Netherlands,

This chapter is a preliminary draft for a manuscript to be submitted to the journal *Nature (Geoscience)* or *Geology*. The author list is preliminary and given in alphabetical order.

There is an ongoing debate on how (ultra) high-pressure (UHP) rocks, such as eclogites, can be brought to the surface from depths well over 100 km (Hacker and Gerya, 2013; Warren, 2013), as indicated by high-pressure minerals such as diamond and coesite (Chopin, 1984; Smith, 1984; Majka et al., 2014). It is generally accepted that this exhumation is related to subduction of oceanic slabs. The enigma is that these rocks move up towards the surface, while the oceanic slab is assumed to descend into the mantle in the subduction zone at the same time (e.g. Schellart and Rawlinson, 2010). We show that a simple and efficient mechanism for exhumation is the reversal of the down-going movement of the subducting slab itself. In this mechanism the exhumation is a direct result of the slab movement and not an indirect effect, as in most current models. Subduction reversal occurs when the downward pull by the weight of the subducted slab is less than the opposing upwards pull on the slab. We present one scenario that is particularly prone to lead to slab extraction: a divergent double subduction zone (DDS-zone; Soesoo et al., 1997; Wu et al., 2011; Zhao et al., 2015) (Fig. 1). There are currently at least two active DDS-zones on Earth between Italy and the Balkans (Faccenna et al., 2014) and between the islands of Sulawesi and Halmahera in Indonesia (Hafkenscheid et al., 2001).

Oceanic plates are constantly produced at spreading ridges. As these plates cool, they become denser and in the end slide down into the mantle at subduction zones, such as the Pacific "Ring of Fire". Although the oceanic plate slides down into the mantle, high to ultra-high pressure rocks are commonly found in or

associated with subduction zones (e.g. Ring, 1999). Instead of moving down as the slab does, these rocks moved up from often >100 km depths (Baldwin et al., 2004). These rocks can either derive from the down-going slab, or the base of the overriding plate (Hacker et al., 2013). Exhumation velocities can be very high, well over 10 mm/yr, equivalent to velocities of plates (Rubatto and Hermann, 2001; Parrish et al., 2006). The question of how rocks from great depths can be brought to the surface remains hotly debated.

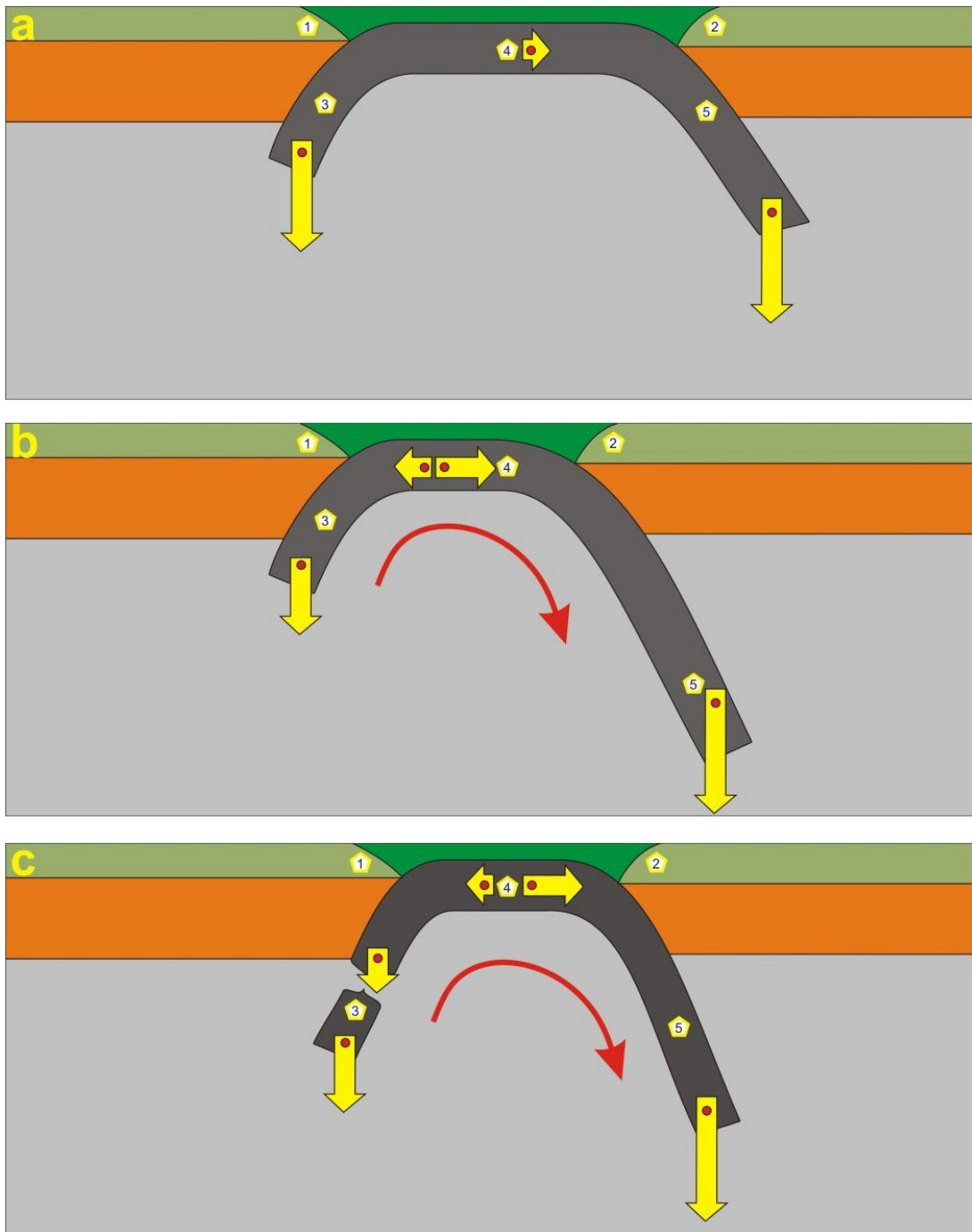


Fig. 1. Schematic sketch of the force balance in typical divergent double subduction situations. (a) As long as the two hinges are far apart, downward pull of each slab mostly results in rollback. (b) If there is a distinct imbalance between the two slabs, one slab pull will exceed the other, leading to the whole oceanic lithosphere sliding in one direction, resulting in exhumation of the short, trailing slab. (c) In case of slab break-off, the force balance is suddenly disturbed, potentially leading to subduction reversal.

Most models have in common that they attempt to reconcile a downward movement of a slab with upward exhumation of UHP rocks. One relatively simple option that has rarely been considered is that the subducted slab may, under circumstances, reverse its sliding direction and move up instead of down. What happens at a subduction zone is the result of the complex interplay of forces that act on the various components: the overriding plate, the not (yet) subducting plate, and the part of that plate that is already subducted (Fig. 1). Under normal circumstances a point on the subducting plate moves towards a point on the overriding plate, forcing the subducting plate to slide underneath the overriding plate. The driving forces are the weight of the slab (slab pull), as well as possible a push from a spreading ridge (ridge push) (Conrad and Lithgow-Bertelloni, 2002). As plates globally form a complex mosaic, an additional factor is the movement of the overriding plate, which may be pushed towards or pulled away from the subduction zone (Webb et al., 2008).

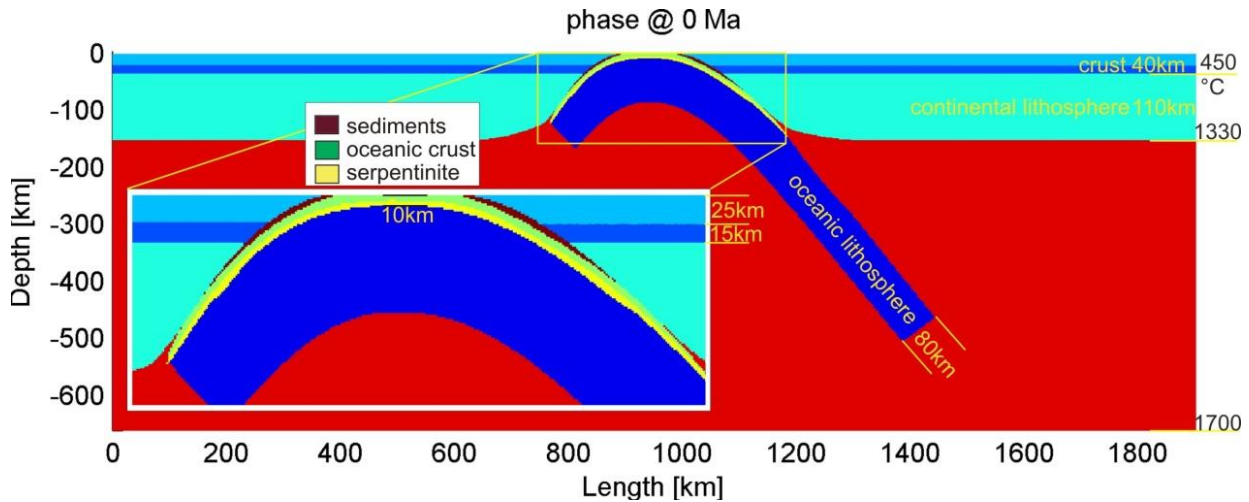


Fig. 2. Initial setup for our FLAMAR model of a divergent double subduction model with a close-up showing the detailed structure of the oceanic crust. For beginning rheological setting up are in Appendix C.

Now we consider the case where points on the subducting and overriding plate diverge. Continued downward sliding of the slab then necessitates so-called "hinge rollback" and the extension of the overriding plate, typically by the formation of a back-arc basin (Jolivet et al., 2013). If, however, the slab pull is relatively minor (e.g. a short slab) and the plates cannot stretch significantly, the forces that pull the plates apart may exceed the slab pull, with reversal of the slab movement a consequence (Fig. 1b).

When subduction of the slab is reversed, UHP rocks from the slab and overriding plate are brought back to the surface. It has been suggested by Hacker et al. (2000) and Webb et al. (2008) that subduction reversal may have been caused by rotation of a microplate in the Triassic Dabie Shan orogeny in eastern China and currently in eastern Papua New Guinea (see below), respectively. The scenario is also close to the "eduction" model of Andersen et al. (1991) and Duretz et al. (2012) for the Western Gneiss Region in Norway. That model envisages subduction of continental crust, dragged down by an oceanic slab. Once the heavy oceanic slab tears off, the continental crust rises by its own buoyancy. Here we argue, with field examples and numerical modeling, that subduction reversal is probably a more common and general mechanism for the exhumation of UHP rocks, not restricted to particular circumstances of microplate rotation or the subduction of buoyant plates.

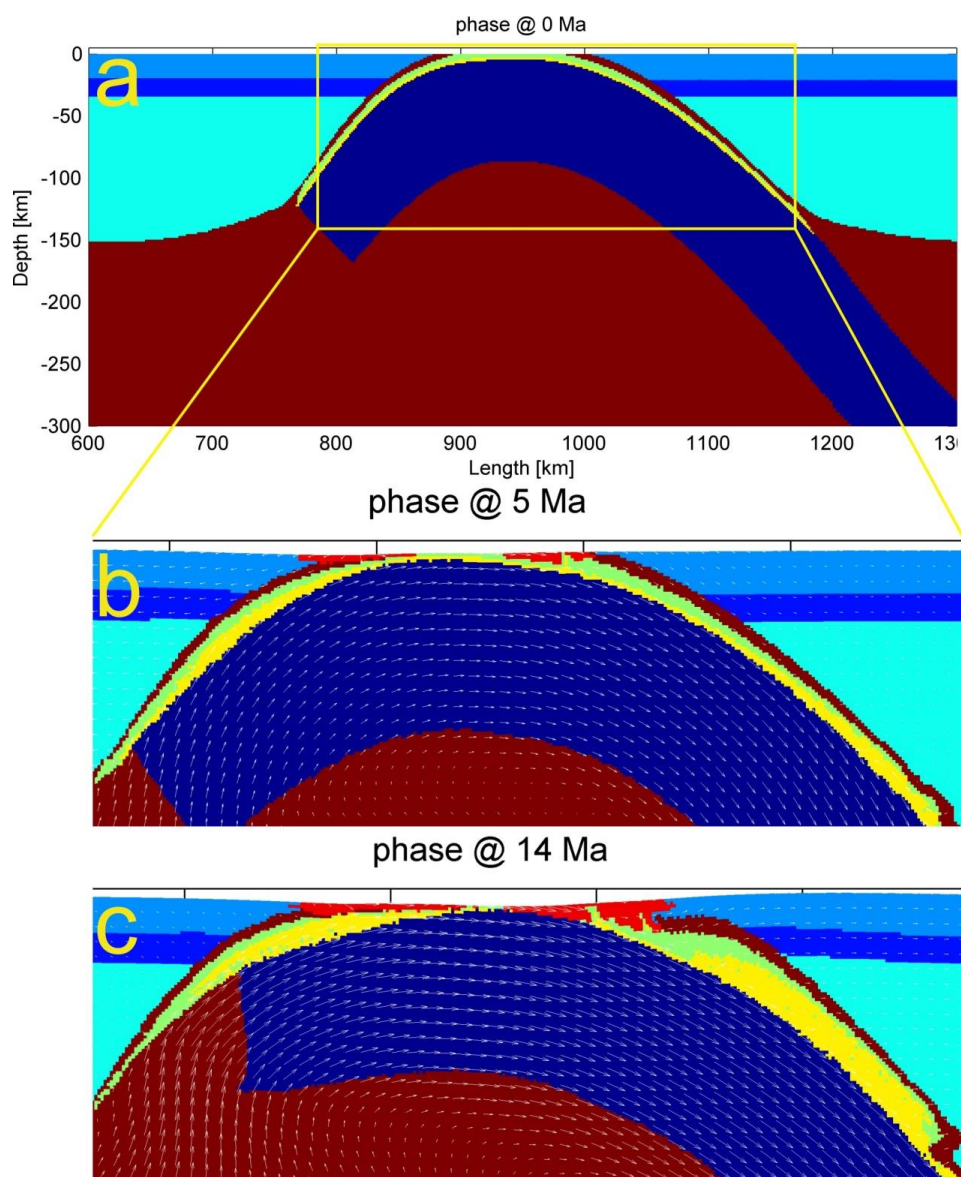


Fig. 3. Example of subduction reversal in a simulation with zero relative velocity between the overriding plates at three points in time: (a) 0 Myr, (b) 5 Myr and (c) 14 Myr, at which stage the extracted oceanic slab begins to separate from the overriding plate and a pull-away basin begins to develop.

A divergent double subduction zone (DDS-zone) (Soesoo et al., 1997; Wu et al., 2011; Zhao et al., 2015) is one scenario that is prone to lead to subduction reversal. In this case one oceanic plate subducts at both sides, which necessitates hinge rollback. As the subduction zones converge, the two slabs will be increasingly affected by each other's pull. As it is highly unlikely that both slabs have equal lengths and densities, one pull will in the end exceed the other, which then experiences a net upwards pull, leading to its upwards extraction from the mantle. This scenario was simulated numerically with FLAMAR (Angiboust et al., 2012, see Methods) for different relative velocities of the overriding plates (Fig. 2).

The simulations start with a DDS-zone with the left slab penetrating down to 150 km and the right one down to 350 km (Fig. 2). As long as the overriding plates do not converge too rapidly (≤ 1 cm/yr), the longer slab slides down and pulls the shorter one up and finally down at the opposite suture, at a rate reaching >5 cm/yr in the simulations. Rocks from >120 km depth exhume to near surface levels within a few million years (exhumation rates up to 5 cm/yr), after which their ascend paths flatten (Fig. 3c, 4). UHP rocks are thus juxtaposed to upper crustal rocks from the overriding plate that are pulled away in what is effectively a giant, lithosphere-scale metamorphic core complex (Whitney et al., 2013) (Fig. 3c). Once the short slab is fully extracted from the mantle, an oceanic basin, which we suggest to call a "pull-away basin", develops as the trailing edge of the plate pulls away from the former suture (Fig. 3b).

One interesting aspect is that the sense of shear at both sutures is the same (Fig. 3a). The exhumed rocks are dragged towards the suture of the down-going slab, where they in the end reach the thrust system. When the two overriding plates finally collide, it is difficult to distinguish which deformation occurred at which suture, as both have the same sense of shear.

Divergent double subduction systems are not the rule, but also not a rare exception. Presently, they are found in the Adria plate, east of Italy (Faccenna et al., 2014) and between the Indonesian Sangehe and Halmahera Islands (Hafkenscheid et al., 2001). Fossil systems are reported in the Australian Lachlan Fold Belt (Soesoo et al., 1997), for closure of the Mongol-Okhotsk ocean (Van der Voo et al., 2015) and the Qiangtang Terrane in Central Tibet (Liu et al., 2011). The simulations show that subduction reversal is only short lived. Because of this, active subduction reversal is expected to be relatively rare at any one time, and may currently only occur at two sites on Earth, which are described below.

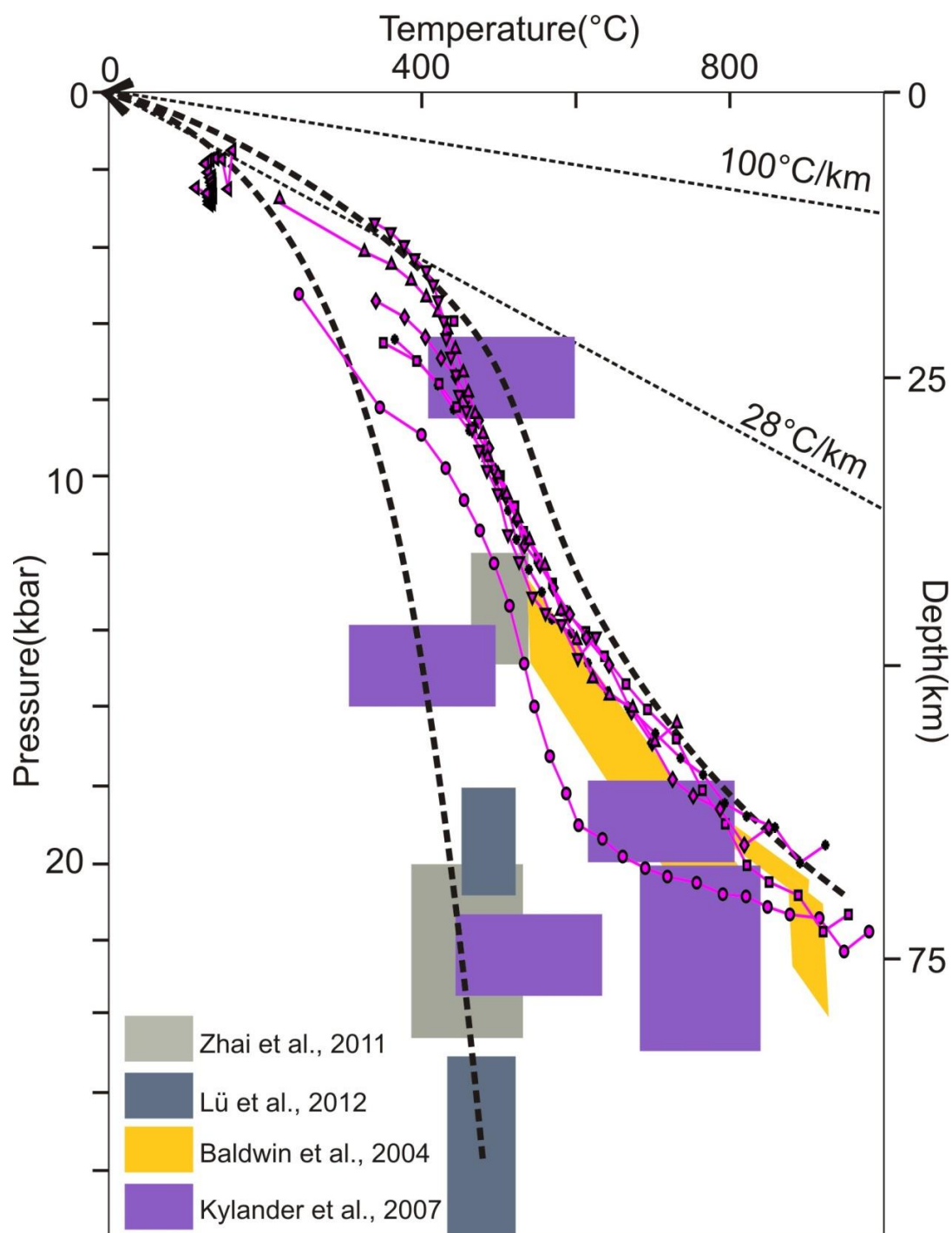


Fig. 4. Temperature-depth paths of selected particles, compared to conditions of UHP metamorphism recorded in Qiangtang, central Tibet (Zhai et al., 2011); Tianshan, northwest China (Lu et al., 2012); Western Gneiss, Norway (Kylander et al., 2007); d'Entrecasteaux Islands, Eastern Papua New Guinea (Baldwin et al., 2004). Pressures are given for reference only and are calculated using a pressure increase of 0.3 kbar/km, thus ignoring possible tectonic over- or underpressure..

Subduction reversal may explain the exhumation of the youngest UHP rocks known on Earth: the eclogite facies rocks of the D'Entrecasteaux Island of the coast of eastern New Guinea (Fig. 5a). These rocks were formed at a depth of ~90 km depth between 4.6 and 5.6 Ma and reached the surface by 1.8 Ma, giving average exhumation rates of ~2 cm/yr (Baldwin et al., 2004; DesOrmeau et al., 2014; Korchinski et al., 2014). The UHP rocks occur in extensional domes, with normal faults separating them from the overlying low-grade upper-plate rocks. Proposed exhumation mechanisms are diapirism of buoyant, and possibly partially molten UHP rocks (Ellis et al., 2011; DesOrmeau et al., 2014), associated with extension due to the NW-ward movement of the Solomon Sea Plate and rapid opening of the Woodlark Basin (Baldwin et al., 2012). In an alternative model, Webb et al. (2008) proposed that the UHP rocks were brought down by northward subduction of the Australian plate and were subsequently exhumed by subduction reversal, due to anti-clockwise rotation of the Solomon Sea Plate (Fig. 5b). However, this subduction of the Australian plate ceases by ≥ 20 Ma (van Ufford and Cloos, 2005), after which the whole system moved another 2000 km to the north. This subduction can therefore not have caused UHP metamorphism around 5 Ma.

Our simulations provide an explanation for the opening of the Woodlark Basin, as well as the exhumation of UHP rocks (Fig. 3b, c). Magmatism along the Maramuni Arc record southward subduction of the Solomon Sea Plate underneath Papua New Guinea in the Miocene (van Ufford and Cloos, 2005) (Fig. 5b), which would have brought down rocks to UHP conditions. The short subducted plate was subsequently pulled up by the NW-ward subducting Solomon Sea Plate at the New Britain trench. Due to the anti-clockwise rotation of the Solomon Sea Plate, it is completely extracted from the mantle in the east, where the Woodlark Basin now opens in its wake as a "pull away basin". The Nabura "Fault" marks the trailing edge of the extracted Solomon Sea Plate.

Another currently active divergent subduction system is that of the Adria plate between Italy and the Dinarides (Wortel and Spakman, 2000; Benoit et al., 2011). One slab currently subducts under the Dinaride coast, while the other slab subducts to the SW under the Apennines. The SW slab is currently in the process of tearing (Wortel and Spakman, 2000; Faure Walker et al., 2012), making it effectively very short (~300 km; Benoit et al. 2011) compared to the NE slab. GPS velocity measurements show that the two overriding plates hardly move relative to each other (Caporali et al., 2009). However, the Adria plate moves at a relative speed of a few mm/yr towards the NE, causing significant extension NE of the axis of the Apennine chain (D'Agostino et al., 2011; Montone et al., 2012). The fact that the whole Adria slab moves to the NE, faster than any rollback of the hinges on either side, must mean that the SW slab is

pulled up in the same direction. However, this has not yet resulted in bringing UHP rocks to the surface in the Apennines. Considering the velocity of the Adria plate, UHP rocks are expected to appear at the surface in about 5-10 million years, which will provide the final proof of our model.

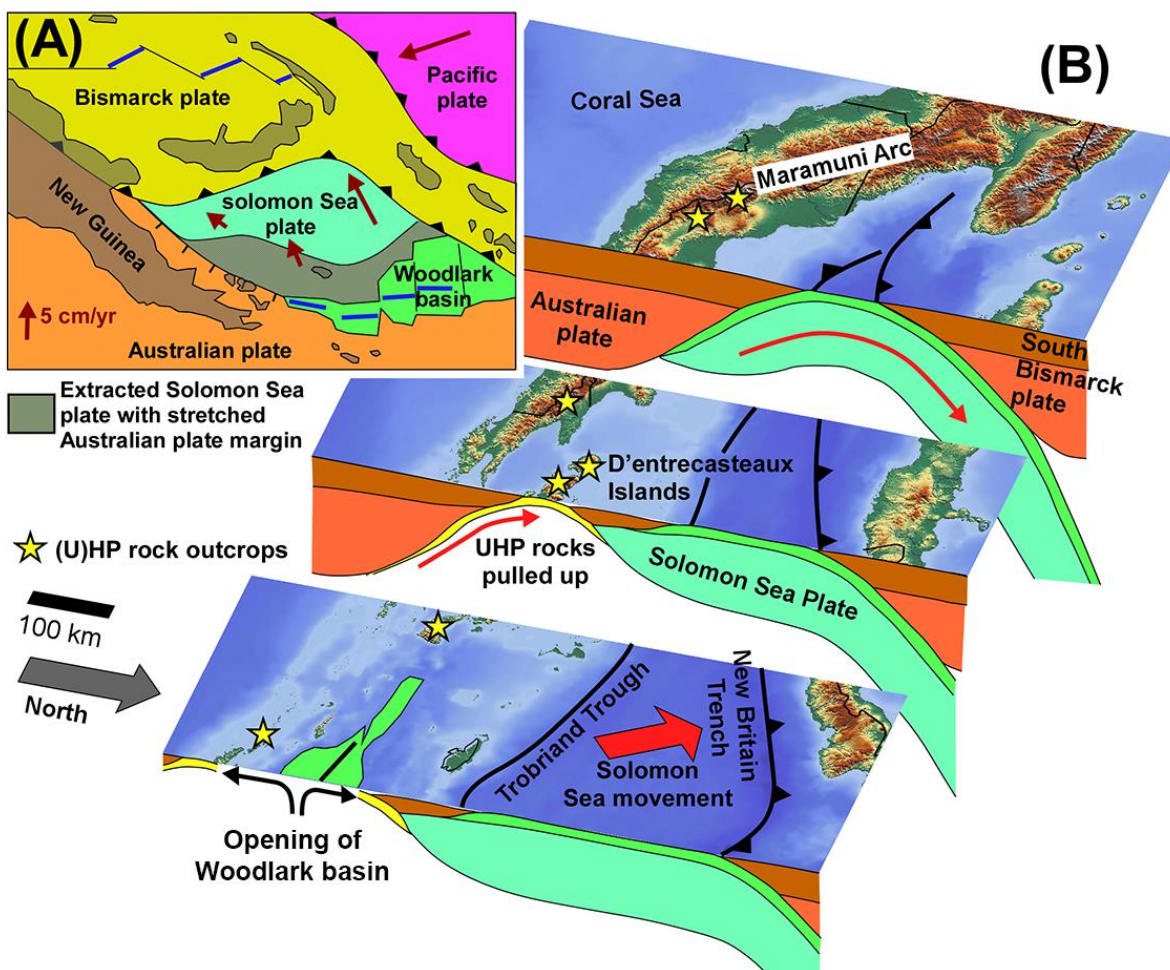


Fig. 5 Model for rapid exhumation of UHP rocks at the d'Entrecasteaux Islands, off the coast of Eastern Papua New Guinea. (A) Regional plate tectonic situation. Red arrows show plate velocities after (Baldwin et al. 2012). (B) Cross sections showing the Solomon Sea plate being extracted from the mantle due to subduction at the New Britain Trench. Map from

http://upload.wikimedia.org/wikipedia/commons/c/c6/Papua_New_Guinea_location_map_Topographic.png

The proposed model provides an efficient mechanism for the rapid exhumation of UHP rocks. It can explain several features typical for UHP rocks, such as initially rapid exhumation, followed by slower exhumation (Kylander-Clark et al., 2012), extension during exhumation (Brueckner and Cuthbert, 2013), close association of UHP rocks with upper-plate rocks. This does not imply that other proposed models are invalidated. However, considering that presently there appear to be at least two cases of subduction

reversal in an active DDS-zone, each with a lifetime in the order of 10-20 myrs, one can expect to have had at least 25 such cases on Earth in the Mesozoic alone. Subduction reversal in a DDS-zone, as well as by other plate tectonic forces, should thus be regarded as an important mechanism for the exhumation of UHP rocks.

Author contributions: The basic idea was conceived by Bons, Zhao and Soesoo. Numerical modelling was carried out by Zhao, Gomez-Rivas and Burov. The paper was written by all authors.

References

- Andersen, T. B., Jamtveit, B., Dewey, J. F., and Swensson, E.: Subduction and exhumation of continental crust: major mechanisms during continent - continent collision and orogenic extensional collapse, a model based on the south Norwegian Caledonides, *Terra Nova*, 3, 303-310, 1991.
- Angiboust, S., Wolf, S., Burov, E., Agard, P., and Yamato, P.: Effect of fluid circulation on subduction interface tectonic processes: Insights from thermo-mechanical numerical modelling, *Earth and Planetary Science Letters*, 357, 238-248, 2012.
- Baldwin, S. L., Monteleone, B. D., Webb, L. E., Fitzgerald, P. G., Grove, M., and Hill, E. J.: Pliocene eclogite exhumation at plate tectonic rates in eastern Papua New Guinea, *Nature*, 431, 263-267, 2004.
- Baldwin, S. L., Fitzgerald, P. G., and Webb, L. E.: Tectonics of the New Guinea region, 2012.
- Benoit, M. H., Torpey, M., Liszewski, K., Levin, V., and Park, J.: P and S wave upper mantle seismic velocity structure beneath the northern Apennines: New evidence for the end of subduction, *Geochemistry, Geophysics, Geosystems*, 12, 2011.
- Brueckner, H. K., and Cuthbert, S. J.: Extension, disruption, and translation of an orogenic wedge by exhumation of large ultrahigh-pressure terranes: Examples from the Norwegian Caledonides, *Lithosphere*, 5, 277-289, 2013.
- Caporali, A., Aichhorn, C., Barlik, M., Becker, M., Fejes, I., Gerhatova, L., Ghitau, D., Greneczy, G., Hefty, J., and Krauss, S.: Surface kinematics in the Alpine-Carpathian-Dinaric and Balkan region inferred from a new multi-network GPS combination solution, *Tectonophysics*, 474, 295-321, 2009.
- Chopin, C.: Coesite and pure pyrope in high-grade blueschists of the Western Alps: a first record and some consequences, *Contributions to Mineralogy and Petrology*, 86, 107-118, 1984.
- Conrad, C. P., and Lithgow-Bertelloni, C.: How mantle slabs drive plate tectonics, *Science*, 298, 207-209, 2002.
- D'Agostino, N., Mantenuto, S., D'Anastasio, E., Giuliani, R., Mattone, M., Calcaterra, S., Gambino, P., and Bonci, L.: Evidence for localized active extension in the central Apennines (Italy)(Zhai et al., 2011; Kylander-Clark et al., 2007) from global positioning system observations, *Geology*, 39, 291-294, 2011.
- DesOrmeau, J. W., Gordon, S. M., Little, T. A., and Bowring, S. A.: Tracking the exhumation of a Pliocene (U) HP terrane: U - Pb and trace - element constraints from zircon, D'Entrecasteaux Islands, Papua New Guinea, *Geochemistry, Geophysics, Geosystems*, 2014.

- Duretz, T., Gerya, T., Kaus, B., and Andersen, T.: Thermomechanical modeling of slab eduction, *Journal of Geophysical Research: Solid Earth* (1978–2012), 117, 2012.
- Ellis, S., Little, T., Wallace, L., Hacker, B., and Buiter, S.: Feedback between rifting and diapirism can exhume ultrahigh-pressure rocks, *Earth and Planetary Science Letters*, 311, 427-438, 2011.
- Faccenna, C., Becker, T. W., Auer, L., Billi, A., Boschi, L., Brun, J. P., Capitanio, F. A., Funiciello, F., Horv  th, F., and Jolivet, L.: Mantle dynamics in the Mediterranean, *Reviews of Geophysics*, 52, 283-332, 2014.
- Faure Walker, J., Roberts, G. P., Cowie, P., Papanikolaou, I., Michetti, A., Sammonds, P., Wilkinson, M., McCaffrey, K., and Phillips, R.: Relationship between topography, rates of extension and mantle dynamics in the actively-extending Italian Apennines, *Earth and Planetary Science Letters*, 325, 76-84, 2012.
- Hacker, B. R., Gnos, E., Ratschbacher, L., Grove, M., McWilliams, M., Sobolev, S. V., Wan, J., and Zhenhan, W.: Hot and dry deep crustal xenoliths from Tibet, *Science*, 287, 2463, 2000.
- Hacker, B. R., and Gerya, T. V.: Paradigms, new and old, for ultrahigh-pressure tectonism, *Tectonophysics*, 603, 79-88, 2013.
- Hacker, B. R., Gerya, T. V., and Gilotti, J. A.: Formation and Exhumation of Ultrahigh-Pressure Terranes, *Elements*, 9, 289-293, 2013.
- Hafkenscheid, E., Buiter, S., Wortel, M., Spakman, W., and Bijwaard, H.: Modelling the seismic velocity structure beneath Indonesia: a comparison with tomography, *Tectonophysics*, 333, 35-46, 2001.
- Jolivet, L., Faccenna, C., Huet, B., Labrousse, L., Le Pourhiet, L., Lacombe, O., Lecomte, E., Burov, E., Denele, Y., and Brun, J.-P.: Aegean tectonics: Strain localisation, slab tearing and trench retreat, *Tectonophysics*, 597, 1-33, 2013.
- Korchinski, M., Vry, J., Little, T., Millet, M. A., Bicknell, R., Smith, E., and Handt, A.: Timing of UHP exhumation and rock fabric development in gneiss domes containing the world's youngest eclogite Facies rocks, southeastern Papua New Guinea, *Journal of Metamorphic Geology*, 32, 1019-1039, 2014.
- Kylander-Clark, A., Hacker, B., Johnson, C., Beard, B., Mahlen, N., and Lapen, T.: Timing of multi-stage metamorphism during ultrahigh-pressure continental subduction and exhumation: Lu/Hf and Sm/Nd geochronology in western Norway, *Chemical Geology*, 232, 137-154, 2007.
- Kylander-Clark, A. R., Hacker, B. R., and Mattinson, C. G.: Size and exhumation rate of ultrahigh-pressure terranes linked to orogenic stage, *Earth and Planetary Science Letters*, 321, 115-120, 2012.
- Liu, Y., Santosh, M., Zhao, Z. B., Niu, W. C., and Wang, G. H.: Evidence for palaeo-Tethyan oceanic subduction within central Qiangtang, northern Tibet, *Lithos*, 127, 39-53, 2011.
- L  , Z., Bucher, K., Zhang, L., and Du, J.: The Habutengsu metapelites and metagreywackes in western Tianshan, China: metamorphic evolution and tectonic implications, *Journal of Metamorphic Geology*, 30, 907-926, 2012.
- Majka, J., Jan  k, M., Andersson, B., Klonowska, I., Gee, D. G., Ros  n,   ., and Ko  smi  nska, K.: Pressure–temperature estimates on the Tjeliken eclogite: new insights into the (ultra)-high-pressure evolution of the Seve Nappe Complex in the Scandinavian Caledonides, *Geological Society, London, Special Publications*, 390, 369-384, 2014.

- Montone, P., Mariucci, M. T., and Pierdominici, S.: The Italian present-day stress map, *Geophysical Journal International*, 189, 705-716, 2012.
- Parrish, R. R., Gough, S. J., Searle, M. P., and Waters, D. J.: Plate velocity exhumation of ultrahigh-pressure eclogites in the Pakistan Himalaya, *Geology*, 34, 989, 2006.
- Ring, U.: Exhumation processes: normal faulting, ductile flow and erosion, Geological Society Pub House, 1999.
- Rubatto, D., and Hermann, J.: Exhumation as fast as subduction?, *Geology*, 29, 3-6, 2001.
- Schellart, W. P., and Rawlinson, N.: Convergent plate margin dynamics: New perspectives from structural geology, geophysics and geodynamic modelling, *Tectonophysics*, 483, 4-19, 2010.
- Smith, D. C.: Coesite in clinopyroxene in the Caledonides and its implications for geodynamics, 1984.
- Soesoo, A., Bons, P. D., Gray, D. R., and Foster, D. A.: Divergent double subduction: tectonic and petrologic consequences, *Geology*, 25, 755-758, 1997.
- van Ufford, A. Q., and Cloos, M.: Cenozoic tectonics of New Guinea, *AAPG bulletin*, 89, 119-140, 2005.
- Van der Voo, R., van Hinsbergen, D. J., Domeier, M., Spakman, W., and Torsvik, T. H.: Latest Jurassic–earliest Cretaceous closure of the Mongol-Okhotsk Ocean: A paleomagnetic and seismological-tomographic analysis, *Geological Society of America Special Papers*, 513, SPE513-519, 2015.
- Warren, C.: Exhumation of (ultra-) high-pressure terranes: concepts and mechanisms, *Solid Earth*, 4, 2013.
- Webb, L., Baldwin, S., Little, T., and Fitzgerald, P.: Can microplate rotation drive subduction inversion?, *Geology*, 36, 823-826, 2008.
- Whitney, D. L., Teyssier, C., Rey, P., and Buck, W. R.: Continental and oceanic core complexes, *Geological Society of America Bulletin*, 125, 273-298, 2013.
- Wortel, M., and Spakman, W.: Subduction and slab detachment in the Mediterranean-Carpathian region, *Science*, 290, 1910-1917, 2000.
- Wu, C., Gao, Y., Frost, B. R., Robinson, P. T., Wooden, J. L., Wu, S., Chen, Q., and Lei, M.: An early Palaeozoic double-subduction model for the North Qilian oceanic plate: evidence from zircon SHRIMP dating of granites, *International Geology Review*, 53, 157-181, 2011.
- Zhai, Q. G., Zhang, R. Y., Jahn, B. M., Li, C., Song, S. G., and Wang, J.: Triassic eclogites from central Qiangtang, northern Tibet, China: Petrology, geochronology and metamorphic PT path, *Lithos*, 125, 173-189, 2011.
- Zhao, Z., Bons, P., Wang, G., Soesoo, A., and Liu, Y.: Tectonic evolution and high-pressure rock exhumation in the Qiangtang Terrane, Central Tibet, *Solid Earth*, 6, 457-473, 2015.

Chapter 7: Main conclusions and further questions

This PhD-thesis contributes to the ongoing controversy about key questions concerning the exhumation of high-pressure rocks and basement in central Tibet during the evolution of the Tethys-realm. The key highlights of this study are to clarify different units in Qiangtang, central Tibet and propose plausible tectonic explanation of their spatiotemporal relationships. Transversely extending of our model in Qiangtang is one the most important aims to us in future. Additional work should focus on geodynamical process among the small Tibetan terranes of which geological analogues also exists today, such as in southeast Asia and the Mediterranean region. Below, the main conclusions concerning these points as well as open research questions are given.

7.1 The *mélange* in central Qiangtang clarified into several different units.

Detailed lithological and structural mapping in the South Qiangtang Terrane allowed the definition of three main units in the area: (1) the Paleozoic autochthonous basement of the Qiangtang Terrane, (2) the Mesozoic allochthonous unit with ophiolitic and sedimentary *mélange*. The ophiolitic *mélange* consists of gabbro, diabase, basalt and minor cherts, however the sedimentary *mélange* composed by marine sediments, high-pressure rafts and Permian limestone, (3) the overlying Mesozoic autochthonous of Jurassic to Cretaceous sediments.

Detrital zircons and dating of orthogneisses constrain the age of the basement between ~591 and 470 Ma. The basement is unconformably overlain by Ordovician slates with a basal conglomerate and Carboniferous sand- and siltstones. Similarity with the Lhasa and Himalaya areas suggest that the Paleozoic autochthonous basement was part of the northern margin of Gondwana during the Early Paleozoic.

The ophiolitic *mélange* consists of gabbro, diabase and basalt blocks and lenses, intercalated with deep-water siltstone, with minor chert, mudstone, sandstone and limestone. The mafic rocks have ocean-island or MORB affinities and range in age from the Ordovician to Triassic. Most of these mafic rocks preserved their original structures such as amygdules in basalt. The sedimentary *mélange* is highly variable and includes sandstone, siltstone, mudstone, cherts, thinly bedded limestone and minor mafic blocks. Competent lithologies are embedded as lenses in a strongly foliated matrix. Various sedimentary structures are preserved, such as Bouma sequences, graded bedding, load casts and flute marks. That means both the ophiolitic and sedimentary *mélange* was never buried to significant depths.

High-pressure rocks are found in association with the clastic sediments and Permian limestones in the sedimentary *mélange*. Main outcrops of high-pressure rocks are located in Jiaomu Ri and south of Gangtang Co. They consist of phengite-quartz schists, blueschists and eclogites. Peak metamorphic age is ~ 244 Ma and exhumation occurred around 220–214 Ma. Maximum temperature and pressure ranges are 410–460 °C and 2.0–2.5 GPa.

After closure of the Longmu Co-Shuanghu suture zone, Upper Triassic sedimentation commenced in the south in a foreland setting and progressively extended to the north where extensive bimodal volcanic activity occurred, which is interpreted as the result of mantle upwelling due to the final sinking of the paleo-Tethys oceanic slab. Jurassic marine sediments deposited both on north and south flanks of Qiangtang Culmination. Cretaceous to recent terrestrial sediments, mostly conglomerates, covers the area in scattered, usually fault-bounded basins.

7.2 Structural relationships of different units.

Boundaries between units could be determined in the field, as well as using ASTER satellite images. The high topography makes it possible to determine the orientation of contacts and map units by using the interaction between these and topography, which was done with Move™ by Midland Valley. This provides orientations on the map scale, which is preferable to using outcrop-scale observations and measurements, due to the often chaotic deformation on the small scale, and the potential overprinting of multiple deformation phases.

In the Rongma area, the main units form a stack of sheets with Precambrian to Carboniferous basement at the base, ophiolitic *mélange* in the middle and sedimentary *mélange* with large rafts of blueschists and non-metamorphic Permian sediments towards the top. Metamorphism in the Central Qiangtang Metamorphic Belt occurred in two unrelated stages. The first, lower greenschist facies event occurred in Pre-/Early-Ordovician times and affected the Precambrian basement. A second event produced the high-pressure rocks that exhumed in the Triassic as a result of the closure at the Longmu Co-Shuang Hu suture zone between the North and South Qiangtang terranes.

As a special case, the high-pressure rocks, as a kilometers scale rafts, are contained within the sedimentary *mélange*. Preservation of fossils and primary sedimentary microstructures show that the sedimentary *mélange* was not metamorphosed. However, the Permian limestones in contact with blueschists NE of Rongma trend towards strongly deformed marbles at that contact. The marbles contain assemblages of calcite + tremolitic amphibole ± epidote ± garnet ± quartz, which indicate elevated

temperatures (up to ~ 500 °C) but relatively low pressure. The garnet, however, appears to have grown post-tectonically, implying a syn- to post-tectonic thermal event.

7.3 Simplified tectonically evolution model of Qiangtang terrane.

The North and South Qiangtang terranes were formerly separated by an Ordovician-Triassic ocean. Opening of the Shuanghu–Tethys between the NQT and the SQT probably commenced in the (Late) Ordovician. The SQT formed the passive northern margin of Gondwana on which sediments were deposited at various stages from the Ordovician to the Permian.

Northward subduction of the Paleo-Tethys underneath the NQT commenced at ~ 275 Ma, as is indicated by arc activity in the NQT. The youngest known passive margin sediments (P_2l) were deposited on the SQT, but no known sedimentation occurred at the active southern margin of the NQT where arc volcanism occurred instead. With (minor) subduction to the south as well, the Shuanghu–Tethys plate would have formed a divergent double subduction zone with a long slab subducting to the north and a short one to the south.

Northward movement of the Shuanghu–Tethys plate, during convergence of the NQT and SQT, carried the mix of sedimentary mélangé and high-pressure rocks northward, towards and in the end on top of the accreted material at the northern suture, the ophiolitic mélangé. As the two terranes collided, all these rocks were thrust onto the SQT, producing the sheet stack as is now observed. Formation of the sheet stack by S- to SW-thrusting took place between about 220 and 210 Ma. It was postdated by intrusion of the undeformed, 210 Ma Gangtang Co granite and onset of Late Triassic foreland sediment deposition and volcanic activity. Coeval foreland basin developed in front of this thrust sheet.

Following the closure of Longmu Co–Shuanghu suture zone, the Bangong–Nujiang suture zone opened between the amalgamated Qiangtang terrane and the north Lhasa terrane. Jurassic shallow marine deposits unconformably overlie Late Triassic sediments and volcanics on the NQT. Jurassic the deep-water flysch sediments cover all the older units in the southern SQT. These are thought to represent the opening of the Bangong–Nujiang suture zone.

Thermochronology results illustrate that the Qiangtang Terrane experienced strong shorting during closure of the Bangong–Nujiang suture and concomitant collision between the Lhasa and Qiangtang terranes. During the Early Cretaceous, the large obducted mélangé sheet was shortened and restacked during this Lhasa-Qiangtang collision. During this shortening, the basement exhumed and ramped up and

over Cretaceous terrestrial conglomerate. Middle Cretaceous terrestrial conglomerate commenced at 90Ma which has not strongly deformed and indicated end of Qiangtang-Lhasa collision.

7.4 New efficient exhumation model of high-pressure rocks.

To explain the current structural relationships of different units, a new high-pressure rocks exhumation model, "subduction reversal" is proposed. The northward-subducting longer oceanic slab pulled a short, south-dipping slab from underneath the South Qiangtang terrane and brought this in contact with the sedimentary mélangé and Permian margin sediments. The proposed slab extraction model provides a very efficient mechanism for the rapid exhumation of UHP rocks. It can explain several features typical for UHP rocks, such as initially rapid exhumation, followed by slower exhumation rate, extension during exhumation, close association of UHP rocks with upper-plate rocks. However, this does not imply that other proposed models are invalidated.

7.5 Open questions and further research aims.

1) The mapping only focused on central Qiangtang. Are the results still applicable to the whole EW extent of the Qiangtang terrane(s)? Are any other regions comparable with Qiangtang and can the results be applied there? The main geodynamical principles that control small terrane evolution remain enigmatic. 2) What was the shortening mechanism, thin- or thick-skinned, during Lhasa-Qiangtang collision? This spectacular issue influences understanding pre-Cenozoic evolution of the Tibetan Plateau. 3) Exhumation of high-pressure rocks is another hotly debated issue for decades. How and where could the 'slab reverse' model be applied or further developed?

Appendix

Appendix A: Original paper (in Chinese) for Chapter 3

Chapter 3 is translated from Chinese version which is also available on online.

http://www.ysxb.ac.cn/ysxb/ch/reader/create_pdf.aspx?file_no=20140819&year_id=2014&quarter_id=8&falg=1

藏北羌塘奥陶纪平行不整合面的厘定及其构造意义^{*}

杨耀^{1,2} 赵中宝^{3,4} 苑婷媛^{2,3} 刘焰^{2**} 李聪颖⁵

YANG Yao^{1, 2}, ZHAO ZhongBao^{3, 4}, YUAN TingYuan^{2, 3}, LIU Yan^{2**} and LI CongYing⁵

1. 成都理工大学地球科学学院, 成都 610059

2. 大陆构造与动力学国家重点实验室, 中国地质科学院地质研究所, 北京 100037

3. 中国地质大学, 北京 100083

4. Department of Geosciences, Eberhard Karls University Tübingen, Tübingen D-72074

5. 中国科学院广州地球化学研究所, 广州 510640

1. College of Earth Sciences, Chengdu University of Technology, Chengdu 610059, China

2. State Key Laboratory of Continental Tectonics and Dynamics, Institute of Geology, Chinese Academy of Geological Sciences, Beijing 100037, China

3. China University of Geosciences, Beijing 100083, China

4. Department of Geosciences, Eberhard Karls University Tübingen, Tübingen D-72074, Germany

5. Guangzhou Institute of Geochemistry, Chinese Academy of Sciences, Guangzhou 510604, China

2014-02-10 收稿, 2014-05-14 改回.

Yang Y, Zhao ZB, Yuan TY, Liu Y and Li CY. 2014. Ordovician parallel unconformity in Qiangtang terrane, northern Tibet: Implications to Early Paleozoic evolution of northern Tibetan regions. *Acta Petrologica Sinica*, 30(8):2381–2392

Abstract Several issues have been disputed for a long time in Qiangtang terrane, northern Tibet, such as whether it has the metamorphic basement, as well as the pre-Cenozoic tectonic history. Here we report the Tashishan Formation, which is located in the northern portion of southern Qiangtang terrane, of Middle and Late Ordovician is parallel unconformity on thick-bedded fossil-free low-grade metamorphic quartz sandstones which has been interbedded by thin layer of marl. Nearly 600 detrital zircons dating results indicate that the maximum sedimentary age of the low-grade metamorphic quartz-sandstone is 527 ± 7 Ma. And more than 300 detrital zircons dating results indicate that the maximum sedimentary age of quartz sandstone at the bottom of Tashishan Formation is 471 ± 6 Ma. The sedimentary age gap between the quartz sandstones above the unconformity and the underlying low-grade metamorphic quartz sandstones is up to 56 Myr, indicative of an obvious depositional hiatus between the two quartz sandstones. This further confirms that the unconformity between the two quartz sandstones is Early Ordovician. An independent piece of evidence is that the fossil-free low-grade quartz sandstones were intruded by Early Ordovician granitoids ($471 \sim 477$ Ma). The sedimentary rock underlying the unconformity is, therefore, named as Rongma Formation and classified in Late Cambrian era in this study. Cathodoluminescence images and geochronological studies indicate that detrital zircons of the quartz sandstones above the unconformity were mainly from crystalline rocks which formed in the late period of the Pan-African event and close to their provenance. This implies that the Late Pan-African crystalline rocks had exhumed in Early Ordovician, and then, underwent denudation, providing material sources for the Middle and Late Ordovician sedimentary rocks. The discovery of the parallel unconformity of Ordovician reflects that the south Qiangtang terrane is one portion of the Gondwana supercontinent, as Himalayan and Lhasa terranes. The distinctive difference in Paleozoic strata between South Qiangtang and North Qiangtang terranes shows that there is an ancient ocean basin between the two terranes in the Early Ordovician at least, and the two terranes evolved independently.

Key words Detrital zircon; Ordovician parallel unconformity; Pan-African event; South Qiangtang, northern Tibet; Gondwana supercontinent

* 本文受中国地质调查局青藏专项项目(1212011121271)资助.

第一作者简介: 杨耀, 男, 1988 年生, 硕士生, 地质学专业, E-mail: yangyao_cdut@163.com

** 通讯作者: 刘焰, 男, 1969 年生, 研究员, 岩石学和构造地质学专业, E-mail: yanliu0315@126.com

摘要 西藏羌塘块体有无变质基底、其前新生代构造属性与演化过程是长期争论的议题。本文报道南羌塘块体北部、中、上奥陶统塔石山组底砾岩平行不整合于浅变质中厚层石英砂岩夹薄层泥灰岩之上。近 600 粒碎屑锆石测年结果表明浅变质石英砂岩的最大沉积年龄为 $527 \pm 7\text{Ma}$, 300 余粒碎屑锆石测年结果表明塔石山组底部石英砂岩的最大沉积年龄为 $471 \pm 6\text{Ma}$ 。不整合面上、下石英砂岩最大沉积年龄之差达 56Myr, 表明这两套石英砂岩之间存在明显的沉积间断, 证实了该平行不整合面的时代为奥陶纪早期。另一独立的证据是在邻区发现了早奥陶世花岗岩类岩石 ($471 \sim 477\text{Ma}$) 侵位于该浅变质石英岩, 因此将不整合面之下的浅变质石英岩暂命名为荣玛组, 归入寒武系地层。阴极发光与年代学研究进一步表明不整合面之上的碎屑锆石主要来源于在“泛非”运动晚期形成的结晶岩, 为近源锆石, 表明“泛非运动”晚期所形成的结晶岩在奥陶纪早期就已隆升, 遭受剥蚀, 为区内中上奥陶统沉积岩的形成提供物质来源。该奥陶纪平行不整合面的发现, 表明南羌塘块体与喜马拉雅、拉萨等块体相似, 同属冈瓦纳大陆体系。南、北羌塘早古生代地层系统之间的显著差异表明在寒武-奥陶纪之交, 南、北羌塘块体就被古大洋盆分隔开, 开始各自独立演化。

关键词 碎屑锆石; 奥陶纪不整合面; 泛非运动; 藏北南羌塘; 冈瓦纳大陆

中图法分类号 P534.42; P597.3

1 引言

在藏北羌塘中部, 有一近东西向延长达 500km 的山脉产出, 被称为羌中隆起 (吴瑞忠等, 1986), 大体将羌塘一分为二, 这就是南、北羌塘的由来 (图 1)。长期以来, 对羌中隆起的构造属性及其演化过程的认识截然不同, 争论不休。吴瑞忠等 (1986) 最早将出露于羌中隆起一带的变质杂岩称为阿木岗群, 由下至上, 再细分为片麻岩段、石英岩段、绿片岩段和硅质岩段, 认为这些变质杂岩构成了羌塘盆地前泥盆纪变质基底。黄继钧 (2001) 进一步阐述了羌塘盆地具有双层结构, 即“结晶硬基底”和“变质软基底”。王国芝和王成善 (2001) 对羌塘基底变质岩系进行了解体, 认为果干加年日 (山) 群年龄为 1111Ma, 戈木日群大于 1111Ma, 戈木日群和果干加年日 (山) 群均属于元古宙变质基底。李日俊等 (1997) 则认为该套变质岩是晚三叠世的构造混杂岩, 不能作为羌塘地块的变质基底, 这一观点得到了李才 (2003) 的支持。与此变质岩带相伴, 还常有基性-超基性岩块产出, 最近在吴瑞忠等 (1986) 称为绿片岩相变质杂岩带中发现了以低温榴辉岩、石榴石蓝闪石片岩为代表的低温高压变质杂岩 (李才等, 2006; Kapp *et al.*, 2000, 2003; Zhang *et al.*, 2006; Liu *et al.*, 2011), 并且羌中隆起两侧的沉积地层、古生物面貌差异较大, 因此许多学者认为该隆起应代表了一重要的古板块边界 (李才等, 1987; Zhang *et al.*, 2001): 北羌塘地块属欧亚陆块, 南羌塘地块则亲冈瓦纳大陆, 龙木错-双湖缝合带代表了冈瓦纳大陆之北界。但这一观点争议颇大, 例如 Yin and Harrison (2000)、Kapp *et al.* (2000, 2003) 等认为该区的变质杂岩系从北侧 200km 之外的金沙江缝合带低角度南向俯冲所形成的高压变质杂岩, 然后从羌塘中部拆离剥露出来, 南、北羌塘属同一构造单元, 羌中隆起则类似弧后盆地。最近, Pullen *et al.* (2008) 修正了该模型, 不再强调长距离低角度俯冲, 转而提出了该变质杂岩系岛弧岩石南向俯冲于南侧羌塘地块之下的观点, 但依然强调该变质杂岩系从弧后盆地处, 羌塘地块中部拆离剥露、仍然坚持南、北羌塘同

属一构造单元等观点, 认为金沙江缝合带才是冈瓦纳大陆之北界 (Gehrels *et al.*, 2011; Pullen *et al.*, 2011)。潘桂棠等学者则认为羌中隆起混杂岩具有典型的蛇绿构造混杂岩特征, 是青藏高原内部规模最大、最壮观的古洋壳遗迹, 南羌塘不是独立地块, 而是一巨型增生杂岩带, 其北侧的龙木错-双湖-澜沧江带与其南侧的班公湖-怒江缝合带同属一巨型缝合带的不同分支, 共同代表了冈瓦纳大陆的北界 (潘桂棠等, 2012; Pan *et al.*, 2012)。本文报道南羌塘块体北缘的奥陶纪平行不整合面, 确定该不整合面下伏的浅变质石英砂岩为寒武纪沉积岩, 暂命名为荣玛组, 试图为丰富当前研究程度较低的羌塘地块的认识提供新的科学依据。

2 区域地质背景

研究区位于藏北高原尼玛县荣玛乡 (图 1)。区内广泛出露增生杂岩、荣玛组浅变质石英砂岩、中、上奥陶统塔石山组石英砂岩和泥灰岩、晚古生代粉砂岩、新近纪康托组紫红色磨拉石等岩石单元 (图 1)。印支期花岗斑岩侵位于荣玛组浅变质石英砂岩之中 (Zhao *et al.*, 2014)。增生杂岩为一套完全无序的构造混杂岩, 可根据岩相, 将增生杂岩进一步细分为: 镁铁质、超镁铁质岩石, 如枕状熔岩、辉长岩、蛇纹岩等岩石、印支期的高压低温变质杂岩, 如石榴蓝片岩、蓝片岩 (李才等, 2006; Pullen *et al.*, 2008; Liu *et al.*, 2011)、绿片岩相变质杂岩, 如深灰色细粒二云母石英片岩、绿泥石二云母石英片岩、硅质岩、大理岩等岩石类型。空间上绿片岩相变质杂岩分布较广, 吴瑞忠等 (1986) 称其为阿木岗群中的绿片岩段。这套绿片岩相变质岩韧性变形强烈, 常发育紧闭褶皱、无根褶皱等, 与荣玛组浅变质石英砂岩、奥陶系塔石山组岩石构造并置在一起 (图 2、图 3)。荣玛组是本文暂命名的岩石地层单元, 以中、厚层状浅变质石英砂岩为主, 其中夹有薄层泥灰岩, 顶部与中、晚奥陶统塔石山组直接接触 (图 2、图 4)。这套浅变质石英砂岩空间上出露广泛, 东起双湖, 西至改则北部的鲁谷地区, 在东西长达近 500km、南北宽约 50km 范围内均有出露。吴瑞忠等 (1986) 称其为阿木岗群的

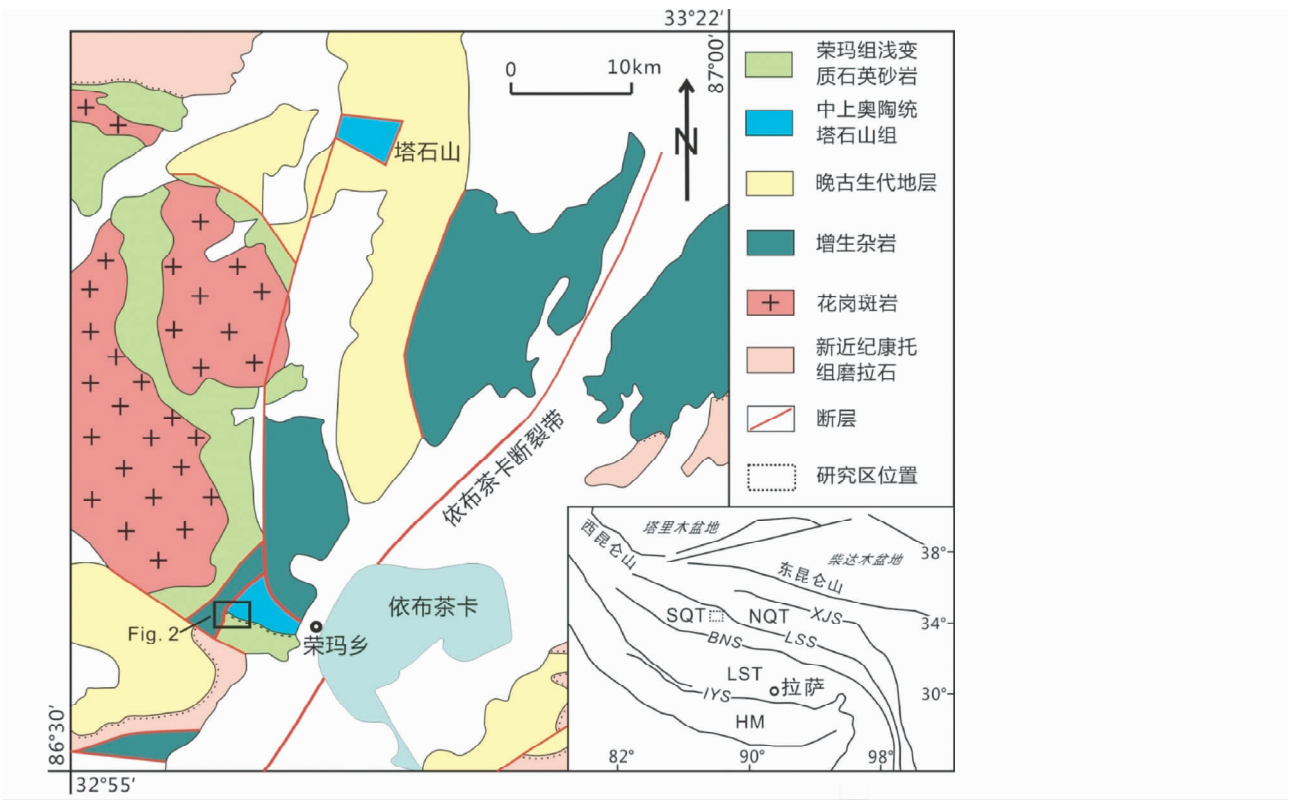


图 1 藏北羌塘荣玛地质简图,右下角插图示意研究区的大地构造位置(据 Liu *et al.* , 2011; Zhao *et al.* , 2014 修改)
LST-拉萨地体;SQT-南羌塘地体;NQT-北羌塘地体;HM-喜马拉雅地体;IYS-雅鲁藏布江缝合带;BNS-班公湖-怒江缝合带;LSS-龙木错-双湖缝合带;XJS-西金乌兰-金沙江缝合带

Fig.1 Simplified geological map of Rongma, northern Tibet (modified after Liu *et al.* , 2011; Zhao *et al.* , 2014)

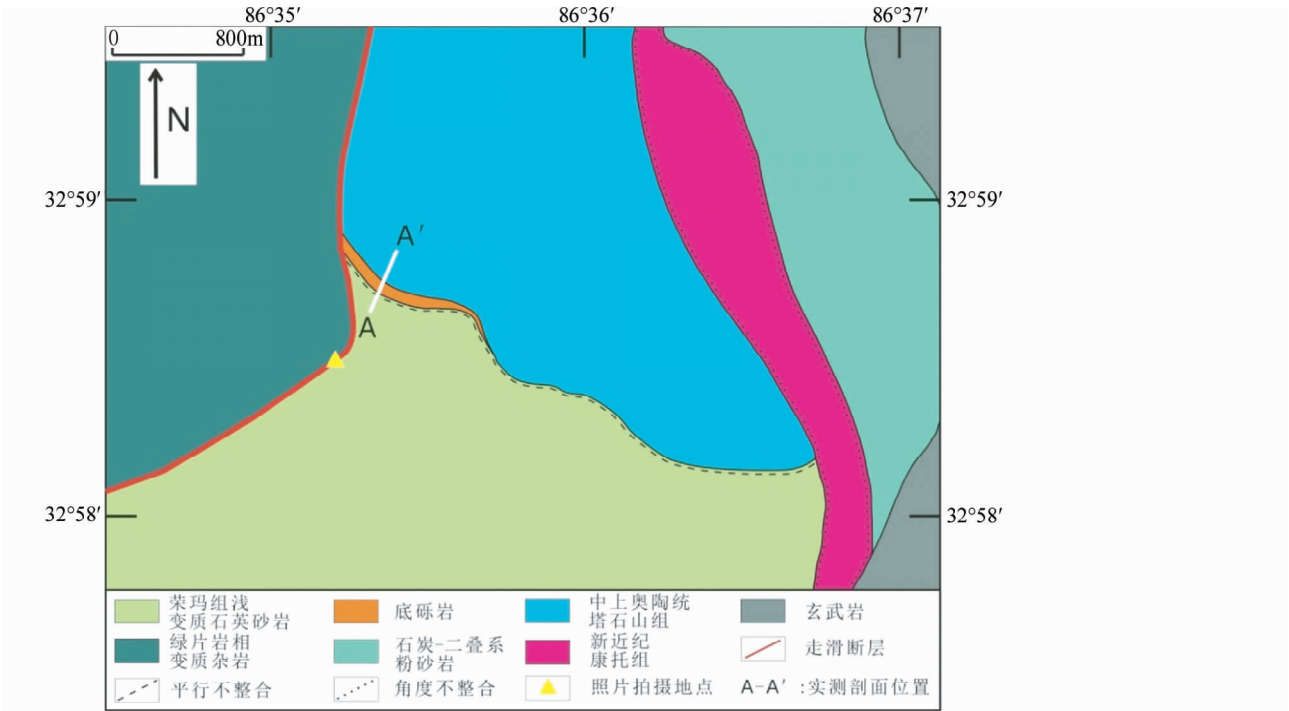


图 2 藏北南羌塘荣玛乡温泉地质简图(位置详见图 1)

Fig.2 Geological sketch map of Rongma area, northern Tibet (location sees Fig. 1)



图3 绿片岩相变质杂岩与浅变质石英砂岩构造并置关系

图中红线代表走滑断层接触面,红色圆圈指示走滑方向,拍摄地点位于图2中黄色三角形处

Fig. 3 Structure juxtaposed relationship between greenschist facies metamorphic rocks (left) and Rongma low-grade metamorphic quartz sandstones (right)

石英岩段。在本研究区内(图2),荣玛组的浅变质石英砂岩常呈中、厚层状产出,岩石变形较强,但依然可根据其中所夹薄层泥灰岩,恢复其原始层理。塔石山组是吉林大学地质调查研究院(2005)在1:25万区域地质调查期间新建立的一个岩石地层单元,建组地点为塔石山(图1)。在塔石山一带,塔石山组出露面积约20km²,呈断块产出于晚古生代地

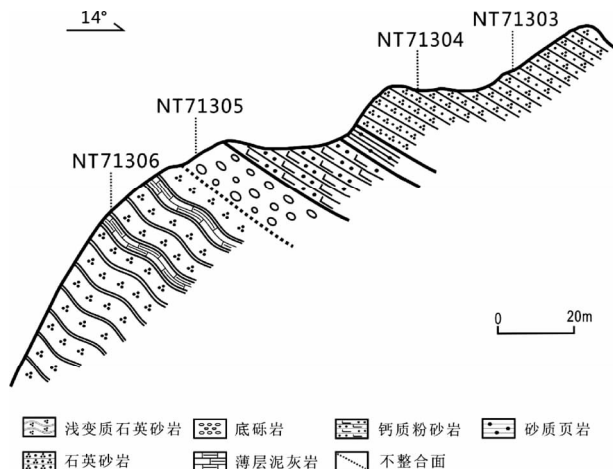


图4 藏北南羌塘荣玛乡奥陶纪不整合面地质剖面图

NT71306-荣玛组浅变质石英砂岩; NT71305-塔石山组底砾岩, NT71304、NT71303-塔石山组下部石英砂岩

Fig. 4 Geological cross-section of Ordovician unconformity in Rongma area, northern Tibet

层中(图1)。因为断层发育,未见该组底部。该组中上部的泥灰岩、碳酸盐岩地层中常含有鹦鹉螺类角石化石,因此被归入中、晚奥陶世地层(吉林大学地质调查研究院,2005)。在荣玛乡附近(图1、图2),塔石山组地层出露更佳,底部为角砾岩层,厚约20m。底砾岩之上为钙质粉砂岩,整合接触(图5)。钙质粉砂岩之上多为石英粉砂岩、细砂岩夹薄层泥



图5 藏北南羌塘荣玛乡寒武-奥陶纪地层宏观照片

(a)-塔石山组底砾岩与上覆石英砂岩整合接触;(b)-中、上奥陶统含角石化石的泥灰岩;(c)-塔石山组底砾岩与下伏荣玛组浅变质石英砂岩平行不整合接触,红线指示接触面;(d)-塔石山组底砾岩宏观照片,以下伏浅变质石英砂岩角砾为主

Fig. 5 Photos of Cambrian-Ordovician strata in Rongma area, northern Tibet

灰岩,向上,泥灰岩、碳酸盐岩、钙质粉砂岩逐渐增多,而石英砂岩含量则下降。在该地区的塔石山组中、上部的泥灰岩、碳酸盐岩中同样可见鸚鵡螺类角石化石(图5)。虽然塔石山组的沉积岩变形也较强,灰岩中的角石化石发生了明显的塑性流变,横截面发育典型的S-C组构,岩石层理常被 S_1 替代,但还是可以根据石英砂岩中的泥灰岩夹层恢复原始层理。根据原始层理面判断,上部的塔石山组与下伏荣玛组之间的地层产状是平行的(图5)。研究区内未见石炭-二叠系沉积岩与奥陶系地层直接接触,从笔者所填地质图的图面关系推测为断层接触(图2),新近纪康托组则大角度不整合于奥陶系和石炭-二叠系粉砂岩之上(图2)。

3 不整合面地质特征

该不整合位于尼玛县荣玛乡之西约3km(图1、图2),其剖面岩性特征从上到下依次为(图4):

不整合面上覆塔石山组地层:上部为中层状石英粉砂岩、细砂岩夹薄层泥灰岩和页岩,厚度大于50m,倾角在 $10^{\circ} \sim 20^{\circ}$ 之间。石英砂岩主要由石英组成,有少量白云母、自形-半自形锆石和电气石等矿物,颗粒粒径一般为0.1~0.2mm(图6)。下部为一套灰白色钙质粉砂岩夹灰白色砂质页岩、泥灰岩,厚约30m,底部与底砾岩整合接触。目前未能在塔石山组下部岩层中发现可辨识的化石。

底砾岩:底砾岩厚度约为20m,砾石成分单一,以不整合面下伏的石英岩角砾为主,如灰白色中、粗粒浅变质石英砂岩(图5d),有少量白色石英脉。砾石多呈椭圆状-次棱角状产出,具有一定的磨圆度,分选性较好。直径一般为3~12cm,较大的砾石可超过20cm(图5d)。该砾石层序清楚(图5c),由下往上砾石的粒径逐渐变小,胶结物多为碳酸盐矿物(图5d、图6b)。砾石层理面平行上、下沉积岩的原始层理面(图5a),据此判断为沉积角砾岩,不是断层角砾岩。

不整合面之下伏荣玛组地层:以灰白色,灰黄色浅变质石英砂岩为主,上与塔石山组之底砾岩接触(图2、图4和图5),下未见底。未能在此套石英砂岩找到可辨识的化石。显微镜下,浅变质石英砂岩为近等粒结构,块状构造,碎屑物主要包括石英、长石和少量的云母(图6c)。其中石英含量占75%左右,粒度在0.05~0.5mm。在正交偏光下,常见石英颗粒具有波状消光特征,反映石英颗粒变形较强。长石含量介于5%~10%之间,包括斜长石和微斜长石(图6c)。其中,斜长石粒度约为0.1mm,微斜长石粒度大约为0.25mm,由此推测其为近源沉积岩。胶结物以泥质为主,次为碳酸盐。泥质胶结物多变质成细粒的绢云母、绿泥石等矿物。副矿物可见自形-半自形锆石(图6c)。

4 分析方法

本次分析样品共4件,分别为不整合面下伏荣玛组浅变

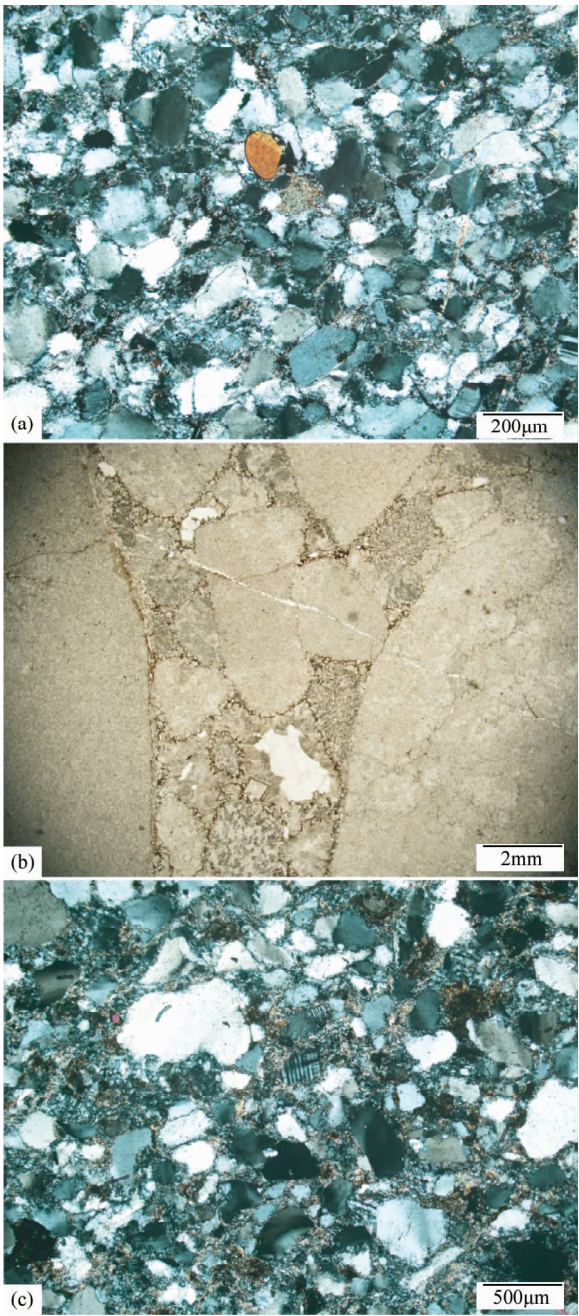


图6 藏北南羌塘荣玛乡奥陶纪不整合面上下岩石显微照片

(a)-不整合面上覆塔石山组石英砂岩显微照片(正交偏光);(b)-塔石山组底砾岩显微照片(单偏光);(c)-不整合面下伏荣玛组浅变质石英砂岩显微照片(正交偏光),基质已部分变质为绢云母和绿泥石

Fig. 6 Photomicrographs of rocks above and beneath the unconformity in Rongma area, northern Tibet, respectively

质石英砂岩(NT71306),不整合面之上塔石山组底砾岩(NT71305)和石英砂岩(NT71303、NT71304)(图4),样品坐标为 $32^{\circ}58'40''N, 86^{\circ}35'20''E$ 。锆石的分选工作在国土资源部河北省地质矿产局廊坊实验室完成,样品粉碎后经常规浮

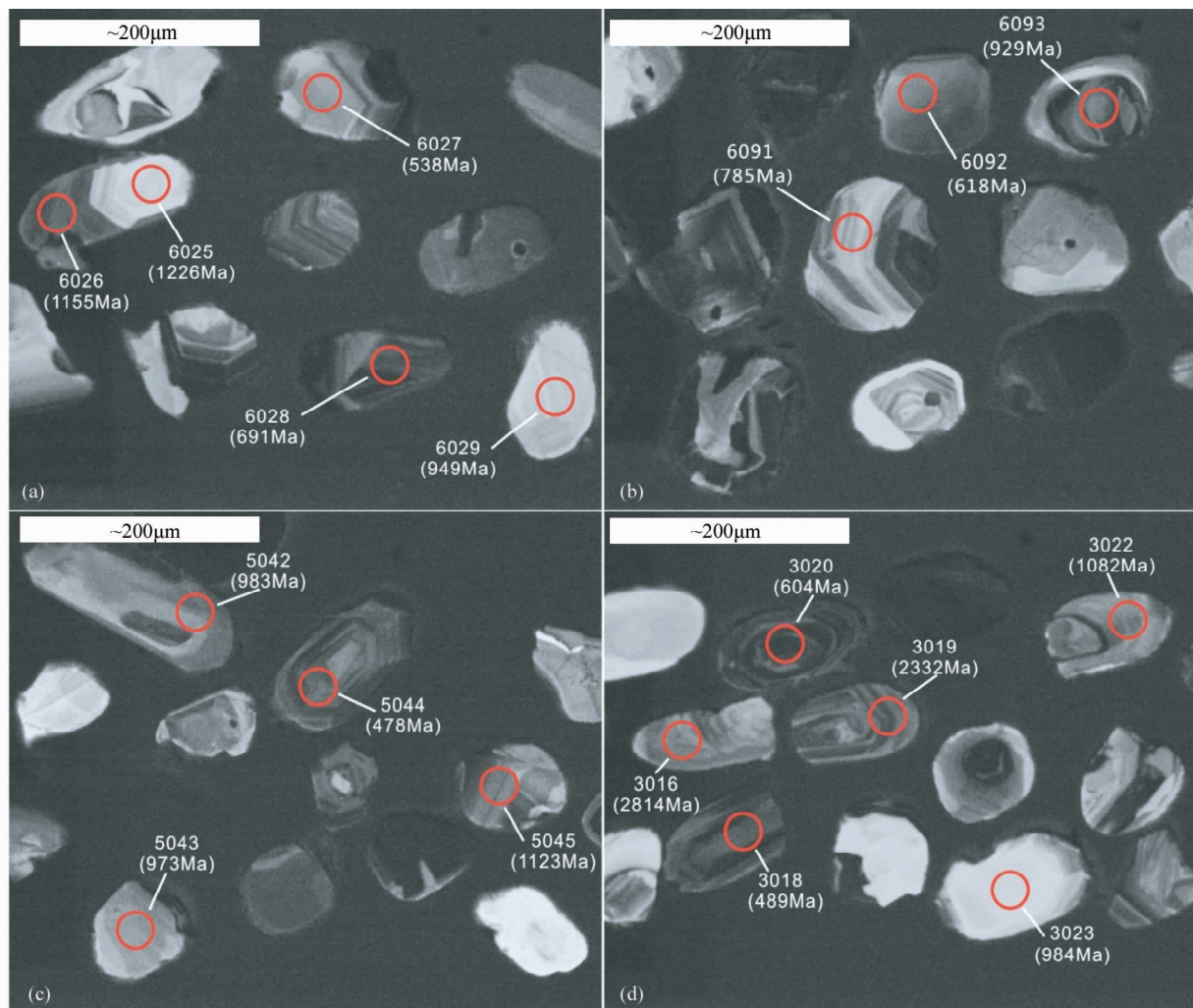


图7 藏北荣玛乡奥陶纪不整合面上、下碎屑岩中碎屑锆石阴极发光图

(a,b)-荣玛组浅变质石英砂岩碎屑锆石阴极发光图;(c,d)-塔石山组石英砂岩碎屑锆石阴极发光图。锆石普遍具有振荡环带,部分锆石存在变质增生边,少数锆石具有明显的磨圆。红色圆圈指示锆石测年位置,括号外和内的数字分别为数据点编号与 $^{206}\text{Pb}/^{238}\text{U}$ 年龄值

Fig. 7 Cathodoluminescence images of detrital zircons from the rocks under and above the unconformity in Rongma area, northern Tibet, respectively

选、磁选和重液分选后分离出锆石。在双目镜下挑选出形态较为完整,没有明显裂痕和包裹体的锆石,制备锆石微区定年样品靶。在开始锆石 U-Pb 测试之前,先开展锆石反射光和阴极发光 (CL) 分析工作,查明锆石样品的内部结构、确定待测年锆石的类型和测年位置。

在中国地质科学院矿产资源研究所,采用配备 OXFORD MiniCL 阴极发光谱仪的 JXA-8800R 电子探针完成锆石阴极发光照相。在广州地球化学研究所同位素地球化学国家重点实验室,使用 Resonetics 公司生产的 RESolution M-50 激光剥蚀系统和 Agilent 7500a 型的 ICP-MS 联机期,完成 LA-ICP-MS 锆石 U-Pb 及微量元素分析。用美国国家标准计算研究院人工合成硅酸盐玻璃标准参考物质 NIST610 进行仪器校正,使仪器达到最佳的灵敏度、最小的氧化物产率 ($\text{CeO}/\text{Ce} < 3\%$) 和最低的背景值。标样为 TEMORA 锆石,激光剥蚀

直径约为 $33\mu\text{m}$, 频率 8Hz。具体分析过程详见涂湘林等 (2011)。采用 ICPMSDataCal (Liu *et al.*, 2008) 完成测试数据的离线处理(包括对样品和空白信号的选择、仪器灵敏度漂移校正、元素含量及 U-Th-Pb 同位素比值和年龄计算)。采用 Isoplot (Ver3.0) (Ludwig *et al.*, 2003) 完成锆石年龄谱和图和频率图的制作。分析数据详见电子版附表 1。

5 锆石测年结果

不整合面下伏荣玛组浅变质石英砂岩中的锆石多呈长轴状,次为近等轴状和椭圆状,粒度大小通常在 $80 \sim 180\mu\text{m}$ 。在阴极发光图像中,大多数锆石具有振荡环带(图 7a, b),晶型保存完整,反映它们应为岩浆锆石。少数锆石存在暗色的

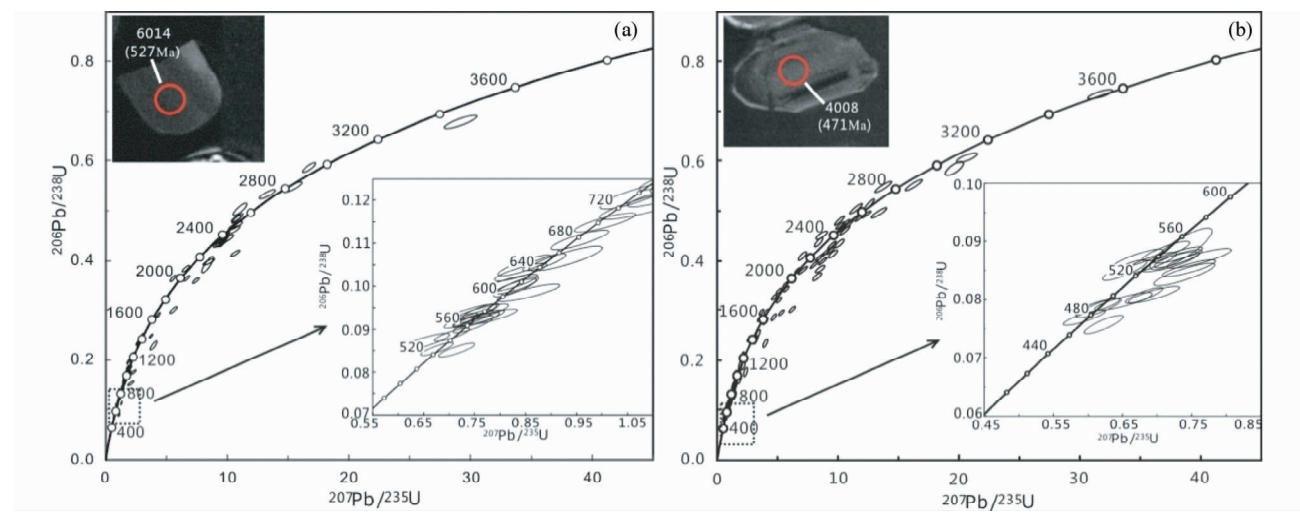


图 8 藏北南羌塘荣玛乡奥陶纪不整合面上、下碎屑岩中的碎屑锆石 U-Pb 谐和图
Fig. 8 Detrital zircon concordia diagrams for clastic rocks under and above the unconformity in Rongma area, northern Tibet, respectively

变质增生边(图 7a)。本次工作对该浅变质石英砂岩样品(NT71306)的 123 颗锆石进行了 128 个数据点分析,其中有 5 粒大颗粒锆石分别测试了核部与暗色边部。分析结果表明这些锆石的 Th、U 含量和 Th/U 比值变化极大,分别为 $0.6 \times 10^{-6} \sim 674.7 \times 10^{-6}$, $23.9 \times 10^{-6} \sim 856.8 \times 10^{-6}$ 和 $0.01 \sim 2.42$,但 Th/U 比值普遍大于 0.1(附表 1)。浅变质石英砂岩中的碎屑锆石年龄分布范围为 527 ~ 3340Ma(图 8a)。最年轻的碎屑锆石年龄为 527 ± 7 Ma(图 8a),谐和度为 96%,最老年龄为 3340 ± 33 Ma,其谐和度为 96%。

不整合面上覆塔石山组石英砂岩、底砾岩中的锆石多呈等柱状和长柱状,少部分呈椭圆状,粒径大小变化悬殊,为 60 ~ 200 μ m。阴极发光图像同样显示大多数锆石具有振荡环带(图 7c, d)。部分锆石同样具有暗色变质增生边,少数锆石颗粒内部相对较亮,且无振荡环带(图 7d)。对此 3 个样品(NT71303、NT71304、NT71305)的 302 颗锆石进行了 311 个数据点分析,其中有 9 粒大颗粒锆石分别分析了核部与边部暗色增生边。结果表明这些锆石的 Th、U 含量和 Th/U 比值变化也比较大,分别为 $1.2 \times 10^{-6} \sim 281.5 \times 10^{-6}$, $28.0 \times 10^{-6} \sim 1391.7 \times 10^{-6}$ 和 $0.01 \sim 3.32$,Th/U 比值普遍大于 0.1(附表 1)。塔石山组沉积岩碎屑锆石年龄分布范围为 471 ~ 3552Ma(图 8b),最年轻的碎屑锆石年龄为 471 ± 6 Ma,谐和度为 95%;最老年龄为 3552 ± 26 Ma,谐和度为 99%。与荣玛组浅变质石英砂岩碎屑锆石相比,最大的不同是:塔石岩组底砾岩、下部的石英砂岩中均出现了年龄为 470 ~ 480Ma 的锆石颗粒群(图 8b),阴极发光进一步表明年龄为 470 ~ 480Ma 的锆石主要来源于结晶岩,其它年龄段的碎屑锆石则非常相似(图 7c, d)。

(图 2)附近的浅变质石英砂岩开展了碎屑锆石年代学研究工作。本文结果与前人结果高度相似,进一步表明本文工作区与邻区的荣玛组浅变质石英砂岩中碎屑锆石来源一致,因此本文结合 Pullen *et al.* (2008) 的 323 个数据点和董春艳等(2011)的 145 个数据点,重新计算近 600 个数据点的年龄分布频率图,从而获得荣玛乡浅变质石英砂岩碎屑锆石年龄频率分布图(图 9),该图清楚地显示了碎屑锆石存在 525 ~

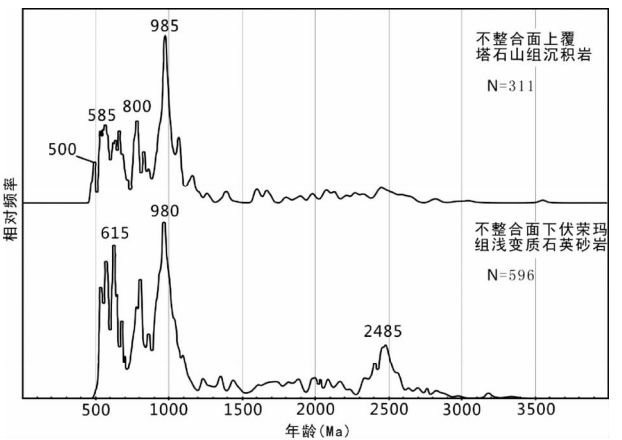


图 9 藏北南羌塘荣玛乡奥陶纪不整合面上、下碎屑岩中的碎屑锆石年龄频率图
不整合面下伏浅变质石英砂岩碎屑锆石年龄频率图,由本文实测 128 个数据、Pullen *et al.* (2008) 323 个数据和董春艳等(2011)145 个数据组成;不整合面上覆石英砂岩碎屑锆石年龄频率图,本文实测数据. 当年龄 ≤ 1200 Ma 时,采用 $^{206}\text{Pb}/^{238}\text{U}$ 年龄,反之采用 $^{207}\text{Pb}/^{206}\text{Pb}$ 年龄
Fig. 9 Detrital zircon age frequency diagram for clastic rocks under and above the unconformity in Rongma area, northern Tibet, respectively

6 讨论

Pullen *et al.* (2008) 和董春艳等(2011)曾对本文研究区

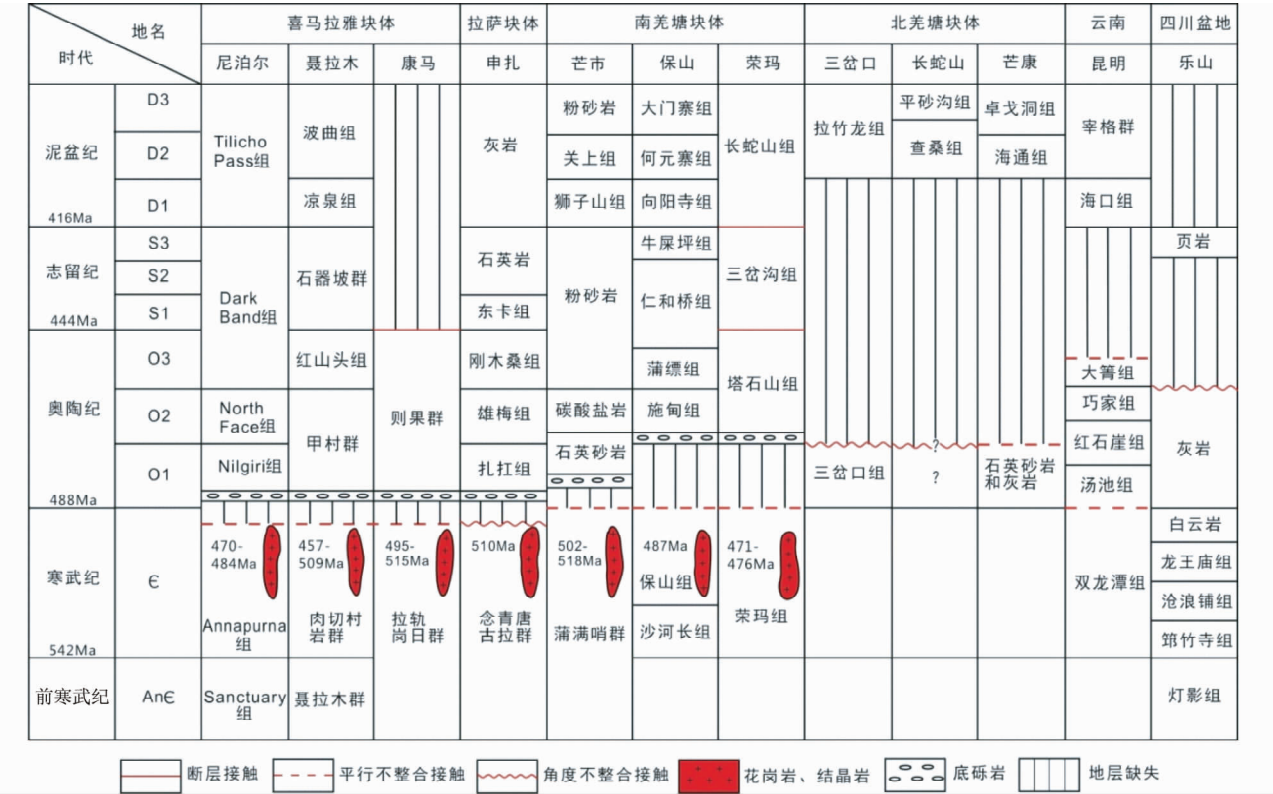


图 10 青藏高原及东部邻区早古生代地层对比

尼泊尔地层据 Gehrels *et al.*, 2003, 2011; 花岗岩年龄据 Schärer and Allègre, 1983; Johnson *et al.*, 2001. 聂拉木地层据朱同兴等, 2003; 中国科学院青藏高原综合科学考察队, 1984; 结晶岩年龄据许志琴等, 2005; Liu *et al.*, 2007a. 康马地层据周志广等, 2004; 花岗岩年龄据许志琴等, 2005; Lee *et al.*, 2000. 申扎地层据中国科学院青藏高原综合科学考察队, 1984; 计文化等, 2009; 结晶岩年龄据 Gehrels *et al.*, 2011; 计文化等, 2009. 芒市据蔡志慧等, 2013. 保山地层据黄勇等, 2012; 谭雪春等, 1982; 花岗岩年龄据宋述光等, 2007. 荣玛地层据吉林大学地质调查研究院, 2005 和本文; 花岗岩年龄据 Pullen *et al.*, 2011; 胡培远等, 2010. 三岔口地层据夏军等, 2006. 长蛇山地区地层据吉林大学地质调查研究院, 2005 和本文. 芒康地区地层据中国科学院青藏高原综合科学考察队, 1984. 昆明地区地层据方润森等, 2000; 张举等, 2013. 乐山地区地层据许海龙等, 2012. 各区地理位置详见图 11

Fig. 10 Stratigraphic correlation in Tibetan regions

700Ma, 885 ~ 1100Ma, 2350 ~ 2580Ma 三个年龄范围, 其中 615Ma, 980Ma 和 2485Ma 的年龄峰值最为明显(图 9)。不整合面之上, 300 余粒塔石山组石英砂岩中的碎屑锆石则存在 470 ~ 520Ma, 580 ~ 800Ma, 950 ~ 1100Ma 三个年龄变化范围, 其中 500Ma, 585Ma, 800Ma 和 985Ma 的年龄峰值显著(图 9)。不整合面上、下石英砂岩碎屑锆石频率分布样式差异比较大, 主要差别表现为下伏岩石的碎屑锆石没有出现年龄小于 525Ma 的锆石, 且年龄频率图在小于 620Ma 区间的样式完全不同, 充分反映了这两套沉积砂岩形成时间不同, 存在沉积间断。在阴极发光图像(图 7)中, 虽有少数锆石有一定程度的磨圆, 但大多数锆石为自形半自形, 具有典型的岩浆振荡环带, 表明锆石主要来源于结晶岩的物源区, 并且搬运距离不远(图 7)。需要指出的是, 从阴极发光图像与测年结果看, 不整合面上覆塔石山组石英砂岩中的碎屑锆石与 Pullen *et al.* (2011)、胡培远等(2010)报道的结晶岩中的锆石非常相似, 他们所报道的结晶岩分别位于本文研究区西侧 100km

和西北侧约 50km(图 11), 这反映了塔石山组石英砂岩中的碎屑锆石很可能来自周边“泛非”晚期的结晶岩, 同时还表明“泛非运动”晚期所形成的结晶杂岩在奥陶纪时已折返至地表之上, 遭受风化和剥蚀, 为区内中、上奥陶统石英砂岩等沉积岩的形成提供物质来源, 因此推测在这个时期存在一个古隆起或山脉, 类似现今的羌中隆起。

前已指出, 由于荣玛组浅变质石英砂岩中没有发现化石, 长期以来对其形成时代争议较大(李才, 2003), 这导致了人们对南羌塘块体构造属性的认识尚不清晰明了, 因此本文试图探讨荣玛组浅变质石英砂岩的形成时代。本文与前人的近 600 粒碎屑锆石测年结果表明荣玛组浅变质石英砂岩的最大沉积年龄为 $527 \pm 7\text{Ma}$ 。不整合面之上石英砂岩的最大沉积年龄为 $471 \pm 6\text{Ma}$ 。因此, 荣玛组浅变质石英砂岩的形成时代应介于 $527 \pm 7\text{Ma}$ 与 $471 \pm 6\text{Ma}$ 之间。另一独立的证据是: 据笔者实地调查, Pullen *et al.* (2011)报道的锆石 U-Pb 年龄介于 471 ~ 476Ma 的正片麻岩, 实质是韧性变形较强

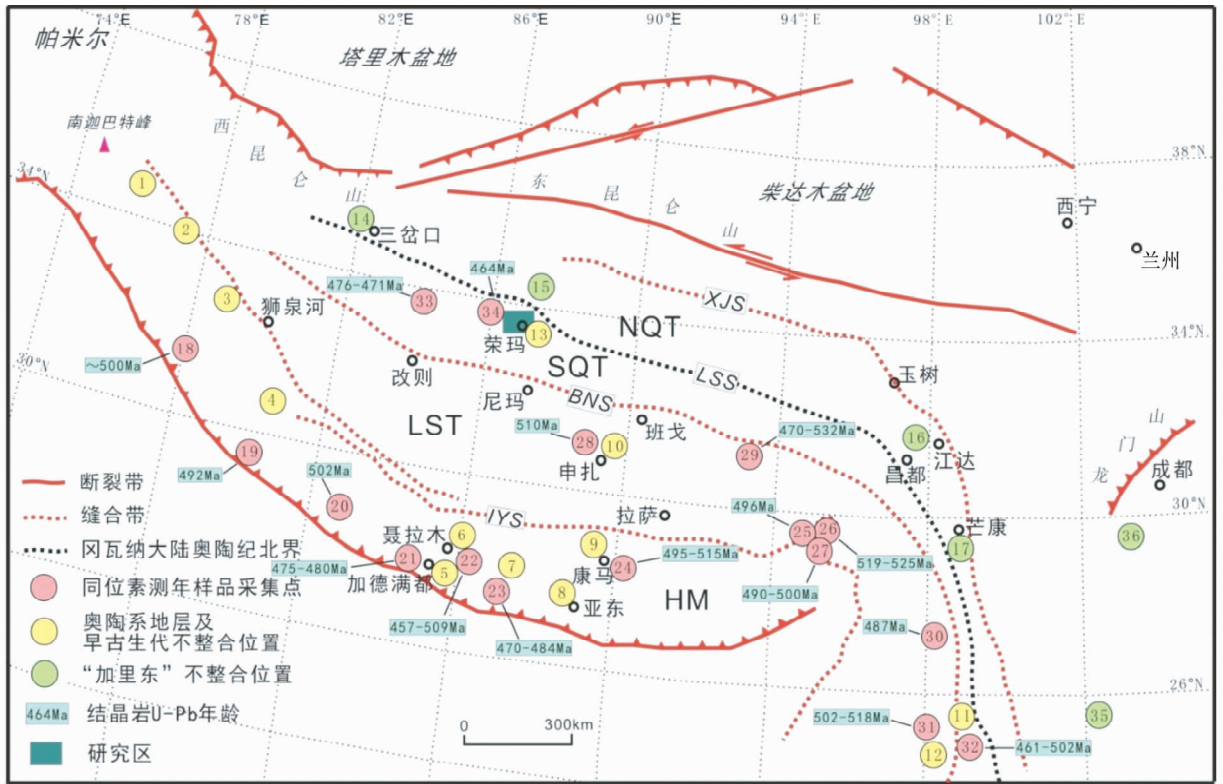


图 11 青藏高原大地构造单元及早古生代造山事件记录

1-Baig *et al.*, 1988; 2-Garzanti *et al.*, 1986; 3-Miller *et al.*, 2007; 4-Valdiya *et al.*, 1995; 5-Gehrels *et al.*, 2003; 6-朱同兴等, 2003; 7-尹集祥等, 1974; 8、9-周志广等, 2004; 10-Gehrels *et al.*, 2011; 11-黄勇等, 2012; 12-蔡志慧等, 2013; 13-吉林大学地质调查研究院, 2005 和本文; 14-夏军等, 2006; 15-吉林大学地质调查研究院, 2005 和本文; 16、17-中国科学院青藏高原综合科学考察队, 1984; 18-Miller *et al.*, 2001; Spencer *et al.*, 2012; 19-Decelles *et al.*, 1998; 20-Godin *et al.*, 2001; 21-Gehrels *et al.*, 2003; 22-许志琴等, 2005; Liu *et al.*, 2007a; 23-Schärer *et al.*, 1983; Johnson *et al.*, 2001; 24-Lee *et al.*, 2000; 25-董昕等, 2009; 26-Liu *et al.*, 2007b; 27-张泽明等, 2008; 28-Gehrels *et al.*, 2011; 29-解超明等, 2010; Guynn *et al.*, 2012; 30-宋述光等, 2007; 31-蔡志慧等, 2013; 32-董美玲等, 2012; 刘琦胜等, 2012; Liu *et al.*, 2009; 33-Pullen *et al.*, 2011; 34-胡培远等, 2010; 35-方润森等, 2000; 张举等, 2013; 36-许海龙等, 2012. LST-拉萨地体; SQT-南羌塘地体; NQT-北羌塘地体; HM-喜马拉雅造山带; IYS-雅鲁藏布江缝合带; BNS-班公湖-怒江缝合带; LSS-龙木错-双湖缝合带; XJS-西金乌兰-金沙江缝合带

Fig. 11 Tectonic units and records of the Early Paleozoic orogenic events in Tibetan regions

的二云母花岗岩,该强变形二云母花岗岩位于本文研究区之西侧约 100km。笔者关于该二云母花岗岩的未刊锆石 U-Pb 年龄数据与 Pullen *et al.* (2011) 报道的数据一致。该二云母花岗岩的围岩即为荣玛组的变质石英砂岩。此外,最近 Zhao *et al.* (2014) 也报道了一个强变形花岗岩侵位于荣玛组浅变质石英砂岩的案例,该强变形花岗岩位于本研究区西北侧约 30km,其锆石结晶年龄为 471Ma。这充分证明了荣玛组浅变质石英砂岩的形成时代应介于 527 ± 7 Ma 和 476Ma 之间。考虑石英砂岩形成之后,尚须经历埋藏、压实以及浅变质作用等作用之后,才易于被花岗岩侵位,因此南羌塘块体北部的荣玛组沉积岩最可能形成于寒武纪中、晚期。荣玛组沉积岩与其上覆之塔石山组石英砂岩之间则存在明显的沉积间断,两者之间为平行不整合关系。

青藏高原及东部邻区早古生代地层对比见图 10 和图 11。早古生代区域地质对比发现,大体仍以现今的羌中隆起为界,南、北区域的地质特征差异颇大(图 10、图 11):从南部

的喜马拉雅块体至北部的南羌塘块体,再东至滇西的保山块体,寒武-奥陶之交均发生了显著的沉积间断(图 10):下伏的寒武系与上覆奥陶系之间多为假整合,局部为角度不整合(谭雪春等, 1982; 中国科学院青藏高原综合科学考察队, 1984; 朱同兴等, 2003; 周志广等, 2004; 吉林大学地质调查研究院, 2005; 计文化等, 2009; 黄勇等, 2012; 蔡志慧等, 2013; Gehrels *et al.*, 2003, 2011)。块体内部,则广泛发育 460~510Ma 的岩浆活动(图 10、图 11),花岗岩常常侵位于寒武系地层内(图 10、图 11)(许志琴等, 2005; 宋述光等, 2007; 计文化等, 2009; 胡培远等, 2010; 蔡志慧等, 2013; Schärer *et al.*, 1983; Johnson *et al.*, 2001; Liu *et al.*, 2007a, b; Pullen *et al.*, 2011; Gehrels *et al.*, 2011)。中、晚奥陶世以来,这些地区则连续接受沉积作用,没有发生明显的沉积间断,岩浆活动微弱。与此相对应,东部的滇东地区、四川盆地等地区,寒武、奥陶纪则为连续沉积,不存在明显的沉积间断(图 10)(方润森等, 2000; 许海龙等, 2012; 张举等, 2013),

但在早奥陶世之后,却常发生沉积间断,多缺失上奥陶统、志留系和下泥盆统地层(图10)(中国科学院青藏高原综合科学考察队,1984;方润森等,2000;吉林大学地质调查研究院,2005;夏军等,2006;许海龙等,2012;张举等,2013)。上覆地层多为中上泥盆统磨拉石,大角度不整合覆盖在下奥陶统地层之上(图10),这些地区不发育460~510Ma的岩浆事件,相反却经历了加里东运动(图10、图11)。区域对比充分表明,早在寒武-奥陶纪之交,南羌塘块体就与北羌塘块体就有显著的地质差异(图10、图11),充分反映了这两块体的大地构造属性完全不同。南羌塘块体与其南侧的拉萨、喜马拉雅,及其东部的保山块体有大地构造的亲缘性,均经历了约500Ma左右的晚泛非运动,参与了冈瓦纳超级大陆的形成过程。在中、晚奥陶世时,很可能由于冈瓦纳超级大陆的裂解,海水上侵,形成中上奥陶统海相沉积地层,平行不整合于寒武系地层之上。北羌塘块体则亲扬子块体,经历了强烈的加里东褶皱造山运动。这表明有一古大洋在寒武奥陶纪之交,就分隔开了南、北羌塘块体。

7 结论

(1)南羌塘荣玛组浅变质石英砂岩形成于寒武纪中晚期,与上覆中、上奥陶统塔石山组为平行不整合接触。

(2)中、上奥陶统塔石山组物源多来自本地“泛非运动”晚期所形成的结晶岩,反映“泛非运动”晚期所形成的变质杂岩在奥陶纪早期就已折返至地表之上,遭受剥蚀。即在奥陶纪时,就有类似现今羌中隆起的古山脉,为中、上奥陶统沉积地层的形成提供物质来源。

(3)在寒武-奥陶纪之交,南、北羌塘块体被一古大洋分隔开,各自独立演化。

致谢 野外调查承蒙袁国礼教授、梁晓博士和郑艺龙博士的大力支持与帮助;廖含英女士帮助完成反射光照相、陈振宇博士帮助完成阴极发光照相、孙卫东研究员帮助完成锆石定年分析;张斌硕士帮助完成图表制作;两位审稿人的审阅提升了本文;在此一并表示衷心感谢。

References

Baig MS, Lawrence RD and Snee LW. 1988. Evidence for Late Precambrian to Early Cambrian orogeny in northwest Himalaya, Pakistan. *Geological Magazine*, 125(1): 83–86

Cai ZH, Xu ZQ, Duan XD, Li HQ, Cao H and Huang XM. 2013. Early stage of Early Paleozoic orogenic event in western Yunnan Province, southeastern margin of Tibet Plateau. *Acta Petrologica Sinica*, 29(6): 2123–2140 (in Chinese with English abstract)

DeCelles PG, Gehrels GE, Quade J, Ojha TP, Kppa P and Upreti BN. 1998. Neogene foreland basin deposits, erosional unroofing, and the kinematic history of the Himalayan fold-thrust belt, western Nepal. *Geological Society of America Bulletin*, 110(1): 2–21

Dong CY, Li C, Wan YS, Wang W, Wu YW, Jie HQ and Liu DY.

2011. Detrital zircon age mode of Ordovician Wenquan quartzite south of Lungmuco-Shuanghu Suture in the Qiangtang area, Tibet: Constraint on tectonic affinity and source regions. *Scientia Sinica (Terrae)*, 41(3): 299–308 (in Chinese)

Dong ML, Dong GC, Mo XX, Zhu DC, Nie F, Xie XF, Wang X and Hu ZC. 2012. Geochronology and geochemistry of the Early Palaeozoic granitoids in Baoshan Block, western Yunnan and their implications. *Acta Petrologica Sinica*, 28(5): 1453–1464 (in Chinese with English abstract)

Dong X, Zhang ZM, Wang JL, Zhao GC, Liu F, Wang W and Yu F. 2009. Provenance and formation age of the Nyingchi Group in the southern Lhasa terrane, Tibetan Plateau: Petrology and zircon U-Pb geochronology. *Acta Petrologica Sinica*, 25(7): 1678–1694 (in Chinese with English abstract)

Fang RS. 2000. A discussion about the Devonian stratigraphy of Yunnan. *Geology of Yunnan*, 19(1): 62–90 (in Chinese with English abstract)

Garzanti E, Casnedi R and Jadoul F. 1986. Sedimentary evidence of a Cambro-Ordovician orogenic event in the northwestern Himalaya. *Sedimentary Geology*, 48(3–4): 237–265

Gehrels GE, Decelles PG, Martin A, Ojha TP, Pinhassi G and Upreti BN. 2003. Initiation of the Himalayan orogen as an Early Paleozoic thin-skinned thrust belt. *GSA Today*, 13(9): 4–9

Gehrels GE, Kapp P, DeCelles P, Pullen A, Blakey R, Weislogel A, Ding L, Guynn J, Martin A, McQuarrie N and Yin A. 2011. Detrital zircon geochronology of pre-Tertiary strata in the Tibetan-Himalayan orogeny. *Tectonics*, 30(5), TC5016, doi: 10.1029/2011TC002868

Godin L, Parrish RR, Brown RL and Hodges KV. 2001. Crustal thickening leading to exhumation of the Himalayan metamorphic core of central Nepal: Insight from U-Pb geochronology and $^{40}\text{Ar}/^{39}\text{Ar}$ thermochronology. *Tectonics*, 20(5): 729–747

Guynn J, Kapp P, George E, Gehrels G and Ding L. 2012. U-Pb geochronology of basement rocks in central Tibet and paleogeographic implications. *Journal of Asian Earth Sciences*, 43(1): 23–50

Hu PY, Li C, Su L, Li CB and Yu H. 2010. Zircon U-Pb dating of granitic gneiss in Wugong mountain area, central Qiangtang, Qinghai-Tibet Plateau: Age records of Pan-African Movement and Indo-China Movement. *Geology in China*, 37(4): 1050–1057 (in Chinese with English abstract)

Huang JJ. 2001. Structural characteristics of the basement of the Qiangtang Basin. *Acta Geologica Sinica*, 75(3): 333–337 (in Chinese with English abstract)

Huang Y, Hao JY, Bai L, Deng GB, Zhang GX and Huang WJ. 2012. Stratigraphic and petrologic response to Late Pan-African movement in Shidian area, western Yunnan Province. *Geological Bulletin of China*, 31(2–3): 306–313 (in Chinese with English abstract)

Institute of Geological Survey, Jilin University. 2005. 1:250000 Mayer Kangri Sheet in Xizang. *Sedimentary Geology and Tethyan Geology*, 25(1–2): 51–56 (in Chinese with English abstract)

Institute of Tibetan Plateau Comprehensive Scientific Expedition. 1984. Strata of Tibet. Beijing: Science Press, 1–405 (in Chinese)

Ji WH, Chen SJ, Zhao ZM, Li RS, He SP and Wang C. 2009. Discovery of the Cambrian volcanic rocks in the Xainza area, Gangdese orogenic belt, Tibet, China and its significance. *Geological Bulletin of China*, 28(9): 1350–1354 (in Chinese with English abstract)

Johnson MRW, Oliver GJH, Parrish RR and Johnson SP. 2001. Synthrusting metamorphism, cooling and erosion of the Himalayan Kathmandu complex, Nepal. *Tectonics*, 20(3): 394–415

Kapp P, Yin A, Manning CE, Murphy M, Harrison TM, Spurlin M, Ding L, Deng XG and Wu CM. 2000. Blueschist-bearing metamorphic core complexes in Qiangtang block reveal deep crustal structure of northern Tibet. *Geology*, 28(1): 19–22

Kapp P, Yin A, Manning CE, Harrison M, Taylor MH and Ding L. 2003. Tectonic evolution of the Early Mesozoic blueschist-bearing Qiangtang metamorphic belt, central Tibet. *Tectonics*, 22(4): 1043, doi: 10.1029/2002TC001383

- Lee J, Hacker BR, Dinklage WS, Wang Y, Gans P, Calver A, Wan JL, Chen WJ, Blüthner AE and McClellan W. 2000. Evolution of the Kangmar Dome, southern Tibet: Structural, petrologic, and thermochronologic constraints. *Tectonics*, 19(5): 872–895
- Li C. 1987. The Longmucuo-Shuanghu-Lancangjiang plate suture and the north boundary of distribution of Gondwana facies Permian-Carboniferous system in northern Xizang, China. *Journal of Changchun College of Geology*, 17(2): 156–162 (in Chinese with English abstract)
- Li C. 2003. Question about the basement of the Qiangtang micro-plate. *Geological Review*, 49(1): 5–9 (in Chinese with English abstract)
- Li C, Zhai QG, Dong YS and Huang XP. 2006. Discovery of eclogite and its geological significance in Qiangtang area, central Tibet. *Chinese Science Bulletin*, 51(9): 1095–1100
- Li YJ, Wu HR, Li HS and Sun DL. 1997. Discovery of radiolarians in the Amugang and Chasang groups and Lugu Formation in northern Tibet and some related geological problems. *Geological Review*, 43(3): 250–256 (in Chinese with English abstract)
- Liu QS, Ye PS and Wu ZH. 2012. SHRIMP zircon U-Pb dating and petrogeochemistry of Ordovician granite bodies in the southern segment of Gaoligong Mountain, western Yunnan Province. *Geological Bulletin of China*, 31(2): 250–257 (in Chinese with English abstract)
- Liu S, Hu RZ, Gao S, Feng CX, Huang ZL, Lai SC, Yuan HL and Liu XM. 2009. U-Pb zircon, geochemical and Sr-Nd-Hf isotopic constraints on the age and origin of Early Palaeozoic I-type granite from the Tengchong-Baoshan Block, western Yunnan Province, SW China. *Journal of Asian Earth Sciences*, 36(2–3): 168–182
- Liu Y, Siebel W, Massonne HJ and Xiao XC. 2007a. Geochronological and petrological constraints for the tectonic evolution of the central Greater Himalayan Sequence in the Kharta area, southern Tibet. *Journal of Geology*, 115(2): 215–230
- Liu Y, Yang ZQ and Wang M. 2007b. History of zircon growth in a high-pressure granulite within the eastern Himalayan syntaxis, and tectonic implications. *International Geology Review*, 49(9): 861–872
- Liu Y, Santosh M, Zhao ZB, Niu WC and Wang GH. 2011. Evidence for palaeo-Tethyan oceanic subduction within central Qiangtang, northern Tibet. *Lithos*, 127(1–2): 39–53
- Liu YS, Hu ZC, Gao S, Günther D, Xu J, Gao CG and Chen HB. 2008. In situ analysis of major and trace elements of anhydrous minerals by LA-ICP-MS without applying an internal standard. *Chemical Geology*, 257(1–2): 34–43
- Ludwig KR. 2003. *ISOPLOT 3.0: A Geochronological Toolkit for Microsoft Excel*. Berkeley Geochronology Center, Spec. Pub., 4: 1–70
- Miller C, Thöni M, Frank W, Grasemann B, Klötzli U, Guntli P and Draganits E. 2001. The Early Paleozoic magmatic event in the Northwest Himalaya, India: Source, tectonic setting and age of emplacement. *Geological Magazine*, 138(3): 237–251
- Pan GT, Wang LQ, Li RS, Yuan SH, Ji WH, Yin FG, Zhang WP and Wang BD. 2012. Tectonic evolution of the Qinghai-Tibet Plateau. *Journal of Asian Earth Sciences*, 53: 3–14
- Pan GT, Wang LQ, Li RS, Yin FG and Zhu DC. 2012. Tectonic model of archipelagic arc-basin systems: The key to the continental geology. *Sedimentary Geology and Tethyan Geology*, 32(3): 5–16 (in Chinese with English abstract)
- Pullen A, Kapp P, Gehrels GE, Vervoort JD and Ding L. 2008. Triassic continental subduction in central Tibet and Mediterranean-style closure of the Paleo-Tethys Ocean. *Geology*, 36(5): 351–354
- Pullen A, Kapp P, Gehrels GE, Ding L and Zhang QH. 2011. Metamorphic rocks in central Tibet: Lateral variations and implications for crustal structure. *Geological Society of America Bulletin*, 123(3–4): 585–600
- Schärer U and Allègre CJ. 1983. The Palung granite (Himalaya): High-resolution U-Pb systematics in zircon and monazite. *Earth and Planetary Science Letters*, 63(3): 423–432
- Song SG, Ji JQ, Wei CJ, Su L, Zheng YD, Song B and Zhang LF. 2007. Early Paleozoic granite in Nujiang River of Northwest Yunnan in the southwestern China and its tectonic Implications. *Chinese Science Bulletin*, 52(17): 2402–2406
- Spencer CJ, Harris RA and Dorais MJ. 2012. Depositional provenance of the Himalayan metamorphic core of Garhwal region, India: Constrained by U-Pb and Hf isotopes in zircons. *Gondwana Research*, 22(1): 26–35
- Tan XC, Dong ZZ and Qin DH. 1982. The Lower Devonian and Silurian-Devonian boundary in western Yunnan Province. *Journal of Stratigraphy*, 6(3): 199–208 (in Chinese)
- Tu XL, Zhang H, Deng WF, Ling MX, Liang HY, Liu Y and Sun WD. 2011. Application of RESOLUTION in-situ laser ablation ICP-MS in trace element analyses. *Geochimica*, 40(1): 83–98 (in Chinese with English abstract)
- Valdiya KS. 1995. Proterozoic sedimentation and Pan-African geodynamic development in the Himalaya. *Precambrian Research*, 74(1–2): 35–55
- Wang GZ and Wang CS. 2001. Disintegration and age metamorphic rocks in Qiangtang basement, Tibet, China. *Science in China (Series D)*, 44(Suppl.): 86–93
- Wu RZ, Hu CZ, Wang CS, Zhang MG, Gao DR, Lan BL and Zhang SN. 1986. The Stratigraphical System of Qiangtang District in Northern Xizang (Tibet). Beijing: Geological Publishing House, 1–31 (in Chinese)
- Xia J, Zhong HM, Tong JS and Lu RK. 2006. Unconformity between the Lower Ordovician and Devonian in the Sanchakou area in the eastern part of the Lungmu Co, northern Tibet, China. *Geological Bulletin of China*, 25(1–2): 114–117 (in Chinese with English abstract)
- Xie CM, Li C, Su L, Wu YW, Wang M and Yu H. 2010. LA-ICP-MS U-Pb dating of zircon from granite gneiss in the Amdo area, northern Tibet, China. *Geological Bulletin of China*, 29(12): 1737–1744 (in Chinese with English abstract)
- Xu HL, Wei GQ, Jia CZ, Yang W, Zhou TW, Xie WR, Li CX and Luo BW. 2012. Tectonic evolution of the Leshan-Longnvsi paleo-uplift and its control on gas accumulation in the Sinian strata, Sichuan Basin. *Petroleum Exploration and Development*, 39(4): 406–414 (in Chinese with English abstract)
- Xu ZQ, Yang JS, Liang FH, Qi XX, Liu FL, Zeng LS, Liu DY, Li HB, Wu CL, Shi DR and Chen SY. 2005. Pan-African and Early Paleozoic orogenic events in the Himalayan terrane: Inference from SHRIMP U-Pb zircon ages. *Acta Petrologica Sinica*, 21(1): 1–12 (in Chinese with English abstract)
- Yin A and Harrison TM. 2000. Geologic evolution of the Himalayan-Tibetan Orogen. *Annual Review of Earth and Planetary Sciences*, 28: 211–280
- Yin JX. 1974. Strata of Everest region (Cambrian-Ordovician). In: *Scientific Expedition Everest Region Report (1966 ~ 1968)*. Beijing: Science Press, 4–21 (in Chinese)
- Zhang J, Zhang YD and Song YY. 2013. Graptolite fauna and age of the Hungshihyen Formation (Ordovician) in eastern Yunnan, Southwest China. *Journal of Stratigraphy*, 37(1): 8–16 (in Chinese with English abstract)
- Zhang KJ. 2001. Blueschist-bearing metamorphic core complexes in the Qiangtang block reveal deep crustal structure of northern Tibet: Comment. *Geology*, 29: 90
- Zhang KJ, Cai JX, Zhang YX and Zhao TP. 2006. Eclogites from central Qiangtang, northern Tibet (China) and tectonic implications. *Earth and Planetary Science Letters*, 245(3–4): 722–727
- Zhang ZM, Wang JL, Shen K and Shi C. 2008. Paleozoic circum-Gondwana orogens: Petrology and geochronology of the Namche Complex in the eastern Himalayan syntaxis, Tibet. *Acta Petrologica Sinica*, 24(7): 1627–1637 (in Chinese with English abstract)
- Zhao ZB, Bons P, Wang GH, Liu Y and Zheng YL. 2014. Origin and pre-Cenozoic evolution of the South Qiangtang basement, Central Tibet. *Tectonophysics*, 623: 52–66
- Zhou ZG, Liu WC and Liang DY. 2004. Discovery of the Ordovician and its basal conglomerate in the Kangmar area, southern Tibet: With a discussion of the relation of the sedimentary cover and unifying

- basement in the Himalayas. *Regional Geology of China*, 23(7): 655–663 (in Chinese with English abstract)
- Zhu TX, Wang AH, Zou GF and Feng XT. 2003. The new discovery of Basal conglomerate of sedimentary cover in Himalayan district. *Geological Bulletin of China*, 22(5): 367–368 (in Chinese with English abstract)

附中文参考文献

- 蔡志慧, 许志琴, 段向东, 李化启, 曹汇, 黄学猛. 2013. 青藏高原东南缘滇西早古生代早期造山事件. *岩石学报*, 29(6): 2123–2140
- 董春艳, 李才, 万渝生, 王伟, 吴彦旺, 颜顽强, 刘敦一. 2011. 西藏羌塘龙木错-双湖缝合带南侧奥陶纪温泉石英岩碎屑锆石年龄分布模式: 构造归属及物源区制约. *中国科学(地球科学)*, 41(3): 299–308
- 董美玲, 董国臣, 莫宣学, 朱弟成, 聂飞, 谢许峰, 王霞, 胡兆初. 2012. 滇西保山地块早古生代花岗岩类的年代学、地球化学及意义. *岩石学报*, 28(5): 1453–1464
- 董昕, 张泽明, 王金丽, 赵国春, 刘峰, 王伟, 于飞. 2009. 青藏高原拉萨地体南部林芝岩群的物质来源与形成年代: 岩石学与锆石 U-Pb 年代学. *岩石学报*, 25(7): 1678–1694
- 方润森. 2000. 云南泥盆系区域地层及有关问题探讨. *云南地质*, 19(1): 62–90
- 胡培远, 李才, 苏犁, 李春斌, 于红. 2010. 青藏高原羌塘中部蜈蚣山花岗岩片麻岩锆石 U-Pb 定年——泛非与印支事件的年代学记录. *中国地质*, 37(4): 1050–1057
- 黄继钧. 2001. 羌塘盆地基底构造特征. *地质学报*, 75(3): 333–337
- 黄勇, 郝家棚, 白龙, 邓贵标, 张国祥, 黄文俊. 2012. 滇西施甸地区晚泛非运动的地层学和岩石学响应. *地质通报*, 31(2–3): 306–313
- 吉林大学地质调查研究院. 2005. 1: 25 万玛依岗日幅地质调查成果与进展. *沉积与特提斯地质*, 25(1–2): 51–56
- 中国科学院青藏高原综合科学考察队. 1984. 西藏地层. 北京: 科学出版社, 1–405
- 计文化, 陈守建, 赵振明, 李荣社, 何世平, 王超. 2009. 西藏冈底斯构造带申扎一带寒武系火山岩的发现及其地质意义. *地质通报*, 28(9): 1350–1354
- 李才. 1987. 龙木错-双湖-澜沧江板块缝合带与石炭二叠纪冈瓦纳北界. *长春地质学院学报*, 17(2): 156–162
- 李才. 2003. 羌塘基底质疑. *地质论评*, 49(1): 5–9
- 李才, 翟庆国, 董永胜, 黄小鹏. 2006. 青藏高原羌塘中部榴辉岩的发现及其意义. *科学通报*, 51(1): 70–74
- 李曰俊, 吴浩若, 李红生, 孙东立. 1997. 藏北阿木岗群、查桑群和鲁谷组放射射的发现及有关问题讨论. *地质论评*, 43(3): 250–256

- 刘琦胜, 叶培盛, 吴中海. 2012. 滇西高黎贡山南段奥陶纪花岗岩 SHRIMP 锆石 U-Pb 测年和地球化学特征. *地质通报*, 31(2): 250–257
- 潘桂堂, 王立全, 李荣社, 尹福光, 朱弟成. 2012. 多岛弧盆系构造模式: 认识大陆地质的关键. *沉积与特提斯地质*, 32(3): 5–16
- 宋述光, 季建清, 魏春景, 苏犁, 郑亚东, 宋彪, 张立飞. 2007. 滇西北怒江早古生代片麻状花岗岩的确定及其构造意义. *科学通报*, 52(8): 927–930
- 谭雪春, 董志中, 秦德厚. 1982. 滇西保山地区下泥盆统兼论志留-泥盆系的分界. *地层学杂志*, 6(3): 199–208
- 涂湘林, 张红, 邓文峰, 凌明星, 梁华英, 刘颖, 孙卫东. 2011. Resolution 激光剥蚀系统在微量元素原位微区分析中的应用. *地球化学*, 40(1): 83–98
- 王国芝, 王成善. 2001. 西藏羌塘基底变质岩系的解体和时代厘定. *中国科学(D 辑)*, 31(增刊): 77–82
- 吴瑞忠, 胡承祖, 王成善, 张懋功, 高德荣, 兰伯龙, 张哨楠. 1986. 藏北羌塘地区地层系统. 北京: 地质出版社, 1–31
- 夏军, 钟华明, 童劲松, 鲁如魁. 2006. 藏北龙木错东部三岔口地区下奥陶统与泥盆系的不整合界面. *地质通报*, 25(1–2): 114–117
- 解超明, 李才, 苏犁, 吴彦旺, 王明, 于红. 2010. 藏北安多地区花岗岩片麻岩锆石 LA-ICP-MS U-Pb 定年. *地质通报*, 29(12): 1737–1744
- 许海龙, 魏国齐, 贾承造, 杨威, 周天伟, 谢武仁, 李传新, 罗贝维. 2012. 乐山-龙女寺古隆起构造演化及对震旦系成藏的控制. *石油勘探与开发*, 39(4): 406–414
- 许志琴, 杨经绥, 梁风华, 戚学祥, 刘福来, 曾令森, 刘敦一, 李海兵, 吴才来, 史仁灯, 陈松永. 2005. 喜马拉雅地体的泛非早古生代造山事件年龄记录. *岩石学报*, 21(1): 1–12
- 尹集祥. 1974. 珠穆朗玛峰地区的地层(寒武-奥陶系). 见: 珠穆朗玛峰地区科学考察报告(1966~1968). 北京: 科学出版社, 4–21
- 张举, 张元动, 宋妍妍. 2013. 滇东地区奥陶系红石崖组的时代. *地层学杂志*, 37(1): 8–16
- 张泽明, 王金丽, 沈昆, 石超. 2008. 环东冈瓦纳大陆周缘的古生代造山作用: 东喜马拉雅构造结南迦巴瓦岩群的岩石学和年代学证据. *岩石学报*, 24(7): 1627–1637
- 周志广, 刘文灿, 梁定益. 2004. 藏南康马奥陶系及其底砾岩的发现并初论喜马拉雅沉积盖层与统一变质基底的关系. *地质通报*, 23(7): 655–663
- 朱同兴, 王安华, 邹光富, 冯心涛. 2003. 喜马拉雅地区沉积盖层底砾岩的新发现. *地质通报*, 22(5): 367–368

附表 1 荣玛组变质石英砂岩 (NT71306) 和塔石山组沉积岩 (NT71303、NT71304、NT71305) 碎屑锆石 LA-ICP-MS U-Pb 年龄
Appendix Table 1 Detrital zircon LA-ICP-MS U-Pb age of the low-grade metamorphic quartz sandstones (sample NT71306) from Rongma Formation and of the sedimentary rocks (sample NT71303 , NT71304 , NT71305) from Tashishan Formation

测点号	Pb	Th	U	Th/U	²⁰⁷ Pb/ ²³⁵ U	1σ	²⁰⁶ Pb/ ²³⁸ U	1σ	²⁰⁷ Pb/ ²³⁵ U	1σ	²⁰⁶ Pb/ ²³⁸ U	1σ	谐和度
	含量(× 10 ⁻⁶)								Age(Ma)		Age(Ma)		
荣玛组变质石英砂岩(NT71306)													
6001	94.8	507.0	357.5	1.42	1.6915	0.0490	0.1720	0.0017	1005	18	1023	10	98%
6002	39.4	138.3	181.4	0.76	1.5490	0.0450	0.1622	0.0018	950	18	969	10	98%
6003	238.2	251.1	435.3	0.58	10.6479	0.2498	0.4148	0.0041	2493	22	2237	19	89%
6004	38.2	239.5	333.5	0.72	0.7055	0.0228	0.0887	0.0010	542	14	548	6	98%
6005	73.1	33.9	734.5	0.05	0.7230	0.0217	0.0920	0.0012	552	13	567	7	97%
6006	151.4	204.4	321.2	0.64	5.5316	0.1656	0.3636	0.0042	1906	26	1999	20	95%
6008	12.0	7.6	32.5	0.23	5.5717	0.1992	0.3004	0.0047	1912	31	1693	23	87%
6009	96.1	248.6	463.8	0.54	1.5581	0.0391	0.1663	0.0016	954	16	992	9	96%
6010	44.2	123.7	151.0	0.82	2.7047	0.0751	0.2325	0.0024	1330	21	1348	13	98%
6011	62.9	136.0	241.3	0.56	2.2770	0.0661	0.2118	0.0026	1205	21	1239	14	97%
6012	28.7	169.0	135.8	1.24	1.3885	0.0508	0.1431	0.0018	884	22	862	10	97%
6013	36.7	83.6	208.6	0.40	1.3795	0.0511	0.1439	0.0016	880	22	867	9	98%
6014	88.2	370.6	856.8	0.43	0.7148	0.0235	0.0851	0.0011	548	14	527	6	96%
6015	68.8	71.5	85.9	0.83	15.3610	0.5090	0.5476	0.0070	2838	32	2815	29	99%
6016	240.8	263.3	829.7	0.32	3.9353	0.1868	0.2292	0.0062	1621	38	1330	32	80%
6017	137.1	151.6	726.2	0.21	1.7837	0.0629	0.1663	0.0022	1040	23	992	12	95%
6018	28.6	91.8	231.6	0.40	0.8405	0.0339	0.1032	0.0014	619	19	633	8	97%
6019	55.5	150.0	244.2	0.61	1.8855	0.0723	0.1752	0.0027	1076	25	1041	15	96%
6020	35.4	141.6	200.0	0.71	1.2824	0.0580	0.1381	0.0023	838	26	834	13	99%
6021	25.4	151.2	204.1	0.74	0.8556	0.0404	0.0985	0.0013	628	22	605	8	96%
6022	32.5	102.0	223.8	0.46	1.0664	0.0464	0.1210	0.0020	737	23	736	11	99%
6023	59.0	238.8	437.8	0.55	0.8273	0.0291	0.1105	0.0014	612	16	676	8	90%
6024	13.8	39.3	62.0	0.63	2.2695	0.1492	0.1758	0.0029	1203	46	1044	16	85%
6025	66.1	107.8	261.4	0.41	2.0634	0.0710	0.2094	0.0025	1137	24	1226	13	92%
6026	16.2	42.2	64.1	0.66	1.8333	0.0770	0.1963	0.0029	1057	28	1155	16	91%
6027	17.2	237.8	115.6	2.06	0.6511	0.0328	0.0870	0.0013	509	20	538	8	94%
6028	81.9	674.7	524.6	1.29	1.2763	0.0406	0.1132	0.0023	835	18	691	13	81%
6029	16.0	42.6	81.5	0.52	1.5781	0.0660	0.1587	0.0023	962	26	949	13	98%
6030	53.6	144.9	282.9	0.51	1.4365	0.0469	0.1525	0.0019	904	20	915	11	98%
6031	270.2	92.6	621.9	0.15	6.6460	0.1639	0.3637	0.0036	2065	22	2000	17	96%
6032	263.3	336.7	383.0	0.88	10.7542	0.2565	0.4831	0.0054	2502	22	2541	23	98%
6033	49.1	75.6	225.2	0.34	1.9432	0.0575	0.1861	0.0023	1096	20	1100	13	99%
6034	44.1	133.1	248.6	0.54	1.3048	0.0359	0.1430	0.0017	848	16	862	9	98%
6035	30.4	112.2	182.0	0.62	1.1867	0.0404	0.1329	0.0017	794	19	804	10	98%
6036	100.2	130.3	207.6	0.63	7.4155	0.1944	0.3594	0.0037	2163	24	1979	18	91%
6037	74.6	72.3	130.7	0.55	9.7085	0.2680	0.4455	0.0054	2408	25	2375	24	98%
6038	41.0	94.6	191.9	0.49	1.7852	0.0576	0.1752	0.0021	1040	21	1041	11	99%
6039	144.2	208.6	288.7	0.72	6.5758	0.2040	0.3836	0.0044	2056	27	2093	20	98%
6040	42.0	120.0	329.7	0.36	0.9566	0.0375	0.1108	0.0015	682	19	677	9	99%
6041	55.9	394.4	287.1	1.37	1.1949	0.0461	0.1363	0.0019	798	21	824	11	96%
6042	96.8	109.3	328.1	0.33	2.9965	0.0952	0.2498	0.0028	1407	24	1437	15	97%
6043	44.9	190.2	383.6	0.50	0.9872	0.0371	0.0973	0.0014	697	19	598	8	84%
6044	174.9	150.6	312.5	0.48	10.0865	0.2852	0.4441	0.0048	2443	26	2369	22	96%
6045	67.1	171.5	626.6	0.27	1.0908	0.0502	0.0894	0.0014	749	24	552	8	79%
6046	16.2	37.9	78.8	0.48	1.8264	0.0782	0.1650	0.0024	1055	28	984	14	93%
6047	167.6	266.2	455.8	0.58	4.0355	0.1081	0.2840	0.0028	1641	22	1612	14	98%
6048	76.3	123.8	234.4	0.53	3.7275	0.0956	0.2484	0.0026	1577	21	1430	14	90%
6049	131.2	130.1	741.1	0.18	1.5164	0.0345	0.1560	0.0019	937	14	934	11	99%

续表 1
Continued Appendix Table 1

测点号	Pb	Th	U	Th/U	²⁰⁷ Pb/ ²³⁵ U	1σ	²⁰⁶ Pb/ ²³⁸ U	1σ	²⁰⁷ Pb/ ²³⁵ U	1σ	²⁰⁶ Pb/ ²³⁸ U	1σ	谐和度
	含量(×10 ⁻⁶)								Age(Ma)		Age(Ma)		
6050	38.4	114.3	235.0	0.49	1.2325	0.0358	0.1339	0.0015	815	16	810	8	99%
6051	166.8	111.5	292.4	0.38	9.5652	0.1688	0.4341	0.0042	2394	16	2324	19	97%
6052	18.5	148.2	82.3	1.80	1.2597	0.0552	0.1334	0.0017	828	25	807	10	97%
6053	40.0	71.6	222.3	0.32	1.4097	0.0375	0.1496	0.0018	893	16	899	10	99%
6054	131.6	426.9	730.8	0.58	1.4675	0.0373	0.1483	0.0019	917	15	892	11	97%
6055	58.1	140.4	388.2	0.36	1.1202	0.0315	0.1245	0.0014	763	15	756	8	99%
6057	64.3	243.9	580.3	0.42	0.7620	0.0237	0.0942	0.0012	575	14	580	7	99%
6058	39.8	211.8	348.8	0.61	0.7472	0.0259	0.0926	0.0013	567	15	571	8	99%
6059	6.8	0.6	67.7	0.01	0.9151	0.0572	0.0924	0.0016	660	30	570	10	85%
6060	70.7	121.3	507.2	0.24	1.1673	0.0476	0.1257	0.0028	785	22	763	16	97%
6061	30.2	70.1	229.9	0.31	1.0056	0.0398	0.1148	0.0015	707	20	701	9	99%
6062	70.0	264.4	666.4	0.40	0.7475	0.0261	0.0911	0.0013	567	15	562	8	99%
6063	160.6	62.9	166.7	0.38	29.1772	0.8969	0.6787	0.0086	3459	30	3340	33	96%
6064	22.6	59.5	124.4	0.48	2.0482	0.1685	0.1534	0.0030	1132	56	920	17	79%
6065	14.0	44.1	88.1	0.50	1.2119	0.0577	0.1285	0.0018	806	27	779	10	96%
6066	10.1	16.6	58.5	0.28	1.4211	0.0825	0.1498	0.0024	898	35	900	14	99%
6067	196.0	633.4	831.5	0.76	1.8724	0.0660	0.1856	0.0025	1071	23	1098	14	97%
6068	14.3	123.0	106.0	1.16	0.7588	0.0379	0.0936	0.0015	573	22	577	9	99%
6069	11.9	94.9	68.5	1.38	1.0887	0.0614	0.1189	0.0022	748	30	724	13	96%
6070	18.0	100.0	131.9	0.76	0.9282	0.0478	0.1064	0.0019	667	25	652	11	97%
6071	103.9	82.0	202.4	0.41	8.4790	0.3148	0.3974	0.0043	2284	34	2157	20	94%
6072	81.7	119.1	399.6	0.30	1.7743	0.0629	0.1768	0.0020	1036	23	1050	11	98%
6073	55.6	212.5	237.1	0.90	1.6635	0.0632	0.1709	0.0021	995	24	1017	12	97%
6074	41.1	144.7	192.8	0.75	1.6146	0.0627	0.1608	0.0021	976	24	961	12	98%
6075	20.8	40.8	147.5	0.28	1.0172	0.0466	0.1205	0.0018	712	23	733	10	97%
6076	6.4	21.6	35.8	0.60	1.2772	0.0876	0.1407	0.0031	836	39	848	17	98%
6077	78.0	283.5	412.7	0.69	1.6596	0.0636	0.1598	0.0033	993	24	956	18	96%
6078	63.1	133.8	555.6	0.24	0.8298	0.0276	0.0999	0.0012	613	15	614	7	99%
6079	98.8	267.7	630.8	0.42	1.1837	0.0381	0.1338	0.0018	793	18	810	10	97%
6080	51.2	185.6	316.9	0.59	1.1409	0.0374	0.1280	0.0014	773	18	776	8	99%
6081	14.5	70.6	82.5	0.86	1.2039	0.0554	0.1317	0.0017	802	26	797	10	99%
6082	78.3	90.2	127.3	0.71	9.7901	0.2588	0.4514	0.0045	2415	24	2401	20	99%
6083	11.9	0.8	119.9	0.01	0.7419	0.0340	0.0937	0.0014	564	20	578	8	97%
6084	155.5	354.2	739.9	0.48	1.7302	0.0460	0.1747	0.0020	1020	17	1038	11	98%
6085	61.2	180.0	220.8	0.82	2.1399	0.0661	0.2102	0.0025	1162	21	1230	13	94%
6086	110.6	221.7	517.3	0.43	1.7358	0.0516	0.1755	0.0020	1022	19	1042	11	98%
6087	57.6	228.5	281.8	0.81	1.4939	0.0450	0.1539	0.0017	928	18	923	10	99%
6088	36.9	67.7	324.8	0.21	0.8314	0.0292	0.0998	0.0015	614	16	614	9	99%
6089	18.1	111.9	69.8	1.60	1.7119	0.0848	0.1691	0.0028	1013	32	1007	16	99%
6090	46.3	73.3	446.6	0.16	0.7526	0.0302	0.0921	0.0012	570	18	568	7	99%
6091	15.2	79.9	86.1	0.93	1.1599	0.0622	0.1295	0.0020	782	29	785	11	99%
6092	22.4	84.0	182.2	0.46	0.8181	0.0370	0.1006	0.0014	607	21	618	8	98%
6093	64.6	247.2	308.8	0.80	1.4973	0.0530	0.1551	0.0022	929	22	929	12	99%
6094	26.0	33.8	120.4	0.28	1.8000	0.0736	0.1852	0.0026	1045	27	1095	14	95%
6095	93.1	94.1	222.4	0.42	7.9407	0.7241	0.3353	0.0143	2224	82	1864	69	82%
6096	30.9	121.1	137.9	0.88	1.5287	0.0699	0.1658	0.0023	942	28	989	13	95%
6097	32.7	188.6	183.1	1.03	1.0884	0.0448	0.1294	0.0017	748	22	785	10	95%
6098	86.8	248.0	379.6	0.65	1.6925	0.0563	0.1781	0.0021	1006	21	1056	12	95%
6099	64.3	85.4	100.8	0.85	9.6800	0.3122	0.4468	0.0051	2405	30	2381	23	99%

续表 1
Continued Appendix Table 1

测点号	Pb Th U			Th/U	²⁰⁷ Pb/ ²³⁵ U	1σ	²⁰⁶ Pb/ ²³⁸ U	1σ	²⁰⁷ Pb/ ²³⁵ U	1σ	²⁰⁶ Pb/ ²³⁸ U	1σ	谐和度
	含量(× 10 ⁻⁶)												
6100	70.4	50.5	125.9	0.40	9.2995	0.3080	0.4345	0.0050	2368	30	2326	22	98%
6101	52.7	92.6	76.2	1.22	10.5140	0.3513	0.4613	0.0059	2481	31	2445	26	98%
6102	105.5	284.5	120.0	2.37	10.7993	0.3145	0.4862	0.0057	2506	27	2554	25	98%
6103	25.6	66.0	108.7	0.61	2.0207	0.0705	0.1844	0.0025	1123	24	1091	14	97%
6104	122.3	498.2	578.0	0.86	1.6651	0.0514	0.1659	0.0022	995	20	989	12	99%
6105	103.3	127.6	367.8	0.35	2.7705	0.0895	0.2341	0.0026	1348	24	1356	14	99%
6106	116.8	162.9	162.2	1.00	11.0247	0.3784	0.5031	0.0080	2525	32	2627	34	96%
6107	28.4	258.3	216.4	1.19	0.7584	0.0330	0.0925	0.0013	573	19	570	7	99%
6108	37.7	119.3	132.2	0.90	2.1383	0.0953	0.2000	0.0043	1161	31	1175	23	98%
6109	22.6	59.9	176.1	0.34	0.8483	0.0348	0.1048	0.0016	624	19	642	10	97%
6110	4.6	3.0	23.9	0.12	1.6447	0.1079	0.1682	0.0037	988	41	1002	21	98%
6111	61.1	116.4	350.3	0.33	1.4788	0.0700	0.1586	0.0031	922	29	949	17	97%
6112	256.7	173.6	354.8	0.49	13.2933	0.4341	0.5330	0.0063	2701	31	2754	26	98%
6113	130.4	228.0	195.6	1.17	9.4913	0.3092	0.4347	0.0048	2387	30	2327	21	97%
6114	220.4	273.2	356.3	0.77	9.5706	0.3195	0.4403	0.0048	2394	31	2352	21	98%
6115	221.8	253.6	339.4	0.75	10.6631	0.3787	0.4702	0.0054	2494	33	2484	24	99%
6116	57.2	110.0	265.3	0.41	1.9360	0.0781	0.1753	0.0021	1094	27	1041	12	95%
6117	122.6	568.2	578.2	0.98	1.5277	0.0507	0.1520	0.0015	942	20	912	9	96%
6118	25.0	105.0	223.4	0.47	0.7857	0.0316	0.0929	0.0012	589	18	573	7	97%
6119	61.8	81.7	306.1	0.27	1.7595	0.0554	0.1710	0.0019	1031	20	1018	11	98%
6120	54.8	337.7	497.7	0.68	0.6766	0.0209	0.0854	0.0010	525	13	528	6	99%
6121	243.7	379.6	567.9	0.67	8.3806	0.3205	0.3917	0.0111	2273	35	2131	51	93%
6122	21.4	105.2	121.1	0.87	1.1690	0.0400	0.1320	0.0016	786	19	800	9	98%
6123	103.9	71.6	130.4	0.55	16.7227	0.3641	0.5871	0.0062	2919	21	2978	25	98%
6124	38.7	107.4	321.0	0.33	0.8865	0.0280	0.1056	0.0013	644	15	647	8	99%
6125	55.1	452.8	186.8	2.42	1.5025	0.0431	0.1635	0.0019	931	18	976	11	95%
6126	19.7	59.4	133.6	0.44	1.1129	0.0418	0.1207	0.0015	760	20	734	8	96%
6127	95.8	123.3	254.3	0.49	4.3322	0.1011	0.2900	0.0036	1700	19	1642	18	96%
6128	42.3	143.2	205.5	0.70	1.4622	0.0448	0.1608	0.0020	915	18	961	11	95%
6129	68.8	165.4	343.4	0.48	1.5659	0.0385	0.1644	0.0018	957	15	981	10	97%
6130	47.8	74.8	165.7	0.45	2.5723	0.0710	0.2338	0.0025	1293	20	1354	13	95%
塔石山组沉积岩(NT71303,NT71304,NT71305)													
3001	220.8	214.5	409.0	0.52	8.7291	0.2869	0.3954	0.0044	2310	30	2148	20	92%
3002	23.5	49.5	120.6	0.41	1.5798	0.0666	0.1624	0.0022	962	26	970	12	99%
3003	148.2	117.8	327.6	0.36	5.8717	0.1627	0.3567	0.0039	1957	24	1967	18	99%
3004	78.0	189.9	386.9	0.49	1.5345	0.0457	0.1626	0.0020	944	18	971	11	97%
3005	165.8	556.3	999.9	0.56	1.1367	0.0350	0.1325	0.0019	771	17	802	11	96%
3006	38.8	127.9	173.9	0.74	2.0077	0.1044	0.1896	0.0057	1118	35	1119	31	99%
3007	39.9	47.3	112.0	0.42	3.5377	0.1217	0.2825	0.0035	1536	27	1604	17	95%
3008	76.3	137.8	364.1	0.38	1.6537	0.0531	0.1692	0.0019	991	20	1008	11	98%
3009	117.0	68.2	234.6	0.29	7.0664	0.2234	0.4094	0.0052	2120	28	2212	24	95%
3010	20.7	87.6	90.6	0.97	1.6975	0.0741	0.1706	0.0026	1008	28	1015	14	99%
3011	30.2	64.8	134.9	0.48	1.8453	0.0720	0.1824	0.0023	1062	26	1080	13	98%
3012	39.4	103.0	199.7	0.52	1.4808	0.0525	0.1640	0.0021	923	21	979	12	94%
3013	58.2	104.1	428.1	0.24	1.0009	0.0325	0.1185	0.0014	704	17	722	8	97%
3014	35.8	82.0	194.8	0.42	1.4095	0.0487	0.1488	0.0016	893	21	894	9	99%
3015	75.9	362.0	328.3	1.10	1.5421	0.0535	0.1651	0.0022	947	21	985	12	96%
3016	164.9	132.5	220.1	0.60	13.7662	0.4497	0.5473	0.0074	2734	31	2814	31	97%
3017	16.7	49.6	122.1	0.41	0.9519	0.0399	0.1105	0.0016	679	21	676	9	99%

续表 1
Continued Appendix Table 1

测点号	Pb	Th	U	Th/U	²⁰⁷ Pb/ ²³⁵ U	1σ	²⁰⁶ Pb/ ²³⁸ U	1σ	²⁰⁷ Pb/ ²³⁵ U	1σ	²⁰⁶ Pb/ ²³⁸ U	1σ	谐和度
	含量(× 10 ⁻⁶)								Age(Ma)		Age(Ma)		
3018	34.7	234.5	348.5	0.67	0.6123	0.0221	0.0788	0.0009	485	14	489	6	99%
3019	215.2	252.8	359.2	0.70	10.1856	0.2630	0.4358	0.0050	2452	24	2332	23	94%
3020	116.6	434.3	1021.3	0.43	0.8839	0.0263	0.0982	0.0015	643	14	604	9	93%
3021	98.3	64.8	878.5	0.07	0.9679	0.0336	0.1022	0.0017	687	17	627	10	90%
3022	53.5	200.7	213.2	0.94	1.9118	0.0523	0.1828	0.0023	1085	18	1082	12	99%
3023	10.6	36.8	48.7	0.76	1.6925	0.0737	0.1650	0.0022	1006	28	984	12	97%
3024	70.5	316.8	299.2	1.06	1.6798	0.0416	0.1690	0.0019	1001	16	1006	10	99%
3025	72.2	197.4	339.7	0.58	1.6696	0.0413	0.1671	0.0018	997	16	996	10	99%
3026	25.5	131.5	139.1	0.95	1.2655	0.0465	0.1354	0.0021	830	21	818	12	98%
3027	45.8	75.9	317.8	0.24	1.0710	0.0299	0.1235	0.0013	739	15	751	8	98%
3028	84.7	128.2	439.4	0.29	1.5792	0.0390	0.1657	0.0020	962	15	988	11	97%
3029	18.9	55.6	75.3	0.74	2.0398	0.0681	0.1938	0.0028	1129	23	1142	15	98%
3030	15.3	39.2	60.3	0.65	2.0964	0.0797	0.1955	0.0029	1148	26	1151	16	99%
3031	35.0	98.9	134.5	0.74	2.0181	0.0605	0.1970	0.0024	1122	20	1159	13	96%
3032	33.0	78.4	128.6	0.61	2.2396	0.0681	0.1974	0.0023	1194	21	1161	12	97%
3033	109.3	126.2	154.6	0.82	11.4692	0.3078	0.5043	0.0062	2562	25	2632	27	97%
3034	44.1	172.4	271.1	0.64	1.1831	0.0363	0.1249	0.0013	793	17	759	8	95%
3035	15.6	68.9	122.7	0.56	0.7962	0.0357	0.1003	0.0013	595	20	616	8	96%
3036	91.8	370.5	638.1	0.58	0.9596	0.0336	0.1155	0.0016	683	17	705	9	96%
3037	72.6	141.6	362.2	0.39	1.5212	0.0479	0.1633	0.0019	939	19	975	11	96%
3038	206.4	195.0	326.5	0.60	10.1379	0.2784	0.4803	0.0063	2447	25	2529	27	96%
3039	30.6	50.8	144.1	0.35	1.7949	0.0808	0.1692	0.0021	1044	29	1007	12	96%
3040	14.7	70.9	129.3	0.55	0.7370	0.0295	0.0915	0.0013	561	17	564	7	99%
3041	18.9	39.9	99.4	0.40	1.3874	0.0540	0.1556	0.0021	884	23	932	11	94%
3042	7.6	11.3	38.9	0.29	1.7129	0.1236	0.1553	0.0026	1013	46	931	15	91%
3043	35.3	111.5	156.7	0.71	1.5479	0.0515	0.1696	0.0021	950	21	1010	12	93%
3044	111.8	688.0	1140.0	0.60	0.5764	0.0195	0.0807	0.0014	462	13	500	8	92%
3045	70.4	71.7	609.3	0.12	0.7762	0.0286	0.1048	0.0015	583	16	643	9	90%
3046	220.3	388.5	324.7	1.20	8.6665	0.3094	0.4504	0.0057	2304	33	2397	25	96%
3047	183.5	362.3	460.8	0.79	3.9278	0.1374	0.2872	0.0046	1619	28	1628	23	99%
3048	80.2	245.0	417.6	0.59	1.4811	0.0486	0.1612	0.0021	923	20	963	12	95%
3049	163.9	426.2	385.1	1.11	3.7123	0.1045	0.2958	0.0031	1574	23	1670	16	94%
3050	221.4	140.6	567.5	0.25	4.7235	0.1369	0.3268	0.0041	1771	24	1823	20	97%
3051	37.7	88.9	292.1	0.30	0.9331	0.0299	0.1097	0.0013	669	16	671	7	99%
3052	33.2	50.5	267.1	0.19	0.8815	0.0265	0.1079	0.0012	642	14	661	7	97%
3053	56.8	192.6	370.0	0.52	1.1392	0.0337	0.1261	0.0015	772	16	766	8	99%
3054	41.2	109.1	194.2	0.56	1.6387	0.0494	0.1650	0.0021	985	19	984	11	99%
3055	87.0	210.5	131.5	1.60	8.0751	0.2329	0.3917	0.0038	2239	26	2130	17	95%
3056	80.9	216.4	266.9	0.81	2.6348	0.0789	0.2207	0.0024	1310	22	1286	13	98%
3057	46.7	87.5	60.8	1.44	10.5952	0.2944	0.4705	0.0054	2488	26	2486	24	99%
3058	58.0	250.2	365.7	0.68	1.0920	0.0328	0.1197	0.0012	749	16	729	7	97%
3059	30.7	81.2	248.6	0.33	0.8752	0.0289	0.1044	0.0013	638	16	640	8	99%
3060	5.9	9.9	30.8	0.32	1.5392	0.0894	0.1590	0.0029	946	36	951	16	99%
3061	47.2	252.9	190.8	1.33	1.5912	0.0529	0.1634	0.0019	967	21	975	11	99%
3062	39.6	178.3	159.4	1.12	1.8256	0.0589	0.1761	0.0026	1055	21	1046	15	99%
3063	21.9	67.3	134.2	0.50	1.1517	0.0396	0.1294	0.0017	778	19	785	10	99%
3064	49.8	135.4	230.2	0.59	1.6121	0.0443	0.1686	0.0019	975	17	1004	10	97%
3065	22.9	58.6	126.9	0.46	1.2830	0.0469	0.1424	0.0018	838	21	858	10	97%
3066	70.0	81.2	102.9	0.79	10.3151	0.2817	0.4701	0.0059	2463	25	2484	26	99%

续表 1
Continued Appendix Table 1

测点号	Pb Th U			Th/U	²⁰⁷ Pb/ ²³⁵ U	1σ	²⁰⁶ Pb/ ²³⁸ U	1σ	²⁰⁷ Pb/ ²³⁵ U	1σ	²⁰⁶ Pb/ ²³⁸ U	1σ	谐和度
	含量(× 10 ⁻⁶)												
3067	100.6	133.5	166.1	0.80	9.2730	0.2264	0.4223	0.0044	2365	22	2271	20	95%
3068	60.5	66.6	136.7	0.49	5.2828	0.1338	0.3431	0.0039	1866	22	1902	19	98%
3069	21.5	124.4	170.1	0.73	0.7795	0.0282	0.0934	0.0011	585	16	576	6	98%
3070	97.8	130.4	125.7	1.04	12.5536	0.2925	0.5116	0.0057	2647	22	2664	24	99%
3071	14.3	11.1	112.4	0.10	0.9350	0.0361	0.1130	0.0015	670	19	690	9	97%
3072	56.9	18.8	575.8	0.03	0.7000	0.0187	0.0898	0.0011	539	11	555	6	97%
3073	22.8	210.2	103.4	2.03	1.1185	0.0444	0.1298	0.0017	762	21	787	10	96%
3074	39.6	146.4	156.5	0.93	1.8443	0.0602	0.1809	0.0020	1061	21	1072	11	99%
3075	10.6	123.6	56.0	2.21	0.9029	0.0430	0.1057	0.0017	653	23	647	10	99%
3076	283.5	135.9	614.3	0.22	6.7286	0.1779	0.3785	0.0042	2076	23	2069	20	99%
3077	41.2	155.7	289.4	0.54	0.9626	0.0314	0.1127	0.0012	685	16	689	7	99%
3078	60.9	203.8	430.8	0.47	1.0017	0.0280	0.1152	0.0012	705	14	703	7	99%
3079	43.0	66.7	403.8	0.17	0.7504	0.0222	0.0924	0.0011	568	13	570	6	99%
3080	50.4	218.0	216.3	1.01	1.6429	0.0510	0.1653	0.0025	987	20	986	14	99%
3081	30.2	68.5	136.8	0.50	1.7968	0.0621	0.1742	0.0022	1044	23	1035	12	99%
3082	38.5	58.4	53.0	1.10	10.3765	0.2817	0.4771	0.0070	2469	25	2515	31	98%
3083	19.3	95.1	81.2	1.17	1.5275	0.0573	0.1614	0.0023	942	23	964	13	97%
3084	28.5	87.9	136.6	0.64	1.5784	0.0599	0.1619	0.0021	962	24	967	11	99%
3085	8.6	65.5	59.5	1.10	0.8007	0.0459	0.1001	0.0016	597	26	615	9	97%
3086	23.5	91.7	112.8	0.81	1.5198	0.0619	0.1568	0.0023	938	25	939	13	99%
3087	20.3	121.2	86.4	1.40	1.3473	0.0565	0.1545	0.0023	866	24	926	13	93%
3088	51.8	328.6	455.2	0.72	0.6723	0.0240	0.0870	0.0011	522	15	538	6	97%
3090	9.5	46.5	82.9	0.56	0.7076	0.0409	0.0916	0.0016	543	24	565	9	96%
3091	46.1	53.1	443.4	0.12	0.7148	0.0249	0.0914	0.0010	548	15	564	6	97%
3092	32.1	64.1	184.9	0.35	1.2586	0.0433	0.1426	0.0016	827	19	859	9	96%
3093	134.4	402.2	464.7	0.87	2.3200	0.0790	0.2149	0.0028	1218	24	1255	15	97%
3094	38.4	124.5	172.7	0.72	1.6048	0.0635	0.1677	0.0023	972	25	1000	13	97%
3095	17.2	88.9	100.2	0.89	1.0510	0.0525	0.1263	0.0019	729	26	767	11	95%
3096	36.9	201.5	264.5	0.76	0.8491	0.0372	0.1048	0.0015	624	20	642	9	97%
3097	66.1	25.4	319.2	0.08	1.7933	0.0651	0.1833	0.0024	1043	24	1085	13	96%
3098	349.9	267.8	537.6	0.50	11.2510	0.3235	0.4851	0.0051	2544	27	2549	22	99%
3099	57.2	108.5	506.0	0.21	0.8176	0.0272	0.1017	0.0013	607	15	624	7	97%
3100	25.9	37.9	35.2	1.08	11.8666	0.3965	0.4928	0.0071	2594	31	2583	31	99%
3101	48.5	134.6	380.6	0.35	0.9079	0.0285	0.1083	0.0012	656	15	663	7	98%
3102	61.4	105.1	643.6	0.16	0.7346	0.0298	0.0887	0.0023	559	17	548	14	97%
3103	49.1	144.3	289.6	0.50	1.1874	0.0360	0.1369	0.0014	795	17	827	8	96%
3104	32.1	102.1	132.9	0.77	1.7240	0.0683	0.1799	0.0032	1018	25	1066	17	95%
3105	64.4	638.3	630.5	1.01	0.8506	0.0291	0.0921	0.0024	625	16	568	14	90%
3106	20.7	45.7	105.9	0.43	1.4977	0.0642	0.1595	0.0020	929	26	954	11	97%
3107	80.8	107.2	184.3	0.58	4.9834	0.1507	0.3365	0.0039	1817	26	1870	19	97%
3108	107.1	322.6	257.9	1.25	3.6509	0.1060	0.2833	0.0031	1561	23	1608	16	97%
3109	24.2	82.3	116.8	0.70	1.5757	0.0588	0.1639	0.0027	961	23	978	15	98%
3110	43.4	110.6	208.6	0.53	1.5306	0.0512	0.1654	0.0019	943	21	987	10	95%
3111	52.7	63.0	277.8	0.23	1.5590	0.0506	0.1604	0.0017	954	20	959	9	99%
3112	26.9	75.1	237.5	0.32	0.8083	0.0285	0.0952	0.0012	601	16	586	7	97%
3113	46.0	175.0	212.0	0.83	1.6157	0.0576	0.1650	0.0022	976	22	984	12	99%
3114	27.6	53.2	136.2	0.39	1.6921	0.0624	0.1642	0.0019	1006	24	980	11	97%
3115	76.8	214.1	657.9	0.33	0.8293	0.0296	0.0982	0.0013	613	16	604	8	98%
4001	33.9	109.1	198.8	0.55	1.2778	0.0482	0.1378	0.0019	836	21	832	11	99%

续表 1
Continued Appendix Table 1

测点号	Pb	Th	U	Th/U	²⁰⁷ Pb/ ²³⁵ U	1σ	²⁰⁶ Pb/ ²³⁸ U	1σ	²⁰⁷ Pb/ ²³⁵ U	1σ	²⁰⁶ Pb/ ²³⁸ U	1σ	谐和度
	含量(× 10 ⁻⁶)								Age(Ma)		Age(Ma)		
4002	85.6	712.5	251.0	2.84	1.8145	0.0572	0.1816	0.0020	1051	21	1076	11	97%
4003	40.2	362.7	329.4	1.10	0.6533	0.0211	0.0851	0.0012	511	13	526	7	96%
4004	172.3	101.7	261.9	0.39	12.3416	0.2870	0.4950	0.0048	2631	22	2592	21	98%
4005	43.5	219.9	267.4	0.82	1.5483	0.0496	0.1305	0.0022	950	20	791	12	81%
4006	154.7	396.8	575.7	0.69	2.2669	0.0647	0.2064	0.0028	1202	20	1209	15	99%
4007	7.6	16.2	50.1	0.32	1.1345	0.0582	0.1264	0.0017	770	28	767	10	99%
4008	44.1	305.8	460.3	0.66	0.6226	0.0187	0.0757	0.0010	491	12	470	6	95%
4009	40.4	96.8	261.9	0.37	1.2018	0.0336	0.1268	0.0011	801	15	769	6	95%
4010	199.5	202.3	317.4	0.64	10.9919	0.2478	0.4783	0.0054	2522	21	2520	23	99%
4011	130.5	231.2	659.8	0.35	1.8332	0.0484	0.1705	0.0022	1057	17	1015	12	95%
4012	28.2	272.8	116.1	2.35	1.1925	0.0616	0.1322	0.0022	797	29	800	13	99%
4013	39.8	354.3	296.6	1.19	0.7493	0.0234	0.0919	0.0012	568	14	567	7	99%
4014	75.5	256.8	424.9	0.60	1.4351	0.0491	0.1381	0.0023	904	20	834	13	91%
4015	34.3	65.1	278.4	0.23	0.9217	0.0335	0.1055	0.0014	663	18	647	8	97%
4016	24.2	57.6	197.9	0.29	0.9509	0.0410	0.1049	0.0016	679	21	643	9	94%
4017	105.9	108.5	514.7	0.21	1.9903	0.0597	0.1821	0.0025	1112	20	1078	14	96%
4018	266.6	405.6	515.9	0.79	7.0339	0.1915	0.3812	0.0053	2116	24	2082	25	98%
4019	12.3	33.6	60.5	0.56	1.6150	0.0651	0.1634	0.0025	976	25	976	14	99%
4020	36.9	181.8	208.1	0.87	1.1618	0.0366	0.1322	0.0015	783	17	800	9	97%
4021	164.5	96.9	200.6	0.48	19.6913	0.5196	0.5862	0.0098	3076	26	2974	40	96%
4022	48.5	99.4	119.4	0.83	4.1326	0.1005	0.2977	0.0037	1661	20	1680	18	98%
4023	155.6	392.0	601.8	0.65	2.3483	0.0535	0.2037	0.0023	1227	16	1195	13	97%
4024	6.1	18.9	28.0	0.67	1.6187	0.0887	0.1687	0.0034	978	34	1005	18	97%
4025	41.9	57.9	217.3	0.27	1.7312	0.0531	0.1780	0.0025	1020	20	1056	14	96%
4026	63.1	128.0	416.9	0.31	1.1127	0.0317	0.1268	0.0016	759	15	770	9	98%
4027	86.6	268.4	404.7	0.66	1.9351	0.0479	0.1760	0.0016	1093	17	1045	9	95%
4028	171.6	344.2	850.9	0.40	1.7161	0.0368	0.1637	0.0013	1015	14	977	7	96%
4029	131.2	256.2	223.6	1.15	9.6235	0.2665	0.4174	0.0074	2399	26	2249	34	93%
4030	9.7	26.9	92.8	0.29	0.7206	0.0362	0.0898	0.0015	551	21	554	9	99%
4031	28.1	61.2	282.8	0.22	0.7301	0.0228	0.0870	0.0010	557	13	538	6	96%
4032	194.1	539.6	986.0	0.55	1.6378	0.0426	0.1595	0.0020	985	16	954	11	96%
4033	63.6	259.1	335.4	0.77	1.3314	0.0384	0.1442	0.0017	859	17	868	9	98%
4034	115.5	210.8	164.0	1.29	10.2510	0.2765	0.4616	0.0048	2458	25	2447	21	99%
4035	52.8	102.3	75.5	1.36	10.1506	0.3135	0.4557	0.0053	2449	29	2421	24	98%
4036	280.6	559.2	435.4	1.28	9.6787	0.3045	0.4403	0.0054	2405	29	2352	24	97%
4037	39.5	81.1	164.7	0.49	2.1435	0.0720	0.1915	0.0023	1163	23	1129	12	97%
4038	115.2	241.8	349.5	0.69	3.4069	0.1352	0.2506	0.0068	1506	31	1442	35	95%
4039	36.5	103.1	188.3	0.55	1.4928	0.0434	0.1515	0.0015	927	18	909	8	98%
4040	230.2	127.1	390.6	0.33	12.5396	0.3190	0.5119	0.0081	2646	24	2665	34	99%
4041	47.3	230.0	320.0	0.72	0.9509	0.0275	0.1126	0.0012	679	14	688	7	98%
4042	200.8	253.6	875.4	0.29	2.1507	0.0566	0.1876	0.0029	1165	18	1108	16	95%
4043	45.8	327.6	373.0	0.88	0.7267	0.0216	0.0894	0.0009	555	13	552	5	99%
4044	20.2	50.3	88.8	0.57	1.8175	0.0679	0.1790	0.0022	1052	24	1061	12	99%
4045	22.3	192.6	163.3	1.18	0.7738	0.0306	0.0953	0.0013	582	18	587	7	99%
4046	142.4	385.4	730.9	0.53	1.5318	0.0490	0.1564	0.0021	943	20	937	12	99%
4047	136.6	253.6	652.2	0.39	2.3646	0.1059	0.1770	0.0051	1232	32	1051	28	84%
4048	46.4	156.9	226.4	0.69	1.4931	0.0429	0.1558	0.0016	928	17	933	9	99%
4049	18.4	80.5	81.7	0.99	1.6065	0.0594	0.1610	0.0020	973	23	963	11	98%
4050	136.8	426.5	317.2	1.34	3.8697	0.0972	0.2801	0.0026	1607	20	1592	13	99%

续表 1
Continued Appendix Table 1

测点号	Pb	Th	U	Th/U	²⁰⁷ Pb/ ²³⁵ U	1σ	²⁰⁶ Pb/ ²³⁸ U	1σ	²⁰⁷ Pb/ ²³⁵ U	1σ	²⁰⁶ Pb/ ²³⁸ U	1σ	谐和度
	含量(× 10 ⁻⁶)								Age(Ma)		Age(Ma)		
4051	48.9	130.1	481.3	0.27	0.6796	0.0196	0.0892	0.0011	527	12	551	6	95%
4052	16.1	79.4	57.8	1.37	1.8478	0.0727	0.1850	0.0025	1063	26	1094	14	97%
4053	159.9	52.4	911.2	0.06	1.4686	0.0373	0.1605	0.0018	918	15	960	10	95%
4054	94.1	424.3	280.5	1.51	2.3074	0.0671	0.2163	0.0023	1215	21	1262	12	96%
4055	27.7	74.7	156.3	0.48	1.2962	0.0478	0.1443	0.0018	844	21	869	10	97%
4056	69.1	148.0	333.4	0.44	1.5193	0.0526	0.1742	0.0021	938	21	1035	12	90%
4057	56.1	146.7	174.7	0.84	2.6400	0.0860	0.2438	0.0032	1312	24	1406	16	93%
4058	26.9	118.6	123.8	0.96	1.4265	0.0530	0.1581	0.0018	900	22	946	10	95%
4059	27.4	45.0	160.7	0.28	1.3598	0.0475	0.1460	0.0016	872	20	878	9	99%
4060	56.0	121.9	264.9	0.46	1.6786	0.0580	0.1716	0.0018	1000	22	1021	10	97%
4061	83.7	170.3	734.6	0.23	0.8863	0.0308	0.1018	0.0015	644	17	625	9	96%
4062	44.1	119.5	223.4	0.53	1.4973	0.0482	0.1579	0.0018	929	20	945	10	98%
4063	40.7	34.8	45.0	0.77	20.6118	0.6084	0.6056	0.0073	3121	29	3052	29	97%
4065	42.1	80.2	191.8	0.42	1.8482	0.0632	0.1800	0.0023	1063	23	1067	13	99%
4066	16.7	61.6	90.7	0.68	1.3624	0.0615	0.1412	0.0019	873	26	852	11	97%
4067	167.3	297.3	398.0	0.75	5.1805	0.1547	0.3217	0.0034	1849	25	1798	17	97%
4068	77.9	106.5	366.5	0.29	1.9080	0.0602	0.1802	0.0019	1084	21	1068	10	98%
4069	25.5	88.4	193.0	0.46	1.0411	0.0467	0.1045	0.0013	724	23	641	7	87%
4070	52.2	76.3	91.7	0.83	8.6739	0.3456	0.4080	0.0051	2304	36	2206	23	95%
4071	77.7	112.8	167.7	0.67	5.7145	0.2139	0.3452	0.0041	1934	32	1912	20	98%
4072	111.7	22.0	413.1	0.05	3.1003	0.1139	0.2396	0.0036	1433	28	1385	19	96%
4073	8.2	70.8	59.5	1.19	0.8367	0.0503	0.0945	0.0017	617	28	582	10	94%
4075	180.5	279.8	333.6	0.84	8.5865	0.2538	0.3926	0.0038	2295	27	2135	18	92%
4076	73.9	127.4	343.7	0.37	1.7789	0.0580	0.1734	0.0019	1038	21	1031	10	99%
4077	68.6	122.4	125.2	0.98	6.7029	0.1973	0.3792	0.0045	2073	26	2073	21	99%
4078	20.4	212.0	154.4	1.37	0.7607	0.0305	0.0871	0.0011	574	18	538	7	93%
4079	164.4	54.5	277.2	0.20	10.4793	0.2901	0.4635	0.0052	2478	26	2455	23	99%
4080	47.9	238.5	305.9	0.78	1.1144	0.0408	0.1178	0.0016	760	20	718	9	94%
4081	238.0	227.9	341.8	0.67	13.4000	0.4157	0.4975	0.0073	2708	29	2603	31	96%
4082	166.3	582.2	576.5	1.01	4.0488	0.1204	0.2354	0.0052	1644	24	1363	27	81%
4083	284.8	169.4	398.7	0.43	16.2448	0.4405	0.5507	0.0071	2891	26	2828	29	97%
4084	5.7	24.2	32.9	0.73	1.2908	0.0866	0.1328	0.0027	842	38	804	15	95%
4085	55.1	205.2	244.3	0.84	1.8400	0.0663	0.1694	0.0020	1060	24	1009	11	95%
4086	45.8	257.4	218.6	1.18	1.5012	0.0561	0.1489	0.0021	931	23	895	12	96%
4087	13.2	42.9	97.1	0.44	1.0898	0.0545	0.1091	0.0017	748	26	668	10	88%
4088	82.1	437.0	338.0	1.29	1.7030	0.0471	0.1622	0.0016	1010	18	969	9	95%
4089	24.6	222.5	196.2	1.13	0.7458	0.0255	0.0854	0.0010	566	15	528	6	93%
4090	36.8	250.3	301.0	0.83	0.7435	0.0233	0.0901	0.0009	564	14	556	6	98%
4091	46.3	123.9	264.7	0.47	1.2317	0.0373	0.1396	0.0018	815	17	843	10	96%
4092	21.8	60.5	165.6	0.37	0.9082	0.0304	0.1074	0.0013	656	16	658	7	99%
4093	46.6	219.0	417.2	0.52	0.7125	0.0226	0.0883	0.0011	546	13	545	7	99%
4094	90.2	176.2	340.7	0.52	2.1491	0.0608	0.2079	0.0026	1165	20	1218	14	95%
4095	86.1	270.4	392.4	0.69	1.5399	0.0470	0.1653	0.0019	946	19	986	10	95%
4096	13.2	133.0	88.0	1.51	0.7831	0.0362	0.0942	0.0015	587	21	580	9	98%
4097	53.7	122.3	254.7	0.48	1.6324	0.0519	0.1712	0.0023	983	20	1018	12	96%
4098	38.5	64.4	124.5	0.52	2.9527	0.0880	0.2414	0.0029	1396	23	1394	15	99%
4099	67.5	180.8	290.3	0.62	2.1487	0.0658	0.1951	0.0031	1165	21	1149	17	98%
4100	18.9	143.6	139.1	1.03	0.9316	0.1135	0.0953	0.0014	668	60	587	8	87%
4101	19.1	319.6	96.3	3.32	1.4265	0.0656	0.1395	0.0045	900	27	842	26	93%

续表 1
Continued Appendix Table 1

测点号	Pb	Th	U	Th/U	²⁰⁷ Pb/ ²³⁵ U	1σ	²⁰⁶ Pb/ ²³⁸ U	1σ	²⁰⁷ Pb/ ²³⁵ U	1σ	²⁰⁶ Pb/ ²³⁸ U	1σ	谐和度
	含量(×10 ⁻⁶)								Age(Ma)		Age(Ma)		
4102	45.2	152.3	319.5	0.48	0.9775	0.0305	0.1137	0.0012	692	16	694	7	99%
4103	21.0	134.6	161.6	0.83	0.8580	0.0303	0.0958	0.0011	629	17	589	7	93%
4104	46.7	81.4	225.7	0.36	1.6218	0.0488	0.1699	0.0019	979	19	1012	11	96%
4106	163.5	1281.5	940.8	1.36	1.4501	0.0466	0.1267	0.0036	910	19	769	20	83%
4107	208.7	344.3	427.4	0.81	5.9511	0.1534	0.3627	0.0040	1969	22	1995	19	98%
4108	76.6	347.5	474.0	0.73	1.1736	0.0355	0.1300	0.0020	788	17	788	11	99%
4109	62.1	462.0	387.1	1.19	1.2577	0.0366	0.1215	0.0021	827	16	739	12	88%
4110	13.4	47.4	65.6	0.72	1.4992	0.0620	0.1540	0.0021	930	25	923	12	99%
4111	442.9	184.2	406.3	0.45	31.6252	0.7192	0.7350	0.0069	3539	23	3552	26	99%
4112	43.5	141.1	217.5	0.65	1.5823	0.0503	0.1521	0.0017	963	20	913	9	94%
4113	275.1	231.1	520.9	0.44	8.4547	0.2133	0.4374	0.0060	2281	23	2339	27	97%
4114	20.3	109.0	133.9	0.81	1.1033	0.0478	0.1126	0.0018	755	23	688	10	90%
4115	57.7	166.4	255.5	0.65	1.7971	0.0540	0.1750	0.0020	1044	20	1040	11	99%
4116	38.2	189.8	363.9	0.52	0.6894	0.0255	0.0863	0.0012	532	15	534	7	99%
4117	16.6	43.8	142.7	0.31	0.8166	0.0314	0.0980	0.0013	606	18	603	8	99%
4118	17.2	24.7	81.5	0.30	1.8317	0.0650	0.1779	0.0023	1057	23	1055	13	99%
4119	7.2	73.8	49.6	1.49	0.7753	0.0453	0.0949	0.0016	583	26	584	9	99%
4120	22.5	37.1	113.9	0.33	1.6501	0.0650	0.1686	0.0023	990	25	1004	13	98%
4121	73.3	435.6	490.1	0.89	0.9388	0.0299	0.1088	0.0012	672	16	666	7	99%
4122	122.9	314.0	469.3	0.67	2.2551	0.0622	0.1984	0.0021	1198	19	1167	12	97%
4123	65.6	386.6	257.2	1.50	1.6980	0.0497	0.1665	0.0022	1008	19	993	12	98%
4124	56.7	212.9	231.6	0.92	1.7483	0.0507	0.1728	0.0017	1027	19	1027	10	99%
4125	49.3	120.0	239.3	0.50	1.6233	0.0464	0.1635	0.0020	979	18	976	11	99%
4126	123.2	252.1	675.1	0.37	1.4320	0.0415	0.1454	0.0020	902	17	875	11	96%
4127	50.1	141.5	227.7	0.62	1.7072	0.0520	0.1660	0.0017	1011	20	990	9	97%
4128	27.6	81.4	217.3	0.37	0.9061	0.0343	0.1022	0.0011	655	18	627	7	95%
4129	40.2	220.4	379.0	0.58	0.7394	0.0291	0.0843	0.0013	562	17	522	8	92%
4130	65.0	186.0	317.4	0.59	1.7825	0.0762	0.1618	0.0025	1039	28	967	14	92%
5001	33.5	119.0	174.4	0.68	1.3450	0.0477	0.1492	0.0017	865	21	897	10	96%
5002	27.8	112.6	273.5	0.41	0.6952	0.0244	0.0809	0.0009	536	15	501	6	93%
5003	20.2	158.3	92.5	1.71	1.2866	0.0554	0.1301	0.0017	840	25	789	10	93%
5004	207.0	316.5	324.4	0.98	9.4550	0.2014	0.4236	0.0036	2383	20	2277	16	95%
5005	36.5	144.5	197.9	0.73	1.2558	0.0392	0.1378	0.0015	826	18	832	9	99%
5006	21.2	112.0	163.2	0.69	0.9907	0.0413	0.0992	0.0021	699	21	610	12	86%
5007	79.7	206.9	373.4	0.55	1.6773	0.0436	0.1655	0.0017	1000	17	987	9	98%
5008	43.6	189.6	398.9	0.48	0.7304	0.0230	0.0877	0.0009	557	13	542	5	97%
5009	16.2	100.9	83.1	1.21	1.2790	0.0478	0.1265	0.0016	836	21	768	9	91%
5010	107.6	111.8	181.5	0.62	9.4706	0.2462	0.4310	0.0044	2385	24	2310	20	96%
5011	130.0	303.3	1391.7	0.22	0.6810	0.0179	0.0807	0.0009	527	11	501	5	94%
5012	155.0	229.2	379.0	0.60	6.2382	0.1398	0.3020	0.0029	2010	20	1701	14	83%
5013	16.9	86.7	95.0	0.91	1.2938	0.0523	0.1284	0.0020	843	23	779	11	92%
5014	61.6	114.3	406.6	0.28	1.2792	0.0307	0.1302	0.0011	837	14	789	6	94%
5015	56.0	239.4	247.6	0.97	1.6622	0.0480	0.1559	0.0026	994	18	934	14	93%
5016	48.1	103.2	384.2	0.27	0.9469	0.0254	0.1088	0.0013	676	13	666	7	98%
5017	83.8	98.3	389.2	0.25	2.0095	0.0465	0.1836	0.0018	1119	16	1087	10	97%
5018	10.0	26.1	85.8	0.30	0.8442	0.0347	0.1003	0.0016	621	19	616	9	99%
5019	59.0	278.3	236.0	1.18	1.9420	0.0516	0.1701	0.0024	1096	18	1013	13	92%
5020	15.7	38.2	131.6	0.29	0.8642	0.0294	0.1023	0.0014	632	16	628	8	99%
5021	60.9	74.9	408.3	0.18	1.2061	0.0335	0.1306	0.0016	803	15	791	9	98%

续表 1
Continued Appendix Table 1

测点号	Pb Th U			Th/U	²⁰⁷ Pb/ ²³⁵ U	1σ	²⁰⁶ Pb/ ²³⁸ U	1σ	²⁰⁷ Pb/ ²³⁵ U	1σ	²⁰⁶ Pb/ ²³⁸ U	1σ	谐和度
	含量(×10 ⁻⁶)												
5022	132.2	188.1	877.7	0.21	1.2473	0.0298	0.1288	0.0013	822	13	781	8	94%
5023	79.1	333.0	269.6	1.24	2.2750	0.0570	0.2005	0.0019	1205	18	1178	10	97%
5024	54.9	240.6	393.3	0.61	0.9742	0.0274	0.1109	0.0013	691	14	678	8	98%
5025	14.2	45.3	52.6	0.86	2.2011	0.0832	0.1995	0.0029	1181	26	1173	15	99%
5026	64.1	123.5	289.6	0.43	1.9522	0.0551	0.1795	0.0018	1099	19	1064	10	96%
5027	50.9	111.3	268.8	0.41	1.4928	0.0481	0.1518	0.0025	927	20	911	14	98%
5028	33.3	196.4	166.1	1.18	1.3648	0.0453	0.1387	0.0016	874	19	838	9	95%
5029	30.6	53.4	153.1	0.35	1.6263	0.0460	0.1649	0.0019	980	18	984	11	99%
5030	22.0	106.9	228.8	0.47	0.6155	0.0217	0.0786	0.0011	487	14	488	7	99%
5031	234.7	536.6	292.7	1.83	10.2260	0.2818	0.4643	0.0071	2455	26	2458	31	99%
5032	94.6	67.2	530.1	0.13	1.8626	0.0776	0.1784	0.0039	1068	28	1058	21	99%
5033	191.6	315.4	943.6	0.33	1.7709	0.0461	0.1665	0.0026	1035	17	993	14	95%
5034	186.1	428.5	1060.7	0.40	1.5301	0.0425	0.1385	0.0015	943	17	836	9	88%
5035	485.6	201.3	973.6	0.21	9.3509	0.3092	0.4155	0.0090	2373	30	2240	41	94%
5036	24.6	8.0	203.0	0.04	1.0692	0.0614	0.1048	0.0020	738	30	643	12	86%
5037	39.4	177.5	167.7	1.06	1.6225	0.0562	0.1633	0.0020	979	22	975	11	99%
5038	64.7	189.0	592.7	0.32	0.7514	0.0210	0.0922	0.0011	569	12	568	7	99%
5039	190.5	227.6	1291.6	0.18	1.1974	0.0339	0.1312	0.0019	799	16	795	11	99%
5040	82.0	544.1	540.8	1.01	1.1522	0.0387	0.1096	0.0014	778	18	670	8	85%
5041	17.2	70.2	124.8	0.56	0.8643	0.0348	0.1093	0.0017	632	19	669	10	94%
5042	49.5	165.9	238.2	0.70	1.6334	0.0545	0.1647	0.0023	983	21	983	12	99%
5043	28.9	44.0	150.4	0.29	1.6285	0.0538	0.1629	0.0021	981	21	973	12	99%
5044	37.3	42.4	430.5	0.10	0.5948	0.0201	0.0769	0.0009	474	13	478	5	99%
5045	63.0	300.4	222.7	1.35	1.8991	0.0659	0.1903	0.0028	1081	23	1123	15	96%
5046	34.0	135.5	160.6	0.84	1.4808	0.0599	0.1571	0.0021	923	25	940	12	98%
5047	38.0	185.3	161.5	1.15	1.5400	0.0573	0.1583	0.0020	947	23	947	11	99%
5048	95.8	151.0	233.6	0.65	5.3480	0.1514	0.2954	0.0028	1877	24	1668	14	88%
5049	53.2	87.4	395.0	0.22	0.9948	0.0319	0.1157	0.0014	701	16	706	8	99%
5050	69.2	226.2	333.8	0.68	1.5134	0.0502	0.1577	0.0019	936	20	944	10	99%
5051	44.2	89.7	215.2	0.42	1.6218	0.0540	0.1655	0.0020	979	21	987	11	99%
5052	49.0	143.3	224.4	0.64	1.6499	0.0501	0.1636	0.0017	990	19	977	10	98%
5053	49.9	127.0	242.2	0.52	1.5916	0.0500	0.1634	0.0020	967	20	976	11	99%
5054	158.4	265.4	299.7	0.89	8.3352	0.2550	0.3694	0.0058	2268	28	2027	27	88%
5055	10.5	1.4	100.3	0.01	0.7950	0.0398	0.0961	0.0013	594	23	592	8	99%
5056	64.2	331.3	591.4	0.56	0.7190	0.0275	0.0865	0.0012	550	16	535	7	97%
5057	97.8	108.8	152.3	0.71	10.5101	0.2870	0.4606	0.0047	2481	25	2442	21	98%
5058	22.3	35.1	32.4	1.08	10.6687	0.3279	0.4679	0.0068	2495	29	2474	30	99%
5059	77.8	219.2	330.1	0.66	1.9098	0.0470	0.1820	0.0018	1085	16	1078	10	99%
5060	16.5	175.9	136.1	1.29	0.6511	0.0276	0.0797	0.0010	509	17	494	6	97%
5061	34.0	2.2	334.0	0.01	0.7865	0.0235	0.0932	0.0010	589	13	575	6	97%
5062	119.4	147.7	250.6	0.59	6.1195	0.1401	0.3601	0.0035	1993	20	1983	17	99%
5063	88.3	114.7	172.2	0.67	7.1668	0.1932	0.3832	0.0050	2132	24	2091	24	98%
5064	21.3	97.5	99.8	0.98	1.5351	0.0554	0.1530	0.0018	945	22	918	10	97%
5065	102.1	417.0	486.2	0.86	1.5258	0.0478	0.1557	0.0019	941	19	933	10	99%
5066	18.2	38.1	87.0	0.44	1.6909	0.0677	0.1670	0.0022	1005	26	995	12	99%
5067	30.4	61.5	51.5	1.19	8.5385	0.2749	0.3840	0.0050	2290	29	2095	23	91%
5068	252.4	116.0	751.6	0.15	4.7188	0.1449	0.2857	0.0051	1771	26	1620	25	91%
5069	24.1	68.6	152.4	0.45	1.1807	0.0437	0.1292	0.0015	792	20	783	9	98%
5070	13.1	16.9	82.0	0.21	1.3621	0.0632	0.1362	0.0017	873	27	823	10	94%

Appendix

Appendix B: Table of thermochronologic data (chapter 5)

sample	Elevation (m)	Latitude (N)	Longitude (E)	Lithology	Unit age (Ma)	4-He (mol)	238-U (mol)	235-U (mol)	232-Th (mol)	Ft	Alpa-corr Age (Ma)	Mean Age (Ma)	Error 1s
0729-RZ1	5076	490800	3644371	sandstone	<90	8.73E-13	5.58E-12	4.10E-14	5.58E-12	7.46E-01	130.63		
	5076	490800	3644371	sandstone		1.64E-12	1.89E-11	1.39E-13	4.63E-12	7.70E-01	81.87		
	5076	490800	3644371	sandstone		5.74E-13	4.61E-12	3.39E-14	2.98E-12	7.79E-01	106.79	106.43	24.38
0729-RZ1	5076	490800	3644371	sandstone	<90	1.27E-12	4.87E-12	3.58E-14	2.76E-12	7.69E-01	228.52		
	5076	490800	3644371	sandstone		1.46E-12	9.14E-12	6.71E-14	1.84E-12	7.78E-01	149.82		
	5076	490800	3644371	sandstone		1.98E-12	7.03E-12	5.17E-14	3.81E-12	7.85E-01	241.60	206.65	49.64
0819-RZ4	4990	466328	3674038	granite	210	7.13E-12	4.24E-11	3.11E-13		8.03E-01	159.70		
	4990	466328	3674038	granite		8.94E-12	6.69E-11	4.91E-13		7.71E-01	132.45		
	4990	466328	3674038	granite		1.12E-11	7.14E-11	5.24E-13	3.64E-11	8.22E-01	130.99	141.05	16.17
0819-RZ7	4698	471005	3658968	mélange	>210	8.45E-13	3.39E-12	2.49E-14	3.45E-12	7.59E-01	202.79		
	4698	471005	3658968	mélange		1.45E-12	4.81E-12	3.53E-14	2.32E-12	7.56E-01	271.50		
	4698	471005	3658968	mélange		9.81E-13	5.83E-12	4.28E-14	1.28E-12	7.71E-01	158.52	210.94	56.93
0819-RZ7	4698	471005	3658968	mélange	>210	5.78E-13	1.95E-12	1.43E-14	3.01E-12	7.85E-01	212.20		
	4698	471005	3658968	mélange		8.51E-13	4.56E-12	3.35E-14	2.36E-12	7.70E-01	165.29		
	4698	471005	3658968	mélange		8.77E-13	4.43E-12	3.26E-14	1.98E-12	7.46E-01	183.17	186.89	23.68
0819-RZ2	5321	464806	3677369	granite	210	1.16E-11	5.24E-11	3.85E-13	7.64E-12	8.11E-01	201.01		
	5321	464806	3677369	granite		6.61E-12	3.43E-11	2.52E-13	2.85E-12	8.06E-01	178.70		
	5321	464806	3677369	granite		1.57E-11	1.01E-10	7.38E-13		7.89E-01	150.63	176.78	25.24
0819-RZ5	4932	469855	3663776	mélange	>210	9.26E-13	3.92E-12	2.88E-14	3.32E-12	8.04E-01	187.40		
	4932	469855	3663776	mélange		1.11E-12	4.75E-12	3.49E-14	4.34E-12	7.76E-01	189.88		
	4932	469855	3663776	mélange		6.64E-13	2.79E-12	2.05E-14	1.27E-12	7.74E-01	211.35		
	4932	469855	3663776	mélange		2.05E-12	1.03E-11	7.54E-14	2.69E-12	7.93E-01	180.43	192.26	13.34
0819-RZ3	5217	464714	3678211	granite	210	1.02E-11	7.11E-11	5.22E-13	3.14E-11	8.10E-01	123.08		
	5217	464714	3678211	granite		3.91E-11	2.32E-10	1.70E-12	1.29E-10	8.14E-01	140.57		
	5217	464714	3678211	granite		1.74E-11	1.06E-10	7.78E-13	9.45E-11	7.73E-01	134.53	132.72	8.88
0819-RZ1	5409	464526	3676742	granite	210	3.88E-12	2.32E-11	1.71E-13	1.23E-11	7.90E-01	144.32		
	5409	464526	3676742	granite		6.48E-12	3.73E-11	2.74E-13	1.57E-11	7.52E-01	160.94		
	5409	464526	3676742	granite		9.55E-12	6.14E-11	4.51E-13	2.06E-11	7.68E-01	143.74	149.67	9.77
0825-RZ1	5557	470896	3700948	basement	520-490	6.83E-13	4.00E-12	2.93E-14	2.05E-12	7.66E-01	152.33		
	5557	470896	3700948	basement		7.48E-13	4.85E-12	3.56E-14	1.63E-12	7.52E-01	145.50		
	5557	470896	3700948	basement		8.12E-13	4.84E-12	3.56E-14	2.23E-12	7.67E-01	151.04		
	5557	470896	3700948	basement		1.39E-12	8.91E-12	6.54E-14	3.91E-12	7.59E-01	143.07	147.99	4.42

Appendix

Appendix C: Numerical setup (chapter 6)

Table1. Rheological setup.

	$\text{Log}_{10}(A)$ ($\text{Mpa}^{-n} \cdot \text{s}^{-1}$)	n	E ($\text{kJ} \cdot \text{mol}^{-1}$)	$\sin(\phi)$	Cohesive	Density	Experimental material	Flow law reference
Continental upper crust	-3.7	1.9	141	0.5	20.e+6	2750	Wet westerly granite	Hansen and Carter (1983)
Continental lower crust	-1.2	3.1	276	0.5	20.e+6	2980	Maryland diabase	Caristan (1980)
Continental lithosphere	3.84	3	510	0.6	200.e+6	3330	Dry olivine	Goetze and Evans (1979)
Sediments	-67	31	98	0.08	10.e+6	2800	Micaschist	Shea and Kronenberg (1992)
Serpentinite	-12.6	5.8	18	0.08	10.e+6	2600	Serpentinite	Hilalret et al., (2007)
Oceanic crust	-1.2	3.1	276	0.5(0.08)	20.e+6	2980	Maryland diabase	Caristan (1980)
Oceanic lithosphere	3.84	3	510	0.6	500.e+6	3330	Dry olivine	Goetze and Evans (1979)
mantle	3.84	3	510	0.6	500.e+6	3330	Dry olivine	Goetze and Evans (1979)

Table2. Boundary condition.

T_moho (°C)	A (oceanic lithosphere)	Vx (lift) (cm/yr)	Length differences	T_base of lithosphere (°C)
400	7.e+3	0	270km	1330

Zhongbao Zhao

EDUCATION

Universität Tübingen

Ph.D., Structural Geology,

Expected August 2015

Dissertation: “*Tectonic evolution of Qiangtang Terrane, central Tibet*”

Supervisors: Prof. P.D. Bons and Prof. Genhou Wang

M.A., Structural Geology, China University of Geosciences (Beijing),

2008.9—2011.6

B.A., Geology, Lanzhou University, China

2004.9—2008.6

AWARDS

‘**State Scholarship Fund**’ on Ph.D study abroad from CHINESE SCHOLARSHIP COUNCIL with Nr. 2011640017.

PUBLICATIONS

Zhao, Z., Bons, P., Wang, G., Soesoo, A., and Liu, Y.: Tectonic evolution and high-pressure rock exhumation in the Qiangtang Terrane, Central Tibet, *Solid Earth*, 6, 457-473, 2015.

Zhao, Z., Bons, P. D., Wang, G., Liu, Y., and Zheng, Y.: Origin and pre-Cenozoic evolution of the south Qiangtang basement, Central Tibet, *Tectonophysics*, 623, 52-66, <http://dx.doi.org/10.1016/j.tecto.2014.03.016>, 2014.

Yang, Y., **Zhao, Z. B.**, Yuan, T. Y., Liu, Y., and Li, C. Y.: Ordovician parallel unconformity in Qiangtang terrane, northern Tibet: Implications to Early Paleozoic evolution of northern Tibetan region. *Acta Petrologica Sinica*, 30, 2381-2392, 2014.

Liu, Y., Santosh, M., **Zhao, Z. B.**, Niu, W. C., and Wang, G. H.: Evidence for palaeo-Tethyan oceanic subduction within central Qiangtang, northern Tibet, *Lithos*, 127, 39-53, 2011.

Zhao, Z., Bons, P. D., Gomez-Rivas, E., Soesoo, A., and Burov E.: Efficient exhumation of (ultra) high-pressure rocks by slab extraction, EGU General Assembly Conference Abstracts, 2015, 6610,

Zhao, Z., and Bons, P. D.: Two radically different exhumation models for the Qiangtang Terrane, Central Tibet, EGU General Assembly Conference Abstracts, 2014, 11745,

Zhao, Z., Bons, P. D., and Wang, G.: Origin and pre-Cenozoic evolution of the Qiangtang terrane basement, central Tibet, EGU General Assembly Conference Abstracts, 2013, 1067,